Transcription Factor Dysfunction in Ovarian Cancer: The Roles of ZIC2 and RUNX3

by

Huachen Chen

A thesis submitted in partial fulfillment of the requirements for the degree of

Doctor of Philosophy

in

Cancer Sciences

Department of Oncology
University of Alberta

Abstract

Ovarian cancer is the most lethal gynecological cancer, and epithelial ovarian cancer (EOC) accounts for about 90% of ovarian cancers. Despite advancements in medical technology, the overall survival rate of EOC has improved only slightly, with a 5-year survival rate of less than 50%. One cause is the development of chemoresistance in EOC after conventional chemotherapy, which may be due to the presence of cancer stem cells (CSCs). ZIC2 is a transcription factor that is expressed in embryonic stem cells but not in adult tissues except the brain and testis. Upregulation of ZIC2 is pro-tumorigenic in a variety of human cancers. However, limited studies have been conducted on ZIC2-mediated regulation of tumorigenic phenotypes and the related molecular mechanisms of ZIC2 in EOC. We hypothesized that ZIC2 promotes tumorigenic phenotypes in EOC. Herein, we reported that ZIC2 is expressed in a subpopulation of EOC samples and is associated with poor survival in patients with advanced EOC. ZIC2 promotes cell growth, single-cell survival, anchorage-independent growth, and CSC stemness, but it is cell-context dependent. Furthermore, we demonstrated potential underlying mechanisms for ZIC2-mediated regulation of tumorigenic phenotypes in EOC.

We also investigated the role of the transcription factor RUNX3 in a rare subtype of ovarian cancer, granulosa cell tumor of the ovary (GCT). GCTs are classified as adult granulosa cell tumors (AGCT) and juvenile granulosa cell tumors (JGCT). Although most GCTs are diagnosed at early stages, patients with advanced GCTs have a poor prognosis and are prone to relapse. RUNX3 has

been shown to play an important role in normal tissues and human cancers. RUNX3 plays a role in inhibiting or promoting tumor progression in various human cancers. In EOC, RUNX3 promotes cell proliferation, anchorage-independent growth, and chemoresistance. We hypothesized that RUNX3 promotes the tumorigenic phenotypes in GCT. We reported the expression of RUNX1, RUNX2, and RUNX3 in GCT, where RUNX3 showed low levels of variable expression in GCT samples but not in the normal human granulosa cell line SVOG or normal ovarian tissues. RUNX3 also promotes cell growth, anchorage-independent growth, cell motility, and tumor formation in the AGCT cell line KGN, while inhibition of RUNX3 in the JGCT cell line COV434 reduces cell growth. Moreover, RUNX3 upregulates the expression of cyclin D2 and reduces the expression of $P27^{Kip1}$ in KGN cells.

Collectively, this study suggests that ZIC2 and RUNX3 play a pro-tumorigenic role in ovarian cancer in a context-dependent manner and are potential therapeutic targets for ovarian cancer.

PREFACE

This thesis is a collaborative work led by Dr. YangXin Fu and Dr. Lynne-Marie Postovit at the University of Alberta. The patient-derived tumor models of high-grade serous ovarian cancer were a gift from Dr. Lynne-Marie Postovit and were originally obtained from Charles River Laboratories International, Inc. The high-grade serous ovarian cancer tumor microarray was provided by Dr. Cheng Lee. The granulosa cell tumor samples were obtained from the Alberta Cancer Research Biobank and the Baylor College of Medicine Tissue Repository. Animal studies involving SKOV3 and OVCAR3 cells in this thesis have received ethical approval from the Animal Care and Use Committee (ACUC) on Feb 12, 2018 (study title: Targeting the pro-tumorigenic signaling pathways in ovarian cancer, approval number: AUP000004444). Animal studies involving KGN cells in this thesis have received ethical approval from the Animal Care and Use Committee (ACUC) on May 12, 2015 (study title: Analysis of novel therapies for the treatment of granulosa cell tumors, approval number: AUP000001435).

The RUNX3 part of this thesis has been published as:

Chen, H., Crosley, P., Azad, A.K., Gupta, N., Gokul, N., Xu, Z., Weinfeld, M., Postovit, L.M., Pangas, S.A., Hitt, M.M. and Fu, Y., 2019. RUNX3 promotes the tumorigenic phenotypes of KGN, a human granulosa cell tumor-derived cell line. *International journal of molecular sciences*, *20*(14), p.3471. I am the first author of this article. I have completed most of the experimental work. The animal

research involving KGN cells was done by Powel Crosley. The rest of the experimental work was done by Abul K. Azad, Nidhi Gupta, Nisha Gokul, Zhihua Xu and Dr. YangXin Fu. Drs. Michael Weinfeld, Lynne-Marie Postovit, Stephanie A. Pangas, Mary M. Hitt and YangXin Fu participated in the experiment design and manuscript editing. Dr. YangXin Fu contributed to the experiment design and manuscript writing.

The ZIC2 part (Chapter 3 and Chapter 4) of this thesis is ready to be submitted as:

Chen H, Lee L, Vincent K, Xu Z, Liu, J, Zhang G, Postovit, L M, Fu Y. Transcription factor ZIC2 regulates the tumorigenic phenotypes of epithelial ovarian cancer in a context-dependent manner (in preparation). I am the first author of this article. I wrote the first draft and drew the figures. I designed and performed most of the experimental work in the study. I analyzed and interpreted all the data except RNA-seq data for differentially expressed genes and the clustering heatmaps processed and generated by Laura Lee. Zhihua Xu performed RT-qPCR. Jiahui Liu and Guihua Zhang did the animal injections. Drs. Lynne-Marie Postovit, YangXin Fu and I participated in the experimental design. I prepared the first draft and participated in the editing of the manuscript. The final version of the manuscript was written by Dr. YangXin Fu. Dr. Lynne-Marie Postovit participated in the editing of the manuscript.

Acknowledgment

I would like to express my heartfelt gratitude to the following people, without whom this thesis would not have been possible.

First, I would like to express my most sincere gratitude to my supervisor, Dr. Yangxin Fu. Dr. Fu is the supervisor who has instructed and trained me the most in my life. He taught me critical thinking and guided me to try a range of novel experiments to tackle challenges throughout the Ph.D. program. Without his keen insights and help from the academic field, I would fall into doubt and pause. His care and guidance, as well as the spirit of truth and factuality in academia, ignited my passion for science. Without the hard work and dedication of Dr. Fu, I would not have completed these studies.

I would like to express my sincere gratitude to my co-supervisor, Dr. Lynne-Marie Postovit, and the supervisory committee member Dr. Alan Underhill, for their continuous care, supports, guidance, and insights into my research project throughout my Ph.D. program. It was your inspiration that made the completion of this thesis possible.

I would like to express my sincere gratitude to Dr. Postovit for providing the high-grade serous ovarian cancer tumor array and patient-derived xenografts. I would like to thank Laura Lee in the Postovit laboratory for her help in the analysis of RNA-seq results. I would like to thank all the other members of the Fu Laboratory, especially Mrs. Zhihua Xu. Mrs. Zhihua Xu is a technician in Fu laboratory. She helped with RT-qPCR in my thesis, and her help was indispensable for me to

complete this thesis. Furthermore, thanks to her well-organized management in the laboratory, the laboratory runs smoothly. I would like to thank Dr. Gabrielle Siegers for her help in analyzing the flow cytometry data. I would like to thank Dr. Jiahui Liu, Dr. Guihua Zhang, and Dr. Olena Bilyk for their guidance in immunohistochemistry staining. I would like to thank Drs. Guihua Zhang and Jiahui Liu for their help in animal injections.

I would like to express my sincere gratitude to the Li Ka-Shing Foundation, the WCHRI Innovation Grant and the WCHRI Bridge Fund, the Yau family foundation for their financial support during my Ph.D. program. I would like to express my sincere gratitude to Professor Jen-Fu Chiu, the supervisor of my master's program at Shantou University, for giving me the opportunity to study at the University of Alberta. I would also like to thank Yvette Labiuk, Tara Schuetz-Zawaduk, Jennifer Freund, and Courtney Klein, the members of the Oncology Department, for their excellent supports to international students. I would like to thank Manager Aja Rieger, and Sabina Baghirova at the Flow Core Facility for their superb training and flow cytometry services.

Table of Contents

List of Tables

List of Figures

List of Abbreviations

ABC – ATP-Binding Cassette Transporter

ABCB1 – ATP Binding Cassette Subfamily B Member 1

ABCG2 – ATP Binding Cassette Subfamily G Member 2

AD – Transactivation Domain

AE1 – Anion Exchanger 1

AE3 – Anion Exchanger 3

AGCT – Adult Granulosa Cell Tumor

AKT – Protein Kinase B

ALDH – Aldehyde Dehydrogenase

ALDH1A1 – Aldehyde Dehydrogenase 1 Family Member A1

Alu – Arthrobacter Luteus Restriction Endonuclease

APS – Ammonium Persulfate

ARID1A – AT-Rich Interaction Domain 1A

ASO – Antisense Oligonucleotide

ATCC – American Type Culture Collection

ATM – Ataxia Telangiectasia Mutated

ATP – Adenosine Triphosphate

ATR – Ataxia Telangiectasia and Rad3 Related

BARD1 – BRCA1-Associated RING Domain Protein 1

bFGF – Basic Fibroblast Growth Factor

BMI1 – B Lymphoma Mo-MLV Insertion Region 1 Homolog

BRAF – B-Rapidly Accelerated Fibrosarcoma

Cas9 – CRISPR Associated Protein 9

CBFβ – Core-Binding Factor Subunit B

CBP – CREB-Binding Protein

CCND2 – Cyclin D2

CD10 – Enkephalinase

CD117 – KIT Proto-Oncogene Receptor Tyrosine Kinase

CD133 – Prominin1

CD24 – Small Cell Lung Carcinoma Cluster 4 Antigen

CD44 – Chondroitin Sulfate Proteoglycan 8

CD99 – Antigen Identified by Monoclonal 12E7, Y Homolog

CDKN1B – Cyclin-Dependent Kinase Inhibitor 1B

ChIP – Chromatin-Immunoprecipitation

CHK2 – Checkpoint Kinase 2

cIAP – Apoptosis Inhibitor 1

CPM – Counts of Reads per Million

CRBN – Cereblon

CRISPR – Clustered Regularly Interspaced Short Palindromic Repeats

CSC – Cancer Stem Cell

CTLA-4 – Cytotoxic T-Lymphocyte-Associated Protein 4

CTNNB1 – Catenin B 1

Cyp19a1 – Cytochrome P450 Family 19 Subfamily A Member 1

DAB – 3,3’-Diaminobenzidine

DAPI – 4',6-Diamidino-2-Phenylindole

dCas9 – Cas9 Endonuclease Dead

DEAB – Diethylaminobenzaldehyde

DNA-Pkcs – DNA Protein Kinase Catalytic Subunit

dnRUNX3 – Dominant-Negative Form of RUNX3

E2F3 – E2F Transcription Factor 3

ECM – Extracellular Matrix

EGF – Epidermal Growth Factor

EMSY – BRCA2-Interacting Transcriptional Repressor

EMT – Epithelial-Mesenchymal Transition

EOC – Epithelial Ovarian Cancer

EpCAM – Epithelial Cell Adhesion Molecule

ESC – Embryonic Stem Cell

ERBB2 – V-Erb-B2 Avian Erythroblastic Leukemia Viral Oncogene Homolog 2

ERK – Extracellular Signal-Regulated Kinases

FACS – Fluorescence-Activated Cell Sorting

FBS – Fetal Bovine Serum

FDA – Food and Drug Administration

FDR – False Discovery Rate

FIGO – Fédération Internationale de Gynécologie et d'Obstétrique

FSH – Follicle-Stimulating Hormone

GCT – Granulosa Cell Tumor of The Ovary

Gli1 – Glioma-Associated Oncogene Homolog 1

GO – Gene Ontology

GSEA – Gene Set Enrichment Analysis

hCG – Human Chorionic Gonadotropin

HEPES – N-2-Hydroxyethylpiperazine-N-Ethanesulfonic Acid

HER2 – Human Epidermal Growth Factor Receptor 2

HGSOC – High-Grade Serous Ovarian Carcinoma

HPE – Holoprosencephaly

HR – Hazard Ratio

HRP – Horseradish Peroxidase

HSC – Hematopoietic Stem Cells

IGF2BP1 – Insulin-Like Growth Factor 2 MRNA Binding Protein 1

IgG – Immunoglobulin G

IHC – Immunohistochemistry

IL2 – Interleukin 2

IMP1 – Insulin-Like Growth Factor 2 MRNA Binding Protein 1

ISWI – Chromatin Remodeling by Imitation Switch

JAK2 – Janus Kinase 2

JARID1B – Jumonji/ARID Domain-Containing Protein 1B

JGCT – Juvenile Granulosa Cell Tumor

Ki-67 – Proliferation Marker Protein Ki-67

KIT – Proto-Oncogene Tyrosine-Protein Kinase Kit

KO – Knockout

KRAS – Kirsten Rat Sarcoma Viral Oncogene Homolog

Ku70/80 – A Heterodimer of About 70kda And 80kda Subunits

LGSOC – Low-Grade Serous Ovarian Cancer

LIN28B – Lin-28 Homolog B

LMP – Low Malignant Potential Tumor

MAL – Malignant Tumor

MAX – MYC Associated Factor X

Mbd3 – Methyl-Cpg-Binding Domain Protein 3

MDM2 – Mouse Double Minute 2, Human Homolog of

MEK – Mitogen-Activated Protein Kinase Kinase 1

MEL18 – Polycomb Group Ring Finger 2

mESC – Mouse Embryonic Stem Cell

MET – Mesenchymal-Epithelial Transition

MIR – Mammalian-Wide Interspersed Repeat

MMP3 – Matrix Metallopeptidase 3

mRNA – Messenger Ribonucleic Acid

mTOR – Mammalian Target of Rapamycin

mTORC1 – Mammalian Target of Rapamycin Complex 1

MYC – V-Myc Avian Myelocytomatosis Viral Oncogene Homolog

MYH11 – Myosin Heavy Chain 11

Na_3VO_4 – Sodium Vanadium Oxide

$Na_4P_2O_7$ – Tetrasodium Pyrophosphate

NANOG – Nanog Homeobox

NF-κb – Nuclear Factor of Kappa Light Polypeptide Gene Enhancer in B-Cells 1

NF1 – Neurofibromatosis Type 1

NLS – Nuclear Localization Signal

NRAS – N-Rat Sarcoma

NSG – NOD-Scid IL2R-Gamma Null

NuRD – Nucleosome Remodeling Deacetylase

NURF – Nucleosome Remodeling Factor

OCT4 – Octamer-Binding Transcription Factor

ODN – Oligodeoxynucleotide

OE – Overexpression

$p27^{Kip}$ – Cyclin-Dependent Kinase Inhibitor 1B

p53 – Tumor Protein P53

PAC – Puromycin N-Acetyl-Transferase

PAK4 – P21-Activated Kinase 4

PALB2 – Partner And Localizer of BRCA2

PARP – Poly (ADP-ribose) polymerase

Pax3 – Paired-Box 3

PAX8 – Paired-Box 8

PBS-T – Phosphate-Buffered Saline Solution with 0.1% Tween™ 20

PD-1 – Programmed Cell Death Ligand 1

PDX – Patient-Derived Xenograft

PI3K – Phosphoinositide 3-Kinase

PIK3CA – Phosphatidylinositol-4,5-Bisphosphate 3-Kinase Catalytic Subunit Alpha

PIP – Pyrrole-Imidazole Polyamide

POU5F1 – POU Class 5 Homeobox 1

PPP2R1A – Protein Phosphatase 2 Scaffold Subunit A, Alpha Isoform

PROTAC – Proteolysis Targeting Chimera

PTEN – Phosphatase and Tensin Homolog

QA – Glutamine (Q)- and Alanine (A)-Rich Sequence

RAD50 – RAD50 Double-Strand Break Repair Protein

RAD51C – RAD51 Homolog C

Raf – Rapidly Accelerated Fibrosarcoma Kinases

RB1 – RB Transcriptional Corepressor 1

RBBP4 – RB Binding Protein 4

RHA – RNA Helicase A

RHD – Runt Homology Domain

RISC – RNA-Induced Silencing Complex

RNA-seq – Ribonucleic Acid Sequencing

RNAi – Ribonucleic Acid Interference

ROR1 – Receptor Tyrosine Kinase Like Orphan Receptor 1

ROR2 – Receptor Tyrosine Kinase Like Orphan Receptor 2

RPS14 – Ribosomal Protein S14

RUNX1 – Runt-Related Transcription Factor 1

RUNX2 – Runt-Related Transcription Factor 2

RUNX3 – Runt-Related Transcription Factor 3

S100 – Damage-Associated Molecular Pattern Molecules

SCCOHT – Small Cell Carcinoma of The Ovary Hypercalcemic Type

Shh – Sonic Hedgehog Homolog

SINE – Short Interspersed Nuclear Elements

siRNA – Small Interfering Ribonucleic Acid

Six3b – SIX3 Homeobox 3b

SMAD2 – Sma- and Mad-Related Protein 2

SMAD3 – Sma- and Mad-Related Protein 3

SMMHC – Myosin Heavy Chain 11

SOX2 – SRY (Sex Determining Region Y)-Box 2

TEMED – Tetramethylethylenediamine

TGFB – Transforming Growth Factor

TLE – Transducin-Like Enhancer of Split

TMA – Tumor Microarray

TP53 – Tumor Protein P53

TRAFTAC – Transcription Factor Targeting Chimeras

UTR – Untranslated Region

VHL – Von Hippel-Lindau Tumor Suppressor

WT – Wild Type

WT1 – Wilms' Tumor Gene 1

YAP – Yes-Associated Protein

ZFD – Zinc-Finger Domain

ZFNC – ZF-N-Terminal Conserved

ZIC2 – ZIC Family Member 2

ZOC – *Zic*/*Opa* [Odd Paired Conserved]

CHAPTER 1: INTRODUCTION

1.1 Ovarian cancer

1.1.1 Classification, staging, and risk factors of ovarian cancer

Ovarian cancer is a disease composed of various subtypes (**Figure 1.1**). Lengyel *et al.* described ovarian tumors from three potential sites: ovarian surface epithelium, fallopian tube, or mesothelial endoperitoneal cavity (1). Ovarian cancer can be classified into four categories according to the origin of cancer: epithelial ovarian cancer, germ cell ovarian cancer, sex cord-stromal ovarian cancer, and borderline ovarian cancer.

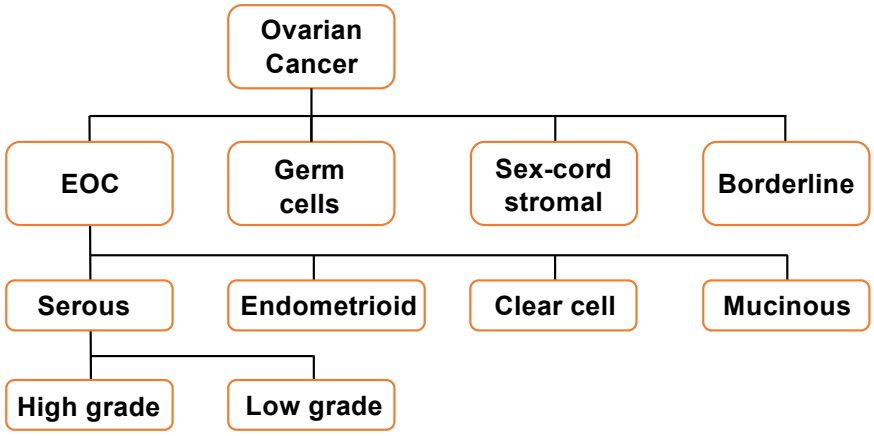

Figure 1.1 Classification of ovarian cancer by origin

This figure shows the four major subtypes of ovarian cancer. There are four subtypes of EOC and two subtypes of serous EOC. These EOC subtypes are primarily categorized based on the origin of ovarian cancer.

Based on the clinical characteristics of ovarian cancer, it is classified into indolent Type I and highly aggressive Type II (**Table 1.1**) (2). Type I ovarian cancer includes low-grade serous, low-grade endometrioid, clear cell, and mucinous carcinomas (3,4). Type II ovarian cancer includes high-grade serous ovarian

cancer, high-grade endometrioid cancer, and undifferentiated cancer (3,4). Most cases of these two types of cancer are diagnosed at different stages. Type II ovarian cancer is highly aggressive and mostly advanced.

Table 1.1 Genetic classification of ovarian cancer

	Type 1	Type 2
Prevalence	About 30%	About 70%
Histology	Serous, endometrioid mucinous, and clear-cell tumors	Serous, mixed malignant mesodermal tumors carcinosarcomas, and undifferentiated tumors
Grade	Low and borderline	High
Mutation	*PTEN, KRAS, BRAF, PIK3CA, ERBB2, CTNNB1, ARID1A, PPP2R1A*, and microsatellite instability	*TP53, BRCA1/2*
Clinical behavior	Typically, large cystic mass confined to the ovary, relatively indolent course	Diagnosed at advanced stages and aggressive behavior

This table is modified from Toss, A., *et al*. (2).

According to the recommendations of the International Federation of Gynecology and Obstetrics (FIGO), ovarian cancer can be classified into stages I to IV depending on the metastasis of cancer (**Table 1.2**) (5). Advanced EOC (stage III or IV) indicates a high degree of infiltration and metastasis (5). In stage I, the

cancer cells remain confined to the ovary or fallopian tube, involving only one ovary and not spreading to the other ovary. In stage II, the cancer cells not only attack one or both ovaries but also metastasize to other organs of the pelvis, such as the uterus, fallopian tubes, bladder, or rectum. In stage III, the cancer cells invade one or both ovaries, involving the visceral peritoneum or dorsal lymph nodes. The highest stage of ovarian cancer is stage IV, when the cancer cells have spread to the peritoneal cavity, including the abdomen and other body parts beyond the pelvis. For instance, at stage IV, the cancer cells have metastasized to liver, distant lymph nodes, and lungs (6).

Table 1.2 The staging of ovarian cancer

Stage	Tumor location
I	Tumor growth limited to the ovaries
Ia	Growth limited to one ovary: no ascites present containing malignant cells. No tumor on the external surface; capsule intact
Ib	Growth limited to both ovaries: no ascites present containing malignant cells. No tumor on the external surfaces; capsules intact
Ic	Tumor either Stage Ia or Ib, but with tumor on surface of one or both ovaries, or with capsule ruptured, or with ascites present containing malignant cells, or with positive peritoneal washings
II	Tumor growth involving one or both ovaries with pelvic extension
IIa	Extension and/or metastases to the uterus and/or tubes
IIb	Extension to other pelvic tissues
IIc	Tumor either Stage IIa or IIb, but with tumor on surface of one or both ovaries, or with capsule(s) ruptured, or with ascites present containing malignant cells, or with positive peritoneal washings
III	Tumor involving one or both ovaries with histologically-confirmed peritoneal implants outside the pelvis and/or positive retroperitoneal or inguinal nodes. Superficial liver metastases equals Stage III. Tumor is limited to the true pelvis, but with histologically-proven malignant extension to small bowel or omentum
IIIa	Tumor grossly limited to the true pelvis, with negative nodes, but with histologically-confirmed microscopic seeding of abdominal peritoneal surfaces, or histologic proven extension to small bowel or mesentery
IIIb	Tumor of one or both ovaries with histologically-confirmed implants, peritoneal metastasis of abdominal peritoneal surfaces, none exceeding 2 cm in diameter: nodes are negative
IIIc	Peritoneal metastasis beyond the pelvis > 2 cm in diameter and/or positive retroperitoneal or inguinal nodes
IV	Growth involving one or both ovaries with distant metastases. If pleural effusion is present, there must be positive cytology to allot a case to Stage IV. Parenchymal liver metastasis equals Stage IV

This table is modified from Pecorelli, S., *et al*. (5).

According to epidemiological reports, risk factors for ovarian cancer mainly include five factors, including family history, age, race, hormone and reproductive factors, and lifestyles (7-25). Family history refers to women with *BRCA1* and *BRCA2* germline mutations, who are at high risk for ovarian cancer (7,20-22,26). Women with *BRCA1* mutations have a 44% risk of developing ovarian cancer at the age of 80 years, while women with *BRCA2* mutations have a 17% risk of developing ovarian cancer at this age (26). Age is an important risk factor that is strongly associated with the risk of ovarian cancer, among which elderly women are at the highest risk. Multiple reports showed that the median age at diagnosis of ovarian cancer patients ranges from the age of 50 to 79 years (23-25). According to studies, Asians are less likely to develop ovarian cancer than Caucasians and are more likely to develop Type I ovarian cancer (27-30). Hormonal and reproductive factors include the use of menopausal hormones and oral contraceptives (31,32). Long-term use of oral contraceptives and reduced use of menopausal hormones have been shown to help reduce the risk of ovarian cancer (13,33). Lifestyle factors include dietary habits, smoking, and body weight. Studies showed that smoking and obesity are associated with a high risk of ovarian cancer (34-39).

1.1.2 Classification, histology, and molecular biology of EOC

The majority of ovarian cancers are epithelial ovarian cancers (EOC), accounting for about 90% of all ovarian cancers (40). Based on microscopic morphology and histological architecture, EOCs are classified as serous

carcinoma, endometrioid carcinoma, clear cell carcinoma, and mucinous carcinoma (40). Serous carcinoma accounts for 75% of all EOCs (41,42). This subtype of EOC is categorized into high-grade (HGSOC) and low-grade (LGSOC) serous ovarian cancer. HGSOC is the most commonly diagnosed ovarian cancer, accounting for about 70% of all diagnosed ovarian cancers (43). Although all these subtypes of EOC are ovarian cancers, they do not all originate in the ovary. For a long time, it has been recognized that EOC originates from ovarian epithelial cells, but different EOC subtypes exhibit different histological architectures and molecular genetic characteristics. Therefore, the notion that ovarian cancer originates from ovarian surface epithelial cells is challenged. In particular, although both HGSOC and LGSOC are serous carcinoma, they originate in different parts of the body (4,44). Although the origin of serous ovarian cancer is controversial, it is generally accepted that most HGSOCs originate in the fallopian tubes (45-47). Endometrioid carcinoma is believed to be raised in endometriosis lesions based on its histological architectures (40,48). For clear cell carcinoma, it may arise from ciliated cell lineage at the fallopian tubes (49). Mucinous carcinoma is believed to originate in the borderline precursors at the ovary (50).

Different subtypes of EOC present different histological architectures (**Figure 1.2**) (51). HGSOC is characterized by solid masses of cells with slit-like fenestrations. HGSOC also has cribriform, papillary, or glandular architecture in some areas (**Figure 1.2A**) (52). Depending on the degree of differentiation of these papillary protrusions, they can be divided into well differentiated, moderately differentiated, and poorly differentiated. Poorly-differentiated serous ovarian

cancer is more malignant and accompanied by extensive necrosis (52). Unlike HGSOC, LGSOC has only mild nuclear atypia and a low nuclear-to-cytoplasmic ratio, although it also has a papillary structure (**Figure 1.2B**) (52). Mucin-filled cells are seen in mucinous adenocarcinoma. Tumors of this subtype of cancer can be very large and sometimes even occupy the entire abdominal cavity, with a multilocular shape and papillary hyperplasia within the cyst accompanied by hemorrhagic necrosis (**Figure 1.2C**) (53). For endometrioid adenocarcinoma, the formation of endometrial glands can be observed (**Figure 1.2D**) (54). In endometrioid carcinoma, the grade and prognosis of the patient are related to the number of glandular-forming cancer cells. For instance, patients with high-grade endometrioid carcinoma have fewer gland-forming cancer cells than patients with low-grade endometrioid carcinoma. Clear cell carcinoma is a malignant tumor characterized by large atypical cells with clear cytoplasm and hyaluronic acid in the nuclear matrix (**Figure 1.2E**) (53).

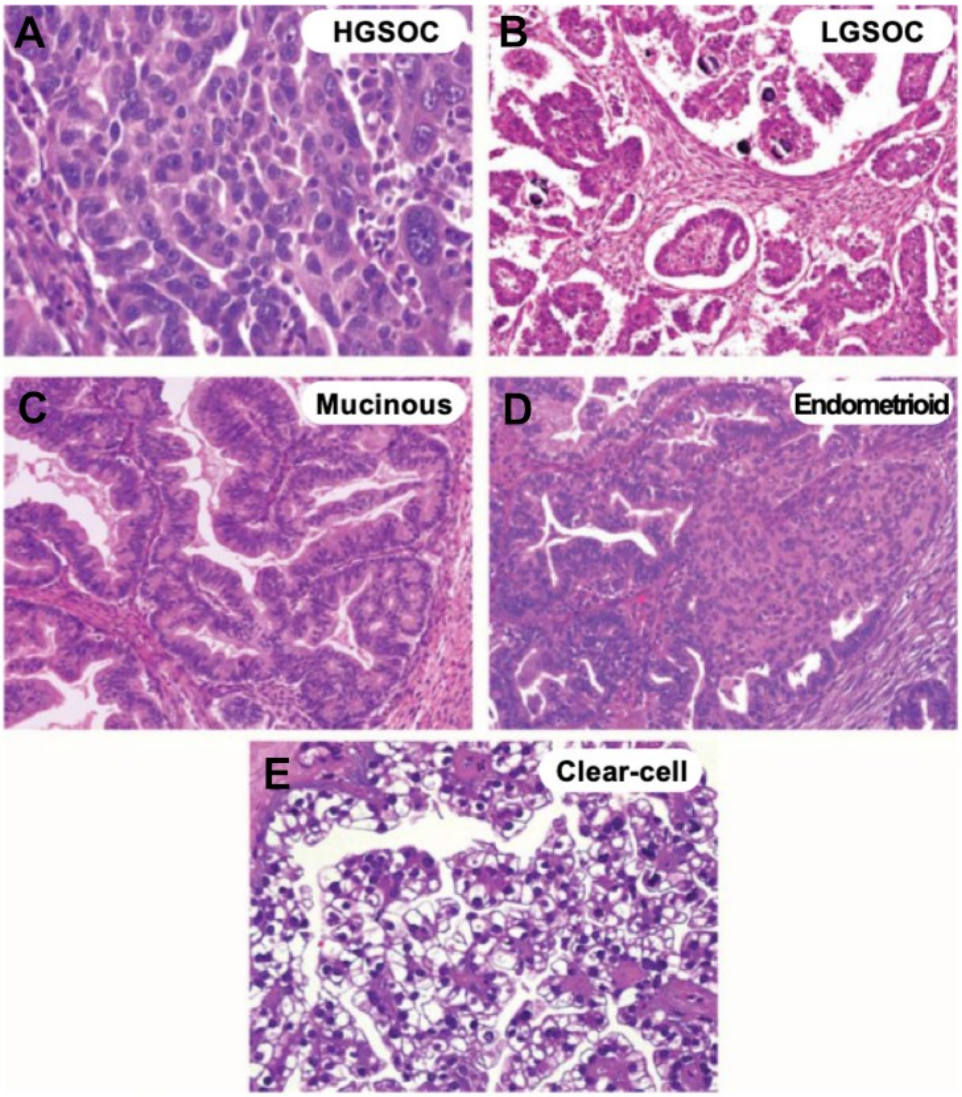

Figure 1.2. The histology of five subtypes of EOC

Images are modified from Prat, J. (51). Images show the histological architectures of four common EOC subtypes, including **(A)** high-grade serous ovarian cancer (HGSOC), **(B)** low-grade serous ovarian cancer (LGSOC), **(C)** mucinous carcinoma, **(D)** endometrioid carcinoma, and **(E)** clear cell carcinoma. Images show tissue sections from different EOC subtypes stained with hematoxylin and eosin.

Different subtypes of EOC have different molecular genetic characteristics (**Figure 1.3**) (55). Type I ovarian cancer is more genetically stable than Type II and exhibits a unique mutation pattern (55,56). About one-third of LGSOC (Type I ovarian cancer) has mutations in *KRAS*, *BRAF*, and *ERBB2* (HER2), whereas mutations in *TP53* are rare. Mutations in *PIK3CA*, *PTEN*, *ARID1A*, and *CTNNB1* have also been reported in endometrioid carcinoma. Similar to low-grade endometrioid carcinoma, clear cell carcinomas are frequently accompanied by *PIK3CA* activating mutations. In mucinous cancers, about half of the cancer cells have *KRAS* mutations. Most Type II ovarian cancers, including HGSOC and rare high-grade endometrioid carcinomas, have *TP53* mutations, but rarely have the mutations found in Type I ovarian cancers.

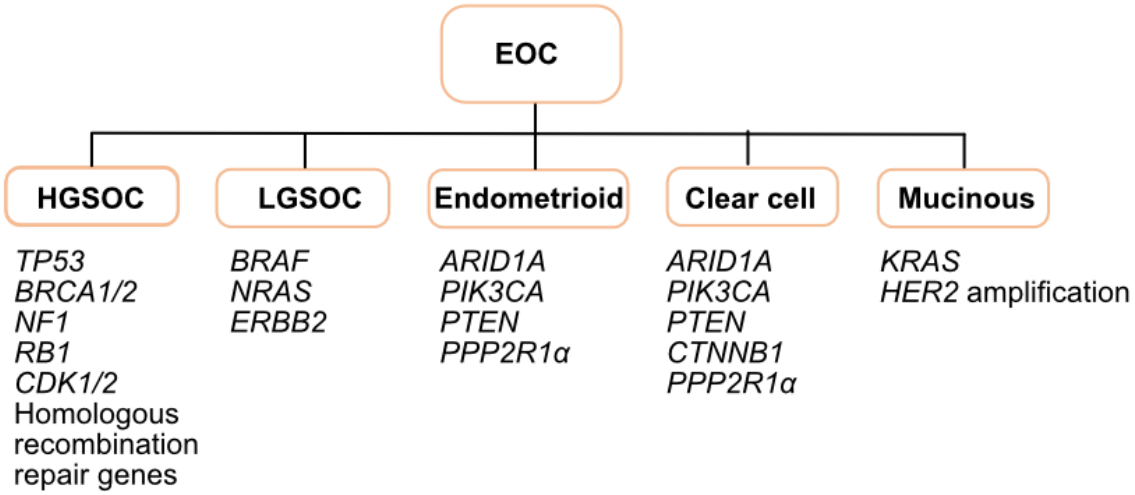

Figure 1.3. Molecular genetic features of five EOC subtypes

This figure is modified from Banerjee, S. and S.B. Kaye (55). EOC consists of five major subtypes including HGSOC, LGSOC, endometrioid, clear cell, and mucinous carcinomas. The corresponding genes that are frequently mutated in

these subtypes are listed below the subtypes. *Homologous recombination repair genes: *CHK2*, *BARD1*, *BRIP1*, *PALB2*, *RAD50*, *RAD51C*, *ATM*, *ATR*, and *EMSY.*

1.1.3 Diagnosis, treatment, survival, and recurrence of EOC

Ovarian cancer is the most lethal gynecological malignancy, ranking fifth among all deaths from gynecological cancer worldwide. It is estimated that there were about 313,959 new cases and 207,252 deaths from ovarian cancer worldwide in 2020 (57). Only about 20% of patients are diagnosed early and about 80% are already at advanced stages (stages II, III, and IV) when diagnosed (16,58-60).

The median overall survival for HGSOC was 40.7 months, with an overall 5-year survival rate of about 39% (61,62). The median overall survival for endometrioid carcinoma was 48 months, with an overall 5-year survival rate of about 41% (63). The median overall survival for clear cell carcinoma is unknown, with a reported overall 3-year survival rate of 75.9% (64).

EOC is asymptomatic in the early stages and easily overlooked in the advanced stages (65-67). As ovarian cancer progresses to advanced stages, the tumor enlarges and squeezes into the digestive tract system, and patients may experience lower abdominal pain or loss of appetite, dyspepsia, weight loss, and nausea. In addition, when the tumor oppresses the intestine, it causes changes in bowel habits; when the tumor oppresses the bladder, it causes frequent urination. In addition, the majority of patients with ovarian cancer at advanced stages (stage

III or stage IV) may include ascites (68). In severe cases, EOC patients in advanced stages may experience bleeding, dyspnea, and vomiting (69-72).

Screening tests for early-stage EOC are limited. In clinical practice, ovarian cancer is usually screened by blood tests for the cancer antigen CA-125 and transvaginal ultrasonography (65,73-78). Although CA-125 is highly sensitive, it lacks specificity (65). Other symptoms, such as endometriosis, ascites due to liver disease, pregnancy, and other non-ovarian cancers such as cervical cancer can also lead to an increase in CA-125. Despite early screening for ovarian cancer, reports suggest that this does not significantly improve survival in patients with ovarian cancer (79,80). In addition, for patients with known familial inherited *BRCA1* and *BRCA2* mutations, they may choose to have their fallopian tubes or the ovaries, or both, removed at an age when ovarian cancer is prone to occur (81,82). The recommended age for surgical excision of the fallopian tubes or ovaries, or both, is 35 to 40 years for women with *BRCA1* mutations and 40 to 45 years for women with *BRCA2* mutations (82).

The main therapeutic regimens for ovarian cancer are complete cytoreductive surgery and chemotherapy (83-87). For patients with early-stage ovarian cancer, complete staging operations, such as hysterectomy, bilateral oophorectomy and salpingo-oophorectomy, as well as debulking of the involved lymph nodes and mesentery can be performed (88). EOC patients often require chemotherapy after surgery. The first-line chemotherapy is carboplatin combined with paclitaxel (89,90). Combination of carboplatin and paclitaxel chemotherapy has a synergistic effect and eliminates most of the cancer cells in the early stages.

For most patients with advanced EOC, cytoreductive surgery is used to maximize resection of all detectable tumors, thereby reducing tumor burden and improving chemotherapy efficacy and patient prognosis. For patients with recurrence, only those sensitive to platinum-based chemotherapy should undergo cytoreductive surgery again (85,91,92). In patients with advanced severe metastases, adjuvant palliative surgery is used to relieve severe comorbid symptoms (93,94). Surgical palliative care includes pleural effusion and ascites drainage (95,96).

Most patients with EOC relapse after primary surgery (97,98). The recurrence of EOC is often accompanied by chemoresistance, which limits the therapeutic options (99,100). Although most EOCs are sensitive to chemotherapy, about 85% of patients with advanced EOC relapse after primary treatment (100). Recurrent ovarian cancer can be classified into platinum-sensitive and platinum-resistant types (100-102). The median survival of patients with recurrent platinum-sensitive ovarian cancer is about 3 years, and the median survival of patients with recurrent platinum-resistant ovarian cancer is about 1 year (103). Patients with recurrent EOC who are susceptible to platinum-based drugs may be treated with surgery (85). However, recurrence of EOC is often accompanied by extensive metastasis of cancer cells. Therefore, resection of all recurrent metastases is challenging (104,105).

Targeted therapy is a new direction in the treatment of ovarian cancer. This treatment targets cancer cells that carry specific gene mutations. Olaparib is the first small molecule PARP inhibitor approved by the FDA (US Food and Drug Administration) for the treatment of ovarian cancer. Oral administration of this small

molecule PARP inhibitor has been shown to significantly improve progression-free survival in HGSOC patients with mutations in *BRCA1* and *BRCA2* genes (106-109). In addition to Olaparib, there are Rucaparib and Niraparib, both small molecule PARP inhibitors approved by the FDA (109-111).

Furthermore, immunotherapy is a promising treatment for ovarian cancer. Immunotherapies use the anti-PD-1 antibody Nivolumab to treat patients with recurrent platinum resistance in EOC (112). In the study by Zamarin *et al*., combination immunotherapy with Nivolumab and Ipilimumab improved objective response rates and progression-free survival in patients with persistent or recurrent EOC in the phase II NRG Oncology Trail (NRG GY003) (112).

1.1.4 Classification, histology, and molecular biology of granulosa cell tumor of the ovary

Granulosa cell tumor of the ovary (GCT) is a rare malignant ovarian cancer that belongs to the sex cord-stromal tumor (113). GCT can be divided into adult GCT (AGCT) and juvenile GCT (JGCT) (114-117). AGCT is the more common subtype of GCT, accounting for about 95% of all GCT cases. In a report of 51 GCT cases in the United Kingdom, the age of GCT patients ranged from 8 months to 88 years and included prenatal and postnatal patients, as well as premenopausal and postmenopausal patients (118). In this report, JGCT occurred predominantly in premenstrual girls and adolescent girls, with very little virilization caused by androgen secreted by GCT (114,116,118,119). In addition, AGCT is more common in premenopausal and postmenopausal women, with a concentration of AGCT

patients between 50 and 55 years of age, and sometimes AGCT patients have virilization due to androgen secretion (116,118).

AGCT and JGCT have different histological architectures and molecular genetic characteristics. AGCT tumors present as very large, single-compartment or multi-cavity thin-walled cystic masses (119). In JGCT, the tumor is solid or cystic, while the cystic tumor is serous, although the tumor is also large, reaching 12 cm in diameter (119). GCT has specific molecular genetic characteristics. In AGCT, trisomy 12, monosomy 22, and chromosome 6 deletion have been detected (116,120,121). In JGCT, the deletion of chromosome 12 and chromosome segment of trisomy 6q has been detected (116). However, *BRCA1* and *BRCA2* mutations affecting EOC are not risk factors for GCT (116). Recent studies reported the presence of somatic missense mutations in *FOXL2* in most AGCT (c.402C>G: Substitution - Missense, position 402, Cytosine→Guanine; p.C134W: Substitution - Missense, position 134, Cysteine→Tryptophan), but these mutations are absent in JGCT (122,123). Research suggests that AGCT and JGCT may be different tumor types (124).

1.1.5 Diagnosis, treatment, survival, and recurrence of granulosa cell tumor of the ovary (GCT)

GCT is the most common subtype of sex cord-stromal tumors, accounting for more than 70% of all sex cord-stromal tumors and 3% to 5% of all ovarian cancers (116). JGCT is extremely rare, accounting for only about 5% of all GCT (116,119). The staging system for GCT is the same as the FIGO staging system

for EOC. GCT is divided into early (stage I) and advanced stages (stages II, III, and IV) (119). In the report by Jalid *et al*., about 80% of patients with GCT were in stage I and about 20% were in stages II to IV (125).

Most patients with GCT are diagnosed in the early stages and have a good overall prognosis (118,126). Median survival data for GCT are not available as the time to relapse may be particularly long. Hines *et al.* reported a case of GCT with a recurrence interval of 37 years (127). The specific survival of GCT patients is closely related to the stage (114). For instance, the 10-year overall survival rate for GCT is 87.2% in stage I, 75% in stage II, 20% in stage III, and 0% in stage IV (125). There is no definitive screening for GCT.

The clinical features of GCT remain unclear. Precocious breast development, vaginal bleeding, and irregular menstruation may occur due to excessive estrogen secretion (119). These patients also showed symptoms such as abdominal swelling and masses. This tumor rarely causes ascites. The uterus enlarges and the endometrium thickens due to estrogen (119). GCT has round or oval white cells showing coffee bean-shaped nuclei (119). AGCT is usually a large, yellowish-brown, and unilateral mass (greater than 10cm in diameter) with solid and cystic areas (116). For JGCT, the mass can reach a larger size of 26 cm, with an average of 12.4 cm. The distinction between AGCT and JGCT can also be identified by microscopic examination (116). For instance, JGCT has round, hyperchromatic nuclei, luteinized theca cell component, and moderate to abundant eosinophilic or vacuolated cytoplasm (116). Immunohistochemistry can also be

applied to help diagnose GCT. Protein expression of α-inhibin, calmodulin, CD99, AE1/AE3, CD10, WT1, and S100 is the characteristic of GCT (116).

Current therapeutic regimens for GCT are similar to those for EOC. Treatment of GCT depends on the stage and age of the patient (116). The primary goal is complete resection of the tumor by surgery and chemotherapy. Most patients with early GCT (stages I and II) have a good prognosis and usually do not require additional postoperative treatment. Patients with advanced GCT (stages III and IV) after surgical resection require platinum-based combination chemotherapy (116).

GCT has a tendency to relapse. Although GCT is a low-grade malignancy, it has a recurrent mortality rate of about 80% (116,128). According to Sun *et al.*, about 21% of patients recurred with a median time to recurrence of 57.6 months (129). Patients with GCT who received optimal cytoreduction at an early stage did not relapse (116). Because of the slow growth of GCT, most recurrences of advanced GCT may occur within 5 to 10 years after the primary surgery (119,123,130). GCT rarely occurs more than 10 years after the patient's first surgery (118,131-133). In patients with recurrent GCT, aggressive cytoreductive surgery combined with chemotherapy, radiotherapy, or hormone therapy is associated with prolonged progression-free survival (130).

1.2 Transcription factor ZIC2

1.2.1 ZIC family members

The human ZIC family consists of five zinc finger transcription factor members, *ZIC1*, *ZIC2*, *ZIC3*, *ZIC4*, and *ZIC5*. Each of these transcription factors has five Cys2His2 zinc fingers (134-136). All *ZIC* genes contain three exons with the zinc finger structures located in the C-terminal region. The first exon was conserved in all *ZIC* family members. The second exon is conserved in *ZIC1*, *ZIC2*, and *ZIC3*, but is different in *ZIC4* and *ZIC5*. *ZIC1* and *ZIC4* are located on the forward and reverse strands of chromosome 3 (3q24), respectively. *ZIC2* and *ZIC5* are located on the forward and reverse strands of chromosome 13 (13q32), respectively. *ZIC3* is located on the forward strand of sex chromosome X (Xq26.3).

ZIC proteins have three important domains: the ZOC (*Zic*/*Opa* [*Odd-paired Conserved*]) domain (ZOC), the ZFNC (*ZF-N*-terminal *conserved*) domain (ZNFC), and the zinc-finger domains (ZFD) (**Figure 1.4**) (137). Among the five ZIC family members, the ZFD domains in ZIC2 through ZIC5 are more conserved than the ZFD domain in ZIC1 (138). Compared to the ZFD domains in other ZIC family members, the ZFD domain in ZIC1 contains a different number of amino acid residues between the two cysteines: the ZFD domain in ZIC1 has 6 to 38 amino acid residues, while the ZFD domains in other ZIC members have 2 or 4 amino acid residues (139). The ZFD domain executes important functions, including DNA binding, cofactor binding, transcriptional activation, and nuclear localization (140). The ZOC and ZFNC domains are conserved among ZIC family members. The

known function of ZOC in mouse ZIC2 is to interact with two proteins, IMFA and PAX3 (141,142). The functionality of ZFNC is unclear.

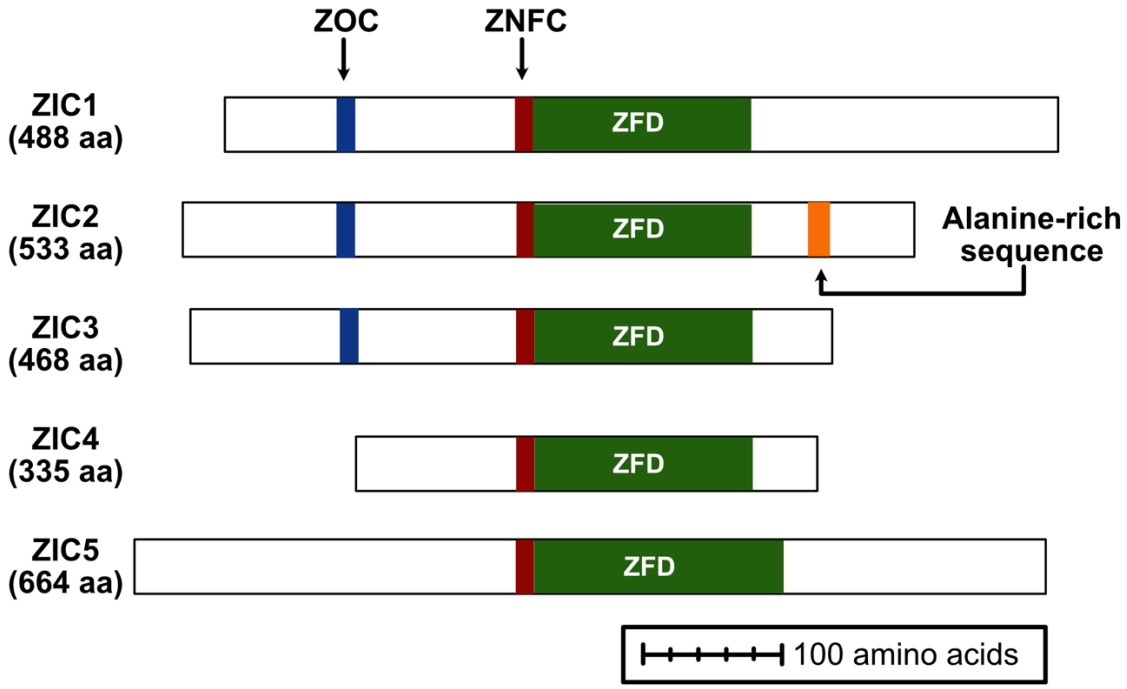

Figure 1.4. The protein domains in the proteins of ZIC family members

This figure is modified from Ali, R.G., H.M. Bellchambers, and R.M. Arkell (137). The figure shows the location of the major domains in the five ZIC proteins. ZOC: *Zic*/*Opa* [*Odd-paired Conserved*] domain; ZNFC: *ZF-N*-terminal *conserved* domain; ZFD: Zinc-finger domain; C-terminal Alanine-rich sequence of ZIC2 is unique to the ZIC2 protein; aa: amino acid.

1.2.2 The role of ZIC2 in development and human cancers

ZIC2 plays a vital role in brain development (143). In humans, heterozygous mutations in *ZIC2* are associated with holoprosencephaly (HPE) (144-146). Studies showed that heterozygous mutations in *ZIC2*, including nonsense, frameshift, missense mutations, and polyadenylation amplification, are present in

3% to 4% of patients with HPE, a severe congenital disorder of forebrain development associated with the mispatterning of the embryonic primitive streak, leading to the failure to separate the forebrain hemispheres during embryonic development.

The role of ZIC2 in development has been extensively investigated in mouse models (141,146-156). In mice, ZIC2 plays an important role in neurodevelopment and the development of bones and muscles of the extremities (141,148-150,154,155). Mice with homozygous mutations in *Zic2* exhibit abnormal behaviors associated with schizophrenia, such as impaired social behavior and social disorders (157,158). In addition, reduced expression of ZIC2 in the mouse brain results in abnormal formation of the dorsal midline and inability of the cerebral cortex to be divided into two hemispheres, leading to incomplete development of structures in the hindbrain and forebrain, such as Call-Exner bodies (134,149,159). In another report, in mice, homozygous mutations in *Zic2* caused the neural delay, as well as defects in the closure of the anterior segment leading to cerebrospinal fluid and anencephaly and defects in the posterior segment of the neural tube concomitant with spina bifida (148).

Normally, ZIC2 is highly expressed only in the brain and testicular tissue in adults (160-162), but its expression is elevated in several human cancers, including EOC (161,163-169). In prostate cancer, knockout of ZIC2 decreased cell proliferation, cell entry into the S phase of the cell cycle, and cell migration in the prostate cell line PC-3 (165). In nasopharyngeal carcinoma, shRNA knockdown of ZIC2 significantly inhibited cell proliferation and invasion in the nasopharyngeal

carcinoma cell line CNE1 (166). Inhibition of ZIC2 expression in cervical cancer cells reduced cell invasion, cell migration, and angiogenesis (170). Overexpression of ZIC2 in hepatocellular carcinoma promotes tumor growth and metastasis (161). In addition, ZIC2 maintained the self-renewal ability of liver CSCs (169).

Research on ZIC2 in ovarian cancer is limited. A study by Marchini *et al.* showed that increased mRNA expression of *ZIC2* in ovarian cancer was associated with poor prognosis in patients (163). In this report, they used EOC samples from an Italian institute and divided the samples into two groups based on clinical data, the MAL (malignant tumor) group and the LMP (low malignant potential tumor) group. Microarray analysis of cDNA samples from both groups showed that the average mRNA level of *ZIC2* was higher in the MAL group than in the LMP group, and the average mRNA level of *ZIC2* was significantly higher in stage III tumor samples than in stage I tumor samples. They found that serous and endometrioid carcinomas expressed *ZIC2* more frequently than clear cell and mucinous carcinomas. Immunoblotting analysis of ZIC2 protein expression in tumors revealed that ZIC2 protein expression was higher in MAL sample than in LMP sample.

In addition, they found that ZIC2 was detected in EOC cell lines, including the SKOV3, IGROV, and OVCAR8, but not in non-tumorigenic human ovarian epithelial (HOSE) and LMP-derived cell lines. They transiently knocked down ZIC2 in the OVCAR8 cell line with siRNAs and found reduced cell proliferation. Moreover, based on *ZIC2* mRNA expression, they divided the stage I patients into *ZIC2* high

(n = 40) and *ZIC2* low groups (n=53), and stage III patients into *ZIC2* high (n = 37) and *ZIC2* low groups (n = 8). They found that the 5-year progression-free survival and 5-year overall survival rates were significantly lower in stage I patients with high *ZIC2* expression than in stage I patients with low *ZIC2* expression. There was no significant difference in 5-year overall survival and 5-year progression-free survival rates in stage III patients.

1.2.3 Molecular mechanism related to ZIC2

ZIC2 is involved in the regulation of gene expression in mouse embryonic stem cells (ESCs). Luo *et al*. reported that ZIC2 interacts with the nucleosome remodeling and deacetylase (Mbd3-NuRD) complex containing the core component MBD3 in mouse ESC (171). In that report, MBD3/NuRD is identified as a chromatin remodeling factor that plays an important role in maintaining pluripotency in mouse ESC, and the depletion of ZIC2 in mouse ESC led to impaired lineage commitment. The authors of that report also found that ZIC2 is involved in epigenetic modifications of mouse ESC chromatin and cell differentiation, acting as an enhancer-specific binding factor during embryonic development.

ZIC2 activates the expression of the stem cell transcription factor *OCT4* in liver CSCs (169). Zhu *et al.* reported that transcriptional activation of *OCT4* by ZIC2 in liver CSCs is achieved through direct interaction with the RBBP4 protein, a component of the nuclear remodeling factor (NURF) complex (169). The NURF complex is a conserved higher eukaryotic ISWI-containing remodeling complex

that catalyzes ATP-dependent nucleosome sliding to control transcriptional activity and genome organization (169). That study also reported that inhibition of the NURF complex, which is required for self-renewal of liver CSCs, reduced the expression of *OCT4*. Ishiguro *et al*. reported a direct interaction between the ZIC2 protein and two complexes (complex I and complex II) in mice by immunoprecipitation assay (172). Complex I consists of DNA protein kinase catalytic subunit (DNA-Pkcs) and Ku70/80 dimer, which are involved in the DNA repair pathway (173). Complex II consists of RNA helicase A (RHA) and Ku70/80 dimer and interacts with other nuclear factors (i.e., NF-κb and BRCA1), in which RHA acts as a transcriptional activator for recruitment of polymerase II and activates transcription recycling of ZIC2 target genes (174-176). Both complexes I and II play key roles in mouse embryonic development (177-181).

ZIC2 is associated with multiple signaling pathways, such as the Wnt/β-catenin, Nodal, and Sonic Hedgehog pathways (182-187). In early embryonic development in *Xenopus*, Zic2 inhibits the Wnt/β-catenin pathway by interacting with the transcription factor Tcf5 (182). Research on the Nodal pathway showed that normal development of mouse embryos depends on ZIC2 and NODAL, and that the heterozygous mutation in *Zic2* leads to abnormal embryonic development (183). That research demonstrated the physical interaction of ZIC2 with the transcription factors NODAL, SMAD2, and SMAD3 in the ZIC2-overexpressed human embryonic kidney cell line HEK293T by immunoprecipitation (188). In the Nodal pathway, SMAD2 and SMAD3 are the NODAL-responsive SMADs. Overexpression of ZIC2 in HEK293T cells leads to phosphorylation of endogenous

SMAD2 and SMAD3 and the formation of a complex of SMAD2 and SMAD3, suggesting a positive role for ZIC2 in Nodal/Smad signaling.

Regarding the Sonic Hedgehog pathway, a study showed that the expression of *zic2a*, a homolog of human ZIC2 in zebrafish, is activated by the growth factor Sonic hedgehog (Shh) and then represses the transcription of the transcription factor *six3b*, which is essential for the normal thalamus formation (187). Similarly, the role of ZIC2 in the Sonic Hedgehog pathway has been investigated in cervical cancer, in which ZIC2 interacts directly with GLI1, a key transcription factor in the Sonic Hedgehog pathway, and enhances the activity of this pathway by promoting nuclear retention of GLI1 (186). In addition, *ZIC2* was reported to be targeted and inhibited by miR-129-5p in cervical cancer and reduced the mRNA and protein levels of *SHH*, *GLI1*, and *GLI2*, suggesting that ZIC2 may be involved in the positive regulation of the Sonic hedgehog pathway (170). In hepatocellular carcinoma, ZIC2 upregulates *PAK4* expression and promotes tumor growth and metastasis; knockdown of PAK4 by RNA interference (RNAi) reduces ZIC2-mediated cell growth via the Raf/MEK/ERK pathway (161). In nasopharyngeal carcinoma, the combination of miR-873 and PI3K inhibitor LY294002 was reported to inhibit ZIC2, thereby impairing the self-renewal capacity of nasopharyngeal carcinoma cells, suggesting that the PI3K/AKT pathway might be a positive regulator of ZIC2 (189).

Taken together, accumulating evidence suggests that ZIC2 acts as a transcription factor or co-activator, or both, and interacts with chromatin

remodeling complexes and signaling molecules to regulate gene expression and signaling pathways in multiple biological processes.

1.3 Transcription factor RUNX3

1.3.1. RUNX family members

The human RUNX family members include *RUNX1*, *RUNX2*, and *RUNX3*. These three RUNX family members differ in gene size (190-192). *RUNX1* is located on the reverse strand of chromosome 21 (21q22.12). It is the largest gene in the RUNX family, containing 12 exons. The size of the gene containing introns is about 261 kb (192). *RUNX2* is located on the forward strand of chromosome 6 (6p21.1) and has eight exons. The size of the gene containing introns is about 222 kb. *RUNX3* is located on the reverse strand of chromosome 1 (1p36.11). The size of the *RUNX3* gene containing introns is about 67 kb, and it is the smallest of the three genes, with six exons. *RUNX3* is the most conserved member of the mammalian RUNX family. The percentage of repetitive Alu (Alu element) and MIR (mammalian-wide interspersed repeat) in the SINE (short interspersed nuclear elements) of the *RUNX3* gene is 4% and 7%, respectively (192). Among the three *RUNX* genes, *RUNX3* has the highest proportion of repeated MIR, suggesting that the repeated MIR sequences in the *RUNX1* and *RUNX2* genes might have been replaced by other reverse transcripts during evolution (193). The human *RUNX3* gene and the mouse *Runx3* gene are highly similar in size and organization. For instance, the percentage of repetitive elements in the human *RUNX3* gene is as low as 21%, compared to an average of 40% to 50% in the human genome. The

percentage of repetitive sequences in the mouse *Runx3* is low, and the MIR in the SINE repetitive sequences is also consistent with that in the human *RUNX3* gene (193).

There are six domains in each RUNX protein, five of which are common to all three RUNX proteins, including RHD (a conserved Runt homology domain), NLS (a nuclear localization signal), AD (a transactivation domain), ID (an inhibitory domain), and the C-terminal Groucho/transducin-like enhancer of split (TLE) binding site (VWRPY motif) (**Figure 1.5**) (194). RHD is a conserved domain responsible for DNA binding and protein-protein interactions. NLS is located between RHD and AD and is responsible for the nuclear localization of RUNX proteins. AD and ID are located at the C-terminus of RUNX protein and show low conservation. AD interacts with the transcriptional co-activator p300/CBP, while ID located at the C-terminus of RUNX proteins counteracts the effects of AD. The extreme C-terminal VWRP motif mediates the interactions with the transcriptional co-repressor Groucho/TLE. In addition to these five common domains, there is a unique QA (glutamine/alanine-rich) domain in RUNX2. It was shown that this domain alters transactivation, which may be related to the shape and evolution of the mammalian skull (195).

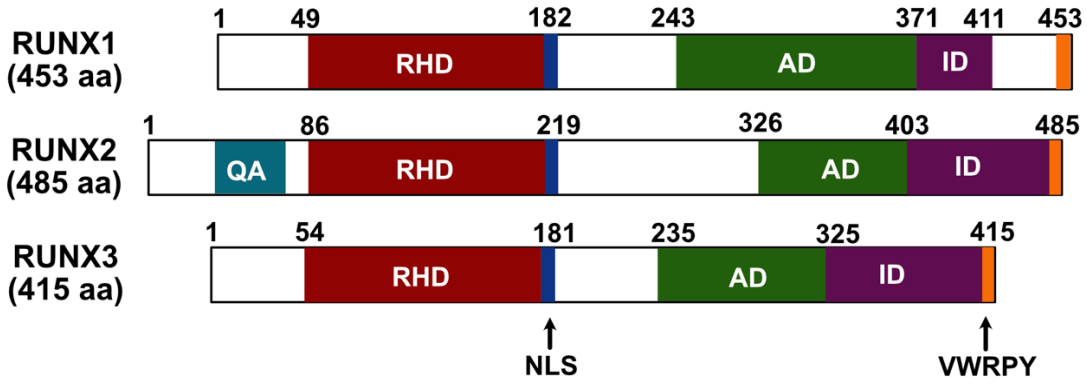

Figure 1.5. The protein domains of RUNX family members

This figure is modified from Mevel, R., *et al.* (194). The human RUNX family has three members, including RUNX1, RUNX2, and RUNX3. The main domains of these three proteins and the locations of these domains are shown in the figure. RHD: conserved Runt homology domain; NLS: nuclear localization signal; AD: transactivation domain; ID: inhibitory domain; VWRPY: Groucho/transducin-like enhancer of split (TLE) binding site. QA: glutamine (Q)- and alanine (A)-rich sequence.

1.3.2 The expression of RUNX3 during embryonic development and human cancers

RUNX3 plays an important role in development (194,196-206). It plays the following roles in development: **1)** neurogenesis (198,199); **2)** specification of lymphocyte and bone marrow lineage commitment (204-206); **3)** multiple stages of complex cell fate determination involving thymic T-lymphocyte development in the immune system, including active regulation of T-cell Cd8 expression (196,197); **4)** endochondral ossification in mice (203); **5)** maturation of myeloid dendritic cells (201,202); and **6)** streaks and hair germination stages (200).

The dysfunction of RUNX3 in human cancers varies from cancer to cancer and may be due to promoter hypermethylation, mutational inactivation, gene deletions, and protein mislocalization (207-212). Expression of *RUNX3* is inhibited in several human cancers (207-220). In human cancers, such as gastric, cholangiocarcinoma, pancreatic, and lung cancers, there is a hemizygous deletion

of the *RUNX3* gene and reduced expression of *RUNX3* (208-215). In most reported human cancers, *RUNX3* is considered a tumor suppressor gene. The main cause of loss of *RUNX3* expression in cancers such as gastric, colon, esophageal, breast, and hepatocellular carcinomas is hypermethylation of the *RUNX3* promoter (207,212,216-218,220).

In addition to the silencing of *RUNX3* by hypermethylation, mislocalization of RUNX3 protein was found in gastric, breast, colorectal polyps, liver cancer, and EOC (212,218,221,222). The truncated form of the RUNX3 protein (RUNX3 protein with its C-terminal truncated, 1-187) is expressed only in the cytoplasm of the gastric cancer cell line SNU16 (212). Notably, the cytoplasmic RUNX3 protein could not function as a tumor suppressor because RUNX3 needs to enter the nucleus and bind to the heterodimer partner CBFβ to function (223). *RUNX3* is increased in some human cancers such as EOC, head and neck cancer, and human basal cell carcinoma, and is considered pro-tumorigenic in these types of cancers (222,224).

1.3.3 The role of RUNX3 in ovarian cancer

Research on RUNX3 in ovarian cancer has been limited to EOC (222,225-227). Nevadunsky *et al.* reported that RUNX3 was expressed in some EOC samples and EOC cell lines, but not in non-tumorigenic ovarian epithelial cell lines (222). They also found that RUNX3 positively regulates the proliferation of EOC cells. Lee *et al.* also confirmed the expression of *RUNX3* in EOC samples and cell lines (225). The study by Lee *et al.* also examined RUNX3 expression in different

subtypes and found that *RUNX3* was expressed in 40% of endometrioid carcinomas and 33% of HGSOCs, but not in clear cell carcinomas. The authors also demonstrated that RUNX3 promotes proliferation and anchorage-independent growth in EOC cell lines. Research published in our laboratory showed that RUNX3 promotes carboplatin resistance in EOC cell lines (226).

The role of RUNX3 in GCT remains to be investigated. In mice, RUNX3 has been shown to play a role in folliculogenesis and steroidogenesis in granulosa cells (228,229). Ojima *et al.* reported that the female *Runx3-/-* mice had ovulation disorders and an atrophied uterus that suggested a decrease in estrogen production in ovaries (229). In addition, that report indicated that the corpus luteum was not detected in *Runx3-/-* adult mice and that the number of follicles in the ovaries was decreased compared to normal adult mice. Therefore, the authors suggested that *Runx3* is involved in follicular development in mice. Follicle formation includes an early non-gonadotropin-dependent growth phase and a late gonadotropin-dependent growth phase (230-233). During the early phase, the recruitment of primordial follicles is regulated by the estrogen required for follicle development into pre-ovulatory follicles. Granulosa cells of the ovary are involved in follicle formation and luteinization. Ojima *et al.* found that *Runx3* and Aromatase (*Cyp19a1*, a key enzyme for estrogen synthesis) were co-expressed in granulosa cells of the ovary from *Runx3* wild-type mice, while mRNA expression of Aromatase was reduced in granulosa cells of the ovary from *Runx3-/-* mice (228). Therefore, the authors suggested that *Runx3* deficiency results in decreased Aromatase expression, which might lead to decreased estrogen secretion in

granulosa cells of the ovary (229). Therefore, *Runx3* in mouse granulosa cells of the ovary may promote follicle formation and estrogen secretion.

1.4 Cancer stem cells (CSCs)

1.4.1 The development of CSC theory

The CSC-related theory has undergone three major stages of development: clonal evolution, CSCs, and cancer cell plasticity (**Figure 1.6-1.8**) (234-238). The first clonal evolutionary model suggested that tumors originated from normal cells (**Figure 1.6**) (235). Inspired by Darwinian evolution, Nowell proposed a continuous evolution model of cancer in 1976, which revealed how common genetic variation and selection on cancer cells contributed to the development and proliferation of cancer cells in a more malignant direction (234). However, the model suggested that the clones were mutually exclusive, as associations between heterogeneous clones are not considered, and clones without genetic variation and small clones in tumors, as well as functional interactions between these clones, were ignored (238,239).

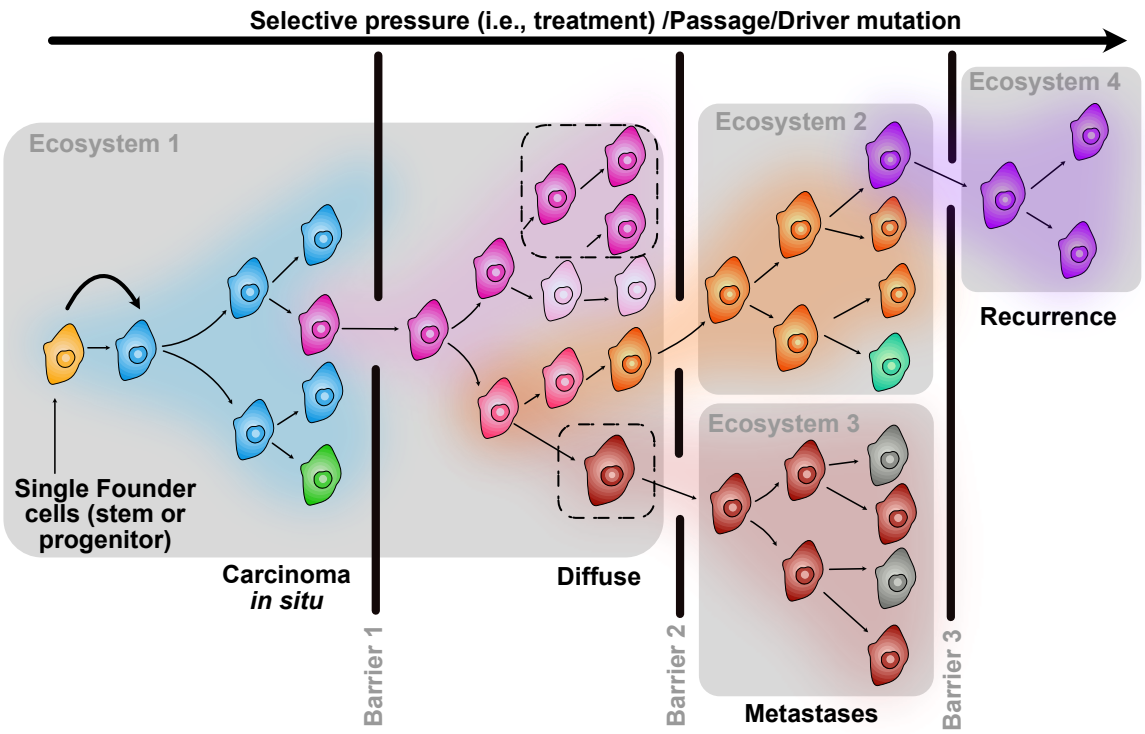

Figure 1.6 The model of clonal evolution

This figure is modified from Greaves, M. and C.C. Maley (235). The figure shows a preliminary model of a CSC-related theory: the clonal evolution model. The horizontal lines with arrows indicate the clonal evolution of cancer cells under therapeutic and driver mutation pressures. The gray boxes represent different tissue ecosystems or habitats. The small boxes with dashed lines in Ecosystem 1 represent local habitats or niches, and the vertical lines represent independent pressures during clonal evolution. Each cell in the figure represents a genetically distinct subclone.

The second model is the CSC model (**Figure 1.7**) (238). The CSC model was inspired by the hierarchical hematopoietic cells found in human acute myeloid leukemia by John Dick *et al.* in 1994 (236). This report proposed a model in which

a subpopulation of leukemia cells (CSCs) located at the top of the hierarchical pyramid could differentiate into other types of cancer cells and was subsequently used to explore CSCs in solid tumors (237). The model showed that only a few cancer cells with the properties of stem or progenitor cells could promote the malignant progression of cancer. However, the second model ignored genetic heterogeneity within the tumor, overemphasized the function of CSCs, and suggested that the remaining differentiated cancer cells had no selective advantage in maintaining the cell differentiation phenotype (236). In fact, cancer cells with genetic and epigenetic heterogeneity, both CSCs and non-CSCs, drive tumorigenesis and progression.

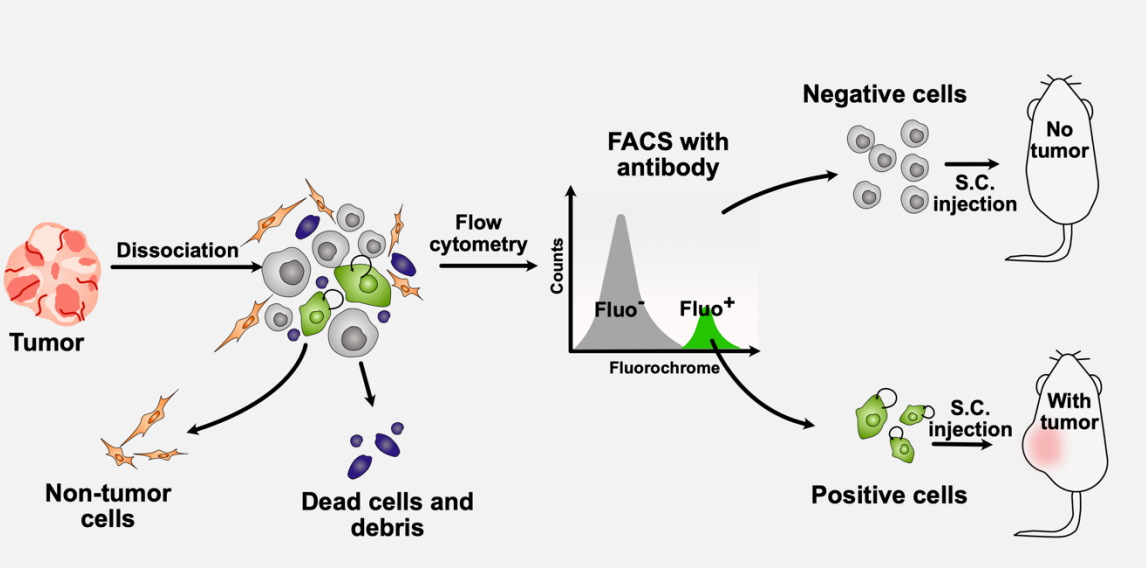

Figure 1.7. The model of cancer stem cells (CSCs)

This figure is modified from Shackleton, M., *et al.* (238). The figure shows a preliminary model of the CSC-related theory: the CSC model. It shows that CSCs are a small population of tumorigenic cells (Positive cells) in comparison to non-tumorigenic cells (Negative cells). Negative and positive cells are sorted based on

the signal of fluorochrome-conjugated antibodies of the CSC-markers. *S.C. injection: subcutaneous injection; $Fluo^+$: fluorochrome-positive; $Fluo^-$: fluorochrome-negative.

The cancer cell plasticity model proposed that there was considerable plasticity between differentiated cancer cells and CSCs (**Figure 1.8**) (240). Corbin Meacham proposed a cancer cell plasticity model in 2013 (241). This model explained the phenomenon that some differentiated cancer cells display CSC characteristics in response to stimuli from a specific environment. For instance, differentiated cancer cells and CSCs could be interconverted. The CSC plasticity is mainly manifested in two aspects:

On the one hand, some cancer cells can switch in different states to promote tumor growth. For instance, breast cancer cells in the mesenchymal state have a higher tumorigenic capacity than cells in the epithelial state (242); in melanoma, cancer cells can reversibly control the expression of some genes (e.g., *JARID1B*) through epigenetic modifications (e.g., histone methylation) to maintain tumor growth (243); in gliomas, exposure of cancer cells to perivascular carbon monoxide reversibly promote tumorigenesis (244).

On the other hand, some cancer cell subpopulations develop resistance to multiple chemotherapeutic drugs or radiotherapy, or both (241,245-248). In cancer cells treated with chemotherapeutic drugs, the plasticity of some cancer cells appears to reversibly produce progeny cells that are sensitive or resistant to chemotherapy. In some cancers, cancer cells with enhanced tumorigenicity are

also resistant by nature to chemotherapy or radiotherapy, or both. For instance, in breast cancer cells treated with chemotherapy and in glioma cells treated with radiotherapy, treatment-induced resistant cell subpopulations are enriched and more tumorigenic (245,246).

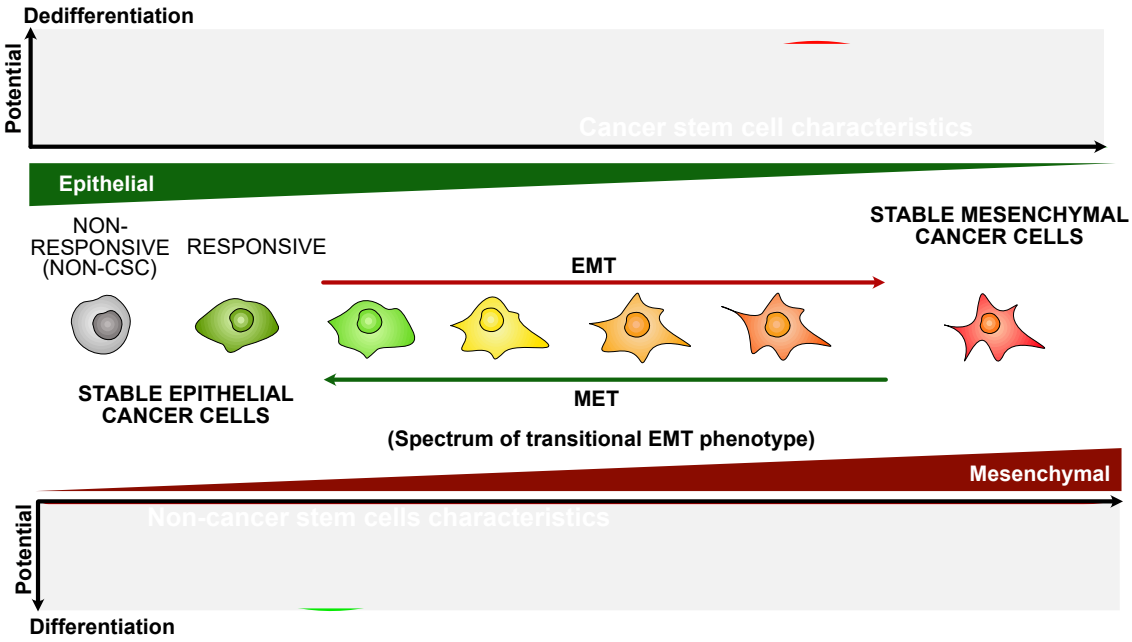

Figure 1.8. The model of cancer cell plasticity

This figure is modified from Chaffer, C.L., *et al.* (240). The figure shows a preliminary model of CSC-related theory: the cancer cell plasticity model. It suggests that cancer cells contain cells that are responsive (Responsive) or non-responsive to EMT (Non-responsive). Cells that are responsive to EMT may undergo EMT and achieve maximum CSC properties (self-renewal ability) in a specific state that tends to be mesenchymal. However, cells in a stable mesenchymal state do not achieve the maximum CSC properties (self-renewal ability). In addition, this model shows that CSC properties of epithelial cells (not necessarily CSCs) can be obtained by EMT.

1.4.2 The characteristics of CSC

CSCs are cancer cells with characteristics similar to normal stem cells (249). From this perspective, CSCs have the potential for self-renewal and differentiation. Self-renewal refers to the fact that after a cell is divided into two cells, the two progeny cells remain in the same undifferentiated state as the parental cell *in vitro* and *in vivo*. Differentiation potential refers to the phenotype of differentiated cancer cells after CSCs undergo cell division *in vivo* or *in vitro*. For instance, differentiated cancer cells have phenotypes of rapid proliferation and rapid cell cycle but lack expression of specific stem cell markers. CSCs are tumor-initiating cells and the proportion of CSCs in a tumor depends on the asymmetric division of CSCs to maintain a dynamic balance that gives rise to CSCs and differentiated cancer cells. The self-renewal and differentiation potential of CSCs is one of the causes of tumor recurrence and metastasis (250,251).

CSCs are tumorigenic. Initially, researchers identified the presence of heterogeneous cells in tumors (252). They sorted cancer cell subpopulations based on cell surface markers by fluorescence-activated cell sorting (FACS) and injected a limited number of sorted cells into immunodeficient mice (252). They found that a specific subpopulation of cancer cells formed tumors in mice that could be passaged serially. This specific subpopulation of cancer cells was interpreted as being enriched in CSCs. Otherwise, under the same conditions, a subpopulation of cancer cells in immunocompromised mice that had difficulty

forming tumors or passaged serially was interpreted as differentiated cancer cells. Thus, based on this fact, CSCs are tumorigenic.

CSCs are quiescent or rapidly proliferating (253-256). Since CSCs were first discovered in leukemia, researchers referred to the characteristics of normal hematopoietic stem cells (HSCs) and concluded that CSCs rarely divide and have a relatively quiescent cell cycle (257,258). When HSCs divide asymmetrically, they give rise to rapidly dividing progeny cells and new quiescent HSCs. Subsequent studies confirmed that most CSCs are quiescent. However, there are several reports showing that CSCs proliferate rapidly (256,259,260). For instance, these studies showed that quiescent CSCs are reactivated after chemotherapy and rapidly proliferate to repopulate the tumor, which is one of the causes of cancer recurrence after chemotherapy.

CSCs have metastatic potential (261-264). One feature of cancer cell plasticity suggests that the phenotype of cancer cells could be reversibly transformed. Studies showed that phenotypic changes occur during the process of CSC metastasis (265-269). These studies demonstrated that these changes include epithelial-mesenchymal transition (EMT) and mesenchymal-epithelial transition (MET). EMT is a process by which cancer cells of epithelial origin lose some of their epithelial features and acquire a mesenchymal state, while MET is the reverse process of EMT (269,270). EMT enables cancer cells to invade blood vessels, enter the circulatory system, and reach metastatic sites during tumor progression. Furthermore, MET allows cancer cells to form new metastases and to proliferate rapidly as the tumor progresses. Thus, the ability of CSCs to switch

between mesenchymal and epithelial states renders cancer cells the potential to metastasize (240,271,272).

CSCs are resistant to chemotherapy and radiotherapy. The effectiveness of conventional anti-proliferative chemotherapy and radiotherapy is usually limited due to the presence of CSCs (273). Most chemotherapy drugs work by attacking the DNA of cancer cells, inhibiting their division and proliferation, and killing rapidly growing cancer cells (252,274). Nevertheless, chemotherapy has no significant effect on CSCs in a relatively quiescent state (252). Kurtova *et al.* indicated that although chemotherapy kills rapidly proliferating differentiated cancer cells in bladder cancer, it activates quiescent CSCs that rapidly repopulate the tumor after treatment is stopped (256). Radiation therapy is based on the use of ionizing radiation to damage DNA directly or to generate charged groups such as free radicals, which indirectly damage DNA and kill cancer cells (275,276). Similar to chemotherapy, radiotherapy is based on rapidly proliferating cancer cells that are more sensitive than normal tissues. Similarly, radiotherapy is not practical for CSCs in a relatively quiescent state. Lagadec *et al.* demonstrated that radiotherapy can reprogram differentiated cancer cells into CSCs in breast cancer (277). The above studies explain the possible causes of cancer recurrence from the perspective of radiotherapy, suggesting that the presence of CSCs in the tumor might be one cause of chemoresistance and radiotherapy resistance.

In addition, CSCs have been shown to express a large number of anti-apoptotic proteins that inhibit apoptosis in cancer cells, DNA repair enzymes that enhance DNA repair, and ATP-binding cassette (ABC) transporters that counteract

chemotherapeutic drugs by increasing drug excretion and decreasing intracellular drug concentrations (278-281).

Therefore, these CSC properties make this subpopulation of cancer cells a key challenge for the treatment of human cancers.

1.4.3 The factors that regulate ovarian CSCs

With the development of the CSCs model and the further additions of the cancer cell plasticity model, CSCs are considered one of the causes of tumor progression. Ovarian CSCs have been demonstrated to be involved in primary tumor growth, peritoneal spread, recurrence, and the development of chemoresistance (282-285). Ovarian CSCs are regulated by multiple factors during tumor progression. These factors include extrinsic factors and intrinsic factors, which ultimately determine the acquisition and maintenance of biological characteristics associated with CSC stemness. Extrinsic factors include the tumor microenvironment, whereas intrinsic factors include signaling pathways and epigenetic modifications (286-297).

The tumor microenvironment is an extrinsic regulator of ovarian CSCs (286-288). The tumor microenvironment is important because it could act on the CSCs and affect intrinsic factors such as gene expression profile, epigenetic modifications, signaling pathways, which are ultimately reflected in the stemness regulation of ovarian CSCs (298-302). The cancer cell plasticity model proposed that CSC plasticity was coordinated by the tumor microenvironment, and that cancer cells could dynamically switch between stem and non-stem cell states with

the involvement of the tumor microenvironment (241,286,303). The tumor microenvironment includes the unique anatomical site where ovarian cancer tumors are located, also known as the stem cell niche (304). In addition to CSCs, the tumor microenvironment includes non-CSCs, other host cells, extracellular matrix, and cytokines (287,305).

Differences in tumor microenvironment result in different states of CSCs, such as determining whether the state of these cells is quiescent, differentiated, symmetrical, asymmetrical, epithelial, or mesenchymal (306). Stem cell niches in ovarian CSCs might be associated with normal stem cells in the ovarian surface epithelium (OSE) and fallopian tubes, which are considered the origins of ovarian cancer (307-311). Flexken-Nikitin *et al.* inferred somatic stem cells and stem cell niches in the hilum region of mouse ovaries, fallopian tubes, and mesothelial region (307,309,312). In other studies, scientists showed that somatic stem cells in OSE are also widely distributed throughout the ovary rather than in specific regions (309,312). Thus, the stem cell niche of OSE may contain mature OSE cells, stroma under OSE, follicles, and follicular fluid (313). Reports showed that somatic and stem cell niches are found at the distal end of the fallopian tubes (i.e., the base of the tubal villi) and that the distal fallopian tubes and ovaries may share some niche components and signals (308,310,311). Therefore, it can be predicted that the niche of ovarian CSCs may benefit from the niche of normal somatic stem cells, such as OSE and fallopian tubes (314).

The above information refers to the tumor microenvironment of primary ovarian cancer located in the ovary. However, as tumors progress, advanced

ovarian cancer may also spread to other organs, such as the peritoneum, which increases the complexity of the tumor microenvironment in which ovarian CSCs are located (315,316). The tumor microenvironment of metastatic ovarian CSCs remains unclear.

There are various intrinsic factors involved in the stemness regulation of ovarian CSCs. Signaling pathways are one of them. Studies showed that a series of signaling pathways involved in tumor progression are associated with ovarian CSCs, such as the Wnt/β-catenin, Notch, JAK/STAT (Janus Kinase and Signal Transducer and Activator of Transcription), Hedgehog, and NF-κB pathways (289-294,317). The following is a brief overview of the roles of these pathways in normal organisms and ovarian CSCs:

1) The roles of the Wnt/β-catenin pathway in normal tissues include regulation of cell survival, proliferation, fate determination, and asymmetric division of stem cells (318,319). The Wnt/β-catenin pathway is aberrantly activated in a variety of cancers and is associated with maintenance of CSC stemness and CSC-mediated cancer metastasis. In ovarian cancer, CSC stemness is regulated by the Wnt/β-catenin pathway (289,317). Studies showed that *ALDH1A1* is a direct target of β-catenin in ALDH1A1-enriched ovarian CSCs (289,290). In xenograft tumor models, knockdown of β-catenin and inhibition of ALDH1A1 leads to decreased self-renewal ability and cell viability of EOC cells as well as inhibits tumor growth and peritoneal metastasis (289,290).

2) The roles of the Notch pathway in embryonic development include regulating the fate of cells in the central nervous system, hematopoietic system,

heart, eyes, and other organs, as well as regulating the differentiation of stem and progenitor cells (320-322). The Notch pathway maintains the proportion of ovarian CSCs. One study reported that the expression of Notch pathway-related proteins, including NICD1 (NOTCH1 intracellular domain), NICD2 (NOTCH2 intracellular domain), and NICD3 (NOTCH3 intracellular domain), was significantly higher in ovarian CSCs enriched in the side population than cells in the non-side population. (322). In contrast, a report showed that treatment of EOC cells with the Notch pathway inhibitor γ-Secretase inhibitor (GSI) reduced the proportion of the side population (291). In addition, that report showed that overexpression of NICD3 in EOC cells increased mRNA expression of the stem cell marker *CD44* gene and increased cisplatin resistance in EOC cells, and that the proportion of the side population in NICD3-overexpressed EOC cells did not change after treatment with GSI, except for a negative dose-dependent proportion of the side population in control cells after treatment with GSI (291). The above studies suggest that the Notch pathway is important for maintaining ovarian CSCs enriched in the side population.

3) The JAK/STAT pathway maintains the self-renewal ability, hematopoiesis in normal tissues, and neurogenesis in embryonic stem cells (323,324). In ovarian cancer, activation of this pathway is associated with the maintenance of CSC stemness. One study demonstrated that cancer cells from recurrent ovarian cancer ascites treated with paclitaxel display increased expression of CSC markers and showed activation of the JAK/STAT pathway, such as increased phosphorylation of STAT3 protein, compared with cancer cells

from recurrent ovarian cancer ascites that were not treated with paclitaxel. Furthermore, after treatment with a JAK2 inhibitor (e.g., CYT387) and paclitaxel, the activity of the JAK/STAT3 pathway was inhibited in ascites-derived tumor cells, such as decreased phosphorylation of JAK2 and STAT3 and decreased expression of CSC markers, compared with ascites-derived tumor cells treated with paclitaxel alone (292).

4) The Hedgehog pathway plays a vital role in the correct patterning of the nervous system, bone, heart, and intestine during embryonic development (325,326). In adults, the pathway is active only in some somatic stem cells, including the central nervous system, skin, and hair (325,326). In ovarian cancer, this pathway is activated and is associated with the ability of CSCs to maintain self-renewal. One study reported that the Hedgehog pathway is activated in spheres formed by EOC cells (293). For instance, mRNA and protein expression of the *GLI1* gene was increased in sphere-derived cells compared to cells cultured in a monolayer. Furthermore, the growth of spheres formed by these cells was inhibited by the Hedgehog pathway inhibitor dopamine (293).

5) The roles of the NF-κB pathway in normal tissues include regulation of inflammation and immune response, cell proliferation, survival, and differentiation (327). In ovarian cancer, this pathway is constitutively activated in CSCs and is associated with CSC-mediated inflammation. A study showed that the NF-κB pathway was constitutively activated in CD44+-enriched CSCs from malignant ovarian cancer ascites and ovarian tumors and that the use of an inhibitor of the

NF-κB pathway (eriocalyxin B) reduced the CSC-mediated inflammatory response and promoted the death of these CSCs (294).

Although all the above pathways are involved in maintaining the stemness of ovarian CSCs, the roles of these pathways in ovarian CSCs are not isolated but interact with each other. For instance, one study showed that treatment of EOC cells with the Hedgehog pathway inhibitor GANT61 not only inhibited the expression of genes downstream of the Hedgehog pathway in these cells, but also downregulates the expression of multiple genes involved in the Notch and the Wnt/β-catenin pathways (290).

Epigenetic modifications that determine gene expression profiles are another intrinsic factor in the regulation of ovarian CSC stemness. Ovarian cancer consists of heterogeneous populations of cancer cells, which is partly due to the different gene expression profiles of CSCs and non-CSCs in ovarian cancer. Researchers found a large number of differentially expressed genes in the gene expression profile of CSCs compared to non-CSCs in EOC, some of which are activated by transcription factors and play important roles in signaling pathways (295).

There is evidence that ovarian CSC stemness is regulated by epigenetic modifications. In a study, epigenetic modifications were shown to regulate ovarian CSC stemness and chemoresistance (296). The authors found that treatment of EOC cell lines and tumor cells from HGSOC patients with the DNA methyltransferase inhibitor SGI-110 decreased the proportion of $ALDH^{high}$ cells, and increased chemosensitivity compared to the untreated cells (296). In addition,

treatment of EOC cells with this inhibitor reduced self-renewal ability and single-cell survival. In a mouse xenograft model, they found that the inhibitor reduced the tumorigenicity of ovarian CSCs by targeting $ALDH^{high}$ EOC cells. They demonstrated that in a mouse model treated with carboplatin, CSC markers (e.g., *ALDH1A1*, *BMI1*, *NANOG*, and *POU5F1*) were overexpressed in the $ALDH^{high}$ cell population of EOC cells and that treatment with this inhibitor reduced the expression of the methyltransferase *DNMT1* gene, increased the expression of the differentiation gene *HOXA10*, and reduced the total mass and volume of xenografts (296). Thus, these studies above suggest that CSC stemness might be regulated by epigenetic modifications in EOC.

In particular, although gene mutations are one of the key drivers of tumor progression, one study showed that differences in gene mutations do not account for differences in gene expression profiles between ovarian CSCs and non-CSCs (297). There was no difference in gene mutations between CSC ($CD44^+/CD117^+$) and non-CSC pairs isolated from five independent HGSOC ascites samples (297). Therefore, epigenetic modifications rather than gene mutations might be an intrinsic factor regulating ovarian CSC stemness.

1.4.4 CSC markers of ovarian cancer

Current identification of ovarian CSCs relies on stem cell markers (**Figure 1.9**) (328-360). These markers include cell surface transmembrane glycoproteins (e.g., CD24-, $CD44^+$, $CD133^+$, and $EpCAM^+$), tyrosine kinase receptors (e.g., $CD117^+$ and ROR1), cytoplasmic aldehyde dehydrogenase (i.e., $ALDH^{high}$), stem

cell-associated transcription factors (e.g., OCT4, SOX2, NANOG, and MYC), and ATP-binding cassette transporters (e.g., ABCGB1 and ABCG2) (337,343,344,346-352,355-365).

Tyrosine kinase receptor CD117 (c-KIT) was the first identified marker of ovarian CSCs associated with poor prognosis, enhanced tumorigenicity, and chemoresistance (337,361,362,366). The cell surface transmembrane glycoprotein CD133 is one of the most commonly used cell surface markers to identify ovarian CSCs associated with poor prognosis, enhanced tumorigenicity, and chemoresistance (301,363-365). In addition to cell surface markers, aldehyde dehydrogenase ALDH1A1 is a widely accepted marker of ovarian CSCs that positively correlates with cell proliferation, metastatic capability, poor prognosis, and chemoresistance (343,344,358). *OCT4 (POU5F1)*, *SOX2*, and *NANOG* are transcription factor genes expressed in normal stem cells for the identification of ovarian CSCs (344,346-352,359). Increased expression of these three transcription factors is associated with poor prognosis in ovarian cancer patients (347,349,350,359). The transcription factor c-MYC is a pro-tumorigenic factor associated with tumor pathogenesis (352,360). Moreover, expression of the ATP-binding cassette transporters *ABCB1* and *ABCG2* increases the ability of cancer cells to excrete a DNA-binding dye (Hoechst 33342), which makes it possible to screen for side population by flow cytometry (355-357). Because the side population cells show chemoresistance, side population has also been used to identify ovarian CSCs.

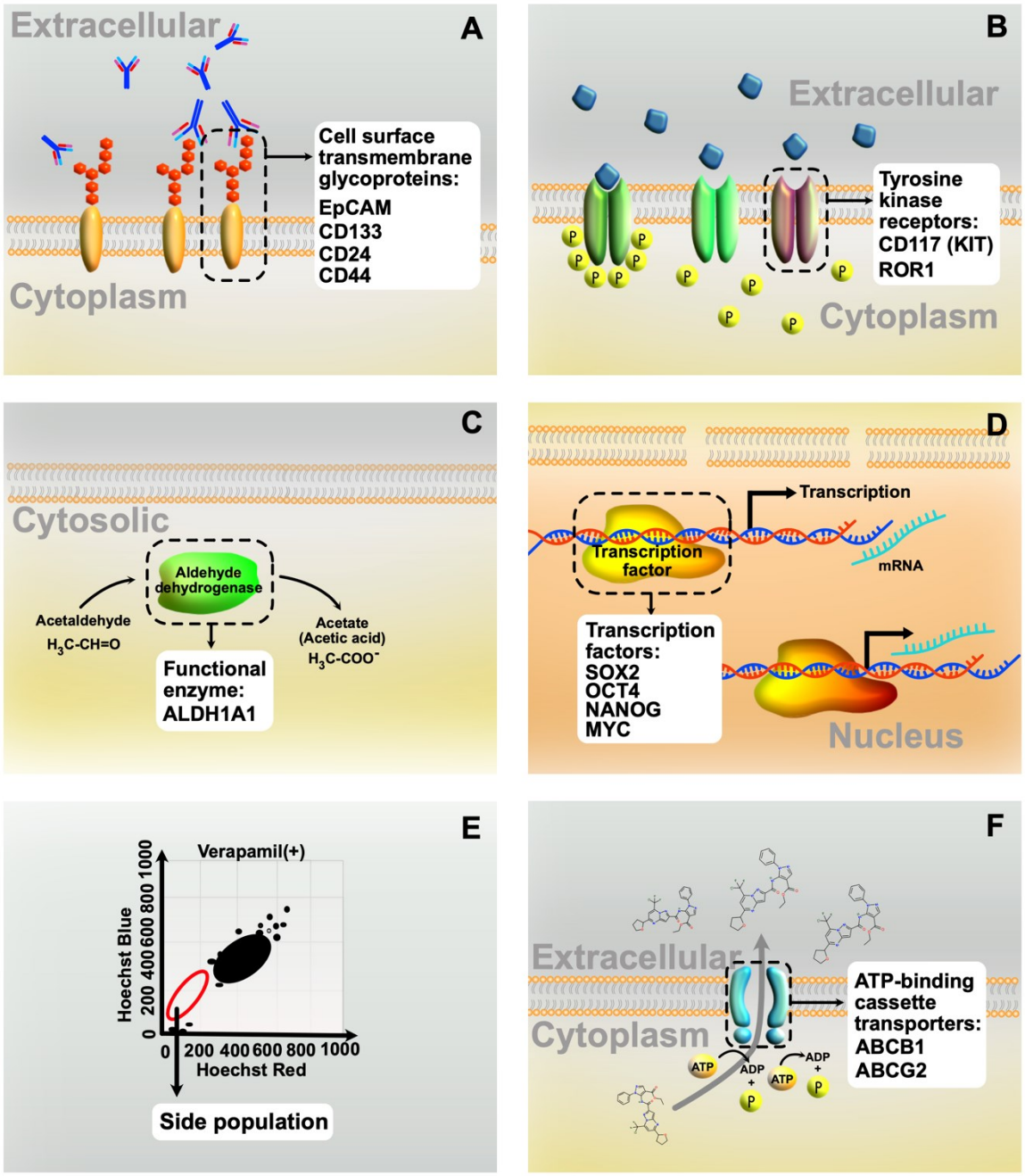

Figure 1.9 The CSC markers of ovarian cancer

This figure is generated based on the contents of multiple publications (337,343,344,346-352,355-365). **(A)** Cell surface transmembrane glycoproteins (EpCAM, CD133, CD24, and CD44). **(B)** Tyrosine kinase receptors (ROR1 and CD117). **(C)** Functional enzyme: ALDH1A1. **(D)** Transcription factors (SOX2,

OCT4, NANOG, and c-MYC). **(E)** Side population by Hoechst 33342. **(F)** ATP-binding cassette transporters (ABCB1 and ABCG2).

1.5 Target transcription factors

1.5.1 The role of transcription factors in EOC

Transcription factors play an important role in cancer. Transcription factors account for about 20% of all oncogenes and have proven biological functions (367). A series of transcription factors become drivers of the different histological subtypes of EOC. In EOC, transcription factors are categorized into those involved in multiple histological subtypes and those displaying histological subtype specificity. The former includes PAX8 and WT1, which are associated with more than one histological subtype of EOC (368,369). The latter group of transcription factors is classified as those specifically expressed or mutated in each subtype, such as HGSOC, LGSOC, endometrioid carcinoma, clear cell carcinoma, and mucinous carcinoma (368,370-384). These transcription factors are as follows:

1) The transcription factors that are expressed in multiple histological subtypes of EOC include PAX8 and WT1. PAX8 is expressed in four major histological subtypes of EOC, including HGSOC, LGSOC, endometrioid, and clear cell subtypes, with the exception of the mucinous subtype (385,386). PAX8 is used clinically as a biomarker for serous, endometrioid, and clear cell subtypes, and its expression in these advanced EOCs is associated with poor overall survival (40,387,388). In HGSOC, PAX8 directly targets *WT1* and *MUC16*, the biomarkers of HGSOC (389). Inhibition of PAX8 in EOC *in vitro* attenuates the tumorigenic

phenotypes, including reduced cell proliferation, migration, and invasion (390-392). In addition, inhibition of PAX8 in HGSOC significantly reduces cell viability, while inhibition of PAX8 in cell lines of other EOC subtypes does not affect cell viability, suggesting that the pathobiological role of PAX8 is HGSOC lineage-dependent despite its expression in multiple EOC subtypes (393).

WT1 is another transcription factor that is highly expressed in HGSOC, LGSOC, and a small subset of endometrioid carcinoma (394-396). The combination of overexpression of *WT1*, *PAX8*, and loss of function mutations of *TP53* and *BRCA1/2* is considered a biomarker of HGSOC (397). *WT1* has been recognized as a tumor suppressor gene in human cancers (398). In particular, *WT1* expression in HGSOC is associated with better patient prognosis, but its expression in other EOC subtypes is unfavorable (388,399-401). However, its pathobiological roles in EOC, its upstream regulators and downstream effectors, and its direct target genes are not clear.

2) The transcription factors specifically expressed or mutated in HGSOC include *TP53*, *BRCA1*, *BRCA2*, *FOXM1*, and *MYC*. *TP53* is one of the most common mutated genes in most cancers (402). Almost all HGSOCs have *TP53* mutations (368,370-372). Missense mutations in exons of the *TP53* DNA-binding domain accounted for about 60% of all *TP53* mutation types in HGSOCs (372). These missense mutations include R175 (R175H), R248 (R248W or R248Q), and R273 (R273H), of which R273 is the most common mutation in HGSOC (403,404). The *TP53* R273 mutant retains the ability of *TP53* to bind to DNA, but its sequence of binding to target DNA is altered (405,406). The *TP53* R273 mutant is associated

with increased ATP-dependent efflux pump protein, *MDR1*-encoded multidrug resistance protein 1, and paclitaxel resistance (404). Furthermore, *TP53* R248 and R175 mutants are associated with increased genomic instability and chemoresistance in HGSOC (403,407,408).

BRCA1 and *BRCA2* are two other transcription factors that are frequently mutated in HGSOC. Germline mutations in these two genes occur in about 10% of HGSOC but rarely in other subtypes of EOC (368,371,373). The primary role of these two genes is to participate in homologous recombination repair of DNA double-strand breaks (409). Wild-type BRCA1 protein can bind to other transcription factors to form complexes that regulate the signaling pathways related to cell proliferation, and loss of function mutation in this gene impairs these pathways and promotes tumorigenicity (410-412). Taking advantage of the fact that HGSOC tumors with *BRCA1*/*2* mutations are dependent on DNA single-strand break repair and are particularly sensitive to the inhibition of PARPs (DNA repair enzymes that promote single-stranded break repair), PARP inhibitors (e.g., Olaparib) originally developed for *BRCA1/2* mutant breast cancer are applied to treat *BRCA1/2* mutant EOC (413-415).

FOXM1 is also a transcription factor frequently overexpressed in HGSOC. *FOXM1* is upregulated in up to 84% of HGSOC and its overexpression is associated with poor overall survival in HGSOC patients (368,371,374,375). Inhibition of *FOMX1* expression in HGSOC by shRNA attenuates the tumorigenic phenotype in mice, including inhibition of cell proliferation, migration, invasion, and tumorigenesis (416). Moreover, FOXM1 also promotes the expression of the two

transcription factors, *BRCA1* and *PAX8,* in HGSOC (392,417). Thus, inhibition of *FOXM1* in HGSOC leads to decreased expression of *BRCA1*, which might sensitize cancer cells to PARP inhibitors.

MYC is a transcription factor that is frequently overexpressed in HGSOC. Upregulation of *MYC* is associated with reduced overall and progression-free survival in patients with HGSOC (418-421). *MYC* is overexpressed in all stages of HGSOC and is associated with cancer metastasis and the development of chemoresistance (422,423). Overexpression of *MYC* in human fallopian tube secretory epithelial cells, which are considered HGSOC precursors, promotes tumorigenic phenotypes *in vivo* and *in vitro* (424,425).

3) PAX2 is considered one of the transcription factors specifically expressed in LGSOC. In one study, scientists compared gene expression profiles of normal ovarian surface epithelium, tumor samples from LGSOC and HGSOC and confirmed that *PAX2* is one of the genes significantly upregulated in LGSOC (376). *PAX2* plays an important role in organogenesis, such as brain development (376). Although the pathobiological role of PAX2 in ovarian cancer is unclear, studies showed that overexpression of PAX2 in ovarian surface epithelial cells promotes tumorigenic phenotypes, such as cell proliferation, survival, and chemoresistance (426).

4) β-catenin, encoded by *CTNNB1*, is specifically and highly expressed in endometrioid carcinoma (377). β-catenin is a key transcription factor in the Wnt/β-catenin pathway (427-429). Normally, in the absence of Wnt stimulation, β-catenin is degraded by the destruction complex of tumor suppressors, such as Axin,

colorectal adenomatous polyposis (APC), glycogen synthase kinase-3β (GSK-3β), and casein kinase 1 (CK1). Upon Wnt stimulation, this destruction complex-mediated degradation of β-catenin is inhibited, resulting in the entry of β-catenin into the nucleus and its binding to other transcription factors to regulate transcription of downstream genes (430). The high expression of β-catenin-encoding gene *CTNN1B* in endometrioid carcinoma is due to mutations in the third exon of this gene or mutations in genes of protein factors that mediate β-catenin degradation (e.g., Axin and APC), leading to constitutive activation of the Wnt/β-catenin pathway (377,431). As described above, the Wnt/β-catenin pathway is involved in maintaining the stemness of ovarian CSCs.

5) HIF1A and HNF1B are transcription factors with high specific expression in clear cell carcinoma. HIF1A is highly expressed in hypoxic tumor regions away from blood vessels. Although HIF1A expression has been detected in other histological subtypes of EOC, the high expression of this gene is specific to clear cell carcinoma (378). Consistent with the high expression of HIF1A, clear cell carcinomas are considered to be abnormally hypoxic (378). In addition, because *HIF1A* is located downstream of the PI3K/AKT/mTOR pathway, it promotes the expression of genes associated with hypoxic response, such as *VEGF* and glycolysis-related genes. High expression of HIF1A in clear cell carcinoma might be related to tumor angiogenesis, energy metabolism, and tumorigenesis under hypoxic conditions (378,432,433).

Another transcription factor that is particularly highly expressed in clear cell carcinoma is HNF1B. The promoter of the *HNF1B* gene is methylated in normal

ovarian tissue and other EOC subtypes. Thus, overexpression of HNF1B could be used as a specific biomarker for clear cell carcinoma (379-382). Of interest, HNF1B is also highly expressed in clear cell carcinoma of other human cancers (e.g., uterine cancer, pancreatic cancer, and renal cancer), suggesting that HNF1B is important for the biological characteristics of clear cell carcinoma (434,435). Clear cell carcinoma is believed to originate from endometriosis. Coincidentally, a study showed that overexpression of HNF1B in endometriosis cells induces a multinucleated phenotype similar to that of clear cell carcinoma. Therefore, HNF1B might be one of the important drivers for the progression of endometriosis into clear cell carcinoma (436).

6) *CDX2* is specifically and highly expressed in mucinous carcinoma. *CDX2*, together with *KRT7* (keratin 7) and *KRT20* (keratin 20), is considered a biomarker for mucinous carcinoma (383,384). However, research on *CDX2* in mucinous carcinoma remains at the level of using the protein as a biomarker, and the pathobiological role and molecular mechanism of this gene in this subtype have not been explored. In other cancers, such as colon cancer, the forced expression of *CDX2* upregulates the expression of *MDR1* (multidrug resistance 1). Thus, *CDX2* expression in colon cancer may be associated with increased chemoresistance (437).

In addition, some transcription factors originally expressed in human embryonic stem cells, such as *POU5F1* (*OCT4*), *SOX2*, and *NANOG*, are also expressed in ovarian CSCs (355,438). However, it is unclear whether the expression of these transcription factors in EOC is subtype-specific.

1.5.2 Development of technologies targeting transcription factors and targeted drugs applied in clinical trails

Transcription factors play a key role in tumorigenic progression. However, transcription factors have long been considered undruggable targets. Until recently, new technologies have made the targeting of transcription factors possible (439). Most traditional small-molecule drugs target proteins, but about 80% of proteins cannot be effectively targeted by these drugs. These proteins include transcription factors necessary for tumor progression. Unlike protein kinases, transcription factors lack an active binding cavity. The active binding cavity in kinases is bound by small molecular drugs that block the entry of endogenous substrates and block the function of the kinase. Transcription factors are intracellular proteins. Therefore, antibody-based drugs targeting cell surface proteins are not suitable for transcription factors. For the above reasons, these proteins, including transcription factors, which cannot be interfered with by conventional drug development approaches are known as undruggable targets.

In recent years, an increasing number of pharmaceutical companies have developed new drugs targeting transcription factors based on their role in the cells. These drugs aim to inhibit the expression of transcription factors, block the interaction of transcription factors with cofactors, prevent the binding of transcription factors to target DNA, and induce protein degradation of transcription factors (**Figure 1.10 to 1.13**) (440-461).

The first type of drug is nucleic acid drugs. Most pharmaceutical companies use such drugs, such as antisense oligonucleotides (ASOs) nanoparticle-

encapsulated small interfering RNAs (siRNA), and single-guide RNAs in CRISPR technology to inhibit the expression of transcription factors by manipulating their mRNA levels, the DNA sequences of their genes, or mRNA translation (66,440-452,462-464). ASOs are short single-stranded DNA oligodeoxynucleotide fragments complementary to RNA that can recruit ribonuclease H (RNase H) to mediate the cleavage of the target transcript mRNA, thereby inhibiting gene expression (**Figure 1.10A**). This type of ASOs is already in clinical trials (450).

RNA interference (RNAi) technology using nanoparticle-encapsulated siRNA is similar to that of ASOs. siRNA inhibits the expression of transcription factors by targeting and degrading their mRNAs (**Figure 1.10B**). In addition, high-density lipoprotein carriers (nanoparticles) provide the feasibility of cytoplasmic release of siRNA fragments by overcoming the problems of easy degradation, short cycle time, and difficulty in crossing cell membrane barriers of RNAi *in vivo* (451-453). CRISPR technology applies specifically designed single-guide RNAs and different Cas systems to target DNA or pre-mRNA of genes, suppressing protein expression (**Figure 1.10C**) (447,449,465).

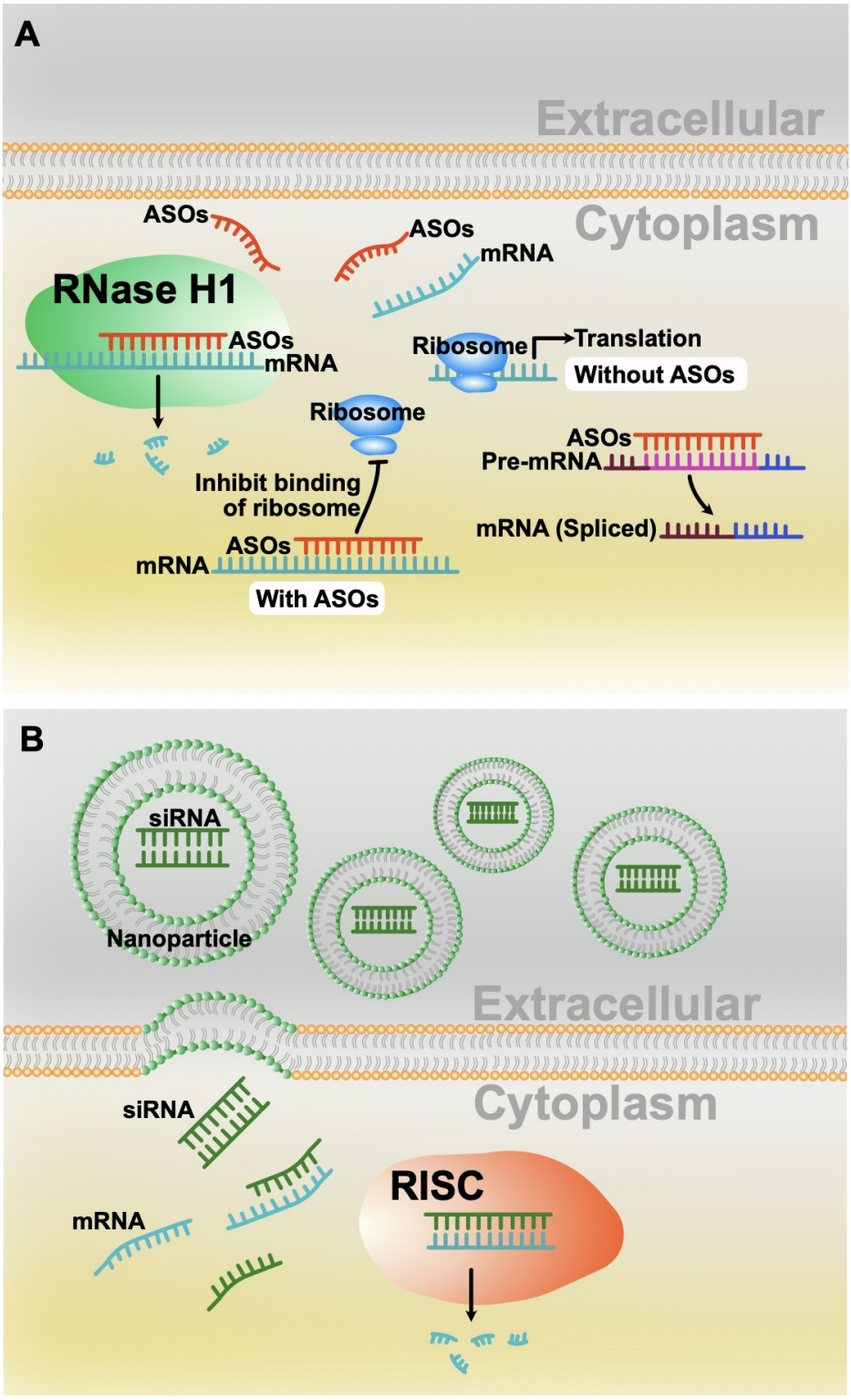
A
Extracellular
Cytoplasm
ASOs
ASOs
mRNA
RNase H1
ASOs
mRNA
Ribosome
Translation
Without ASOs
Ribosome
ASOs
Pre-mRNA
Inhibit binding
of ribosome
mRNA (Spliced)
ASOs
mRNA
With ASOs
B
siRNA
Nanoparticle
Extracellular
Cytoplasm
siRNA
mRNA
RISC

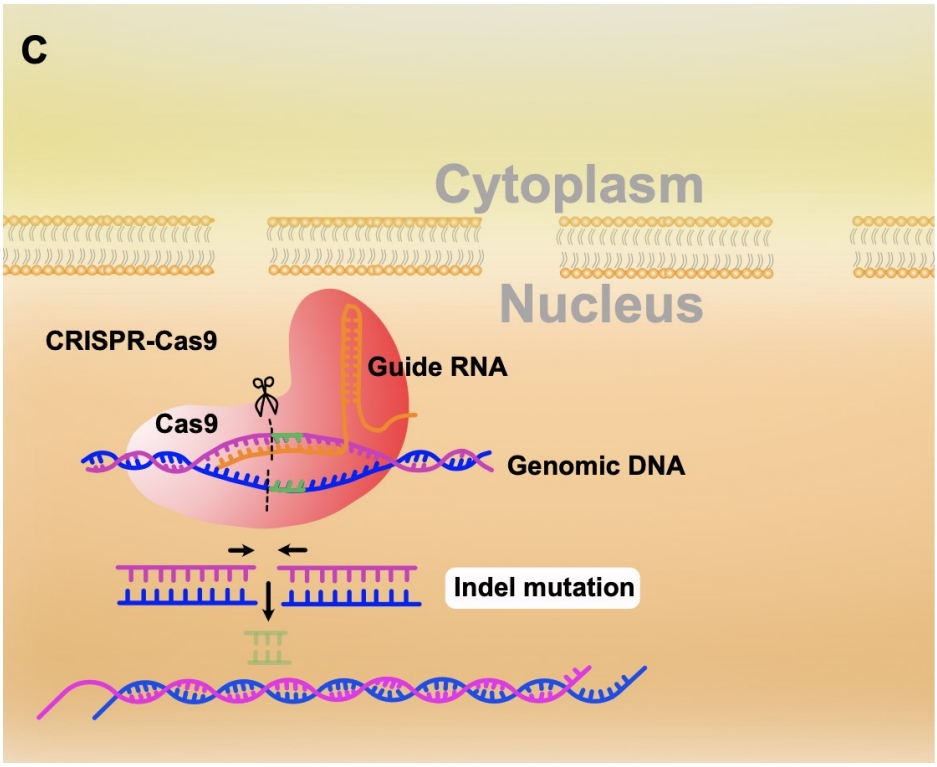

Figure 1.10 The first type of technologies developed for targeting transcription factors

The first type of technology (nucleic acid technologies) that targets transcription factors: **(A)** Antisense oligonucleotides (ASOs). ASOs and mRNA bind complementarily in the cytoplasm and then mRNA is degraded under the mediation of RNase H1, or ASO binds to mRNA so that the ribosome cannot bind to mRNA for translation, or ASO binds to pre-mRNA but produce mRNA in which complementary mRNA fragments are spliced. **(B)** RNA interference (RNAi) encapsulated in nanoparticles. Double-strand RNA encapsulated in nanoparticles fused to the cell membrane is released into the cytoplasm and binds to mRNA, which is then degraded under the mediation of RISC (RNA-induced silencing complex). **(C)** CRISPR-Cas9. In the nucleus, indels are introduced into a

transcription factor gene in the genome by a specific guide RNA, knocking out the expression of the transcription factor.

The second type of drug is small-molecule drugs that target the interaction between cofactors and transcription factors (**Figure 1.11**). For instance, small-molecule drugs (e.g., Mycro3) and peptide drugs (e.g., Omomyc) have high specificity and affinity for c-MYC, thus blocking c-MYC-MAX dimerization (454,455,466). Another example is a small-molecule drug known as Nutlins that targets the interaction between p53 and MDM2 to inhibit MDM2 function, thus preventing MDM2 from degrading p53 (456-458).

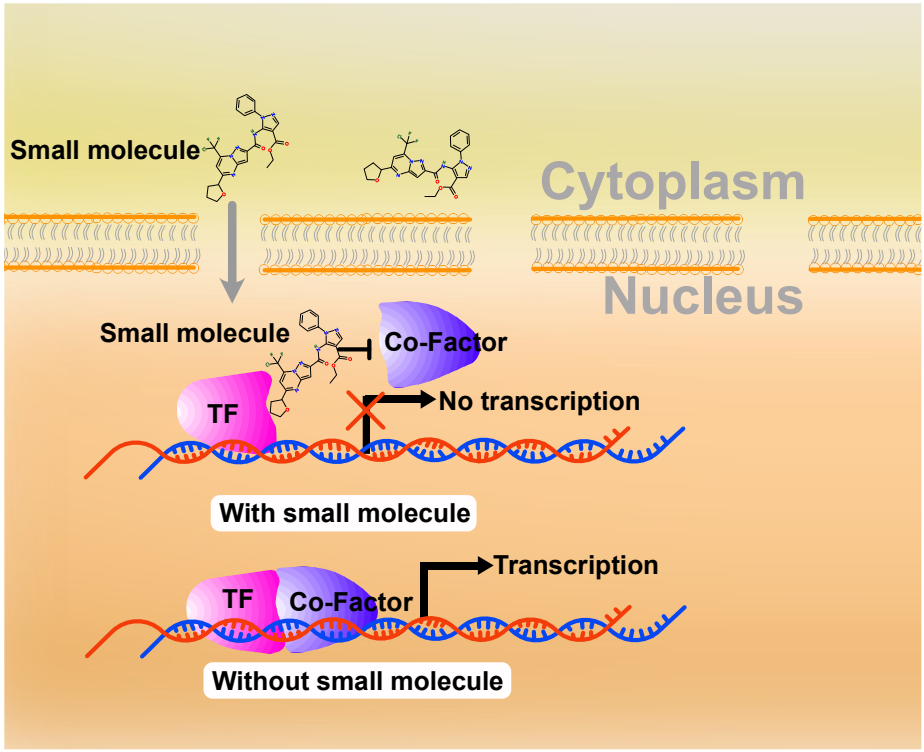

Figure 1.11 The second type of technology developed for targeting transcription factors

The second type of technology: Cofactor blocking. The synthetic small molecules prevent the binding of transcription factors (TF) and co-factors from promoting the activity of transcription factors and inhibit the activity of transcription factors.

The third type of drug is small-molecule drugs that inhibit the expression of downstream genes by preventing the binding of transcription factors to their target DNA (**Figure 1.12**). For instance, Taniguchi *et al.* developed a bioactive synthetic DNA-binding inhibitor based on hairpin pyrrole-imidazole polyamide (PIPs) that binds to the DNA-binding sequence of SOX2 to inhibit the binding of SOX2 to DNA (467).

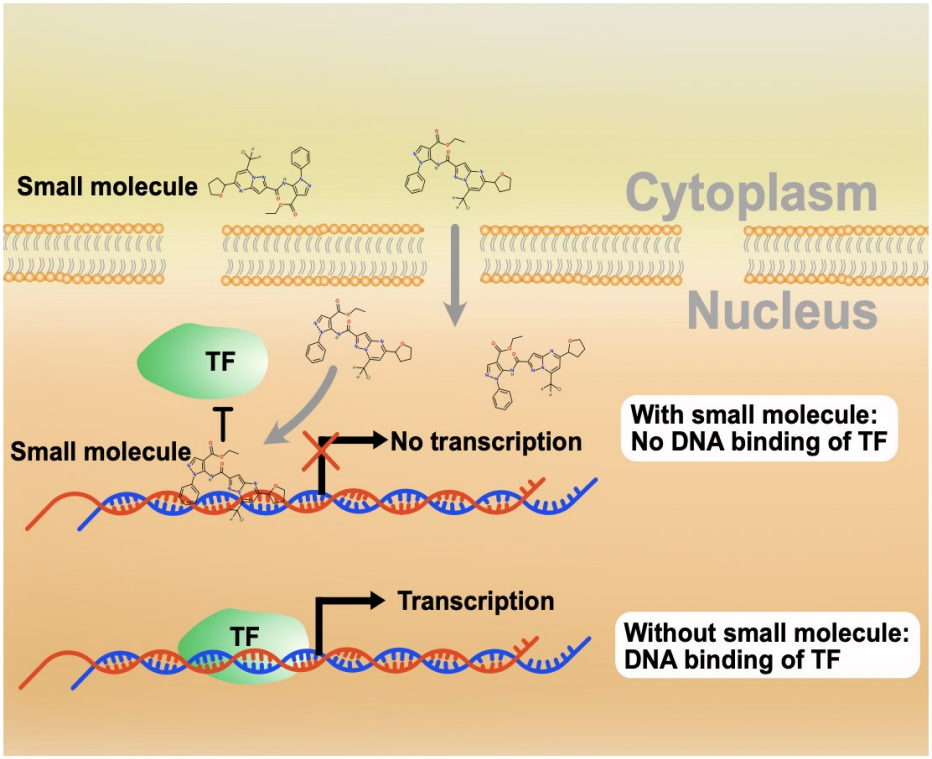

Figure 1.12 The third type of technologies developed for targeting transcription factors

The third type of technology: DNA-binding blocking. Small molecules compete with transcription factors for DNA-binding sequences to prevent transcription factors from transcribing downstream genes.

The fourth type of drug is those developed based on a popular new technology that induces protein degradation. The main principle of this technology is the use of proteasomes present in cells to degrade transcription factors (468,469). Since the 1990s, the technology of inducing protein degradation has undergone three major developments and has become increasingly practical (464,469). This preliminary technology was patented by Proteinex Inc. They designed a bifunctional molecule (proteolysis targeting chimera, PROTAC) that simultaneously recognizes the E3 ubiquitin ligase and the structural fragments of the target protein, resulting in ubiquitination and degradation of the target protein by the proteasome (**Figure 1.13A**) (464,469). This first-generation technology made it possible to degrade the target protein intracellularly, but was not of interest to pharmaceutical companies because of the poor ability of these bifunctional molecules to cross cell membranes (464).

Based on the first generation of bifunctional small molecules, the second-generation technology improved the recognition of the short amino acid sequence of E3 ubiquitin ligase VHL (Von Hippel-Lindau). The problem of poor transmembrane ability was solved by adding cell-penetrating peptide sequences.

The peptide structure of the bifunctional molecule remains different from conventional small-molecule drugs (464,470).

The third-generation technology is based on the discovery of small-molecule ligands for VHL, which makes the degradation of target proteins by small-molecule drugs practical and popular with a large number of pharmaceutical companies (459-461,464,471). More recently, studies proposed the use of an improved PROTAC and CRISPR technology, known as TRAnscription Factor TArgeting Chimeras (TRAFTACs) (**Figure 1.13B**). This technology consists of two major components, such as a kind of PROTAC known as Halo-PROTAC, which ubiquitinates the target protein, and a Cas9 protein subtype (CRISPR-associated protein 9) known as dCas9 (Cas9 endonuclease death) that is fused with an HT7-tag, a high-affinity genetic fusion tag from a modified haloalkane dehalogenase. dCas9 protein interacts with Halo-PROTAC to bind transcription factors to synthetic DNA-binding sites linked to single-guide RNA on dCas9 protein, thereby more efficiently targeting transcription factors as well as ubiquitinating and degrading transcription factor proteins (472). In brief, the fourth type of technology achieves degradation of undruggable transcription factors at the protein level, rapidly and reversibly inhibiting the effects of transcription factors without modifying the genome and avoiding the problem of off-target effects (473).

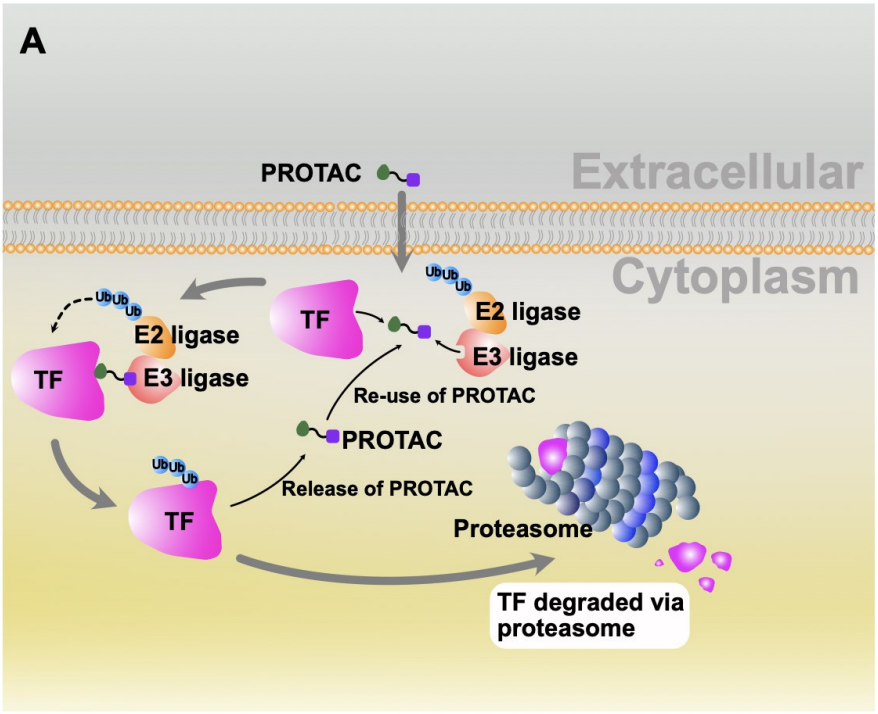
A
PROTAC
Extracellular
Cytoplasm
TF
E2 ligase
E3 ligase
Re-use of PROTAC
PROTAC
Release of PROTAC
Proteasome
TF degraded via proteasome

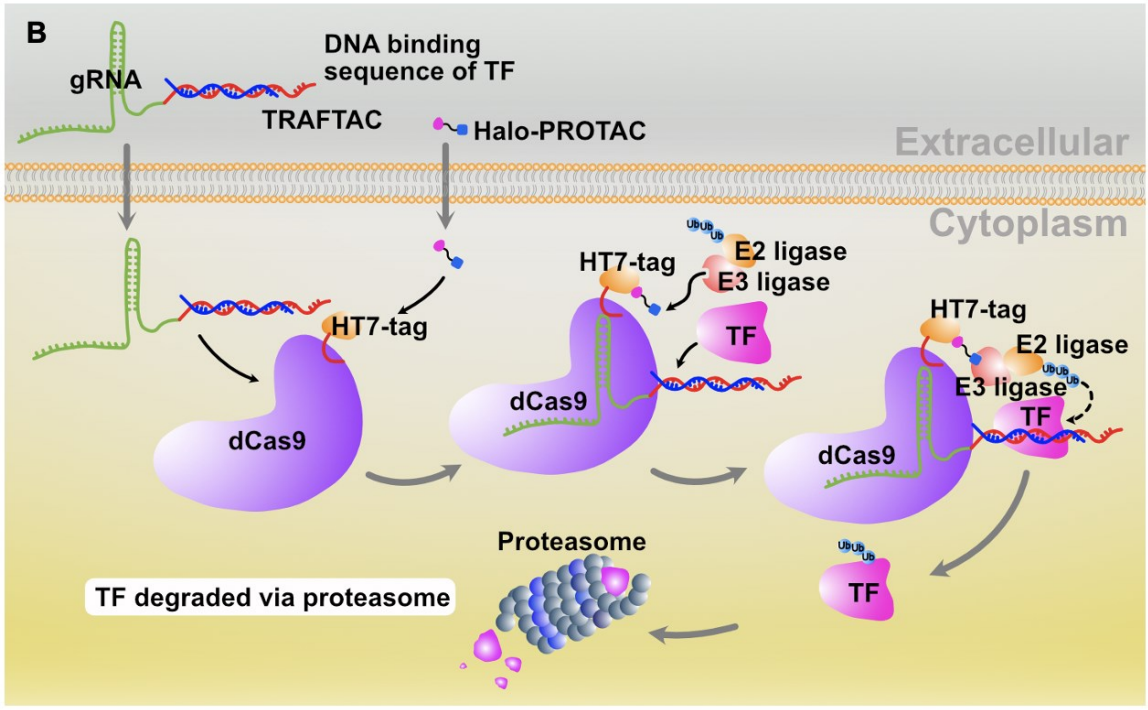
B
gRNA
DNA binding sequence of TF
TRAFTAC
Halo-PROTAC
Extracellular
Cytoplasm
HT7-tag
E2 ligase
E3 ligase
TF
dCas9
Proteasome
TF degraded via proteasome

Figure 1.13 The fourth type of technologies developed for targeting transcription factors

The fourth type of technology: **(A)** Proteolysis Targeting Chimera (PROTAC). Transcription factors are ubiquitinated and subsequently degraded by proteasome through interaction with E3 ubiquitin ligase with the help of a bifunctional small molecule or peptide (PROTAC). **(B)** TRAnscription Factor TArgeting Chimeras (TRAFTAC). In the cytoplasm, TRAFTAC (a single-guide RNA fused with a double-stranded DNA-binding sequence of a transcription factor) binds to the HT7-tag fused dCas9 (Cas9 Endonuclease Dead). The transcription factor binds to the double-stranded DNA on dCas9. The HT7-tag on dCas9 interacts with Halo-PROTAC, a bifunctional molecule that interacts with HT7-tag and E3 ubiquitin ligase, and the other end of Halo-PROTAC interacts with E3 ubiquitin ligase, leading to ubiquitination of the adjacent transcription factor and its proteasomal degradation.

The emergence of new molecular biology technologies and research by pharmaceutical companies on undruggable protein targets, which account for about 80% of proteins in humans, has made targeting transcription factors possible. To address the inability of traditional small-molecule drugs to target transcription factors, research institutions and pharmaceutical companies are targeting transcription factors to reduce the impact of oncogenic transcription factors on cancer by inhibiting gene expression, blocking upstream or downstream

interacting proteins, and directly degrading proteins. Currently, drugs targeting transcription factors are in clinical trials (**Table 1.3**).

Table 1.3 Transcription factor targeted drugs currently in clinical trials

Category	TF target	Disease	Clinical Phase	Year
TFD ODNs (decoy)	E2F	Vascular hyperplasia	2, 3	2002-2005
TFD ODNs (decoy)	NF-κB	Mild-to-moderate atopic dermatitis	1, 2	2005-2008
TFD ODNs (decoy)	STAT3	Head and neck squamous cell carcinoma	1	2008-2015
JAK1/2 inhibitor (Ruxolitinib)	STAT3	Primary myelofibrosis	3	2015-2019
JAK1/2 inhibitor (Ruxolitinib)	STAT3	Advanced cutaneous squamous cell carcinoma	2	2021-
Upstream tyrosine kinase inhibitors (AZD1480)	STAT3	Primary myelofibrosis	2	2009-2017
BET inhibitor (CPI-0610)	BET	Myelodysplastic syndromes	2	2014-2018
BET inhibitor (TEN-010)	BET	Advanced solid tumors	1	2014-2018
Bromodomain inhibitor (GSK525762)	p53	NUT gene midline carcinoma	1	2012-2020
CBP/β-catenin (PRI-724)	CBP/β-catenin	Acute myeloid leukemia, chronic myelogenous leukemia	1, 2	2012-2017
E2F1 transcription factor stimulant (ARQ-761)	E2F1	Solid tumors	1	2012-2020
MDM2 inhibitor (SAR405838)	p53	Solid tumors	1	2012-2018
KLA4 activator (APTO-253)	KLA4	Late-stage acute myelogenous leukemia	1	2014-
MDM2 inhibitor (DS-3032)	p53	Lymphoma, solid tumors	1	2013-2020
MDM2-p53 interaction inhibitor (AMG232)	p53	Acute myeloid leukemia, chronic myelogenous leukemia, solid tumors	1	2012-2017
MDM2 inhibitor (MK-8242)	p53	Solid tumors	1	2011-2018
MDM2-p53 interaction inhibitor (CGM097)	p53	Solid tumor with p53-wild type (wt) status	1	2013-2020
MDM2-p53 interaction inhibitor (RG7112)	p53	Leukemia, sarcoma	1	2007-2016
MDM2-p53 interaction inhibitor (RG7388)	p53	Recurrent plasma cell myeloma	1	2015-2019
MDM2-p53 interaction inhibitor (HDM201)	p53	Advanced solid and hematological TP53-wt tumors	1	2014-2020
Nrf2 (ABT-RTA-408)	Nrf2	Metastatic non-small-cell lung cancer, skin	1	2014-2016

Data source: ClinicalTrials.gov (http://clinicaltrials.gov/); TFD ODNs: Double-stranded transcription factor decoy (TFD) oligodeoxynucleotides (ODN).

1.5.3 The challenges of targeting transcription factors

Currently, drugs targeting transcription factors are in clinical trials, but most approaches to targeting transcription factors still face challenges. Although the first type of nucleic acid-based technology has been widely applied to target transcription factors in basic research, difficulties have been encountered in developing patient-friendly therapies. For instance, the *in vivo* environment is much more complex than the cell culture environment, and the stability of nucleic acid drugs in the blood is relatively poor. There are problems of drug concentration dilution, immunogenicity, and renal aggregation (474-476). As for the CRISPR technology, although its outstanding ease of use and broad application deserve recognition, there are still off-target effects that need to be addressed as it is a new technology similar to all nucleic acid technologies. Optimizing this technology and applying it to humans takes time (449,477,478).

The second type of technology is to interfere with the interaction between transcription factors and cofactors. The challenge of such technology comes from the discovery of co-factors of known transcription factors and the structure of the co-factor interacting sites. Only a few transcription factors, such as p53 and STAT3, have been extensively investigated. Although a large number of transcription factors have been shown to play a pivotal role in cancer, research into the mechanisms of these transcription factors is still ongoing (479-481).

The third type of technology uses small molecules that prevent transcription factors from binding to DNA sequences. The challenge with this type of technology is the lack of specificity. Since transcription factors generally belong to a large family, other members of the family may have similar DNA-binding domains or similar DNA-binding motifs, resulting in the inability to precisely target specific transcription factors (439,482). The lack of specificity reduces the efficacy of drugs targeting specific transcription factors.

The fourth type of technology is the induction of transcription factor protein degradation. Although PROTAC technology is attracting academic institutions, large pharmaceutical companies (e.g., AstraZeneca, Novartis, Bayer, and Pfizer), and biotechnology companies, it also faces challenges. These challenges are as follows:

1) In current clinical trials, drugs developed using this technology are limited to androgen degradation in prostate cancer and estrogen degradation in ER-positive breast cancer based on PROTAC technology (439).

2) The bifunctional small molecules of PROTAC require interaction with E3 ubiquitin ligase and target proteins, placing high demands on their design and optimization (468,473).

3) The dual-function nature of PROTAC is to catalyze the degradation of proteins, but the drugs themselves do not enter the degradation cycle. The pharmacokinetics and pharmacodynamics of these drugs cannot be measured by traditional evaluation approaches and new evaluation approaches are needed (483).

4) Similar to traditional small-molecule drugs, screening for effective target protein ligands is a challenge (473). Currently, E3 ubiquitin ligase ligands (e.g., VHL, cIAP, MDM2, and CRBN) are limited for the small molecule PROTAC. However, more than 600 E3 ubiquitin ligases are present in cells (468,473). Considering that ubiquitination of target proteins requires specific ubiquitin ligases, the development of more E3 ubiquitin ligase ligands might help target more transcription factor proteins.

1.6 Hypothesis and objectives

1.6.1 Rationales and hypothesis

EOC is the major subtype of ovarian cancer and the most lethal gynecological cancer. The lethality of EOC is primarily due to the challenges of lack of effective early screening, cancer recurrence, and chemoresistance (79,80). Conventional therapeutic regimens for ovarian cancer include cytoreductive surgery and platinum-based chemotherapy (83-87). However, recurrence of EOC remains inevitable. In recent years, new advances have been made in the targeted therapy for ovarian cancer. For instance, PARP inhibitors such as Olaparib, Rucaparib, and Niraparib have been approved by FDA for the treatment of advanced ovarian cancer with *BRCA1*/*2* mutations (BRCAm) (106-111). These inhibitors have shown efficacy in the treatment of BRCAm ovarian cancer. *ZIC2* is a transcription factor and co-activator that plays a role in maintaining the stemness in embryonic stem cells and liver CSCs, is upregulated in a variety of human cancers, and promotes multiple pathobiological functions (161,164-168,171). In

addition, ZIC2 overexpression has been reported to be associated with poor prognosis in patients with EOC (161). Therefore, we will examine the hypothesis that ZIC2 acting as an oncogene promotes tumorigenic phenotypes in EOC (**Figure 1.11**). If this is the case, increased ZIC2 in EOC cells promotes tumorigenic phenotypes including cell growth, cell migration, single-cell survival, anchorage-independent growth, and tumor growth. We expect that high-throughput RNA sequencing analysis of the ZIC2-regulated transcriptome will contribute to the understanding of the molecular mechanisms by which ZIC2 regulates gene expression and tumorigenic phenotypes in EOC.

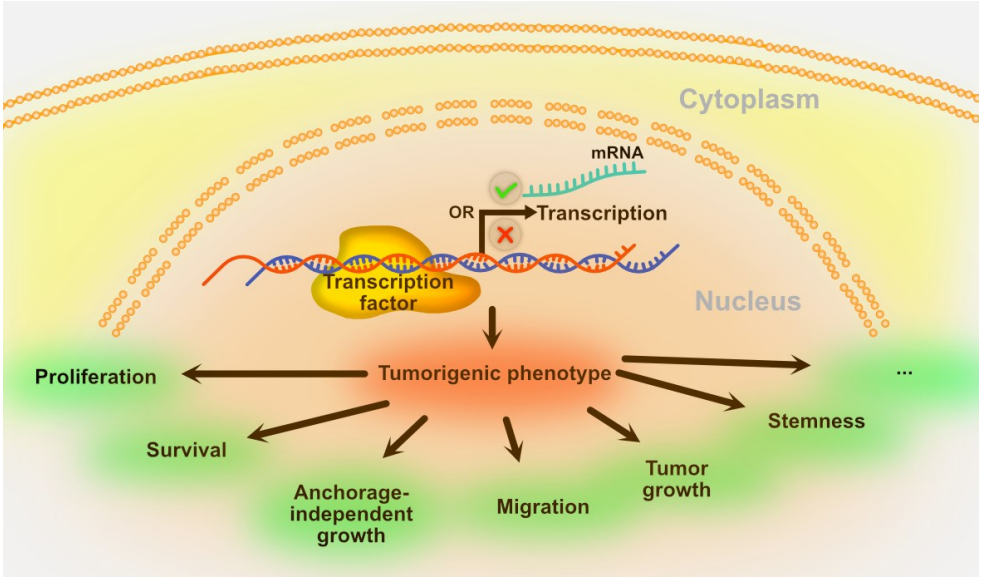

Figure 1.14 Hypothesis of ZIC2 in EOC

Transcription factor ZIC2 promotes tumorigenic phenotypes including proliferation, survival, anchorage-independent growth, migration, tumor growth, and cancer cell plasticity in EOC.

RUNX3 is another upregulated and pro-tumorigenic transcription factor in EOC (222,225,226). RUNX3 plays key roles in the development of normal tissues, such as neurogenesis, lymphocyte development, and fate determination (168,199,204-206). In some human cancers, *RUNX3* is silenced by promoter methylation and acts as a tumor suppressor gene, while *RUNX3* is upregulated and acts as an oncogene in other human cancers (207,212,216,217,225,226). Previous studies in our laboratory and Lee *et al.* showed that RUNX3 promotes tumorigenic phenotypes such as enhanced proliferation and carboplatin resistance in EOC cells (225,226). GCT is a rare subtype of ovarian cancer. Most patients with GCT are diagnosed at the early stages. However, advanced GCT and recurrent GCT are fatal (116,125). GCT is thought to originate from the granulosa cells of the ovary (116). *Runx3* has been reported to be involved in follicle development and ovulation in mice. Follicles are surrounded by granulosa cells of the ovary at the early stage of development, and *Runx3* is involved in follicular development (228,229). Current studies on GCT are limited to elucidating the methylation of the *RUNX3* gene promoter in some GCT tumor samples (484). Whether RUNX3 regulates the tumorigenic phenotypes of GCT remains to be investigated. Therefore, further understanding of the pathobiological roles of RUNX3 in GCT is still warranted for designing new therapeutic strategies. We will determine the hypothesis that RUNX3 promotes the tumorigenic phenotypes of GCT. We will test whether overexpression of RUNX3 promotes tumorigenic phenotypes of GCT, such as cell growth, anchorage-independent growth, cell

migration, and tumorigenesis, and vice versa, and whether inhibition of RUNX3 attenuates the tumorigenic phenotypes.

1.6.2 Objectives

In Chapter 3, we aimed to determine ZIC2 expression in HGSOC-PDX and HGSOC tumor samples, the effect of high or low expression of ZIC2 on the survival in patients with EOC, and the regulation of ZIC2 on the tumorigenic phenotypes. We explored the role of ZIC2 in regulating the tumorigenic phenotypes through the ZIC2-knockout (ZIC2-KO) and ZIC2-overexpression (ZIC2-OE) models of EOC. In biological functions studies, we explored the role of ZIC2 *in vitro* and *in vivo*, including cell growth, single-cell survival, migration, anchorage-independent growth, self-renewal ability, changes in the percentage of $ALDH^{high}$ and $CD133^{high}$ cells, and tumor growth in immunocompromised mice.

In Chapter 4, we aimed to assess the role of ZIC2 in regulating the transcriptome in EOC. We performed RNA-seq analyses to determine the ZIC2-regulated transcriptome in SKOV3 and OVCAR3 cells. We correlated the differentially expressed genes regulated by ZIC2 and hallmarks, biological processes, signaling pathways, and oncogenic signatures in GSEA analyses with the tumorigenic phenotypes of the corresponding cell lines. Our data suggest that the discrepancies in differentially expressed genes between the two cell lines, as well as differences in potential underlying molecular mechanisms regulated by ZIC2, might help elaborate the extensive tumor heterogeneity in EOC.

In Chapter 5, we aimed to determine the expression of *RUNX1*, *RUNX2*, and *RUNX3* in GCT tumor samples and cell lines, and apply the overexpression and inhibition of *RUNX3* in GCT cells to investigate RUNX3 functions and the potential underlying molecular mechanisms behind the tumorigenic functions of *RUNX3* in GCT.

CHAPTER 2: MATERIALS AND METHODS

2.1 Overall, Progression-Free, Post-Progression survival analysis

5-year overall survival, 5-year progression-free survival, and 5-year post-progression survival were analyzed using the online tool provided by Kaplan-Meier plotter [OVARIAN] on KMPlot.com. Expression of ZIC2-high and ZIC2-low expressions was divided by upper quartile, and the follow-up threshold was set to 60 months. The histology was set to serous, and stage was set to 2 + 3 + 4. Grades, *TP53* mutation status, and conditions for debulk and chemotherapy were set to all. Data sources and statistical data Logrank *p*-value and HR (Hazard Ratios) were provided automatically by the tool.

2.2 Patient-derived xenografts and high-grade serous ovarian cancer tumor array

The patient-derived xenograft (PDX) models used for immunohistochemistry (IHC) staining studies, PDX-550 (Oncotest^{TM} PDX OVXF 550), and PDX-899 (Oncotest^{TM} OVXF PDX 899) were originally purchased from and developed by Charles River Laboratories International, Inc. Tumor sections for both models were a generous gift from Dr. Lynne-Marie Postovit. PDX-899 was derived from a 76-year-old Caucasian woman with stage III HGSOC who had received radiation therapy prior to surgery. The tumor was well differentiated with intermediate vasculature and wild-type *TP53*. PDX-550 came from a Caucasian woman with HGSOC, but age, stage, and treatment prior to surgery were unclear. This tumor was poorly differentiated with high vasculature and mutant *TP53*. The HGSOC tumor array was a gift from Dr. Cheng Lee. There are 150 HGSOC tumor

samples on the array (individual tissue samples with less than 50% integrity were not included).

2.3 Cell lines and cell culture

Immortalized ovarian surface epithelial cells (IOSE386) were cultured in M119/MCDB105 medium (Gibico, Carlsbad, CA, USA) supplemented with 5% (v/v) FBS (Gibico, Carlsbad, CA, USA) and 1% (v/v) penicillin-streptomycin (penicillin 100 U/mL, streptomycin: 100 μg/mL, Gibico, Carlsbad, CA, USA). Immortalized fallopian tube cells (FT189) were cultured in DMEM/Hams' F12 medium (Gibico, Carlsbad, CA, USA) (1:1) supplemented with 5% (v/v) Ultroser^{TM} G serum substitute (15950-017, Sartorius, Goettingen, Germany), HEPES buffer (25 mmol/L, pH 7.2-7.5) and 1% L-glutamine. The human embryonic kidney cell line HEK293T cells were cultured in DMEM medium supplemented with 10% FBS and 1% penicillin-streptomycin.

The EOC cell lines SKOV3, A2780s, COV318, JHOS2, and CAOV3, were cultured in DMEM/Hams F12 medium supplemented with 10% FBS and 1% penicillin-streptomycin. OVCAR8 and OVCAR3 were cultured in RPMI-1640 medium (Gibco, Carlsbad, CA, USA) supplemented with 10% FBS and 1% penicillin-streptomycin. TYK-NU was cultured in EMEM medium (Gibico, Carlsbad, CA, USA) supplemented with 15% FBS, 1% penicillin-streptomycin, and 1% L-glutamine. OV90 was cultured in MCDB 105/M199 medium (1:1, Gibco, Carlsbad, CA, USA) supplemented with 15% FBS, 1% penicillin-streptomycin, and 1% L-glutamine.

The adult GCT cell line KGN and the juvenile GCT cell line COV434 were cultured in DMEM/Ham's F-12 (1:1) and DMEM medium, respectively, supplemented with 10% FBS and 1% penicillin-streptomycin. The immortalized granulosa cell line of the ovary SVOG was cultured in MCDB105/M199 medium (1:1) supplemented with 10% FBS, 1% penicillin-streptomycin, and 0.4 μg/mL hydrocortisone (Sigma-Aldrich, St. Louis, CA, USA).

FT189 cells were a gift from Dr. Lynne-Marie Postovit, originally from Dr. Ronny Drapkin (University of Pennsylvania, Philadelphia, PA, USA). A2780s and OVCAR8 cells were gifts from Dr. Benjamin Tsang (Ottawa Hospital Research Institute) and other collaborators. KGN cells were purchased from the RIKEN Cell Bank; COV434 cells were purchased from Sigma (07071909, Oakville, ON, Canada); SVOG cells were from the Canadian Ovarian Cell Bank at the BC Cancer Research Centre; and IOSE386, SKOV3, and OVCAR3 cells were from the cell stock of Fu Laboratory from ATCC (American Type Culture Collection), and COV318, JHOS2, TYK-NU, OV90, CAOV3 cell lines were obtained from the cell stock of Postovit Laboratory. All of the above cell lines were authenticated by short tandem repeat (STR).

2.4 Generation of EOC cell models: ZIC2-knockout (KO) models

The DNA sequences of the single-guide RNA of *ZIC2* exon 1 were designed by searching for DNA sequences potentially targetable by using the CRISPR Tracks function on the UCSC genome browser. G-Blocks containing the DNA sequences of the single-guide RNA were synthesized by the Integrated DNA

Technologies (IDT). These g-Blocks were then inserted into the All_in_one_CRISPR/Cas9_Laz plasmid (Addgene, #74299). This plasmid was generously provided by Dr. Postovit Laboratory. The DNA sequences submitted for synthesis of the single-guide RNAs and g-Blocks are as follows:

>Single_guide_RNA1

AGCTCGGCGTTCACGTCGCA (Forward strand: 5'-3')

>G_block_insert_for_single_guide_RNA1

ATATATCGTCTCGAACTTGAAAGTATTTCGATTTCTTGGGTTTATATATCTTGT

GGAAAGGACGAAACACCGTTTTAGAGCTAGAAATAGCAAGTTAAAATAAGG

CTAGTCC**AGCTCGGCGTTCACGTCGCA**GTTATCAACTTGAAAAAGTGGCAC

CGAGTCGGTGCTTTTTTCTAGACACAATTGCATGAAGAATCTGCTTAGGGTT

AGGCGTTTTGCGCTAGA GACGAATTAT (5'-3')

>Single_guide_RNA2

CGCGCCCGGGTTGAGCTTGA (Reverse strand: 3'-5')

>G_block_insert_for_single_guide_RNA2

ATATATCGTCTCGAACTTGAAAGTATTTCGATTTCTTGGGTTTATATATCTTGT

GGAAAGGACGAAACACC**CGCGCCCGGGTTGAGCTTGA**GTTTTAGAGCTAG

AAATAGCAAGTTAAAATAAGGCTAGTCCGTTATCAACTTGAAAAAGTGGCAC

CGAGTCGGTGCTTTTTTCTAGACACAATTGCATGAAGAATCTGCTTAGGGTT

AGGCGTTTTGCGCTAGAGACGAATTAT (5'-3')

The plasmid (All_in_one_CRISPR/Cas9_Laz) integrated with g-Block was used to transiently transfect SKOV3 and OVCAR8 cells. The plasmid contains a DNA sequence encoding the fluorescent protein mCherry. 48 hours later, the

successfully transfected mCherry-positive cells could be screened by FACS and sorted into wells of a 96-well plate, one cell per well. When enough single cells in the well were expanded, some of the cells were lysed and collected as cell lysate and DNA samples, while some of the cells were kept in cell culture. These samples were then used for subsequent genomic DNA sequencing and immunoblotting to confirm the knockout of *ZIC2* at the genomic DNA and protein levels. Based on the results of genomic DNA sequencing and immunoblotting, clonal cells with indels at the DNA level and no detectable ZIC2 at the protein level were considered ZIC2-knockout clones (i.e., SKOV3 ZIC2-KO and OVCAR8 ZIC2-KO). Those clonal cells without indels at the DNA level but with ZIC2 detected at the protein level were considered ZIC2 wild-type clones (SKOV3 WT and OVCAR8 WT).

2.5 Generation of EOC models: ZIC2-overexpression (ZIC2-OE) models

First, 2 μg plasmid mixture containing the commercial lentiviral plasmid with *ZIC2* encoding sequence (pLenti-ZIC2-C-Myc-DDK-P2A-Puro, Cat#RC220798L3, Origene) and the packaging plasmid psPAX2 (Addgene, #12260) as well as the envelope plasmid pMD2.G (Addgene, #12259) in 1:2:2 molar stoichiometry was transiently transfected into HEK293T cells in a well of 6-well plate using Fugene HD Transfection Reagent (E2311, Promega, Madison, WA, USA). The cells were cultured for three days. The medium supernatant was then filtered through a 0.45 μm Millipore syringe-driven filter (pore size: 0.45 μm, SLHAR33SS, Millipore, Bedford, MA, USA) and collected after three days, and the medium supernatant was added with a final concentration of 8 μg/mL of polybrene (TR-1003-G, Sigma-

Aldrich, St. Louis, CA, USA). The culture medium for OVCAR3 and A2780s cells was replaced with the medium supernatant containing lentivirus. Since the plasmid contains a DNA insert encoding puromycin N-acetyl-transferase (PAC), puromycin (P8833-10MG, Sigma-Aldrich, St. Louis, CA, USA) was used to screen transduced cells to obtain stable ZIC2-overexpressed cells (e.g., A2780s ZIC2-OE and OVCAR3 ZIC2-OE cells). Regarding the generation of the corresponding control cells, a commercial lentiviral plasmid, which is an empty vector (pLenti-C-mGFP-P2A-Puro, Cat#PS100093V, Origene), was adopted and subjected to the same treatments as OVCAR3 and A2780s cells to screen and obtain stable cells with empty vector (A2780s vector and OVCAR3 vector cells).

2.6 Generation of GCT models: KGN RUNX3-overexpression (KGN RUNX3-OE) and COV434 dnRUNX3-overexpression (COV434 dnRUNX3-OE) models

The KGN cells with empty vector (KGN vector) and RUNX3-overexpressed KGN cells (KGN RUNX3-OE) were generated by stable transduction of the empty vector or RUNX3-FLAG using retroviral plasmids as previously described in the report by Barghout *et al.* (226). The COV434 cells with empty vector (COV434 vector) and dnRUNX3-overexpressed COV434 cells (COV434 dnRUNX3-OE) were generated by stable transduction of the pcDNA3.1 (empty vector) plasmid or the pcDNA-FLAG-RUNX3 (1-187) plasmid. PcDNA-FLAG-RUNX3 (1-187) plasmid expressed a truncated form of the RUNX3 protein that contained the runt domain but lacks the C-terminal transactivation domain and was a dominant-

negative form of RUNX3 (dnRUNX3). PcDNA-FLAG-RUNX3 (1-187) plasmid was kindly provided by Yoshiaki Ito at the Cancer Science Institute of Singapore.

2.7 Immunoblotting

Protein expression of the genes was determined by immunoblotting. Briefly, cells were washed with cold 1X PBS followed by 1X RIPA buffer (50 mM Tris pH7.4, 150 mM NaCl, 1% (w/v) sodium deoxycholate, 0.1% (w/v) sodium dodecyl sulfate, 1 mM EDTA, 10 mM $Na_4P_2O_7$, 10 mM Na_3VO_4, 1% (w/v) Triton X-100 with 1X protease inhibitor cocktail (11697498001, Sigma-Aldrich, St. Louis, CA, USA). Cell lysates were then collected and subjected to brief sonication. After centrifugation at 13,000 rpm for 15 minutes at 4°C, supernatants were collected and protein concentration was determined using the DC™ Protein Assay Kit (5000111, Bio-Rad Laboratories, Hercules, CA, USA) according to the manufacturer's instructions. The protein concentration of different samples was adjusted to be consistent according to the protein concentration of the corresponding samples by balancing the volume of cell lysate with additional RIPA buffer. Protein samples were loaded onto 7% (w/v), 10% (w/v) or 12.5% (w/v) SDS-polyacrylamide gel (stacking gel: 4X Upper Buffer, 30% (w/v) Bis-Acrylamide, 10% (w/v) ammonium persulfate (APS), tetramethyl ethylenediamine (TEMED, T9281, Sigma-Aldrich, St. Louis, CA, USA), ddH_2O; separating gel: 4X Lower Buffer, 30% (w/v) Bis-Acrylamide, 10% (w/v) APS (Ammonium persulfate, A3678, Sigma-Aldrich, St. Louis, CA, USA), TEMED, and ddH_2O). Proteins were separated by electrophoresis and then wet transferred to nitrocellulose membranes at 100V for

about 90 minutes. Regions of the membrane indicated by the protein ladder for the proteins of interest were separated as strips and then incubated with indicated primary antibodies (1:1,000) overnight. Immunoblotting was performed using anti-ALDH1A1 (B-5, sc-374149, Santa Cruz Biotechnologies, Santa Cruz, CA, USA), anti-ZIC2 (ab150404, Abcam, Cambridge, MA, USA), anti-cyclin D2 (ab207604, Abcam, Cambridge, MA, USA), anti-RUNX1 (#4334, Cell Signaling Technology, Danvers, CA, USA), anti-RUNX2 (D1H7, #8486, Cell Signaling Technology, Danvers, CA, USA), anti-RUNX3 (ab40278, Abcam, Cambridge, MA, USA), anti-REBP2β/CBFβ (141,4,1) (sc-56751, Santa Cruz Biotechnologies, Santa Cruz, CA, USA), anti-MMP3 (D7F5B, #14351, Cell Signaling Technology, Danvers, CA, USA), anti-LIN28B (D4H1, 11965S, Cell Signaling Technology, Danvers, CA, USA), anti-IMP1 (D33A2, #8482, Cell Signaling Technology, Danvers, CA, USA), anti-ROR2 (D3B6F, #88639, Cell Signaling Technology, Danvers, CA, USA), anti-PARP (46D11, #9532, Cell Signaling Technology, Danvers, CA, USA), anti-β-actin (A5441, Sigma-Aldrich, St. Louis, CA, USA), anti-β-Tubulin (ab59680, Abcam, Cambridge, MA, USA), and anti-FLAG M2 (F1804, Sigma-Aldrich, St. Louis, CA, USA) antibodies.

The next day, the strips were then incubated with IRDyde 800CW anti-rabbit (926-32211, LI-COR Bioscience, Cambridge, UK) or anti-mouse (926-32210, LI-COR Bioscience, Cambridge, UK) secondary antibody (1:15,000) for 1 hour at room temperature, and then images of immunoblots were obtained using an Odyssey IR scanner (LI-COR Bioscience, Cambridge, UK) and quantified through Image Studio Lite software (LI-COR Bioscience, Cambridge, UK).

2.8 Immunohistochemistry

The concentration of anti-ZIC2 (ab150404, Abcam, Cambridge, MA, USA), anti-Ki-67 (8D5, #9449, Cell Signaling Technology, Danvers, CA, USA), and anti-ALDH1A1 antibodies (D9Q8E, #54135S, Cell Signaling Technology, Danvers, CA, USA) were optimized to 1:1,000, 1:500, and 1:1,000, respectively, for immunohistochemistry staining assay. Briefly, sections of HGSOC PDX tumors and HGSOC tumor microarray, as well as tumors from the SKOV3 ZIC2-KO (i.e., SKOV3 WT and SKOV3 ZIC2-KO) and OVCAR3 ZIC2-OE (e.g., OVCAR3 vector and OVCAR3 ZIC2-OE) models, were formalin-fixed and paraffin-embedded, deparaffinized, and hydrated. Afterward, the sections were subjected to heat-induced antigen retrieval using Dako Target Retrieval Solution (pH6) (S2369, DAKO Corp, Carpinteria, CA, USA) in a beaker at 100°C for 20 minutes, followed by incubation with Dako Protein Block Serum-Free Reagent (X090930-2, DAKO Corp, Carpinteria, CA, USA) for 10 minutes. Subsequently, tumors sections from the SKOV3 ZIC2-KO model were incubated with anti-ZIC2, anti-Ki-67, and anti-ALDH1A1 antibodies, respectively, and sections of HGSOC PDX tumors and HGSOC microarray were incubated with anti-ZIC2 antibody for 1 hour at 25 °C in a humidified chamber. Afterward, the tissue sections were washed with 1X TBS-T and then incubated with Dako anti-rabbit IgG (HRP) (P0448, DAKO Corp, Carpinteria, CA, USA) for 30 minutes at room temperature. Next, the sections were incubated with Dako DAB+ (3,3'-diaminobenzidine) chromogen (GV825, DAKO Corp, Carpinteria, CA, USA) to develop color, followed by incubation with

hematoxylin for 1 minute. Images of tumor sections were obtained on an Aperio Digital Pathology Slide Scanner AT2 (Leica Microsystems, Bradford, Ontario, Canada).

2.9 Soft agar colony-formation assay

The cells were mixed with specific 2X culture media and an equal volume of 0.7% (w/v) agar in ddH_2O and layered on a base layer made with 2X specific culture medium and an equal volume of 1.2% (w/v) agar in ddH_2O in a six-well plate. To form colonies, cells were incubated in a cell incubator under 5% CO_2 at 37°C for 2 to 3 weeks. 5,000 cells of EOC cells or 2,000 KGN cells were mixed in the top agar layer per well. Visualization was performed with 1% (w/v) crystal violet solution in 20% methanol and then images of the colonies were obtained, and colonies containing more than 50 cells were counted under an EVOS fl microscope (Advanced Microscopy Group, Bothell, WA, USA). The number of colonies was acquired by counting 18 random fields under a microscope. The colony size of the captured images was measured by ImageJ software (ImageJ1, NIH, Bethesda, MD, USA), and the parameter "Threshold" was set to "Auto" and other settings were defaulted for all measured images. In the measurement, only the size of the entire colonies (colony area) in the image was measured, and the colony area was expressed in μm^2. Non-intact colonies at the edges of the image were excluded.

2.10 Neutral red uptake assay

Cell growth was determined by neutral red uptake assay. The experimental procedure for neutral red uptake assay was obtained from Repetto *et al.* (485). Briefly, cells were seeded in wells of a 96-well plate and incubated in a cell incubator for 1, 3, 5, 7 days. When a specific time point was reached, the medium was aspirated and replaced with fresh media containing 1X neutral red dye (33 µg/mL, N7005, Sigma-Aldrich, St. Louis, CA, USA) and then incubated in the cell culture incubator for 3 hours. The media was then aspirated, washed with 1X PBS to remove excess dye, and lysed with de-staining solution (50% (v/v) ethanol and 1% (w/v) acetic acid in ddH_2O) to release the dye from the cells. The absorbance of the 96-well plates was measured at a wavelength of 540 nm using a FLUORstar Omega microplate reader (BMG LABTECH GmbH, Offenburg, Germany).

Regarding SKOV3, OVCAR8, A2780s cells, cells were seeded at a density of 1,000 cells per well. Regarding OVCAR3 cells, cells were seeded at a density of 3,000 cells per well. Regarding KGN and COV434 cells, cells were seeded at a density of 2,000 cells per well. The relative cell growth was calculated using the following equation: relative cell growth = the absorbance on the test day / the absorbance on the first day × 100%.

2.11 Clonogenic assay

The single-cell survival of the cells was determined by clonogenic assay. Briefly, 200 cells per well were seeded in wells of a six-well plate and allowed to form colonies for 7 to 12 days. When colonies with a cell count greater than 50

were observed under the microscope, the cells were stained with crystal violet. In brief, the medium was aspirated, and the colonies on the plate were washed with 1X PBS and fixed with 4% (w/v) formaldehyde solution in PBS for 20 minutes at room temperature. The fixed colonies were washed with 1X PBS and stained with 5% (w/v) crystal violet solution in 20% methanol. The number of colonies was counted manually from the images taken with an imager. The size of the colonies (colony area) was measured as described in section 2.9.

2.12 Transwell migration assay

5×10^4 cells were seeded into the top chamber of a polyethylene terephthalate (PET) Falcon cell culture insert (pore size: 8.0 μm, Fisher Scientific, MA, USA) and cultured in FBS-free medium. The Inserts were placed in wells of a 12-well plate containing culture medium supplemented with 10% FBS. Cells were allowed to migrate through the pores in the membrane in the wells of the 12-well plate for 24 hours. Afterward, the cells on the membrane were fixed with 4% formaldehyde in PBS and stained with 1% crystal violet solution in 20% methanol for 15 minutes. The unmigrated cells on the upper side of the membrane were removed with a cotton swab. The migrated cells on the bottom side of the membrane were imaged under a microscope with 4X magnification. Migrated cells were counted in 18 random fields on the membrane surface covering each insert.

2.13 ALDEFLUOR assay

The percentage of $ALDH^{high}$ EOC cells was determined by ALDEFLUOR assay using the ALDEFLUOR Assay Kit (01700, STEMCELL Technologies, Vancouver, BC, Canada). Briefly, the single-cell suspension was generated by trypsinization, filtration, centrifugation, and resuspension in the provided ALDEFLUOR buffer. After cell counting, 1×10^6 cells were prepared in 1 mL ALDEFLUOR buffer. Add 5 µL of activated FITC-conjugated ALDEFLUOR Reagent to the cells and immediately mix and dispense equal volume into $ALDH^-$ sample tube containing ALDH inhibitor DEAB (diethylaminobenzaldehyde) reagent and $ALDH^+$ sample tube without any reagent. Immediately incubate the $ALDH^-$ and $ALDH^+$ sample tubes in a 37°C water bath for 40 minutes. Afterward, cells were centrifuged and resuspended in 0.5 mL ALDEFLUOR buffer for flow cytometry or FACS. 10,000 events per sample were collected using a blue laser at 530 nm wavelength (B530) to detect the FITC signal of the cells. The percentage of $ALDH^{high}$ cells was based on DEAB reagent-treated samples as $ALDH^{low}$ cells were gated, i.e., cells without DEAB reagent measured with a stronger B530 signal than cells with DEAB reagent were considered $ALDH^{high}$ cells, otherwise $ALDH^{low}$ cells. $ALDH^{high}$ and $ALDH^{low}$ cells sorted by FACS were immediately subjected to subsequent experiments, such as limiting dilution sphere formation assay.

2.14 Flow cytometry with anti-CD133 antibody

The percentage of $CD133^{high}$ OVCAR3 cells was determined by flow cytometry, and $CD133^{high}$ and $CD133^{low}$ cells were separated by FACS. Briefly,

single-cell suspensions were generated by trypsinization, filtration, centrifugation, and resuspension in flow cytometry staining buffer (FC001, R&D system, Minneapolis, Minnesota, USA). 1×10^6 cells each were prepared for negative controls (Non-stained), samples with Zombie Aqua only incubated with only Zombie Aqua dye (e.g., a cell viability dye for exclusion of dead cells, Zombie Aqua Fixable Viability Kit, 423101, BioLegend, San Diego, CA, USA), samples with CD133 only incubated with CD133/2 PE-conjugated (REA816) antibody (130-112-315, Miltenyi Biotec, Bergisch Gladbach, Germany), and samples with Zombie Aqua and anti-CD133 antibody (Zombie Aqua & CD133) incubated with Zombie Aqua dye and ant-CD133 antibody. Samples with Zombie Aqua only and samples with CD133 only were used as Fluorescence Minus One (FMO) controls. For samples with the Zombie Aqua only and samples with Zombie Aqua and anti-CD133 antibody, cells were treated with Zombie Aqua dye (1:100) for 15 minutes at room temperature, then washed with 1X PBS and resuspended in flow cytometry staining buffer. Samples with Zombie Aqua and anti-CD133 antibody and samples with anti-CD133 antibody only were treated with 2 µL of anti-CD133 PE-conjugated antibody (recommended concentration, 1:50) and placed in an ice bath in the dark for 30 minutes. Afterward, all samples were centrifuged at 250 × g for 5 minutes, washed with cold 1X PBS, and resuspended in flow cytometry staining buffer for flow cytometry or FACS. The signal of Zombie Aqua was detected with a violet laser at a wavelength of 525 nm (V525), and the signal of anti-CD133 PE-conjugated antibody was detected with a yellow laser at a wavelength of 586 nm (Y586). Dead cells and debris were excluded, and

$CD133^{high}$ and $CD133^{low}$ cells were gated based on the samples with Zombie Aqua only (negative control). For instance, cells in samples with Zombie Aqua and anti-CD133 antibodies are considered $CD133^{high}$ cells if the Y586 signal is stronger than cells in the samples with Zombie Aqua only, otherwise, they are considered $CD133^{low}$ cells. $CD133^{high}$ and $CD133^{low}$ cells sorted by FACS were immediately used in subsequent experiments, such as limiting dilution sphere formation assay.

2.15 Immunofluorescence

SKOV3, OVCAR8, OVCAR3, and A2780s cells were seeded and allowed to attach onto glass coverslips for about 24 hours. Afterward, cells were fixed with 4% formaldehyde in 1X PBS for 15 minutes, permeabilized with 0.25% (w/v) Triton X-100 (X100-100ML, Sigma-Aldrich, St. Louis, CA, USA) for 5 minutes, and then treated with 5% goat serum (Gibico, Carlsbad, CA, USA) for protein blocking for 1 hour at room temperature. Cells were incubated with anti-ZIC2 antibody (1:1000) at 4°C overnight. The next day, the cells were washed three times with 1X PBS-T for 5 minutes each, and then incubated with Alexa 594-conjugated donkey anti-rabbit secondary antibody (1:400, R37119, Invitrogen, Carlsbad, CA, USA). Afterward, cells were washed three times with 1X PBS-T for 5 minutes each, stained with 1 µg/mL DAPI (5.08741.0001, CalBiochem, San Diego, CA, USA) for 2 minutes, and then coverslips were mounted onto microscope slides with Dako Fluorescent Mounting Medium. Images were acquired with a Zeiss LSM 710 confocal microscope at 20X magnification using Zeiss ZEN software.

2.16 Limiting dilution sphere formation assay

The self-renewal ability of EOC cells was determined by limiting dilution sphere formation assay. Limiting dilution sphere formation assay was performed by respectively seeding the following number of cells per well in the well of 96-well plate with ultra-low attachment: 200, 150, 120, 100, 75, 50, 25, 20, 10, 5, 2, and 1. The cells were cultured in serum-free culture medium (DMEM/Ham's F-12 medium for SKOV3 and A2780s cells, and RMPI-1640 medium for OVCAR8 and OVCAR3 cells) supplemented with human recombinant EGF (epidermal growth factor, 20 ng/mL, 236-EG, R&D Systems, Minneapolis, MN, USA), human recombinant bFGF (basic fibroblast growth factor, 20 ng/mL, F3685-25UG, Sigma-Aldrich, St. Louis, CA, USA), and 2% (v/v) B27 supplement (Invitrogen, Carlsbad, CA, USA). After 14 days, the number of spheres in each well was counted, and the images of spheres were obtained under an EVOS fl microscope. The size of spheres was measured as described in section 2.9. In the measurement, only the size of the entire spheres (sphere area) in the photos was measured, and the sphere area was expressed in μm^2. Non-intact spheres at the edges of the image were excluded.

2.17 Scratching assay

The mobility of the KGN vector and KGN RUNX3-OE cells was determined by scratch assay. Cells were cultured on 6 cm plates until they reached 100% confluence. A p200 pipette tip was used to generate a scratch on the cell monolayer. Debris and detached cells were removed by washing three times with

culture medium containing 0.2% FBS. The culture medium was then replaced with fresh culture medium containing 0.2% FBS and the cells were allowed to migrate to the center of the scratched area. Images of migrating cells in the scratched area were obtained under an EVOS fl microscope 24 hours after the scratch was completed and the wound areas were quantified using Image J software (ImageJ1, NIH, Bethesda, MD, USA).

2.18 Mouse xenograft models

For SKOV3, 2.5×10^6 cells were injected subcutaneously into four 8-week-old female NOD-scid IL2R-gamma null (NSG) mice (SKOV3 WT) and five 8-week-old female NSG mice (SKOV3 ZIC2-KO), respectively. Mice were palpated weekly. The volume of the transplanted tumor was measured 19 days after injection and used to generate the tumor growth curves. 39 days later, when tumors exceeded 1 cm^3 in size, mice were euthanized, and tumors were then extracted, imaged, and weighed.

For OVCAR3, 1.0×10^7 cells were injected subcutaneously into four 15-week-old female NSG mice (OVCAR3 vector) and four 15-week-old female NSG mice on both flanks. Mice were palpated weekly. The volume of the tumor was measured 52 days after injection. 74 days later, the tumors exceeded 1 cm^3 in size and the mice were euthanized, then the tumors were extracted, imaged, and weighed. The repeated xenograft models of OVCAR3 cells were performed under the same conditions. 89 days later, the mice were euthanized, then the tumors were extracted and imaged in the repeated experiment.

For KGN, 2×10^7 cells of KGN with empty vector (KGN vector) and RUNX3-overexpressed KGN (KGN RUNX3-OE) cells were injected subcutaneously into the left and right flanks of six 7.5-weeks-old female NSG mice, respectively, 12 injections in total. Regarding the injections, mice were injected twice at the same sites over an interval of two weeks and then intermittently observed for tumor formation, as previously described by Kim *et al.* (486). 170 days after the first injection, mice were euthanized and dissected at the time of tumor formation. The tumors were then imaged and collected for subsequent experiments.

Animal experiments related to EOC cells (SKOV3 and OVCAR3) and KGN cells were conducted under the guidance of the Canadian Animal Health Council and approved by the University of Alberta Science Animal Care and Use Committee (study title: Targeting the pro-tumorigenic signaling pathways in ovarian cancer, approval number: AUP000004444) on Feb 12 of 2018 and on May 12 of 2015 (study title: Analysis of novel therapies for the treatment of granulosa cell tumors, approval number: AUP00001435), respectively.

2.19 Genomic DNA sequencing

The DNA fragment covering part of the 5'-UTR and first exon of ZIC2 of the gDNA sequence was amplified with PCR using AmpliTaq Gold™ 360 Master Mix (4398881, Applied Biosystems™, Foster City, CA, USA) with a pair of primers (5'-ATACACTTTGGTTCTCCGCCT-3' and 5'-AAGTCCCGGGTGGAG TTGA-3'). The amplified DNA products were separated by electrophoresis, and the target DNA bands (size: 666 bp) were isolated and extracted using QIAquick Gel Extraction

Kit (Qiagen GmBH, Hilden, Germany) according to the manufacturer's instructions. The purified DNA fragments are integrated into a pCR™4-TOPO® TA vector using the TOPO® TA Cloning® Kit (K4575-01SC, Invitrogen, Carlsbad, CA, USA). The vector with DNA fragment was transformed into One Shot® competent cells and the transformed competent cells were coated on LB plates containing 50 µg/mL ampicillin and pre-coated with X-gal (20 mg/mL, Sigma-Aldrich, St. Louis, CA, USA). Afterward, the plates were incubated in a 37°C cell incubator for no more than 16 hours. White but not blue colonies on the plates were collected and incubated overnight in liquid LB medium containing 50 µg/mL ampicillin. The next day, plasmid DNA from amplified colonies in liquid LB medium was purified using the QIAprep® Spin Miniprep Kit (27104, Qiagen GmbH, Hilden, Germany) according to the manufacturer's instructions. Sanger sequencing of the plasmid DNA with M13-forward primer (5'-GTAAAACGACGGCCAG-3') and M13-reverse primer (5'-CAGGAAACAGCTATGAC-3') was performed through the Molecular Biology Facility at the University of Alberta.

2.20 RNA extraction, cDNA synthesis, and reverse transcription-quantitative PCR

Cells cultured in 60 mm culture plates at about 80% confluence were washed with 1X PBS, lysed, and homogenized with TRIzol Reagent (15596026, Invitrogen, Carlsbad, CA, USA), and then chloroform (0.2 mL per 1 mL TRIzol Reagent) was added for phase separation. After centrifugation at 12,000 × g for 15 minutes at 4°C, the upper phase containing RNA was collected. Next, the upper

phase liquid was collected and separated with 100% isopropanol (0.5 mL per 1 mL of TRIzol Reagent). Subsequently, the upper phase liquid was collected after incubation at room temperature for 10 minutes and centrifugation at 12,000 × g for 10 minutes at 4°C. The RNA was precipitated at the bottom of the tube and then washed with 75% ethanol (1 mL per 1 mL TRIzol Reagent). Afterward, the supernatant was removed and the RNA was dried and dissolved in RNase-free water. The RNA concentration was measured with a DU730 Spectrophotometer (Beckman Coulter, Indianapolis, IN, USA).

cDNA synthesis was prepared using SuperScript II Reverse Transcriptase (18064022, Invitrogen, Carlsbad, CA, USA) supplemented with RNaseOUT Recombinant Ribonuclease Inhibitor (10777019, Invitrogen, Carlsbad, CA, USA) and 25 mM dNTP as well as random primers according to the manufacturer's instructions and performed on a Veriti 96-well thermal cycler (Life Technologies, Gaithersburg, MA, USA). RT-qPCR reactions were prepared with SYBR Select Master Mix (4472903, Applied Biosystems™, Foster City, CA, USA), the primers of specific genes, 50 ng cDNA, and ddH_2O and performed on a Mastercycler ep Realplex real-time PCR system (Eppendorf, Mississauga, Ontario, Canada). Relative fold changes in mRNA expression of specific genes were calculated by normalizing GAPDH followed by control samples according to the 2(-Delta Delta C(T)) method published by Schmittgen *et al.* (487). PCR primers are listed in **Table 2.1**.

Table 2.1 The DNA sequences of primers for specific genes

Gene Symbol	Forward (5'-3')	Reverse (5'-3')
ALDH1A1	CAGGAACAGTGTGGGTGAAT	CTCTCCCAGTTCTCTTCCATTTC
GAPDH	GGACCTGACCTGCCGTCTAGAA	GGTGTCGTTGAAGTCAGAG
IGF2BP1	CCGAAACACCTGACTCCAAA	CTCCTCCTTGAGTTTGCCATAG
LIN28B	GGGAAGACAGGAAGCAGAAT	GAGGAAACGGTGGTGATGTA
MMP3	CTCGTTGCTGCTCATGAAATTG	TCAGGTCTGTGAGTGAGTGATA
CCND2	TTCCCTCTGGCCATGAATTAC	GGGCTGGTCTCTTTGAGTTT
ROR2	CCAACGGGATGAAGACCATTA	GAACCCATCCTCGTGGTAATC
RUNX1	ACTATCCAGGCGCCTTCACCTACT	TAGTACAGGTGGTAGGAGGGCGAG
RUNX2	ACGAATGCACTATCCAGCCACCTT	ATATGGAGTGCTGCTGGTCTGGAA
RUNX3	TGGCAGGCAATGACGAGAACTACT	TGAACACAGTGATGGTCAGGGTGA
ZIC2	CCGTTCCAGTGTGAGTTTGA	GTAGGACTTGTCGCACATCTT

2.21 RNA preparation for RNA-sequencing

RNA extraction from SKOV3 WT and SKOV3 ZIC2-KO cells, as well as the OVCAR3 vector and ZIC2-OE cell lines was performed using the Qiagen RNeasy Mini Kit (74104, Qiagen GmbH, Hilden, Germany) according to the manufacturer's instructions. Briefly, cells cultured in 60 mm culture plates at about 80% confluence were lysed with buffer RLT provided in the kit and then homogenized using a QIAshredder homogenizer (Qiagen GmbH, Hilden, Germany). Afterward, ethanol was added to the homogenized cell lysate. The total RNA was bound to an RNeasy Mini Spin Column and the remaining DNA was eliminated by DNase digestion with an RNase-free DNase Set (79254, Qiagen GmbH, Hilden, Germany). The DNase-treated RNA was then washed and eluted and the RNA concentration was measured using the Qubit RNA BR (Broad Range) Assay Kits (Q10210, Invitrogen,

Carlsbad, CA, USA) on a Qubit™ Fluorometer (Invitrogen, Carlsbad, CA, USA). 0.5 µg of RNA from each sample was submitted to the McGill University and Genome Quebec Innovation Center for Illumina HiSeq (SKOV3) and NOVAseq (OVCAR3).

2.22 Processing of RNA-sequencing data

RNA samples prepared from SKOV3 (SKOV3 WT and ZIC2-KO) and OVCAR3 cells (OVCAR3 vector and ZIC2-OE) were submitted to the McGill University and Genome Quebec Innovation Center for cDNA library construction and high-throughput sequencing. Briefly, the quality of the RNA was determined by an Agilent bioanalyzer. NEB/KAPA libraries were then prepared and sequenced by Illumina HiSeq or NOVAseq. Post-sequencing quality checks of reads and removal of adapter sequences were completed by FastQC and Skewer software, respectively. Reads were aligned to the GRCh37/Hg19 human reference genome using STAR (a fast RNA-seq read mapper). Refseq annotation was used to perform read quantification using FeatureCounts. Differentially expressed genes were determined by the expression values of paired samples (SKOV3 WT vs. ZIC2-KO cells, or OVCAR3 vector vs. ZIC2-OE cells) using exact test within the edgeR package. Differentially expressed genes with FDR< 0.05 were considered significant.

2.23 Gene Set Enrichment Analysis

Differentially expressed genes with FDR< 0.05 were included in Gene Set Enrichment Analysis (GSEA). The analysis was performed using GSEA 4.1.0 software, and the sources of gene set collections were selected as follows: hallmark gene sets (h.all.v7.4.symbols.gmt), ontology gene sets: biological processes (c5.go.bp.v7.4.symbols.gmt), signaling pathways (curated gene sets: canonical pathways, c2.cp.v7.4.symbols.gmt), and oncogenic signature gene sets (c6.all.v7.4.symbols.gmt). All enriched gene sets with FDR< 0.25 were considered significant according to the recommendations of the documentation by the MIT Broad Institute: https://software.broadinstitute.org/cancer/software/gsea/wiki/index.php/Main_Page.

2.24 ZIC2-ChIP-seq and histone-ChIP-seq datasets

ChIP-seq datasets for the study of mouse embryonic stem cells on ZIC2 and histone modifications, the study of human embryonic kidney cell line HEK293 with eGFP-ZIC2 overexpression on ZIC2, and the study of human colon cancer cell line HCT116 with wild-type ZIC2 and ZIC2-knockout on ZIC2 were obtained from the Gene Expression Omnibus (GEO) DataSets. The datasets of mouse embryonic stem cells were obtained with accession number: Series GSE61188. The datasets of HEK293 with eGFP-ZIC2 overexpression were obtained with accession number: Series GSE105882. The datasets of HCT116 with wild-type ZIC2 and ZIC2-knockout were obtained with accession number: Series GSE127960. The information of the datasets was visualized by IGV_2.8.9.

2.25 Statistic analysis

Data are shown as mean ± SD of at least three independent experiments unless otherwise stated. Statistical analyses were generated using the GraphPad Prism 5 (GraphPad Software, La Jolla, CA, USA). Data were considered statistically significant when one-way ANOVA values were defined as $p < 0.05$.

CHAPTER 3: The role of ZIC2 in regulating tumorigenic phenotypes of EOC

3.1 Introduction

Ovarian cancer is the most deadly gynecologic malignancy, and is ranked fifth among all gynecologic cancer deaths worldwide (57). Most EOC patients are diagnosed at advanced stages due to the lack of screening tests and methods for early detection (16,58-60,65-67). Conventional therapeutic regimens for EOC are cytoreductive surgery and chemotherapy (83-87). However, most EOC patients relapse after primary treatment and are frequently accompanied by chemoresistance (97,98). The presence of CSCs in tumors is one cause of chemoresistance (250-252,261,263,264,273). CSCs are cancer cells with properties similar to normal stem cells and are characterized by the potential for self-renewal and differentiation, as well as tumorigenesis and metastasis. EOC is classified into four major EOC subtypes based on histological characteristics, including serous, endometrioid, clear cell, and mucinous carcinomas. These subtypes are believed to originate in different tissues and have different gene expression profiles (55,56).

The transcription factor ZIC2 is considered an oncogene in multiple cancers (161,163-169). ZIC2 is expressed during embryonic development and is highly expressed in the brain and testis in adults (160-162,169). In humans, heterozygous mutations in *ZIC2* gene cause holoprosencephaly (HPE) (144-146); in mice, mutations in the *Zic2* gene cause behaviors associated with schizophrenia (157,158). In a variety of human cancers, upregulation of ZIC2 has been associated with the promotion of tumorigenic phenotypes, including increased cell proliferation, cell migration, invasion, angiogenesis, tumor growth, and metastasis

(161,166,169,170). In addition, ZIC2 has shown the ability to regulate stem cell-associated genes (169,171). For instance, in mouse ESC, ZIC2 regulates the expression of stem cell-associated genes (171). In human liver CSCs, *ZIC2* is upregulated and directly regulates the expression of stem cell gene *OCT4* (169). In EOC, *ZIC2* is upregulated and has been shown to be associated with poor patient prognosis (163). The role of ZIC2 in regulating tumorigenic phenotypes in EOC has not been explored in depth. In this study, we tested the hypothesis that ZIC2 plays a pro-tumorigenic role in EOC. Herein, we show that ZIC2 promotes tumorigenic phenotypes in EOC cells that naturally express ZIC2 and propose that ZIC2 may be a potential therapeutic target for EOCs that naturally express ZIC2. However, the tumorigenic functions of ZIC2 in EOC are cell-context dependent.

3.2 Results

3.2.1 *ZIC2* expression in EOC and its association with the survival in EOC patients

One study showed that *ZIC2* is upregulated in EOC tumors and is associated with poor prognosis in patients (163). To determine *ZIC2* expression in EOC, we first analyzed the mRNA expression levels of *ZIC2* using existing ovarian cancer datasets, including the Lu Ovarian, the Bittner Ovarian, and the Tothill Ovarian datasets from the Oncomine database (Oncomine.org). Among these datasets, the Lu Ovarian dataset was the only one containing normal ovarian surface epithelial tissues. The Lu Ovarian dataset showed that the relative mRNA expression of *ZIC2* was variable in all EOC samples compared to the normal ovarian surface epithelium, except for the mucinous subtype (**Figure 3.1A**). Our

analysis showed that *ZIC2* expression was higher in some EOC samples of the serous subtype than in the other three subtypes. Due to the limited number of tumor samples in this dataset, we further analyzed the Bittner Ovarian and the Tothill Ovarian datasets, which have more EOC tumor samples. Analysis of the Bittner Ovarian dataset showed that the relative mRNA expression of *ZIC2* in EOC tissues was largely variable, except for the mucinous subtype. We found relatively high expression of *ZIC2* in some samples of the endometrioid and serous subtypes (**Figure 3.1B**). The Tothill Ovarian dataset had the largest number of EOC samples. Consistent with the analysis of the Lu Ovarian and Bittner Ovarian datasets, these samples from the Tothill Ovarian dataset also showed large-scale variation in *ZIC2* expression, with only a proportion expressing relatively high levels of *ZIC2* (**Figure 3.1C**).

Collectively, our analysis demonstrates that ZIC2 expression in EOC samples is variable, with a proportion of EOC samples expressing high levels of *ZIC2*, especially in some endometrioid and serous samples, in agreement with the findings by Marchini *et al.* (163).

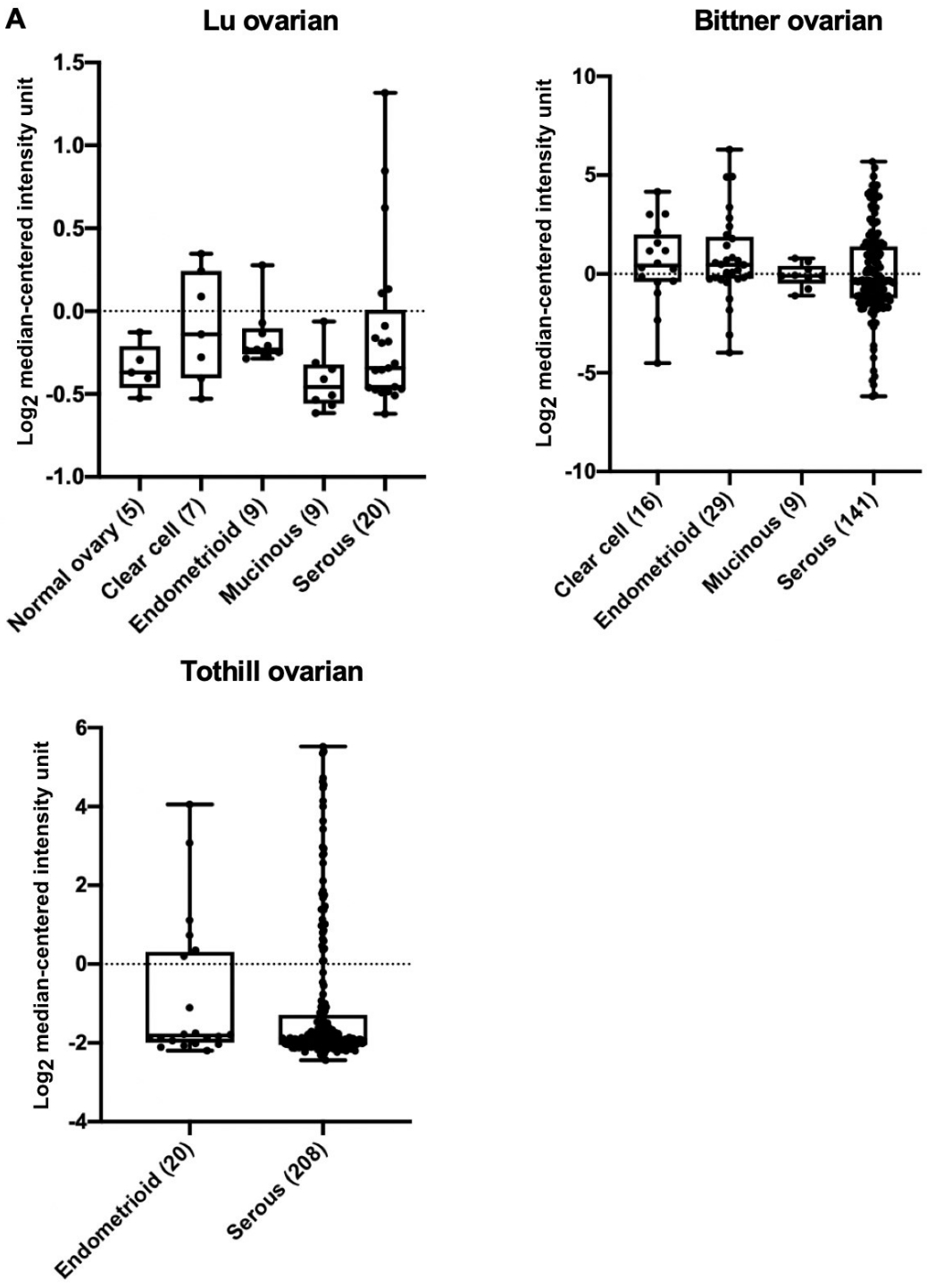

Figure 3.1 The *ZIC2* mRNA expression is variable in EOC patient samples

ZIC2 mRNA expression was analyzed in normal ovarian tissues (ovarian surface epithelium) and in samples of different EOC subtypes from the Oncomine datasets

(Oncomine.org). Relative *ZIC2* mRNA expression levels are shown as Log_2 median-centered intensity unit. The number of samples in each group is shown in parentheses.

Next, we determined the expression of *ZIC2* in tumor samples from patients with different stages of EOC. We analyzed the available staging data from the Bittner Ovarian and Tothill Ovarian datasets (**Figure 3.2**). The data showed that the expression levels of *ZIC2* were variable in tumor samples from patients at all stages, particularly in patients with stage I, III, and IV EOC, and some tumor samples from patients with stage III and IV EOC expressed relatively high levels of *ZIC2*. Marchini *et al*. also showed that the average relative *ZIC2* mRNA expression levels were higher in tumors from stage III EOC patients than in tumors from stage I EOC patients (163). However, our analysis did not show a higher average expression of *ZIC2* in tumors from stage III EOC patients than in tumors from stage I EOC patients. This difference may be related to the limited number and source of EOC samples (n = 232) used in the study by Marchini *et al.* (163).

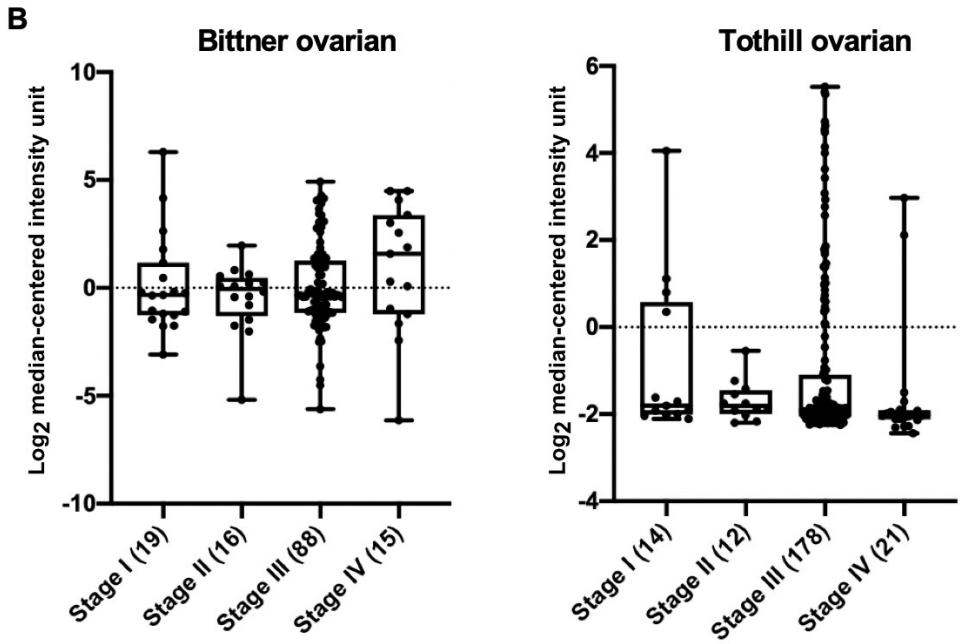

Figure 3.2 *ZIC2* expression is variable in EOC samples of all stages

The mRNA expression levels of *ZIC2* in tumor samples from patients with different stages of EOC from the Bittner Ovarian and Tothill Ovarian datasets (Oncomine.org) were analyzed. Relative *ZIC2* mRNA expression level is shown as Log_2 median-centered intensity unit. The number of samples in each group is shown in parentheses.

We further analyzed the association between *ZIC2* expression and the 5-year overall survival, 5-year progression-free survival, and 5-year post-progression survival in EOC patients using a Kaplan-Meier Plotter (KMplot.com) (**Figure 3.3**) (488). Since patients with early-stage (stage I) EOC usually have a good prognosis, we excluded data from patients with stage I EOC (489). Because only a small number of EOC patients had relatively high *ZIC2* expression, we divided the patients into *ZIC2* high and low groups by upper quartile based on the mRNA

expression levels and adopted ROC (Receiver-Operating Characteristic) analysis for survival analysis (**Figure 3.1 and 3.2**).

The results showed that the 5-year overall survival (p = 0.022) and 5-year post-progression survival (p = 0.017) were significantly shorter in patients with high *ZIC2* expression than in those with low *ZIC2* expression. In terms of 5-year overall survival, the median survival was 11 months shorter in patients with high *ZIC2* expression than in patients with low *ZIC2* expression (33 months vs. 44 months). In terms of 5-year post-progression survival, the median survival was 10.7 months shorter in patients with high *ZIC2* expression than in patients with low *ZIC2* expression (29.7 months vs. 40.4 months). However, we did not find any difference in 5-year progression-free survival between patients with high *ZIC2* expression and those with low *ZIC2* expression (15.9 months vs. 15 months).

In summary, this analysis indicates that *ZIC2* expression is variable in EOC samples and that high *ZIC2* expression is associated with poor overall and post-progression survival in EOC patients.

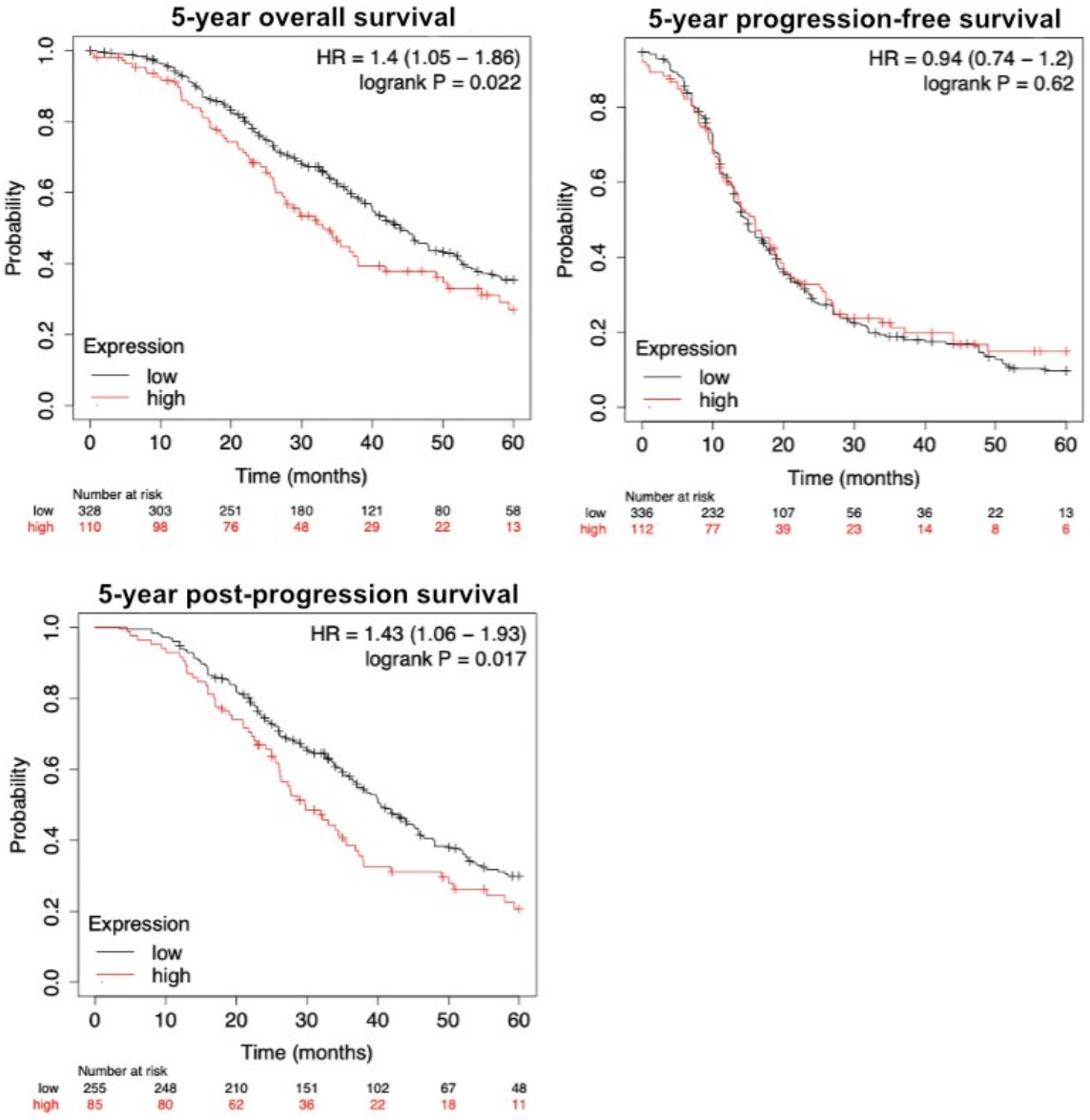

Figure 3.3 High *ZIC2* expression is associated with poor 5-year overall survival and 5-year post-progression survival

The Kaplan-Meier plots show 5-year overall survival, 5-year progression-free survival, and 5-year post-progression survival for EOC patients with high *ZIC2* expression (red line) and low *ZIC2* expression (black line) in the tumors. Number at risk showed the number of EOC patients with high *ZIC2* expression (red) and

low *ZIC2* expression (black) in the tumor that were still alive at the corresponding time points. HR (Hazard Ratio) and the significance values (Logrank *p*-value) were calculated automatically. Patient survival and *ZIC2* mRNA expression data were provided by KMplot.com. Data for analysis were from stage II, III, and IV EOC patients.

3.2.2 ZIC2 is expressed in the HGSOC-PDX and the HGSOC-tumor microarray

To further examine ZIC2 expression in EOC tumors, we carried out immunohistochemistry (IHC) staining to detect ZIC2 expression in two patient-derived xenografts (PDXs) and one HGSOC tumor microarray. PDX-899 and PDX-550 are models created by the Charles River Laboratories International, Inc for oncology experiments that differ in *TP53* status, cell differentiation, and vasculature.

IHC staining showed that ZIC2 protein expression was detected in PDX-550 but not in PDX-899 (**Figure 3.4A**). PDX-899 is well differentiated with moderate vasculature and moderate expression of wild-type *TP53*. PDX-550 is poor differentiated with high vasculature and moderate expression of mutant *TP53* (i.e., C17F, C44F, C83F, C137F, C165F, and C176F). In PDX-550, ZIC2-positive cells were detected in the cystic tumor tissue, while the surrounding mouse-derived fibroblasts were not stained. The results showed that ZIC2 was expressed in HGSOC-PDX.

We further determined ZIC2 expression in one HGSOC-tumor microarray (HGSOC-TMA) containing 150 different HGSOC tumor samples using IHC staining.

IHC staining showed ZIC2 expression in a few samples (5 of 150 samples), consistent with our findings from the analyzed Oncomine datasets, indicating that only a small number of EOC samples had high levels of ZIC2 expression (**Figure 3.4B**).

Taken together, these data suggest that ZIC2 is expressed in a subset of tumor samples from EOC patients.

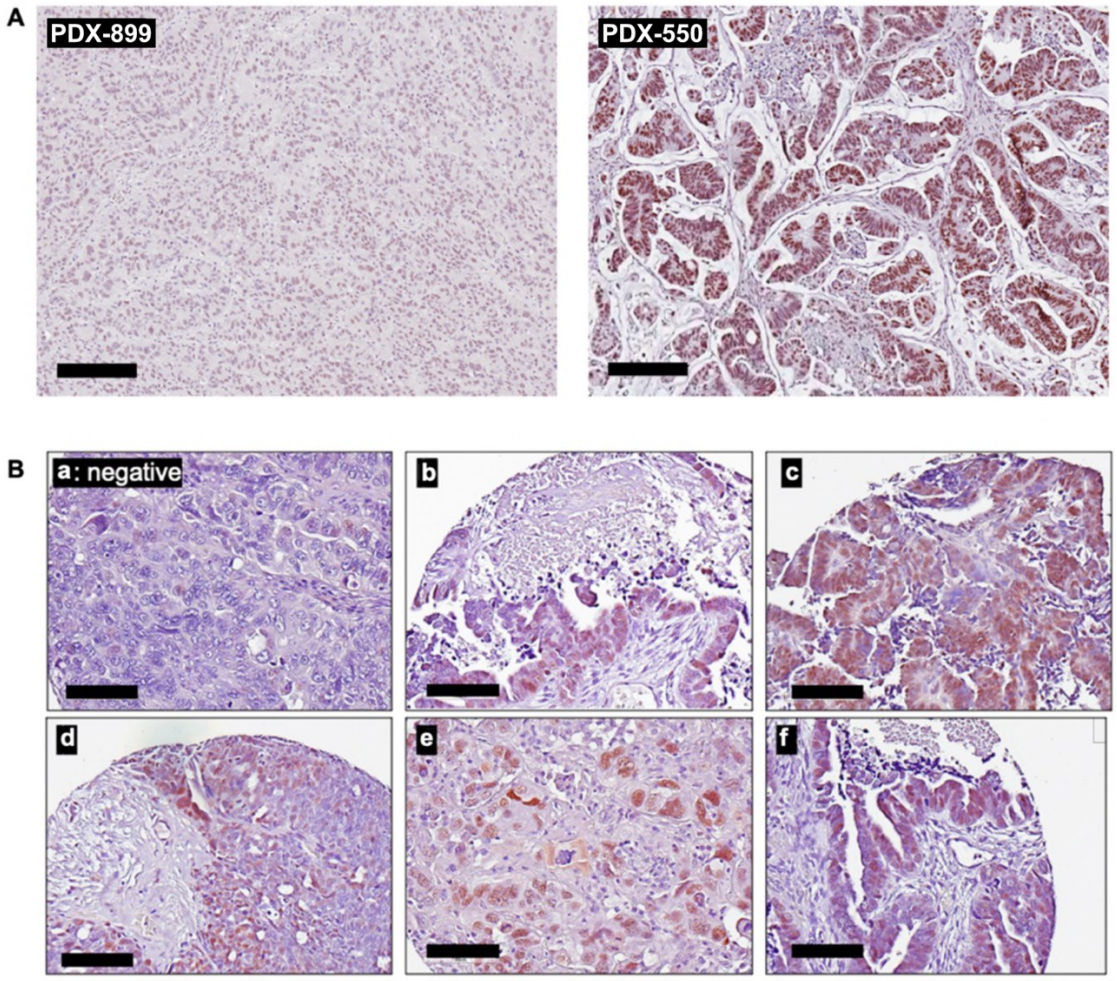

Figure 3.4 ZIC2 is expressed in HGSOC-PDX and HGSOC-TMA samples

(A) Protein expression of ZIC2 in the two HGSOC-PDXs (PDX-899 and PDX-550) was detected by IHC staining. Magnification: 10X. Scale bar = 200 μm. **(B)** Protein expression of ZIC2 in the HGSOC tumor microarray was detected by IHC staining.

Image **(a)** shows ZIC2-negatively stained tissue. Images **(b to f)** show ZIC2-positively stained tissues. Unfortunately, the corresponding clinical data for the sample were not available. Magnification: 10X. The scale bar = 100 μm.

3.2.3 ZIC2 expression in EOC cell lines

Marchini *et al.* showed that ZIC2 is expressed in multiple EOC cell lines (163). To determine whether ZIC2 is expressed in EOC cell lines, we performed immunoblotting (**Figure 3.5A**). Ovarian surface epithelial cells and fallopian tube epithelial cells are considered the origin of EOC (40,490-492). In our analysis, we included a non-tumorigenic immortalized ovarian surface epithelial cell line IOSE386 and an immortalized fallopian tube epithelial cell line FT189. The EOC cell lines we examined included the endometrioid carcinoma cell lines SKOV3 and A2780s, as well as the HGSOC cell lines COV318, OVCAR8, TYKNU, OV90, JHOS2, OVCAR3, and CAOV3 (493,494). As shown in **Figure 3.5A**, ZIC2 was expressed in a subset of cell lines, including SKOV3, COV318, OVCAR8, TYKNU, OV90, and JHOS2 cells, but not in IOSE386, FT189, A2780, OVCAR3, and CAOV3 cells. Among the cell lines that naturally express ZIC2, SKOV3 expresses the highest level of ZIC2.

Next, to further compare the mRNA expression levels of *ZIC2* in these nine EOC cell lines, we analyzed the relative *ZIC2* mRNA levels in ovarian cancer cell lines available in the Cancer Cell Line Encyclopedia database (CCLE, https://portals.broadinstitute.org/ccle) (**Figure 3.5B**). *ZIC2* expression information was available for 47 ovarian cancer cell lines in the CCLE database. Of note, the

mRNA expression levels of *ZIC2* in these nine cell lines were consistent with the immunoblotting results (**Figure 3.5A**). The relative mRNA expression of *ZIC2* in SKOV3, COV318, OVCAR8, TYK-NU, and OV90 cells was above 0 (median central intensity). Consistent with the immunoblotting results, SKOV3 showed the highest expression of *ZIC2* in these nine EOC cell lines. The relative mRNA expression of *ZIC2* was below 0 in A2780s, JHOS2, OVCAR3, and CAOV3 cells.

Overall, these data, as well as previous analyses of the Oncomine dataset and IHC staining of HGSOC-TMA samples, suggest that *ZIC2* expression is variable in EOC and highly expressed in a subset of EOC cells and tissues.

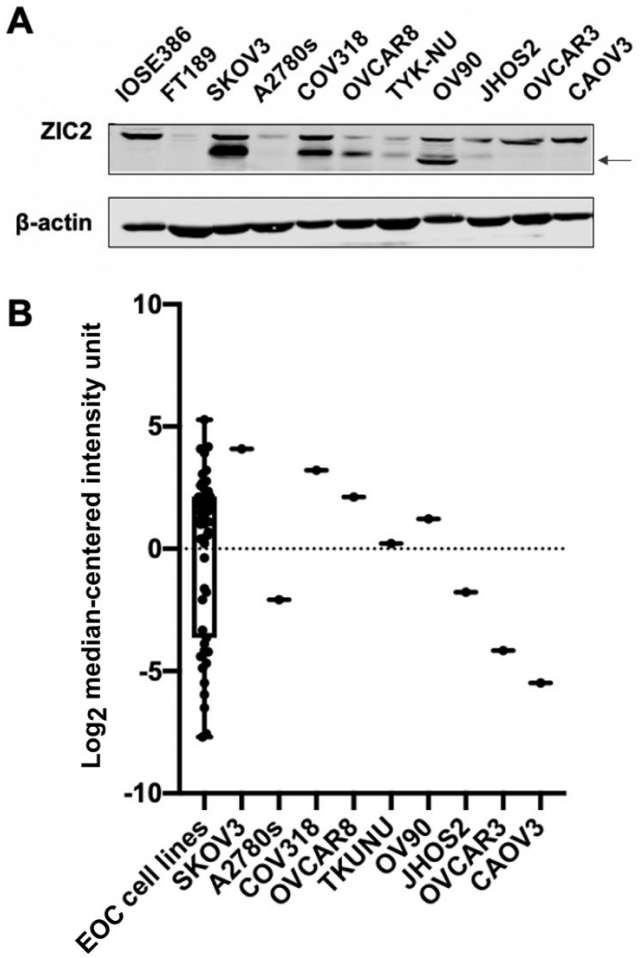

Figure 3.5 *ZIC2* is expressed in the EOC cell lines

(A) Protein levels of ZIC2 in the indicated cell lines were detected by immunoblotting. The band indicated by the arrow is ZIC2. The upper band is non-specific. β-actin is used as a loading control. **(B).** Relative *ZIC2* mRNA expression in 9 EOC cell lines from 47 ovarian cancer cell lines in the CCLE database. mRNA expression of *ZIC2* was shown as Log_2 median-centered intensity unit. Box plot shows the relative mRNA expression of *ZIC2* in 47 ovarian cancer cell lines. Data source: CCLE.

3.2.4 Generation of EOC models: ZIC2-KO and ZIC2-OE models

We showed that *ZIC2* was highly expressed in a subset of EOC tumors and that high *ZIC2* expression was related to the poor overall and post-progression survival in EOC patients. Emerging research demonstrated that ZIC2 promotes tumor progression in human cancers. Next, we determined whether ZIC2 promotes tumorigenic phenotype in EOC. We selected the cell lines SKOV3 and OVCAR8 that naturally express ZIC2 to generate ZIC2-knockout (ZIC2-KO) models and the cell lines OVCAR3 and A2780s that naturally do not express ZIC2 to generate ZIC2-overexpression models (ZIC2-OE). To obtain ZIC2-KO models, we knocked out the ZIC2 expression in these cells using CRISPR-Cas9 technology. We performed DNA sequencing and immunoblotting to identify ZIC2-KO clones and ZIC2 wild-type (WT) clones. These WT clones were used as the corresponding controls for the ZIC2-KO models.

We selected three WT clones (SKOV3 WT) and three ZIC2-KO clones (SKOV3 ZIC2-KO) in SKOV3 cells, as well as three ZIC2 WT clones (OVCAR8 WT clones) and three ZIC2-KO clones (OVCAR8 ZIC2-KO) in OVCAR8 cells. Genomic DNA sequencing confirmed ZIC2 mutations in the SKOV3 and OVCAR8 ZIC2-KO clones, including frameshift mutations or the introduction of an early stop codon in *ZIC2* exon 1 (**Table 3.1**). No *ZIC2* mutations were detected in SKOV3 and OVCAR8 WT clones (sequencing data not shown).

Table 3.1 The DNA sequencing results of ZIC2-knockout (ZIC2-KO) single-cell clones

Cell lines	Allele-1	Allele-2	Category of mutation
SKOV3 ZIC2 KO clone 1	**55 bp deletion:** 99982247 to 99982301, *Homo sapiens*, chromosome 13, GRCh38.p13 Primary Assembly, Sequence ID: NC_000013.11, forward strand	**The same as allele-1**	Frameshift (both alleles)
SKOV3 ZIC2 KO clone 2	**5 bp deletion:** 99982296 to 99982300, *Homo sapiens*, chromosome 13, GRCh38.p13 Primary Assembly, Sequence ID: NC_000013.11, forward strand	**16 bp deletion:** 99982287 to 99982302, *Homo sapiens*, chromosome 13, GRCh38.p13 Primary Assembly, Sequence ID: NC_000013.11, forward strand	Frameshift (both alleles)
SKOV3 ZIC2 KO clone 3	**1 bp deletion:** 99982140, AND **54 bp insertion** between 99982300 and 99982301, *Homo sapiens*, chromosome 13, GRCh38.p13 Primary assembly, Sequence ID: NC_000013.11, forward strand	**204 bp insertion:** 99982300 to 99982301, *Homo sapiens*, chromosome 13, GRCh38.p13, Primary Assembly, Sequence ID: NC_000013.11, forward strand	Insertion contains early stop codon (both alleles)
OVCAR8 ZIC2 KO clone 1	**2 bp deletion:** 99982247 to 99982248, *Homo sapiens*, chromosome 13, GRCh38.p13, Primary Assembly, Sequence ID: NC_000013.11, forward strand	**1 bp deletion:** 99982247, *Homo sapiens*, chromosome 13, Grch38.p13, Primary Assembly, Sequence ID: NC_000013.11, forward strand	Frameshift (both alleles)
OVCAR8 ZIC2 KO clone 2	**5 bp deletion:** 99982296 to 99982300, *Homo sapiens*, chromosome 13, GRCh38.p13, Primary Assembly, Sequence ID: NC_000013.11, forward strand	**1 bp insertion:** between 99982300 and 99982301, *Homo sapiens*, chromosome 13, GRCh38.p13, Primary Assembly, Sequence ID: NC_000013.11, forward strand	Frameshift (both alleles)
OVCAR8 ZIC2 KO clone 3	**1 bp deletion:** 99982247, *Homo sapiens*, GRCh38.p13, Primary Assembly, Sequence ID: NC_000013.11, forward strand	**The same as allele-1**	Frameshift (both alleles)

In addition, we confirmed that ZIC2 protein was detected in SKOV3 WT and OVCAR8 WT cells, but not in SKOV3 ZIC2-KO and OVCAR8 ZIC2-KO cells by immunoblotting (**Figure 3.6A**). In addition, immunofluorescence showed that ZIC2 was presented in the nuclei of SKOV3 WT and OVCAR8 WT cells but not in SKOV3 ZIC2-KO and OVCAR8 ZIC2-KO cells (**Figure 3.6B**). Hence, the WT and ZIC2-KO clones of SKOV3 and OVCAR8 cells were confirmed by genomic DNA sequencing, immunoblotting, and immunofluorescence. In this study, three WT or three ZIC2-KO clones were mixed in a 1:1:1 ratio and used for all the experiments.

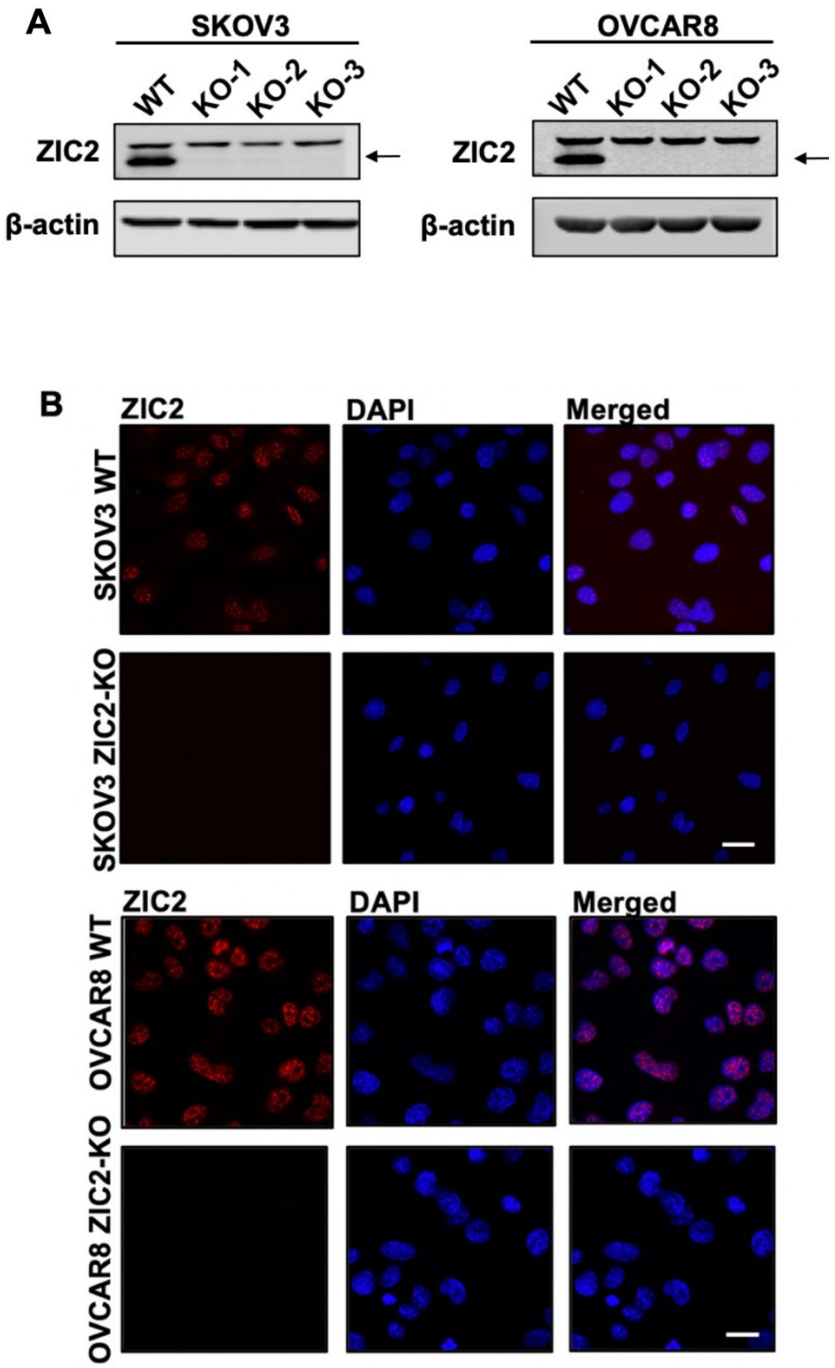

Figure 3.6 The protein expression of ZIC2 in the ZIC2-KO models of SKOV3 and OVCAR8 cells

(A) WT represents a mixture of three SKOV3 WT or OVCAR8 WT clones in a 1:1:1 ratio. KO-1, KO-2, and KO-3 represent three ZIC2-KO clones. β-actin was used as

a loading control. **(B)** Immunofluorescence showed the expression and localization of ZIC2 in SKOV3 and OVCAR8 cells. WT: mixture of three WT clones; KO: mixture of three ZIC2-KO clones. Magnification: 20X. Scale bar = 10 μm.

Next, we generated and confirmed stable ZIC2-overexpressed (ZIC2-FLAG, carboxyl-terminus FLAG-tag) cells (i.e., OVCAR3 ZIC2-OE and A2780s ZIC2-OE) and their respective control cells (i.e., OVCAR3 vector and A2780s vector). Expression of ZIC2-FLAG in the ZIC2-OE cells was confirmed by immunoblotting using an anti-FLAG antibody (**Figure 3.7A**). Similar to ZIC2 in SKOV3 WT and OVCAR8 WT cells, overexpressed ZIC2-FLAG was located in the nuclei of OVCAR3 ZIC2-OE and A2780s ZIC2-OE cells as determined by immunofluorescence using anti-ZIC2 antibody (**Figure 3.7B**). ZIC2 was not detected in OVCAR3 and A2780s vector cells by immunoblotting and immunofluorescence.

In summary, these data confirmed the knockout and overexpression of ZIC2 in the ZIC2-OE models of OVCAR3 and A2780s cells, respectively. Furthermore, we confirmed that ZIC2 is localized in the nucleus, consistent with the role of ZIC2 as a transcription factor.

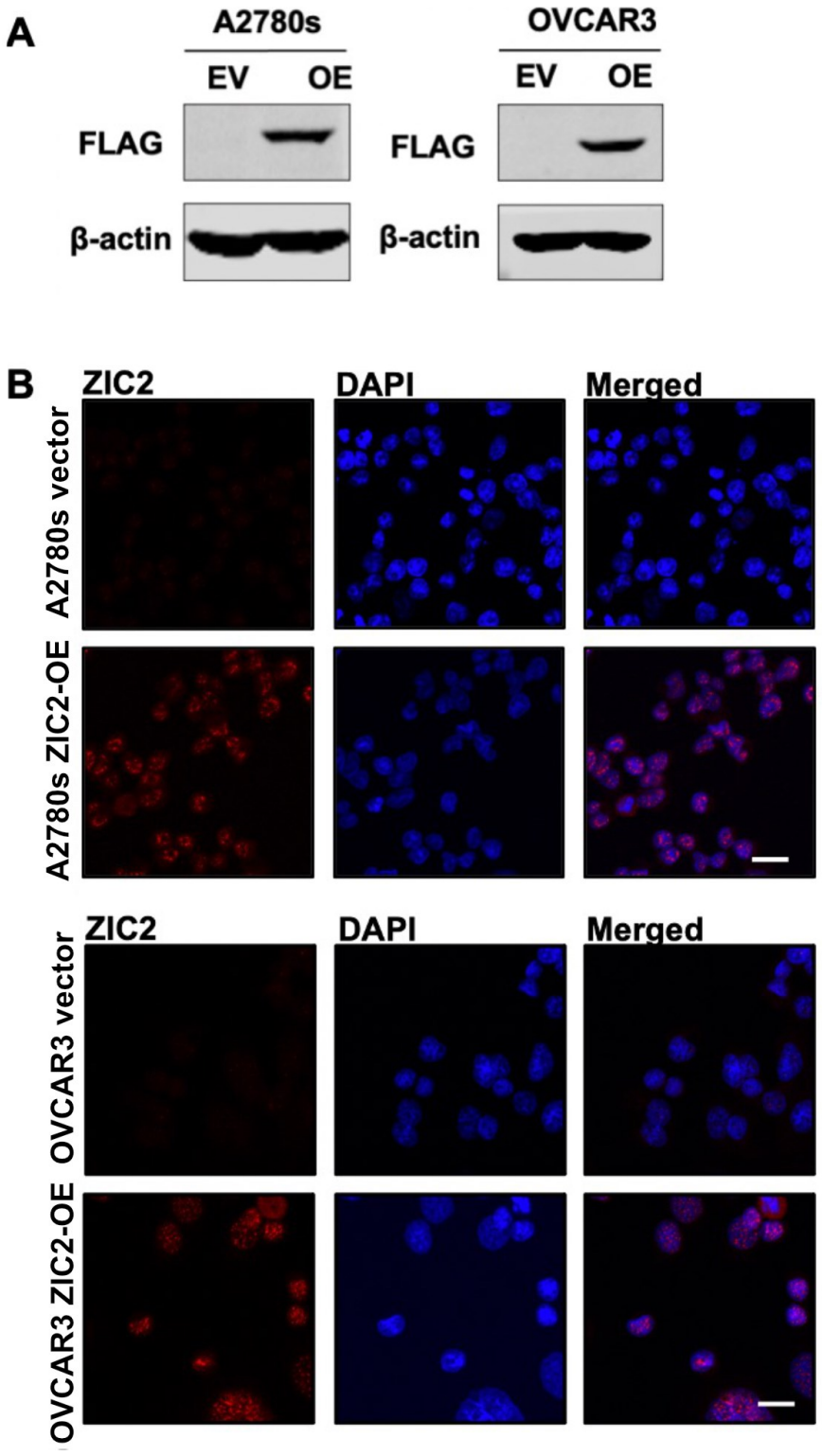
A
A2780s
OVCAR3
EV
OE
EV
OE
FLAG
β-actin
FLAG
β-actin
B
ZIC2
DAPI
Merged
A2780s vector
A2780s ZIC2-OE
ZIC2
DAPI
Merged
OVCAR3 vector
OVCAR3 ZIC2-OE

Figure 3.7 The expression of ZIC2 (ZIC2-FLAG) in the ZIC2-OE models of OVCAR3 and A2780s cells

(A) ZIC2 expression (ZIC2-FLAG) was confirmed by immunoblotting using anti-FLAG antibody in the ZIC2-OE models of OVCAR3 and A2780s cells. EV (empty vector) refers to A2780s vector and OVCAR3 vector cells. OE (ZIC2-OE) refers to OVCAR3 ZIC2-OE and A2780s ZIC2-OE cells. β-actin was used as a loading control. **(B)** Immunofluorescence showed that overexpressed ZIC2-FLAG was localized in the nuclei. Immunofluorescence was performed using anti-ZIC2 antibody. Magnification: 20X. The scale bar is 10 μm.

3.2.5 Knockout of ZIC2 decreases cell growth in SKOV3 and OVCAR8

We generated and validated the ZIC2-KO and the ZIC2-OE models. Next, we determined whether ZIC2 regulates the tumorigenic phenotypes in EOC cells. First, the effect of ZIC2 on cell growth was determined by neutral red uptake assay. To reduce the effect of clonal variation on the experiments, we used the mixture of equal number of cells from three WT or ZIC2-KO clones (1:1:1 ratio) in all experiments associated with ZIC2-KO models. First, we examined the effect of ZIC2 on cell growth using neutral red uptake assay. Neutral red uptake assays showed a 27.0% ($p< 0.01$) reduction in cell growth of SKOV3 ZIC2-KO cells compared to SKOV3 WT cells on day 7 (**Figure 3.8**). Cell growth in OVCAR8 was more sensitive to the knockout of ZIC2. Compared to OVCAR8 WT cells, cell growth of OVCAR8 ZIC2-KO cells was decreased by 40.3% ($p< 0.05$) on day 3, 57.3% ($p< 0.0001$) on day 5, and 37.4% ($p< 0.05$) on day 7. Collectively, these

data suggest that knockout of ZIC2 inhibits cell growth in SKOV3 and OVCAR8 cells.

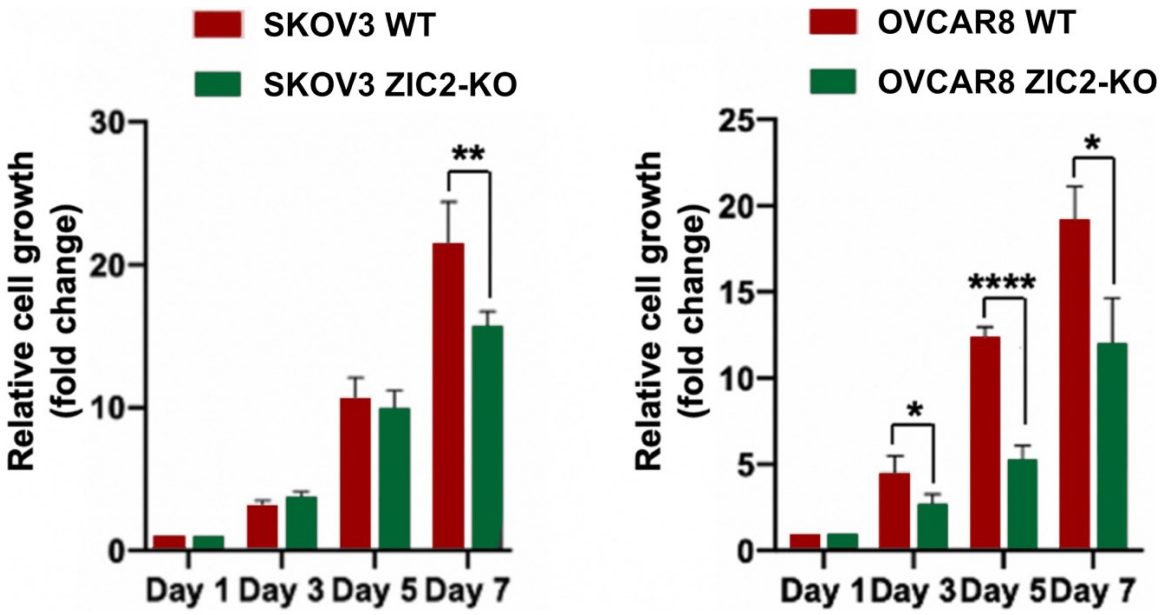

Figure 3.8 Knockout of ZIC2 inhibits the cell growth in SKOV3 and OVCAR8

Cell growth was detected by neutral red uptake assay and expressed as fold changes relative to the data on day 1. Relative cell growth (fold change) shows values as mean ± SD of at least three independent experiments. Statistical significance is determined using the one-way ANOVA (*: $p< 0.05$; **: $p< 0.01$; ****: $p< 0.0001$).

3.2.6 Knockout of ZIC2 decreases the number of colonies formed by SKOV3 cells but decreases the size of colonies formed by OVCAR8 cells

We demonstrated that knockout of ZIC2 reduced cell growth in SKOV3 and OVCAR8 cells. Next, we examined whether ZIC2 regulates the single-cell survival in SKOV3 and OVCAR8 cells using clonogenic assay. The number of colonies in

SKOV3 ZIC2-KO cells was reduced by 20.8% (p< 0.01) compared with SKOV3 WT cells (**Figure 3.9A**). We found that the size of colonies formed by SKOV3 WT was smaller than that formed by SKOV3 ZIC2-KO cells (**Figure 3.9B**). Although there was no significant difference in the number of colonies formed between OVCAR8 WT and ZIC2-KO cells, the size of colonies formed by OVCAR8 ZIC2-KO cells was smaller (**Figure 3.9A and 3.9B**), consistent with neutral red uptake assay in which knockout of ZIC2 decreased cell growth in OVCAR8 cells. Taken together, these data indicate that knockout of ZIC2 decreases single-cell survival and increased the size of the colonies formed by SKOV3 cells and decreases the size of colonies formed by OVCAR8 cells.

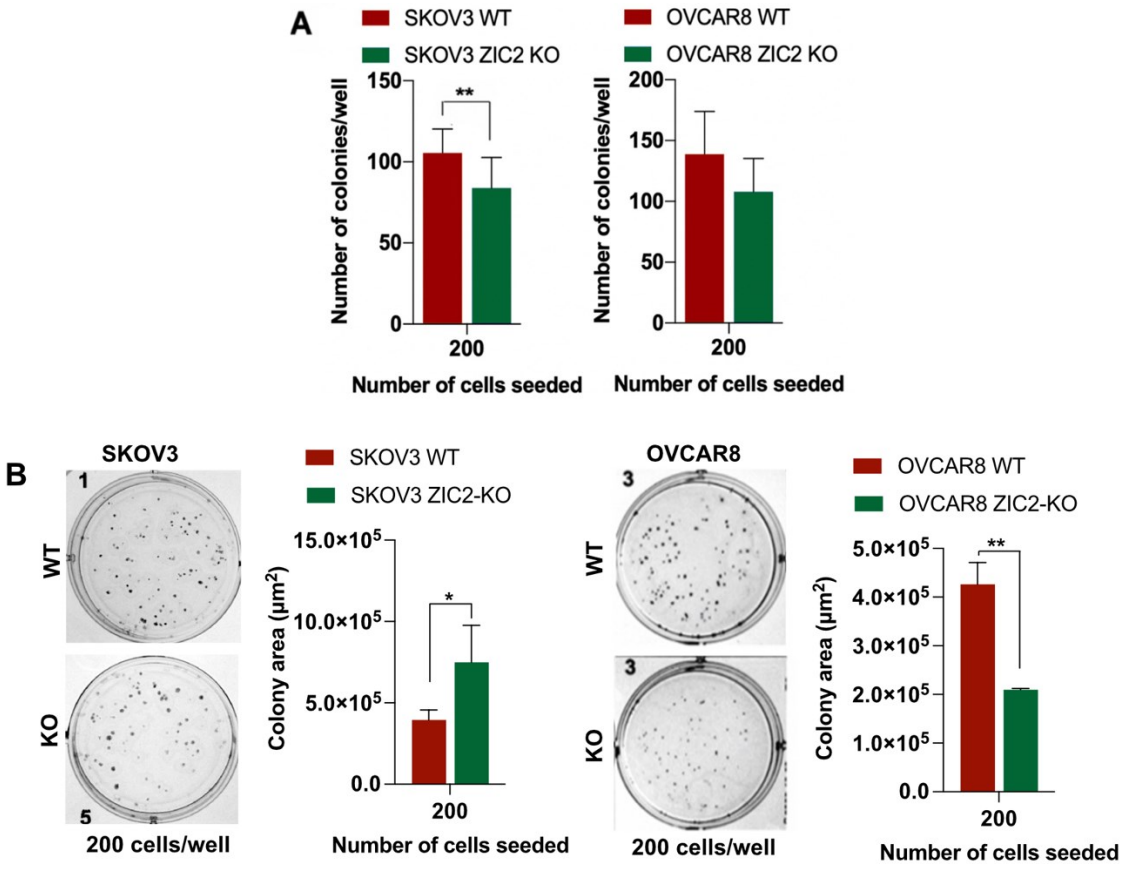

Figure 3.9 Knockout of ZIC2 inhibits single-cell survival in SKOV3 cells and decreases the size of colonies in OVCAR8 cells

Single-cell survival of SKOV3 and OVCAR8 cells was determined by clonogenic assay. **(A)** Histograms show the total number of colonies formed by SKOV3 and OVCAR8 cells seeded at 200 cells per well in six-well plates. **(B)** Images and histograms show the colonies formed by SKOV3 and OVCAR3 cells in six-well plates seeded with 200 cells per well and the size of the colonies (colony area), respectively. Number of colonies/well is shown as mean ± SD of at least three independent experiments. Statistical significance is determined using the one-way ANOVA (*: $p< 0.05$; **: $p< 0.01$).

3.2.7 Knockout of ZIC2 inhibits anchorage-independent growth in SKOV3 cells but does not affect OVCAR8 cells

To determine whether ZIC2 regulates anchorage-independent growth in SKOV3 and OVCAR8 cells, we performed soft agar colony-formation assay. Soft agar colony assay showed that SKOV3 ZIC2-KO cells formed 27.6% ($p< 0.05$) fewer colonies compared to SKOV3 WT cells (**Figure 3.10A**), while OVCAR8 WT and OVCAR8 ZIC2-KO cells formed similar numbers of colonies (**Figure 3.10A**). Interestingly, however, the colonies formed by SKOV3 ZIC2-KO and OVCAR8 ZIC2-KO cells were smaller than their respective WT control cells (**Figure 3.10B**). In summary, these data suggest that knockout of ZIC2 decreases anchorage-independent growth in SKOV3 cells.

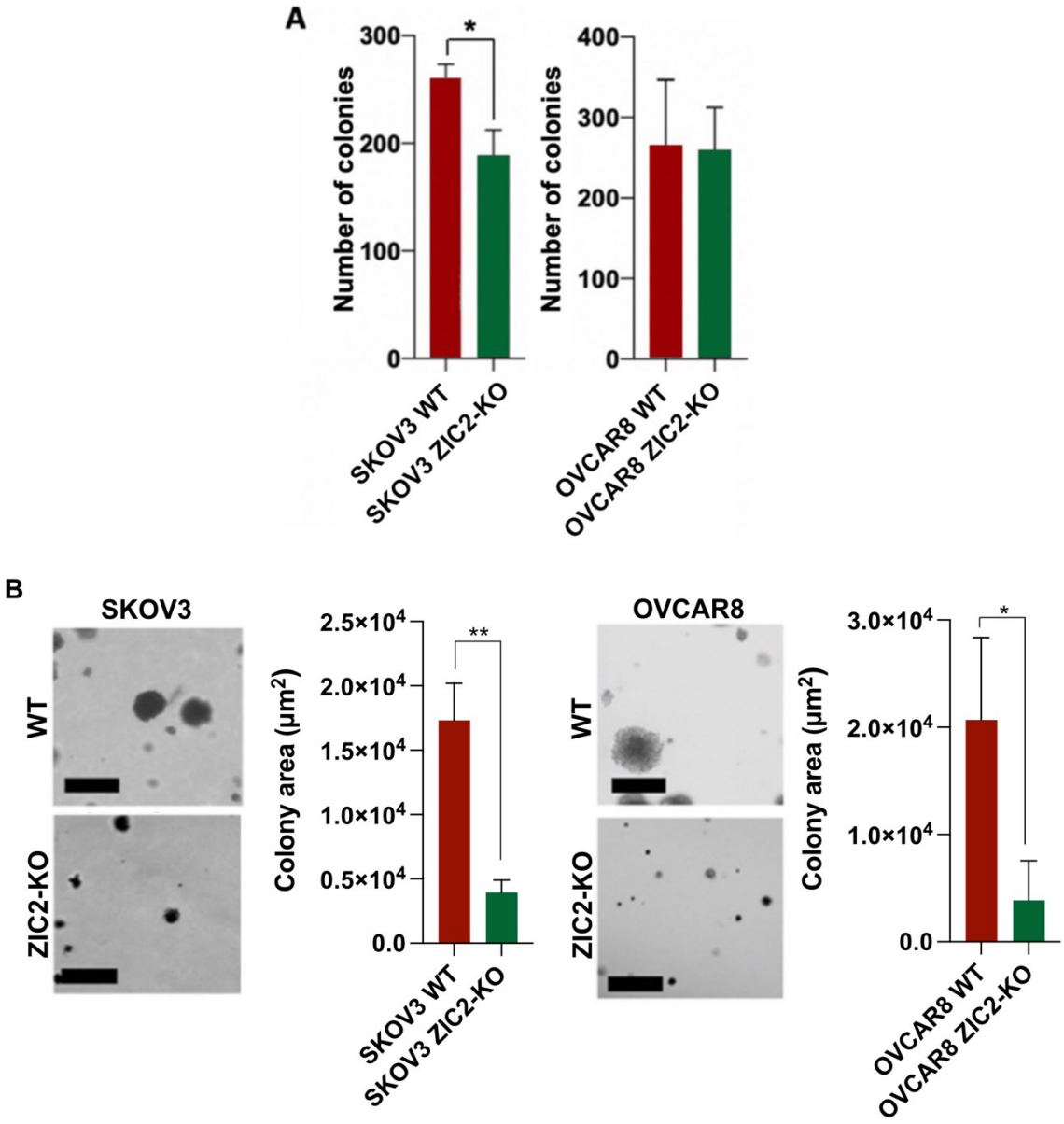

Figure 3.10 Knockout of ZIC2 attenuates anchorage-independent growth in SKOV3 cells but does not affect OVCAR8 cells

Anchorage-independent growth of SKOV3 and OVCAR8 cells was determined by soft agar colony-formation assay. **(A)** Histograms show the number of clones formed by WT and the ZIC2-KO models of SKOV3 and OVCAR8 cells acquired by counting 18 random fields under a microscope. **(B)** Images and histograms show the colonies formed by SKOV3 and OVCAR8 cells in the well of six-well plates and

the size of the colonies (colony area) 21 days after seeding, respectively. The number of colonies showed the total number of colonies acquired by counting 18 random fields under a microscope. Magnification: 4X. The scale bar is 100 μm. Number of colonies is shown as mean ± SD of at least three independent experiments. Statistical significance is determined using the one-way ANOVA (*: $p < 0.05$; **: $p < 0.01$).

3.2.8 Knockout of ZIC2 inhibits cell migration in SKOV3 and OVCAR8 cells

Davis *et al.* demonstrated that ZIC2 promotes cell migration in prostate cancer cells (165). Using transwell migration assay, we determined that knockout of ZIC2 decreased migration by 38.9% reduction ($p < 0.01$) in SKOV3 cells and by 29.4% ($p < 0.05$) in OVCAR8 ZIC2-KO cells (**Figure 3.11**), suggesting that ZIC2 promotes migration in SKOV3 and OVCAR8 cells.

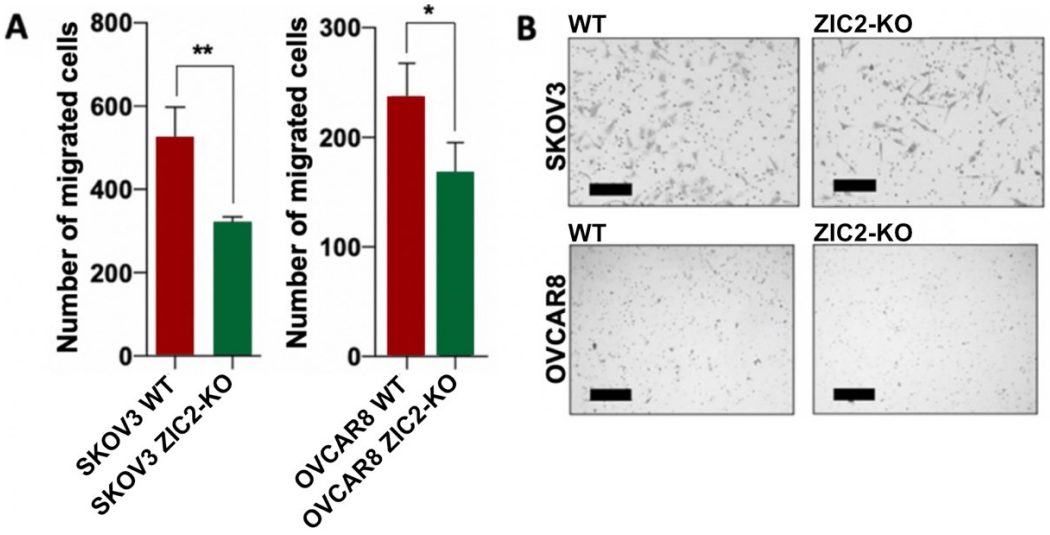

Figure 3.11 Knockout of ZIC2 reduced the cell migration in SKOV3 and OVCAR8 cells

Cell migration of SKOV3 and OVCAR8 was determined by the transwell assay. **(A)** Histograms show the number of migrated SKOV3 and OVCAR8 cells acquired by counting 9 random fields 24 hours after seeding. **(B)** Images show the migrated SKOV3 and OVCAR8 cells. Magnification: 4X. The scale bar = 100 μm. Number of migrated cells is shown as mean ± SD of three independent experiments. Statistical significance is determined using the one-way ANOVA (*: $p< 0.05$; **: $p< 0.01$).

3.2.9 Knockout of ZIC2 decreases self-renewal ability of SKOV3 and OVCAR8 cells

ZIC2 has been shown to be involved in the regulation of target genes for transcription factors expressed in mouse ESC, as well as the activation of the stem cell transcription factor *OCT4* in liver CSCs (169). To determine whether ZIC2 is involved in the regulation of CSCs in EOC cells, we examined the self-renewal ability in the ZIC2-KO models of SKOV3 and OVCAR8 cells *in vitro* by limiting dilution sphere formation assay. Sphere formation assay reflects self-renewal ability by detecting the number of spheres formed, which is one of the important characteristics of CSCs (495,496). Limiting dilution sphere formation assay showed that the number of spheres formed by SKOV3 ZIC2-KO cells was significantly reduced at seeding densities of 20, 25, 50, 75, 100, 120, 150, 200 cells per well compared to SKOV3 WT cells. The number of spheres formed by

OVCAR8 ZIC2-KO cells was significantly reduced at seeding densities of 20, 50, 75, 100, 120, and 200 cells per well compared to OVCAR8 WT cells (**Figure 3.12A**). In addition, knockout of ZIC2 in SKOV3 and OVCAR8 cells resulted in a significant reduction in the size of the spheres formed (**Figure 3.12B**). Our data suggest that knockout of ZIC2 attenuates the self-renewal ability of SKOV3 and OVCAR8 cells.

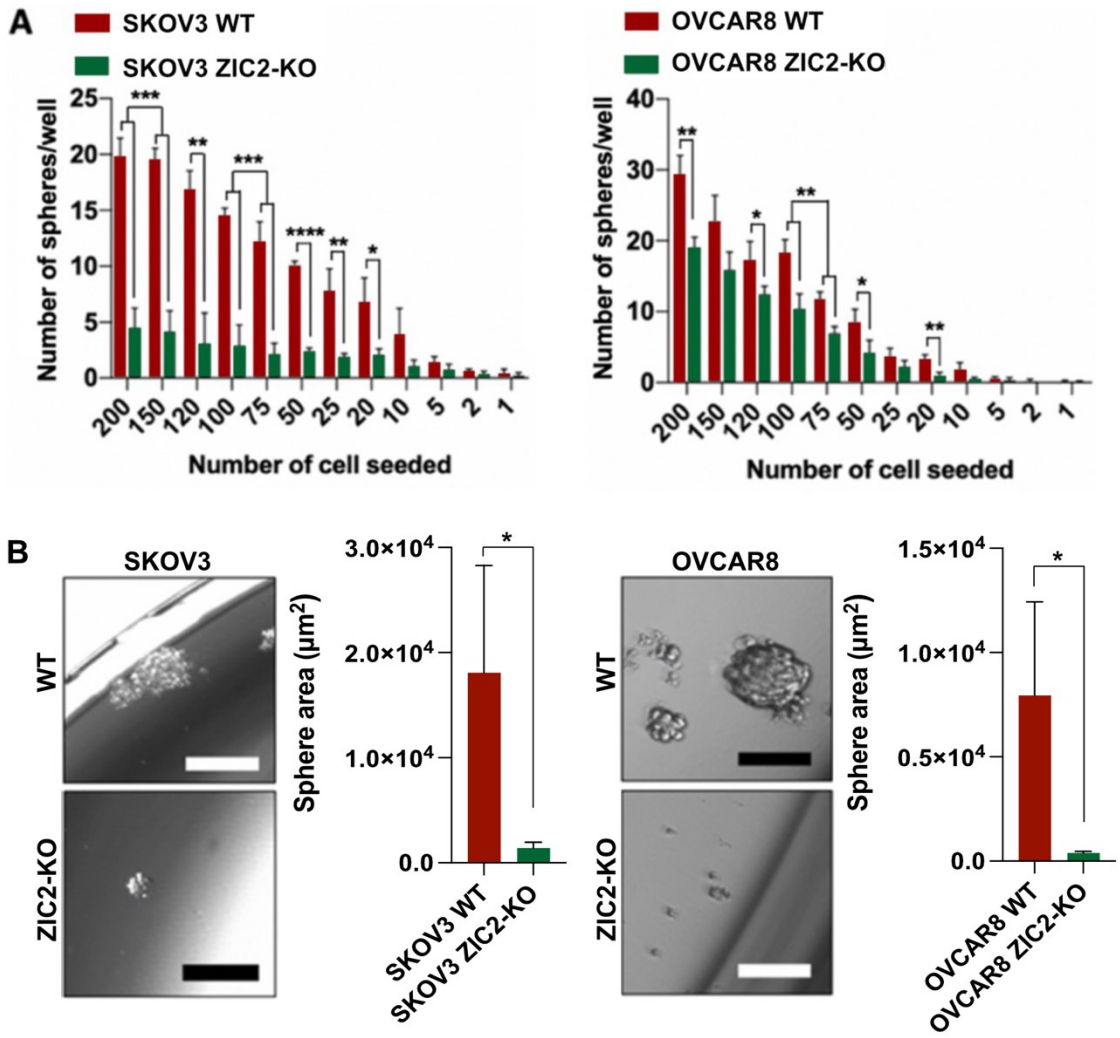

Figure 3.12 Knockout of ZIC2 decreases self-renewal ability of SKOV3 and OVCAR8 cells

Self-renewal ability was determined by limiting dilution sphere formation assay. **(A)** Histograms show the number of spheres formed by SKOV3 and OVCAR8 cells in the wells of 96-well plates 14 days after seeding. **(B)** Images and histograms show the spheres formed by SKOV3 and OVCAR8 cells in the wells of 96-well plates and the size of the spheres (sphere area) 14 days after seeding. Magnification: 10X. The scale bar is 200 μm. Number of spheres per well is shown as mean ± SD of at least three independent experiments. Statistical significance is determined using the one-way ANOVA (*: $p< 0.05$; **: $p< 0.01$; ***$p< 0.001$; ****$p< 0.0001$).

3.2.10 $CD133^{high}$ does not enrich CSC-like cells in SKOV3 or OVCAR8 cells

Our study showed that knockout of ZIC2 reduced the sphere-forming ability of SKOV3 and OVCAR8 cells. We further explored whether ZIC2 regulates the CSC population in SKOV3 and OVCAR8 cells. $CD133^{high}$ is a widely recognized cell surface marker for identifying the CSC populations in ovarian cancer, and $CD133^{high}$ sorting enriches CSC-like cells with tumor-initiating properties (283,337,363-365,497). To determine whether $CD133^{high}$ enriches these cells for CSCs, we performed fluorescence-activated cell sorting (FACS) to sort $CD133^{high}$ and $CD133^{low}$ cells in SKOV3 and OVCAR8 cells, followed by limiting dilution sphere formation assay. We did not find any significant changes in the number of spheres formed by $CD133^{high}$ and $CD133^{low}$ cells in SKOV3 and OVCAR8 cells (**Figure 3.13**). Our results demonstrate that $CD133^{high}$ does not enrich CSC-like

cells in SKOV3 or OVCAR8 cells and that CD133^{high} may not be a CSC marker for these two cell lines.

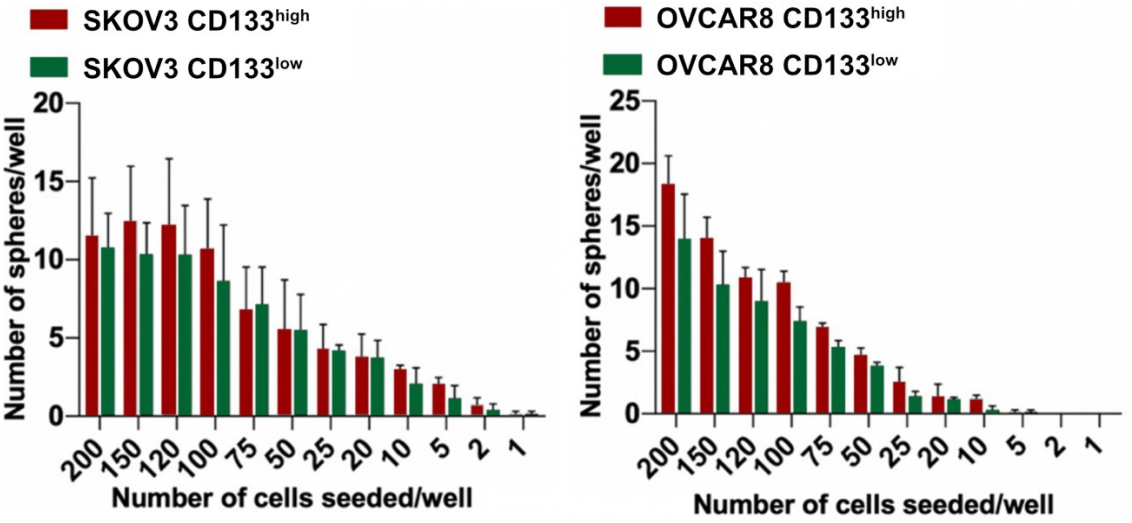

Figure 3.13 CD133^{high} does not enrich CSC-like cells in SKOV3 or OVCAR8 cells

Self-renewal ability of CD133^{high} and CD133^{low} in SKOV3 and OVCAR8 cells were determined by limiting dilution sphere formation assay. The number of spheres formed was counted under a microscope 14 days after seeding. Number of spheres per well is shown as mean ± SD of three independent experiments. Statistical significance is determined using the one-way ANOVA (*: $p< 0.05$; **: $p< 0.01$).

3.2.11 ALDH^{high} enriches CSC-like cells in SKOV3 cells but not in OVCAR8 cells

We determined that CD133^{high} might not be a CSC marker in SKOV3 and OVCAR8 cells. We needed another CSC marker to explore whether ZIC2 regulates the proportion of CSC-like cells in SKOV3 and OVCAR8 cells. ALDH^{high}

is a widely accepted functional marker for identifying the CSC populations in ovarian cancer (498-500). To determine if ALDH^{high} enriches CSC-like cells in SKOV3 and OVCAR8 cells, we sorted ALDH^{high} and ALDH^{low} cells by ALDEFLUOR assay, followed by FACS and limiting dilution sphere formation assay to measure the self-renewal ability of ALDH^{high} cells and ALDH^{low} cells in SKOV3 and OVCAR8 cells. Limiting dilution sphere formation assay showed that the number of spheres formed by ALDH^{high} SKOV3 cells was significantly increased compared with ALDH^{low} SKOV3 cells, while the number of spheres formed by ALDH^{high} OVCAR8 cells was not significantly changed compared with ALDH^{low} OVCAR8 cells (**Figure 3.14**). These data suggest that ALDH^{high} enriches CSC-like cells in SKOV3 cells and that ALDH^{high} may not be a CSC marker in OVCAR8 cells.

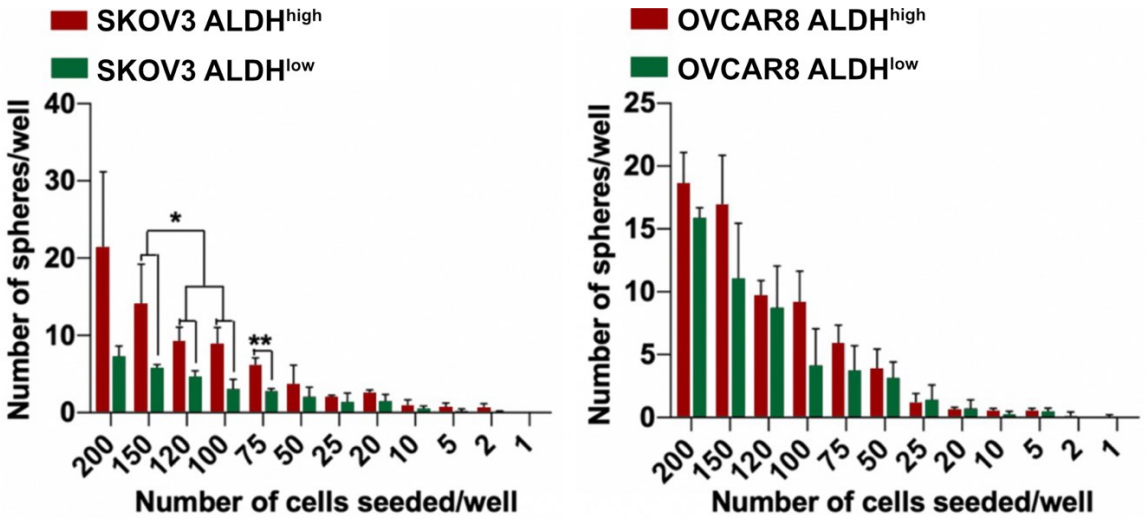

Figure 3.14 ALDH^{high} enriches CSCs in SKOV3 cells

The self-renewal ability of ALDH^{high} and ALDH^{low} cells in SKOV3 and OVCAR8 cells was detected by limiting dilution sphere formation assay. The number of

spheres formed was counted 14 days after seeding. Number of spheres formed per well is shown as mean ± SD of at least three independent experiments. Statistical significance is determined using the one-way ANOVA (*: $p < 0.05$; **: $p < 0.01$).

3.2.12 Knockout of ZIC2 decreases *ALDH1A1* expression in SKOV3 cells but not in OVCAR8 cells

We demonstrated that $ALDH^{high}$ enriched CSC-like cells in SKOV3 cells. ALDH1A1 has been identified as an isoform of ALDH that is associated with CSCs in a range of human cancers (501-504). We demonstrated that the $ALDH^{high}$ enriched CSC-like cells in SKOV3 cells, but not in OVCAR8 cells. To further investigate the effect of ZIC2 on *ALDH1A1* expression in SKOV3 and OVCAR8 cells, we performed RT-qPCR and immunoblotting to detect *ALDH1A1* mRNA and protein expression. Knockout of ZIC2 decreased *ALDH1A1* mRNA level by 99.9% ($p < 0.0001$) and remarkably reduced protein expression in SKOV3 cells (**Figure 3.15**). There were no significant changes in *ALDH1A1* mRNA level and protein level between OVCAR8 WT and OVCAR8 ZIC2-KO cells. These data suggest that ZIC2 increases *ALDH1A1* expression in SKOV3 cells but does not increase ALDH1A1 expression in OVCAR8 cells.

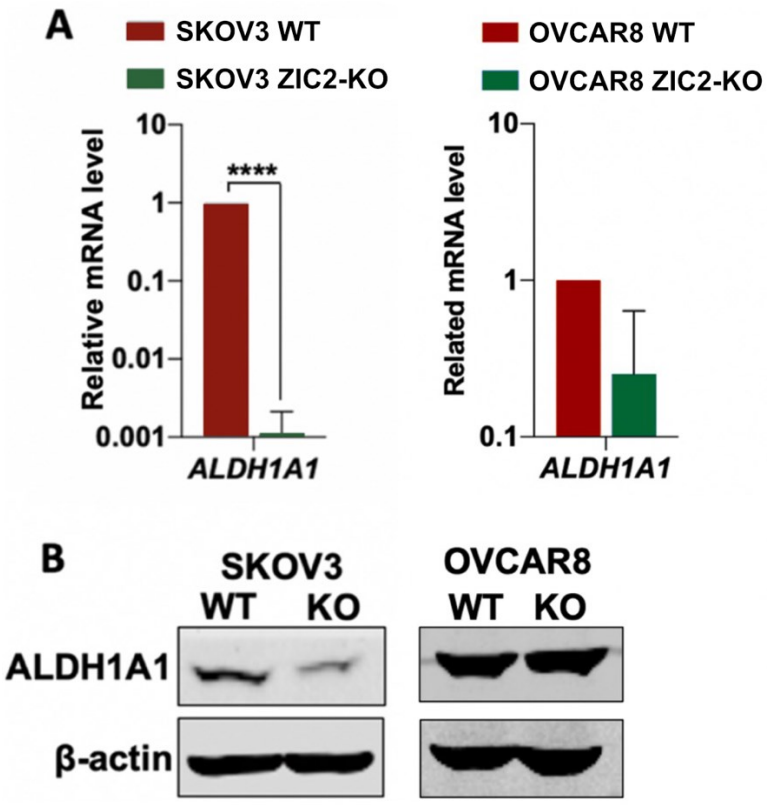

Figure 3.15 Knockout of ZIC2 reduces the expression of ALDH1A1 in SKOV3 cells but not in OVCAR8 cells

The mRNA and protein expression of *ALDH1A1* was determined by RT-qPCR and immunoblotting in SKOV3 and OVCAR8 cells. **(A)** RT-qPCR showed the mRNA expression levels of *ALDH1A1* in SKOV3 and OVCAR8 cells. **(B)** Immunoblotting showed the protein expression levels of ALDH1A1 in SKOV3 and OVCAR8 cells. β-actin was used as a loading control. Relative RNA level is shown as mean ± SD of three independent experiments. Statistical significance is determined using the one-way ANOVA (****: $p < 0.0001$).

3.2.13 Knockout of ZIC2 reduces the proportion of ALDH^{high} cell population in SKOV3 cells

We showed that ZIC2 increased the expression of *ALDH1A1* in SKOV3 cells and that ALDH^{high} enriched CSC-like cells in SKOV3 cells. To explore whether ZIC2 regulates the proportion of ALDH^{high} cells in SKOV3 cells, we performed ALDEFLUOR assay. ALDEFLUOR assay showed that knockout of ZIC2 decreased the proportion of ALDH^{high} cells in SKOV3 cells by 82.4% (p< 0.0001) (**Figure 3.16**).

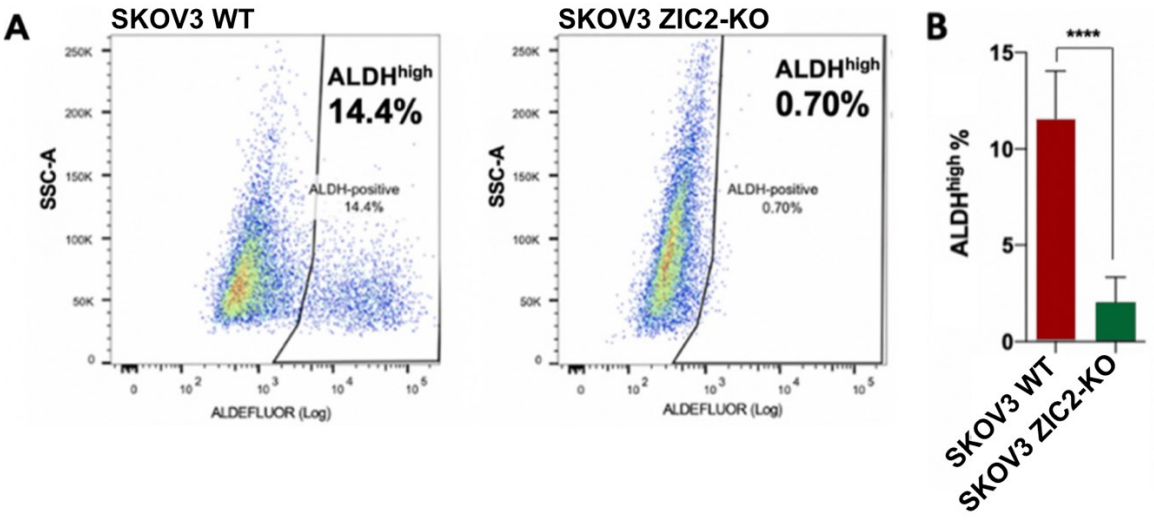

Figure 3.16 Knockout of ZIC2 reduces the proportion of ALDH^{high} cells in SKOV3 cells

The percentages of ALDH^{high} cells in SKOV3 WT and ZIC2-KO cells were determined using ALDEFLUOR assay. 10,000 events were collected for each sample**. (A)** Images show the percentage and distribution of ALDH^{high} cells in SKOV3 WT and SKOV3 ZIC2-KO cells. **(B)** Histogram shows the percentage of ALDH^{high} cells in SKOV3 WT and ZIC2-KO cells. Data were from one

representative experiment of three independent experiments. Statistical significance is determined using the one-way ANOVA (****: $p < 0.0001$).

3.2.14 ZIC2 maintains the ALDH^{high}-enriched CSC population in SKOV3 cells

We showed that knockout of ZIC2 decreased the proportion of ALDH^{high} cells in SKOV3 cells. Asymmetric division is one of the characteristics of CSCs (501). For instance, one CSC can divide into a differentiated progeny, while the other maintains the characteristics of CSCs. To determine whether ZIC2 maintains the ALDH^{high}-enriched CSC population in SKOV3 cells, we performed ALDEFLUOR assay and FACS to isolate ALDH^{high} cells from SKOV3 WT and SKOV3 ZIC2-KO cells. These ALDH^{high} cells were then grown in monolayer culture for 24 hours (day 1), 48 hours (day 2), and 72 hours (day 3). The percentage of ALDH^{high} cells at the three-time points was then determined by ADLEFLUOR assay. Interestingly, the percentage of ALDH^{high} SKOV3 ZIC2-KO cells decreased rapidly over three days, whereas the percentage of ALDH^{high} SKOV3 WT cells decreased only slightly over three days in culture (**Figure 3.17A and 3.17B**). For instance, in the first experiment, the percentage of ALDH^{high} cells in SKOV3 WT cells was 93.6% on day 0 (the day of FACS), 91.4% on day 1, 91.0% on day 2, and 87.5% on day 3. In contrast, the percentage of ALDH^{high} cells in SKOV3 ZIC2-KO cells was 95.8% on day 0, 69.7% on day 1, 41.5% on day 2, 0.7% on day 3. Notably, on day 3, the percentage of ALDH^{high} SKOV3 ZIC2-KO cells decreased to the level before they were enriched (**Figure 3.17A**). We repeated the same experiment and obtained a similar result. The average percentage of ALDH^{high} cells in the two experiments

was shown in **Figure 3.17B**. Our data suggest that ZIC2 maintains the proportion of ALDH^{high}-enriched CSCs in the asymmetric division of SKOV3 cells.

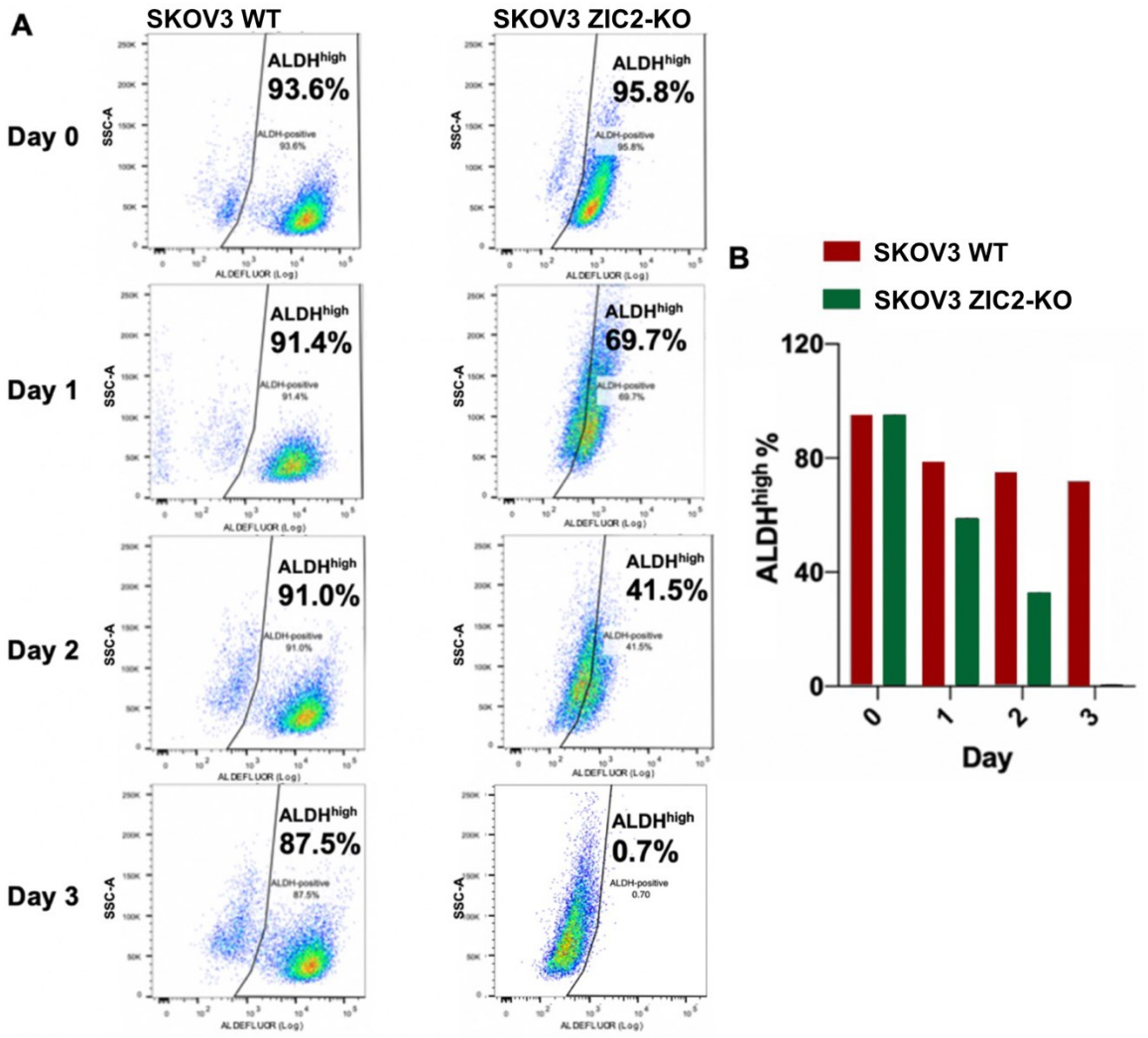

Figure 3.17 ZIC2 maintains the proportion of ALDH^{high}-enriched CSCs in SKOV3 cells

(A) The percentage of ALDH^{high} cells in SKOV3 WT and ZIC2-KO cells was determined by ALDEFLUOR assay. Images show the distribution and percentage of ALDH^{high} cells sorted from SKOV3 WT and the SKOV3 ZIC2-KO cells on days 0, 1, 2, 3 of monolayer culture. Images were taken from one representative

experiment of two independent experiments. 10,000 events were collected for each sample. **(B)** Histogram shows the average percentage of $ALDH^{high}$ cells in SKOV3 WT and SKOV3 ZIC2-KO cells on days 0, 1, 2, and 3 of monolayer culture. Relative $ALDH^{high}$ percentage is shown as mean of two independent experiments.

3.2.15 Knockout of ZIC2 decreases the tumor growth of SKOV3 cells

We indicated that knockout of ZIC2 decreased cell growth, ALDH1A1 expression, and $ALDH^{high}$ population in SKOV3 cells. Next, we explored the effect of knockout of ZIC2 on tumor growth. SKOV3 WT and SKOV3 ZIC2-KO cells were subcutaneously injected into the flanks of female NSG mice to determine tumor formation and growth. The growth of tumors formed by SKOV3 WT cells increased exponentially, while the growth of tumors formed by SKOV3 ZIC2-KO cells increased slightly (**Figure 3.18**). When mice were euthanized on day 39, the tumors formed by SKOV3 WT cells were significantly larger in size and weight than those formed by SKOV3 ZIC2-KO cells (**Figure 3.18A, 3.18B, and 3.18C**). On day 39, the average volume of tumors formed by SKOV3 WT and SKOV3 ZIC2-KO cells was 572.2 mm^3 and 73.54 mm^3, respectively. The average weight of tumors formed by SKOV3 WT and SKOV3 ZIC2-KO cells was 479.0 mg and 20.30 mg, respectively.

In addition, we determined the expressions of ZIC2 and ALDH1A1 by immunoblotting, and the distribution and localization of ZIC2-positive, ALDH1A1-positive, and Ki-67-positive (a proliferation marker) cells in tumors formed by SKOV3 WT and ZIC2-KO cells using IHC (**Figure 3.18D and 3.18E**).

Immunoblotting showed that ZIC2 and ALDH1A1 were expressed in tumors formed by SKOV3 WT cells, but not in tumors formed by SKOV3 ZIC2-KO cells (**Figure 3.18D**). Consistently, ZIC2-positive and ALDH1A1-positive cells were present in tumors formed by SKOV3 WT cells but not in tumors formed by SKOV3 ZIC2-KO cells. The percentage of Ki-67-positive cells was greater in tumors formed by SKOV3 WT cells than in tumors formed by SKOV3 ZIC2-KO cells (**Figure 3.18E**).

Taken together, these data suggest that ZIC2 is required for tumor growth in SKOV3 cells *in vivo*, and that ALDH^{high}-enriched CSCs in SKOV3 WT cells may contribute to tumor growth.

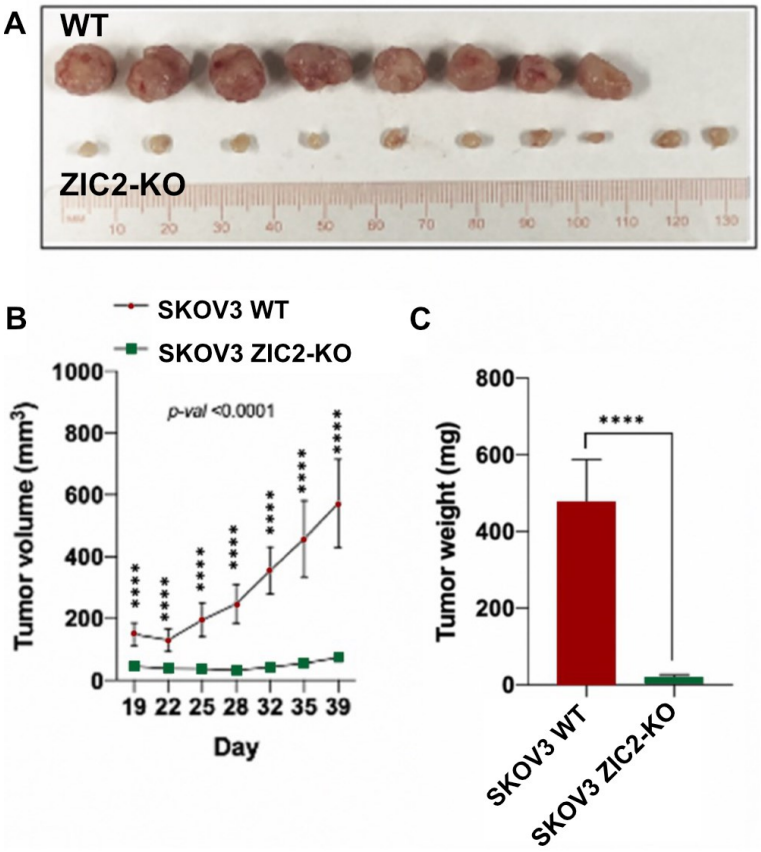

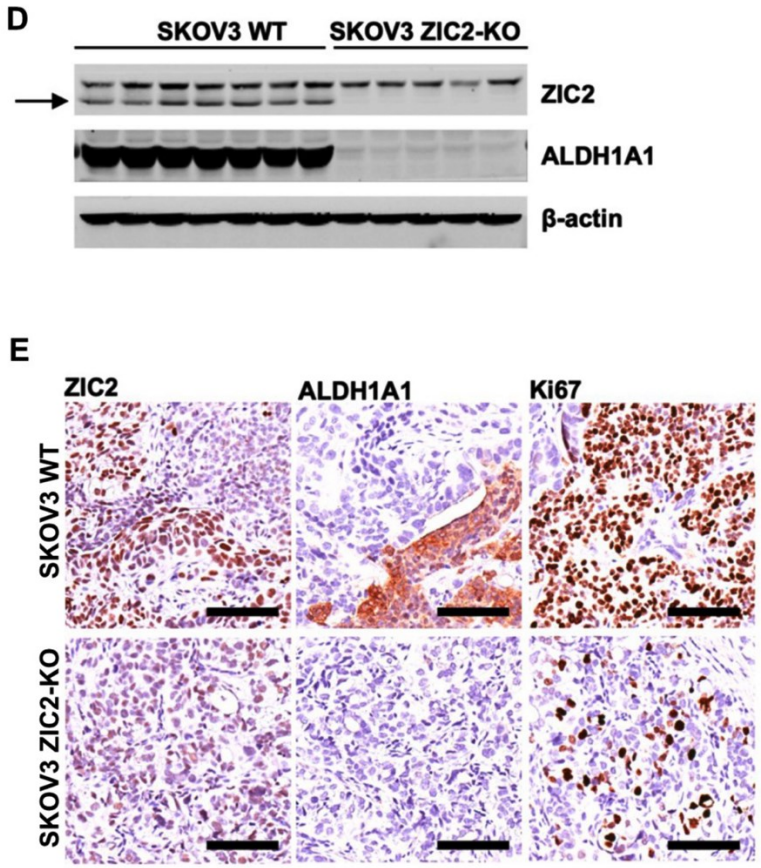

Figure 3.18 Knockout of ZIC2 inhibits the growth of SKOV3 tumors

(A) Images show xenografted tumors of SKOV3 WT (WT) and SKOV3 ZIC2-KO (ZIC2-KO) cells on day 39. **(B)** Line chart shows tumor volumes of SKOV3 WT and SKOV3 ZIC2-KO cells at specific time points. The average volume of 8 xenografted tumors of the SKOV3 WT cells and 10 xenografted tumors of SKOV3 ZIC2-KO cells at specific time points are shown as mean ± SD. **(C)** Histogram shows the tumor weight of SKOV3 WT (n = 8) and SKOV3 ZIC2-KO (n = 10) cells. Tumor weight is shown as mean ± SD. **(D)** Immunoblotting shows protein expression of ZIC2 and ALDH1A1 in tumor lysates. β-actin was used as a loading control. The arrow indicated the bands of ZIC2. The top band is non-specific. **(E)** Localization of ZIC2-positive cells, ALDH1A1-positive cells, and Ki-67-positive

cells in SKOV3 WT and SKOV3 ZIC2-KO tumor sections was determined by IHC staining. Magnification: 20X. The scale bar is 100 μm. Statistical significance is determined using the one-way ANOVA (****: $p < 0.0001$).

3.2.16 Overexpression of ZIC2 decreases cell growth in A2780s and OVCAR3

We showed that knockout of ZIC2 decreased the cell growth in SKOV3 and OVCAR8 cells, as well as the tumor growth in SKOV3 cells. To investigate whether overexpression of ZIC2 regulates cell growth in OVCAR3 and A2780s cells, we performed neutral red uptake assay using the OVCAR3 ZIC2-OE (e.g., OVCAR3 vector and OVCAR3 ZIC2-OE) and A2780s ZIC2-OE (A2780s vector and A2780s ZIC2-OE) models. Unexpectedly, the results of the neutral red uptake assay for both ZIC2-OE models were opposite to those we found in SKOV3 and OVCAR8 cells (**Figure 3.19**). Specifically, cell growth of OVCAR3 ZIC2-OE was significantly decreased on days 3 and 7 compared to OVCAR3 vector cells. The cell growth of OVCAR3 ZIC2-OE cells was decreased by 15.8% ($p < 0.05$) on day 3, 26.5% on day 5, and 37.0% ($p < 0.01$) on day 7 compared to OVCAR3 vector cells. Similarly, cell growth of A2780s ZIC2-OE cells was significantly decreased on days 3, 5, 7 compared to A2780s vector cells. The cell growth of A2780s ZIC2-OE cells was reduced by 62.2% ($p < 0.01$) on day3, 71.8% ($p < 0.01$) on day 5, and 66.9% ($p < 0.01$) on day 7 compared to A2780s vector cells. Together, these data suggest that overexpression of ZIC2 attenuates cell growth in OVCAR3 and A2780s cells.

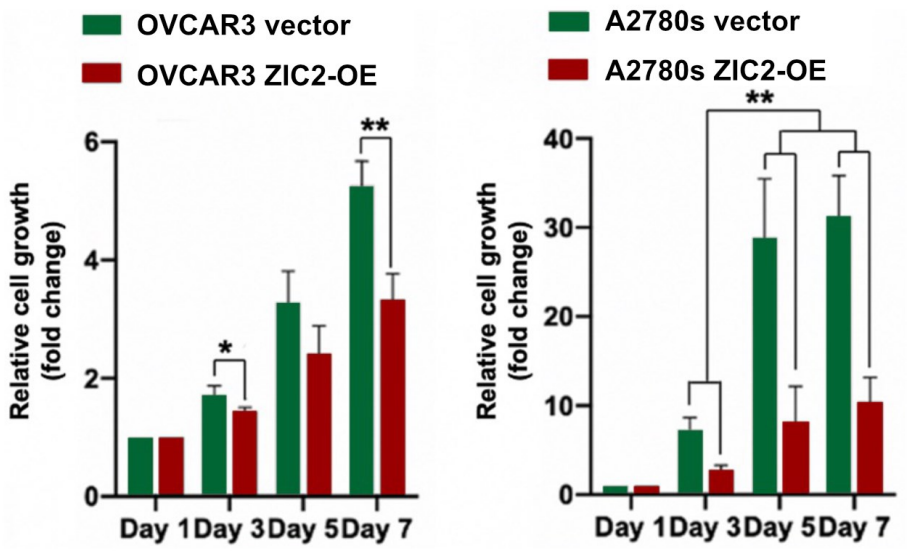

Figure 3.19 Overexpression of ZIC2 decreases cell growth in OVCAR3 and A2780s cells

Cell growth in the OVCAR3 ZIC2-OE and A2780s ZIC2-OE models was determined by neutral red uptake assay. Cell growth was expressed as fold changes relative to the data on day 1. Relative cell growth (fold change) is shown as mean ± SD of at least three independent experiments. Statistical significance is determined using the one-way ANOVA (*: $p< 0.05$; **: $p< 0.01$).

3.2.17 Overexpression of ZIC2 increases the number of colonies formed by OVCAR3 cells but decreases the size of colonies formed by A2780s cells

We showed that knockout of ZIC2 decreased single-cell survival in SKOV3 cells. Next, we performed clonogenic assay to determine whether ZIC2 regulates single-cell survival in OVCAR3 and A2780s cells. Clonogenic assay showed that overexpression of ZIC2 significantly increased ($p< 0.01$) the single-cell survival of OVCAR3 cells but had no effect ($p = 0.1318$) on A2780s cells (**Figure 3.20A**). The

number of colonies formed by OVCAR3 ZIC2-OE cells was increased by 139.2% (p< 0.01) compared to OVCAR3 vector cells. We did not find any significant change in colony size between OVCAR3 vector and OVCAR3 ZIC2-OE cells (**Figure 3.20B**). The number of colonies formed by A2780s ZIC2-OE cells was reduced by 35.5% compared to A2780s vector cells (**Figure 3.20A**). In addition, we found that the size of the colonies formed by A2780s ZIC2-OE cells was significantly decreased compared to A2780s vector cells (**Figure 3.20B**). In summary, our data suggest that overexpression of ZIC2 increases single-cell survival in OVCAR3 cells but decreases colony size in A2780s cells.

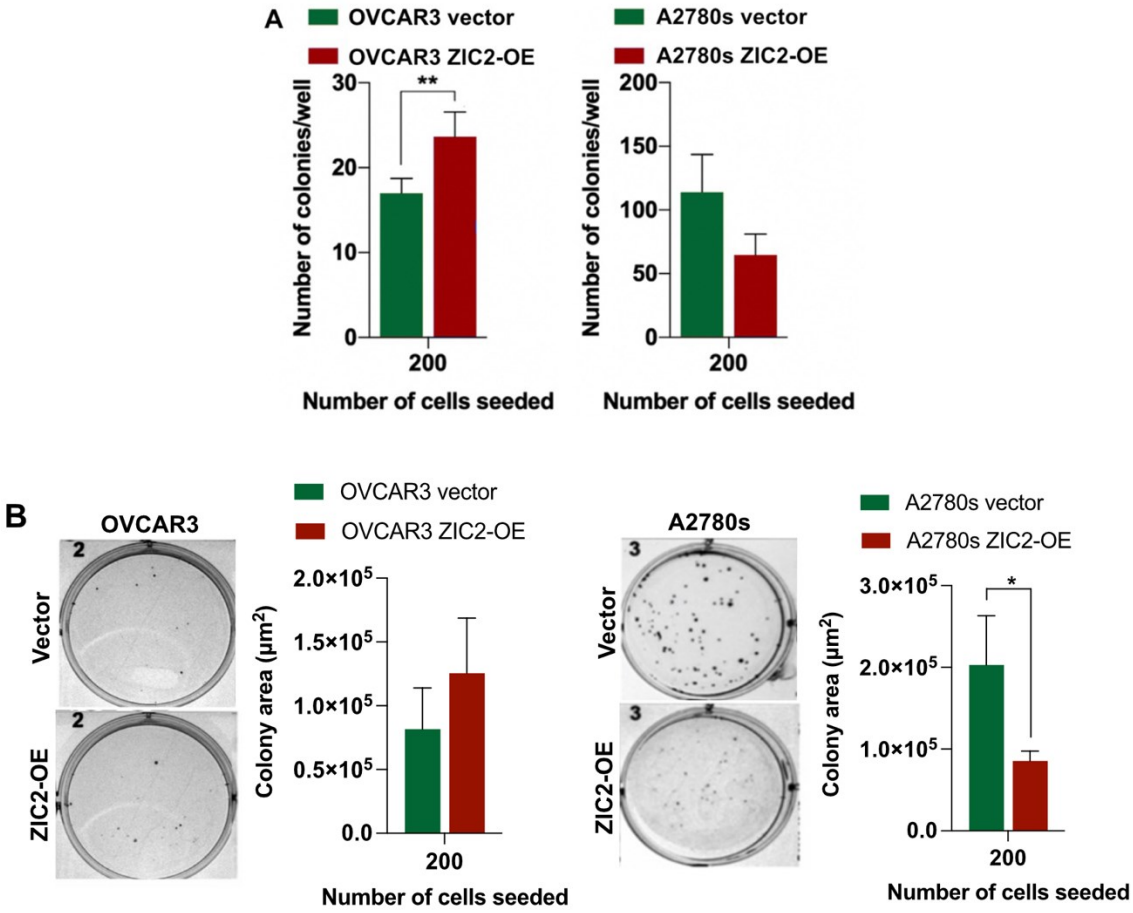

Figure 3.20 Overexpression of ZIC2 promotes single-cell survival of OVCAR3 cells but does not affect single-cell survival in A2780s cells

Single-cell survival in OVCAR3 and A2780s cells was determined by clonogenic assay. **(A)** Histograms show the total number of colonies formed by OVCAR3 and A2780s cells seeded at 200 cells per well in six-well plates. **(B)** The images and histograms show the colonies formed by OVCAR3 and A2780s cells in six-well plates seeded with 200 cells per well and the size of the colonies (colony area), respectively. Number of colonies per well was shown as mean ± SD of at least three independent experiments. Statistical significance was determined using the one-way ANOVA (*: $p< 0.05$; **: $p< 0.01$).

3.2.18 Overexpression of ZIC2 decreases anchorage-independent growth of A2780s cells

To determine whether ZIC2 regulates anchorage-independent growth in OVCAR3 and A2780s cells, we performed soft agar formation assay (**Figure 3.21**). We found that OVCAR3 cells did not form any colonies 21 days after seeding (**Figure 3.21A**). The number of colonies formed by A2780s ZIC2-OE cells was lower by an average of 71.1% ($p< 0.01$) compared to A2780s vector cells (**Figure 3.21B**). In addition, the size of colonies formed by A2780s vector and A2780s ZIC2-OE cells did not change (**Figure 3.21A**). Our data show that overexpression of ZIC2 inhibits anchorage-independent growth in A2780s cells.

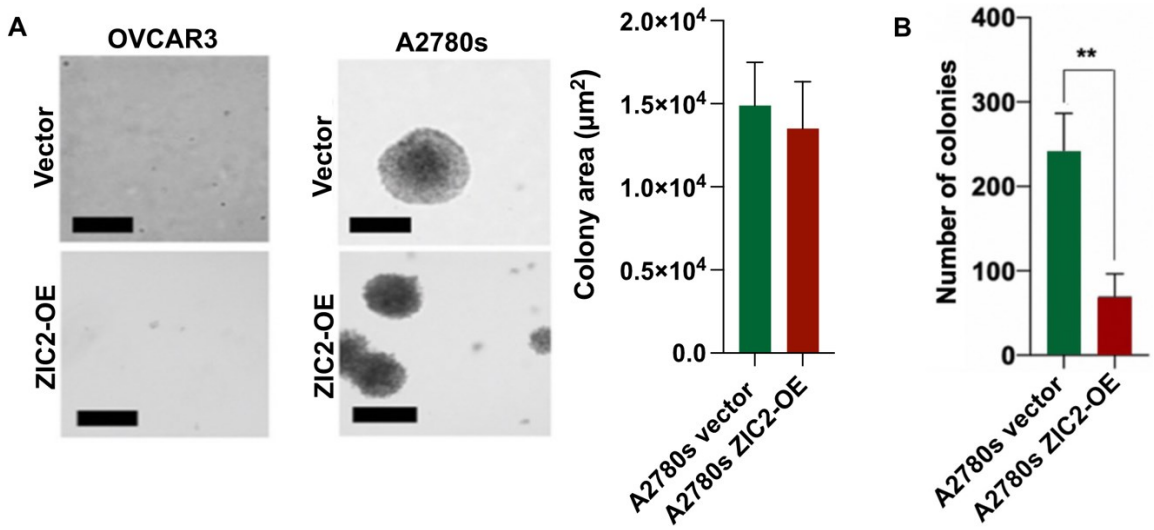

Figure 3.21 Overexpression of ZIC2 decreases anchorage-independent growth in A2780s cells

Anchorage-independent growth of OVCAR3 and A2780s cells was determined by soft agar formation assay. **(A)** Images and a histogram show the colonies formed by A2780s vector and A2780s ZIC2-OE cells and the size of the colonies (colony area) 21 days after seeding, respectively. No colonies were formed by OVCAR3. **(B)** Histogram shows the number of colonies formed by A2780s cells in the well of six-well plates 21 days after seeding. The number of colonies shows the total number of colonies acquired by counting 18 random fields under a microscope. Magnification: 4X. The scale bar = 100 μm. Number of colonies is shown as mean ± SD of at least three independent experiments. Statistical significance is determined using the one-way ANOVA (**: $p < 0.01$).

3.2.19 Overexpression of ZIC2 enhances cell migration in OVCAR3 and A2780s cells

To explore whether ZIC2 regulates cell migration in OVCAR3 and A2780s cells, we performed transwell migration assay. Transwell migration assay showed that ZIC2 significantly enhanced cell migration in OVCAR3 and A2780s (**Figure 3.22**). The number of OVCAR3 ZIC2-OE cells migrated was increased by 5.3-fold ($p< 0.01$) compared to OVCAR3 vector cells. Similarly, the number of migrated A2780s ZIC2-OE cells was increased by 1.9-fold ($p< 0.01$) compared to A2780s vector cells. These data demonstrate that overexpression of ZIC2 promotes cell migration in OVCAR3 and A2780s cells.

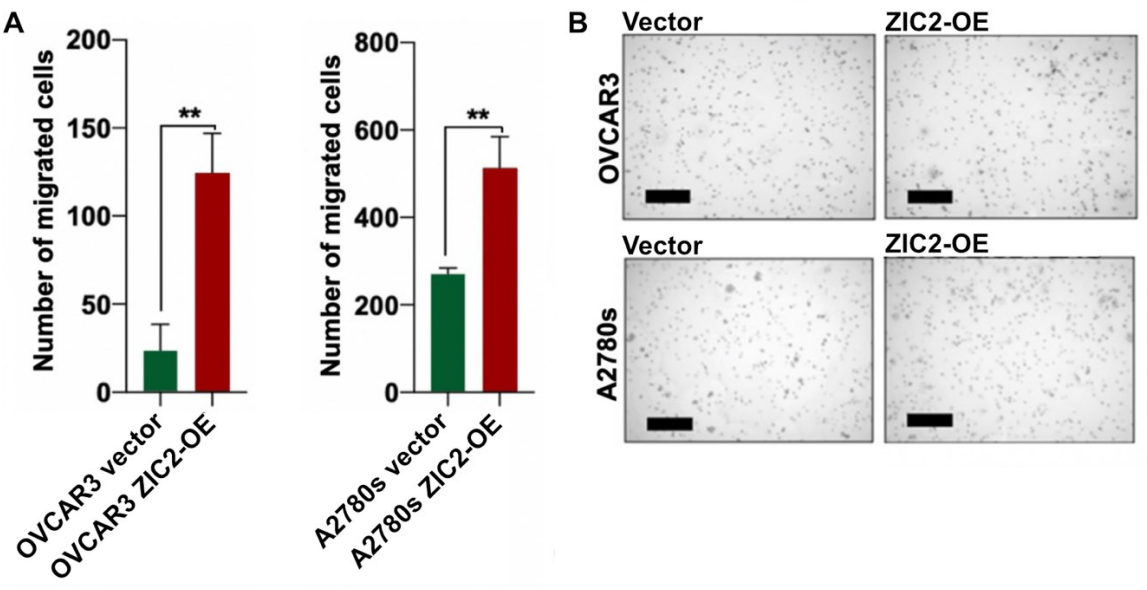

Figure 3.22 Overexpression of ZIC2 promotes cell migration in OVCAR3 and A2780s cells

Cell migration of OVCAR3 and A2780s was determined by transwell assay. **(A)** Histograms show the number of migrated OVCAR3 and A2780s cells acquired by counting 9 random fields 24 hours after seeding. **(B)** Images show migrated

OVCAR3 and A2780s cells. Magnification: 4X. The scale bar = 100 μm. Number of migrated cells is shown as mean ± SD of three independent experiments. Statistical significance is determined using the one-way ANOVA (**: $p < 0.01$).

3.2.20 Overexpression of ZIC2 promotes self-renewal ability in OVCAR3 and A2780s cells

To determine whether ZIC2 regulates the self-renewal ability in OVCAR3 and A2780s cells, we performed limiting dilution sphere formation assay. Limiting dilution sphere formation assay showed that overexpression of ZIC2 promoted the self-renewal ability in OVCAR3 and A2780s cells (**Figure 3.23A**). The number of spheres formed by OVCAR3 ZIC2-OE cells was significantly higher compared to OVCAR3 vector cells at seeding densities of 50, 75, 100, 150, and 200 cells per well; the number of spheres formed by A2780s ZIC2-OE cells was significantly higher compared to the A2780s vector cells at seeding densities of 20, 25, 50, 75, 100, 120, 150, and 200 cells per well. In addition, we found that overexpression of ZIC2 did not alter the size of spheres formed by OVCAR3 cells or A2780s cells (**Figure 3.23B**). Given that ZIC2 overexpression significantly reduced cell growth in A2780s cells, the decrease in sphere size formed by A2780s ZIC2-OE cells might be due to reduced cell growth (**Figure 3.20**). Our data suggest that ZIC2 enhances the self-renewal ability in OVCAR3 and A2780s cells.

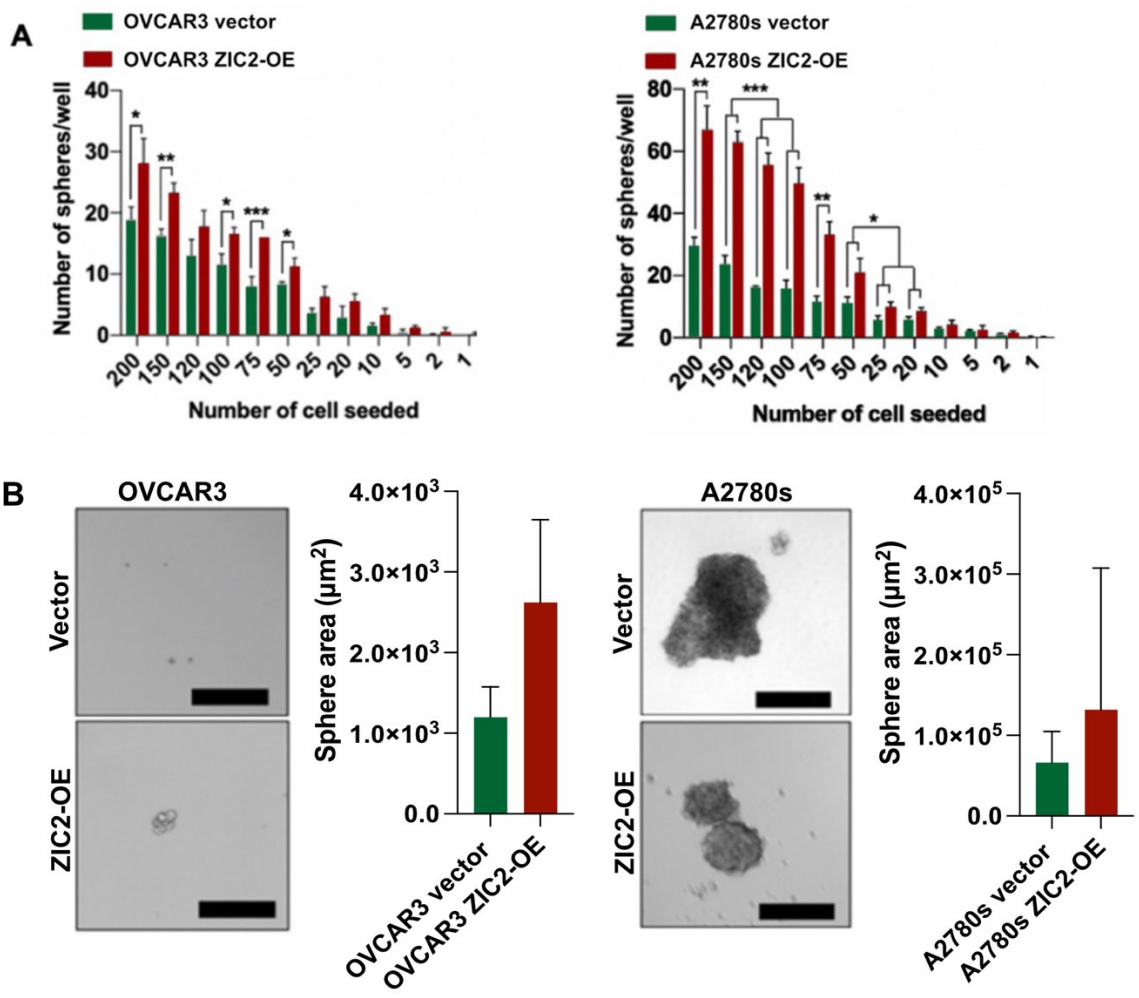

Figure 3.23 Overexpression of ZIC2 enhances self-renewal ability in OVCAR3 and A2780s cells

Self-renewal ability was determined by limiting dilution sphere formation assay. **(A)** Total number of spheres formed by OVCAR3 and A2780s cells in the wells of 96-well plates 14 days after seeding. **(B)** Images and histograms show the spheres formed by OVCAR3 and A2780s cells and the size of the spheres (sphere area), respectively. Magnification: 10X. Scale bar = 200 μm. Number of spheres per well is shown as mean ± SD of three independent experiments. Statistical significance is determined using the one-way ANOVA (*: $p< 0.05$; **: $p< 0.01$; ***$p< 0.001$).

3.2.21 CD133^{high} enriches CSC-like cells in OVCAR3 cells but not in A2780s cells

We further explored whether CD133^{high} is a CSC-marker to enrich CSC-like cells in OVCAR3 and A2780s cells. We performed fluorescence-activated cell sorting (FACS) to sort CD133^{high} and CD133^{low} cells in OVCAR3 and A2780s cells, followed by limiting dilution sphere formation assay. Notably, CD133^{high} OVCAR3 cells formed significantly more spheres 14 days after seeding compared to CD133^{low} OVCAR3 cells, consistent with several reports showing that CD133^{high} enriched CSC-like cells in OVCAR3 cells (**Figure 3.24**) (497,505,506). However, there was no significant difference in the number of spheres formed by CD133^{high} cells and CD133^{low} cells between A2780s vector and A2780s ZIC2-OE cells day 14 days after seeding. Our data suggest that CD133^{high} enriches CSC-like cells in OVCAR3 cells, but not in A2780s cells.

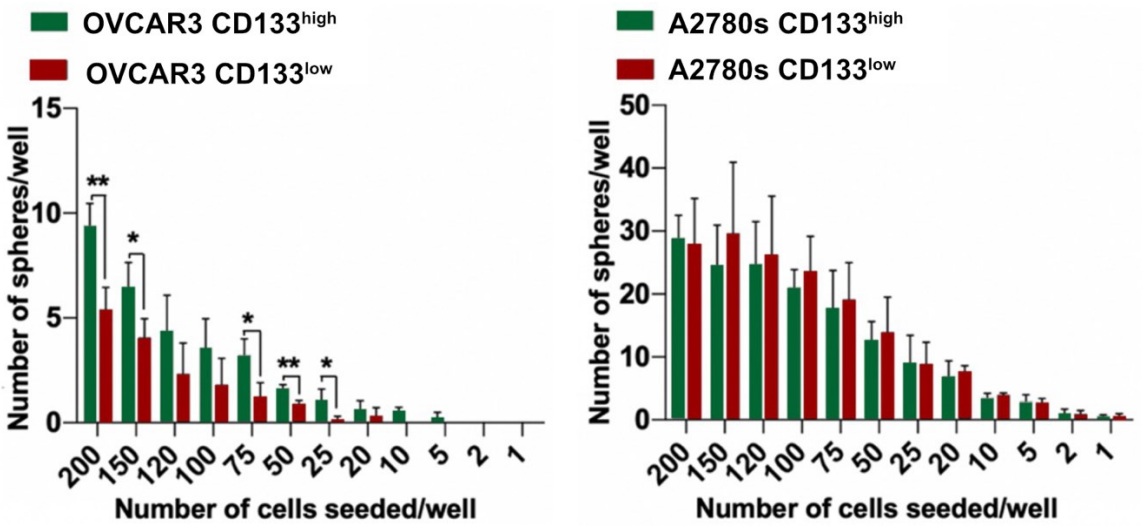

Figure 3.24 CD133^{high} enriches CSC-like cells in OVCAR3 cells but not in A2780s cells

The self-renewal ability of CD133^{high} and CD133^{low} cells sorted from OVCAR3 and A2780s cells was determined by limiting dilution sphere formation assay. The number of spheres formed was counted under a microscope 14 days after seeding. Number of spheres per well is shown as mean ± SD of three independent experiments. Statistical significance is determined using the one-way ANOVA (*: $p< 0.05$; **: $p< 0.01$).

3.2.22 Overexpression of ZIC2 increases the proportion of CD133^{high} cell population in OVCAR3 cells

We indicated that CD133^{high} enriched CSC-like cells in OVCAR3 cells. To determine whether ZIC2 regulates the proportion of CD133^{high} cells in OVCAR3 cells, we incubated the cells with CD133 PE-conjugated antibody and Zombie Aqua dye and then measured the percentage of CD133^{high} cells in OVCAR3 vector and OVCAR3 ZIC2-OE cells by flow cytometry. Flow cytometry analysis showed a significant increase of 187.7% ($p< 0.01$) in the percentage of CD133^{high} cells in OVCAR3 ZIC2-OE cells compared to OVCAR3 vector cells, suggesting that ZIC2 increases the proportion of CD133^{high} cells in OVCAR3 cells (**Figure 3.25A and 3.25B**).

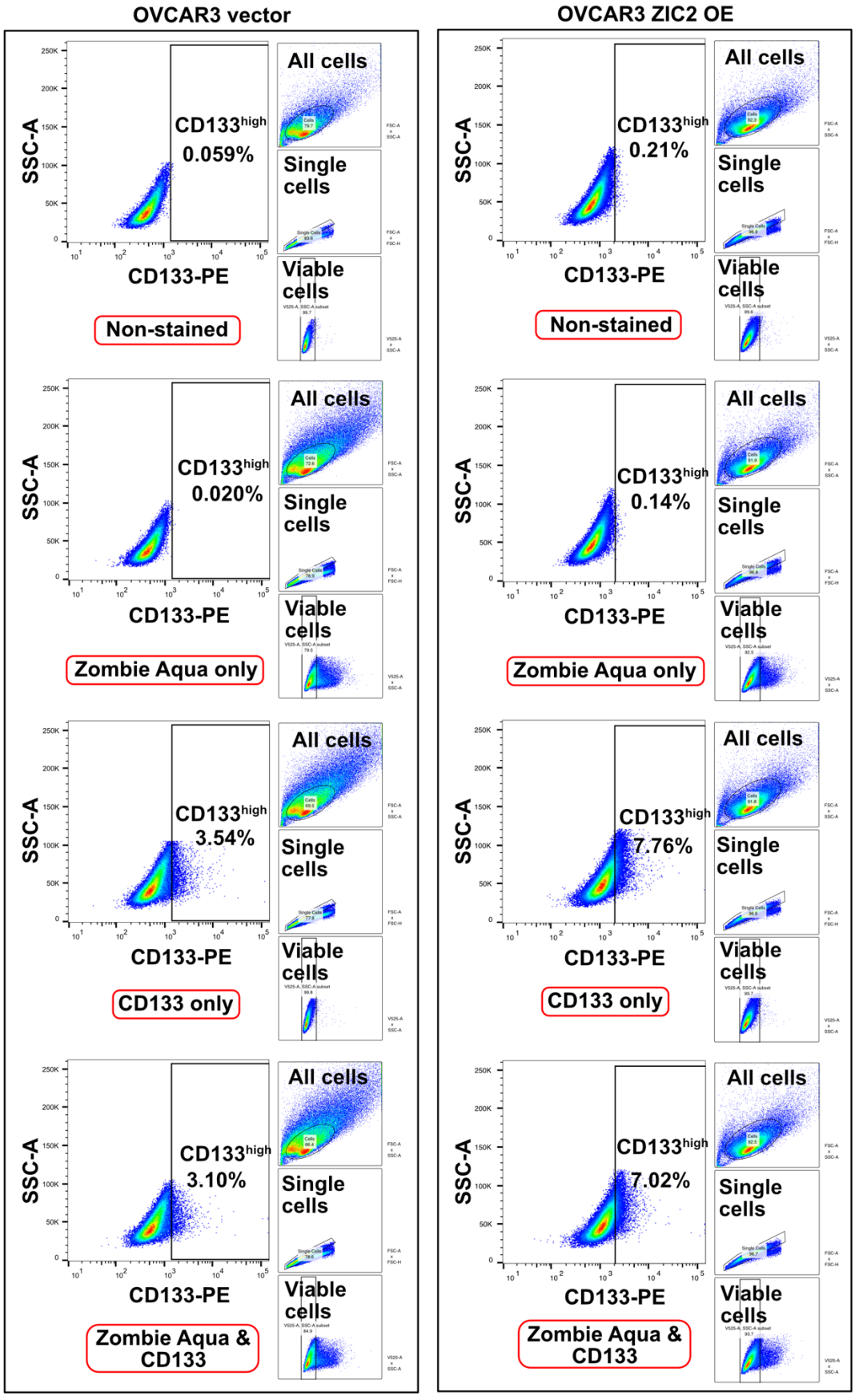
OVCAR3 vector
OVCAR3 ZIC2 OE
SSC-A
CD133-PE
CD133high
0.059%
0.21%
0.020%
0.14%
3.54%
7.76%
3.10%
7.02%
All cells
Single cells
Viable cells
Non-stained
Zombie Aqua only
CD133 only
Zombie Aqua & CD133

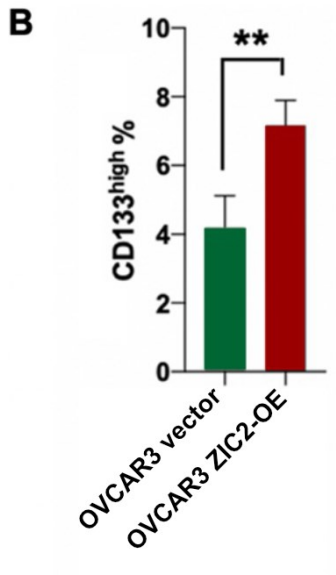

Figure 3.25 Overexpression of ZIC2 increases the proportion of CD133^{high} cells in OVCAR3 cells

The proportion of CD133^{high} cells was determined by flow cytometry using OVCAR3 vector and OVCAR3 ZIC2-OE cells treated with CD133 PE-conjugated antibody and Zombie Aqua dye. **(A)** Images show the percentage of CD133^{high} cells in the negative control group (i.e., Non-stained: cells without any treatment), the Fluorescence Minus One (FMO) control groups (i.e., Zombie Aqua only: cells treated only with Zombie Aqua dye; CD133 only: cell treated only with CD133 PE-conjugated antibody), and the experimental group (i.e., Zombie Aqua & CD133: cells treated with Zombie Aqua dye and CD133 PE-conjugated antibody). All cells: all cells collected by the flow cytometry. Single cells: single cells selected from doublet discrimination. Viable cells: cells with Zombie Aqua-positive cells excluded. Results were from one representative experiment of three independent experiments. 100,000 events were collected for each sample. **(B)** Histogram shows the percentage of CD133^{high} cells in OVCAR3 vector or OVCAR3 ZIC2-OE

cells. CD133^{high} percentage is shown as mean ± SD of three independent experiments. Statistical significance is determined using the one-way ANOVA (**: p< 0.01).

3.3.23 ALDH^{high} enriches CSC-like cells in OVCAR3 and A2780s cells

To determine whether ALDH^{high} enriches CSC-like cells in OVCAR3 and A2780s cells, we sorted ALDH^{high} and ALDH^{low} cells in SKOV3 and OVCAR8 cells by ALDEFLUOR assay followed by FACS and limiting dilution sphere formation assay to examine the self-renewal ability of ALDH^{high} and ALDH^{low} cells. Limiting dilution sphere formation assay showed a significant increase in the number of spheres formed by ALDH^{high} OVCAR3 and ALDH^{high} A2780s cells compared to ALDH^{low} OVCAR3 and ALDH^{low} A2780s cells, suggesting that ALDH^{high} enriches CSC-like cells in OVCAR3 and A2780s cells (**Figure 3.26**).

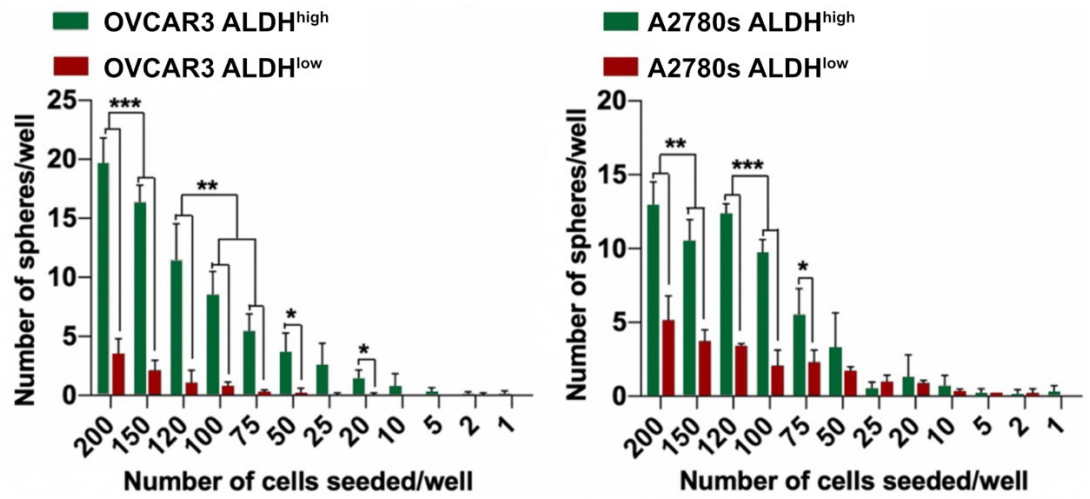

Figure 3.26 ALDH^{high} enriches CSCs in OVCAR3 and A2780s cells

The self-renewal ability of the ALDH^{high} and ALDH^{low} OVCAR3 and A2780s cells was determined using limiting dilution sphere formation assay. Histograms show the number of spheres formed in the wells of 96-well plates. Number of spheres formed per well is shown as mean ± SD of at least three independent experiments. Statistical significance is determined using the one-way ANOVA (*: $p< 0.05$; **: $p< 0.01$; ***$p< 0.001$).

3.2.24 Overexpression of ZIC2 promotes *ALDH1A1* expression in OVCAR3 and A2780s cells

Next, we investigated whether ZIC2 regulates *ALDH1A1* expression in OVCAR3 and A2780s cells. RT-qPCR and immunoblotting showed that the mRNA and protein levels of *ALDH1A1* were significantly increased in OVCAR3 ZIC2-OE and A2780s ZIC2-OE cells compared with the corresponding control cells (**Figure 3.27**). Overexpression of ZIC2 increased *ALDH1A1* mRNA level by 2.35-fold ($p< 0.05$) in OVCAR3 cells and by 2.83-fold ($p< 0.01$) in A2780s cells (**Figure 3.27A**). These data indicate that overexpression of ZIC2 increases *ALDH1A1* expression in OVCAR3 and A2780s cells.

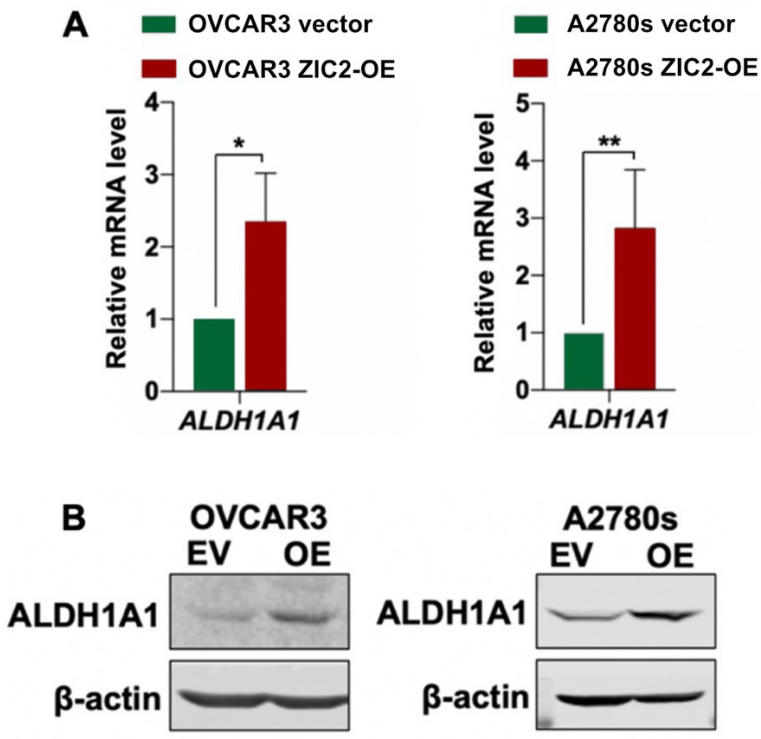

Figure 3.27 Overexpression of ZIC2 increases *ALDH1A1* expression in OVCAR3 and A2780s cells

The mRNA and protein levels of *ALDH1A1* in OVCAR3 and A2780s cells were determined by RT-qPCR and immunoblotting. **(A)** RT-qPCR showed *ALDH1A1* mRNA levels in OVCAR3 and A2780s cells. **(B)** Immunoblotting showed protein levels of ALDH1A1 in OVCAR3 and A2780s cells. β-actin was used as a loading control. Relative RNA level is shown as mean ± SD of at least three independent experiments. Statistical significance is determined using the one-way ANOVA (*: $p < 0.05$; **: $p < 0.01$).

3.2.25 Overexpression of ZIC2 increases the proportion of ALDH^{high} cell population in OVCAR3 and A2780s cells

We demonstrated that overexpression of ZIC2 increased the mRNA and protein levels of *ALDH1A1* in OVCAR3 and A2780s cells. To further investigate whether ZIC2 regulates the proportion of ALDH^{high} cells in OVCAR3 and A2780s cells, we performed ALDEFLUOR assay. ALDEFLUOR assay showed that the percentage of ALDH^{high} cells was 3.8-fold ($p< 0.001$) and 5.6-fold ($p< 0.0001$) higher in OVCAR3 ZIC2-OE cells and A2780s ZIC2-OE cells, respectively, compared to their respective vector control cells, indicating that ZIC2 overexpression increases the proportion of ALDH^{high} cells in OVCAR3 and A2780s cells (**Figure 3.28B**).

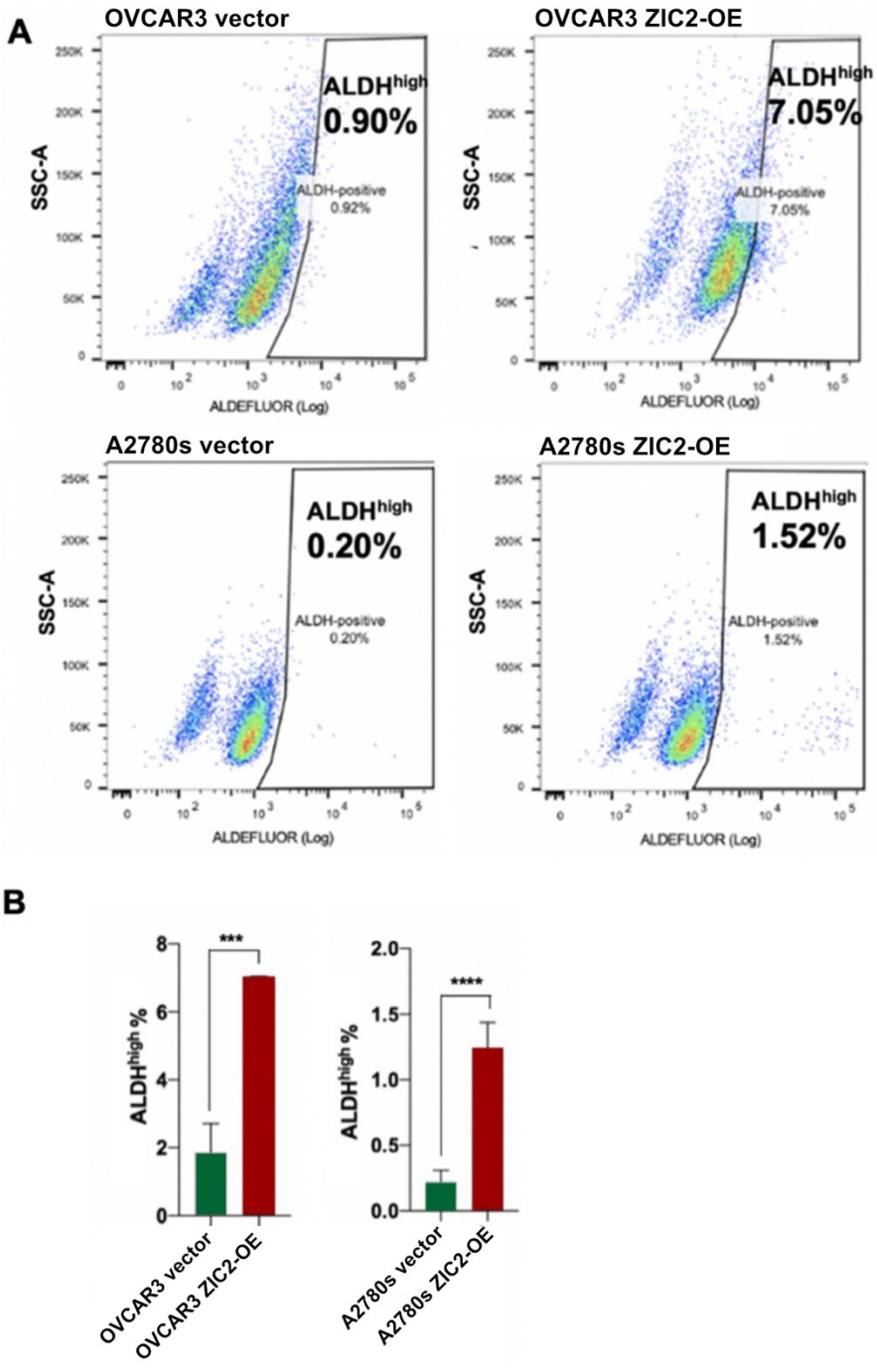

Figure 3.28 Overexpression of ZIC2 increases the percentage of ALDH^{high} cells in OVCAR3 and A2780s cells

The percentage of ALDH^{high} cells in OVCAR3 and A2780s cells was determined by ALDEFLUOR assay. **(A)** Images show the percentage and distribution of

ALDH^{high} cells in OVCAR3 and A2780s cells. The images were from one representative experiment of three independent experiments. 10,000 events were collected for each sample**. (B)** Histograms show the percentage of ALDH^{high} cells in OVCAR3 and A2780s cells. ALDH^{high} percentage was shown as mean ± SD of three independent experiments. Statistical significance was determined using the one-way ANOVA (***: $p< 0.001$; ****: $p< 0.0001$).

3.2.26 Overexpression of ZIC2 maintains the ALDH^{high}-enriched CSC population in A2780s cells

We further determined whether ZIC2 maintains the ALDH^{high}-enriched CSC population in A2780s cells. Due to the relatively low proportion of ALDH^{high} cells in A2780s vector and A2780s ZIC2-OE cells, we first enriched ALDH^{high} cells by culturing A2780s vector and A2780s ZIC2-OE cell in ultra-low attachment plates under sphere culture conditions. Indeed, in A2780s vector and A2780s ZIC2-OE cells, the percentage of ALDH^{high} cells in the spheres was significantly higher than that of ALDH^{high} cells in monolayer culture (**Figure 3.28 and 3.29**). These spheres were then disassociated into single cells and cultured in a monolayer for 0, 1, 2, and 3 days. The percentage of ALDH^{high} cells in these cells cultured in a monolayer was then determined by ADLEFLUOR assay.

ALDEFLUPR assay showed that the proportion of ALDH^{high} A2780s ZIC2-OE cells remained relatively high after three days of monolayer culture compared to A2780s vector cells (**Figure 3.29A and 3.29B**)**.** In contrast, the proportion of ALDH^{high} A2780s vector cells decreased rapidly over three days, approaching that

of the third day under normal monolayer culture (**Figure 3.29A and 3.29B**). For instance, in one experiment, the percentage of ALDH^{high} A2780s vector cells was 38.4% on day 0 (the day of sphere disassociation), 6.45% on day 1 (24 hours after monolayer culture), 4.74% on day 2 (48 hours after monolayer culture), and 3.70% on day 3 (72 hours after monolayer culture), whereas the percentage of ALDH^{high} A2780s ZIC2-OE cells was 45.8% on day 0 (the day of sphere disassociation), 37.4% on day 1 (24 hours after monolayer culture), 32.2% on day 2 (48 hours after monolayer culture), and 24.4% on day 3 (72 hours after monolayer culture) (**Figure 3.29A**). The average percentage of ALDH^{high} cells obtained from three independent experiments was shown in **Figure 3.29B**.

In summary, our data suggest that overexpression of ZIC2 maintains the proportion of ALDH^{high}-enriched CSCs in A2780s cells.

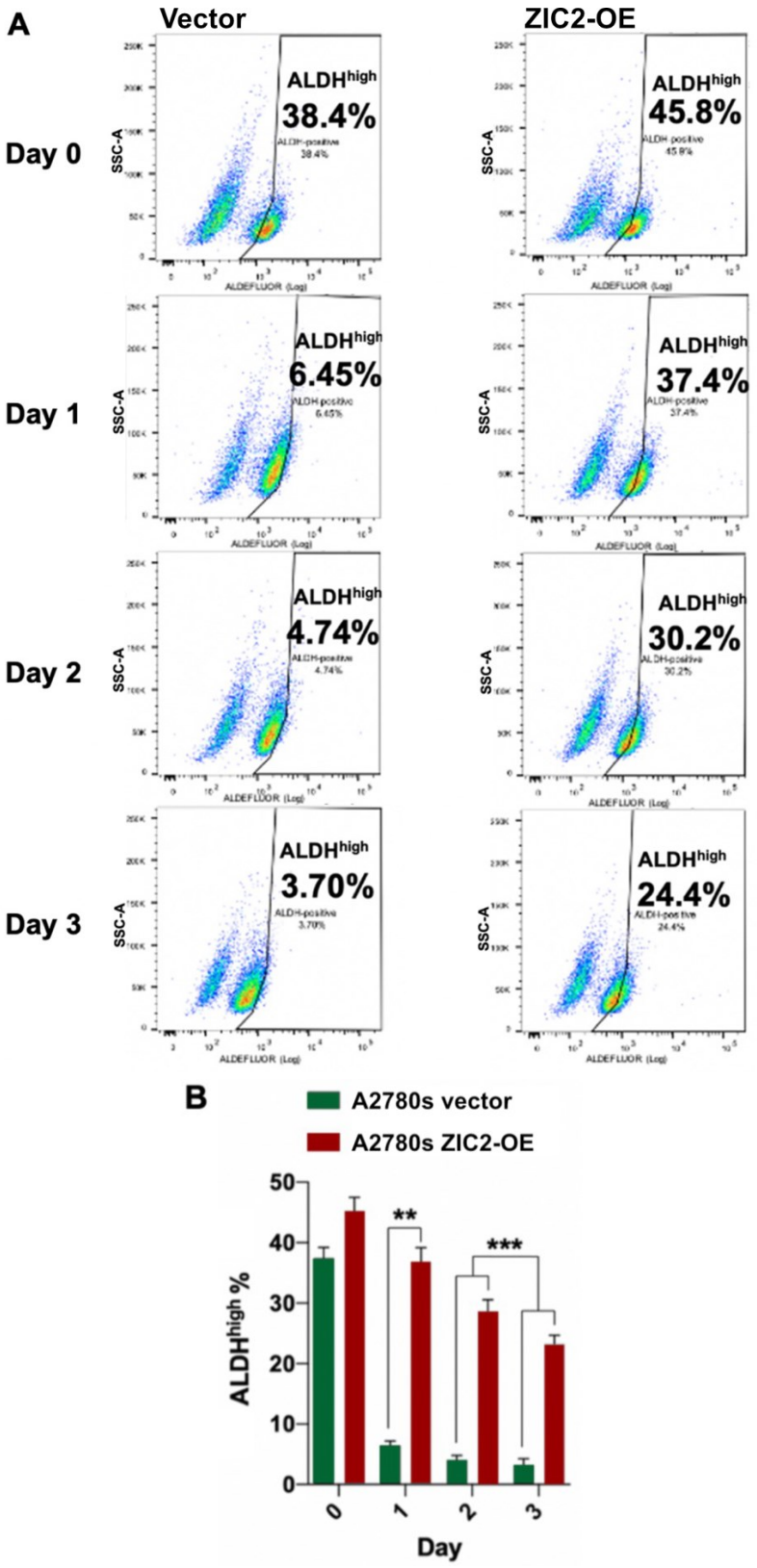
A
Vector
ZIC2-OE
Day 0
Day 1
Day 2
Day 3
ALDHhigh
38.4%
45.8%
6.45%
37.4%
4.74%
30.2%
3.70%
24.4%
SSC-A
ALDEFLUOR (Log)
B
A2780s vector
A2780s ZIC2-OE
ALDHhigh %
Day
**
***
0
1
2
3
10
20
30
40
50

Figure 3.29 Overexpression of ZIC2 maintains the percentage of the ALDH^{high} A2780s cells

(A) ALDH^{high} cells sorted from spheres formed by A2780s vector and A2780s ZIC2-OE cells were grown in monolayer culture. The percentage of ALDH^{high} cells in the culture was measured on days 0, 1, 2, and 3 by ALDEFLUOR assay. Images from one representative experiment of three independent experiments are shown. **(B)** Histograms show the percentage of ALDH^{high} A2780s vector and A2780s ZIC2-OE cells in monolayer culture at specific time points. ALDH^{high} percentage is shown as mean ± SD of three independent experiments. 10,000 events of each sample were collected. Statistical significance is determined using the one-way ANOVA (**p< 0.01; ***: p< 0.001).

3.2.27 Overexpression of ZIC2 decreases tumor growth of OVCAR3 cells

We showed that overexpression of ZIC2 decreased the cell growth in OVCAR3 cells. To determine whether overexpression of ZIC2 regulates tumor growth in OVCAR3 cells, we performed subcutaneous injections using OVCAR3 vector and ZIC2-OE cells. The tumors formed by OVCAR3 ZIC2-OE cells were smaller than those formed by OVCAR3 vector cells (**Figure 3.30A**). The volume and weight of tumors formed by OVCAR3 vector cells. The size, volume, and weight of tumors formed by OVCAR3 vector cells were significantly larger than those formed by OVCAR3 ZIC2-OE cells (**Figures 3.30A, 3.30B, and 3.30C**). When mice were euthanized on day 74, the average volume of tumors formed by OVCAR3 vector and OVCAR3 ZIC2-OE cells was 702.0 mm^3 and 219.7 mm^3,

respectively. The average weight of tumors formed by OVCAR3 vector and OVCAR ZIC2-OE cells was 367.3 mg and 27.5 mg, respectively. We then repeated the experiment to confirm this unexpected finding. In the second experiment, we measured tumor volume twice before collecting tumors due to COVID-19 restrictions during this period. Consistent with the first experiment, the tumors formed by OVCAR3 ZIC2-OE cells were much smaller than those formed by OVCAR3 vector cells (**Figure 3.30D and 3.30E**). Because we wanted to extract RNA from the tumors to confirm *ZIC2* overexpression by RT-qPCR, we did not weigh these tumors. Instead, we prepared tumor lysates with TRIzol immediately after capturing tumor images to minimize RNA degradation. RT-qPCR and immunoblotting confirmed ZIC2 overexpression in tumors formed by OVCAR3 ZIC2-OE cells (**Figure 3.30F and 3.30G**). Monolayer cultured OVCAR3 vector and OVCAR3 ZIC2-OE cells were included as negative controls for RT-qPCR analysis (**Figure 3.30F**).

In addition, we examined the protein expression of ZIC2 and ALDH1A1 by immunoblotting and the distribution and localization of ZIC2-positive, ALDH1A1-positive, Ki-67-positive cells in tumors formed by OVCAR3 vector and OVCAR3 ZIC2-OE cells by IHC staining (**Figure 3.30G and 3.30H**). Immunoblotting using anti-FLAG antibody confirmed that ZIC2 was expressed in tumors formed by OVCAR3 ZIC2-OE cells, but not in tumors formed by OVCAR3 vector cells. Immunoblotting also showed that ALDH1A1 was similarly expressed in all tumors. IHC showed that ZIC2-positive cells were present in tumors formed by OVCAR3 ZIC2-OE cells but not in tumors formed by OVCAR3 vector cells, and that similar

proportions of ALDH1A1-positive cells and Ki-67-positive cells were present in tumors formed by OVCAR3 vector and OVCAR3 ZIC2-OE cells.

In summary, these data indicate that overexpression of ZIC2 inhibits tumor growth of OVCAR3 cells.

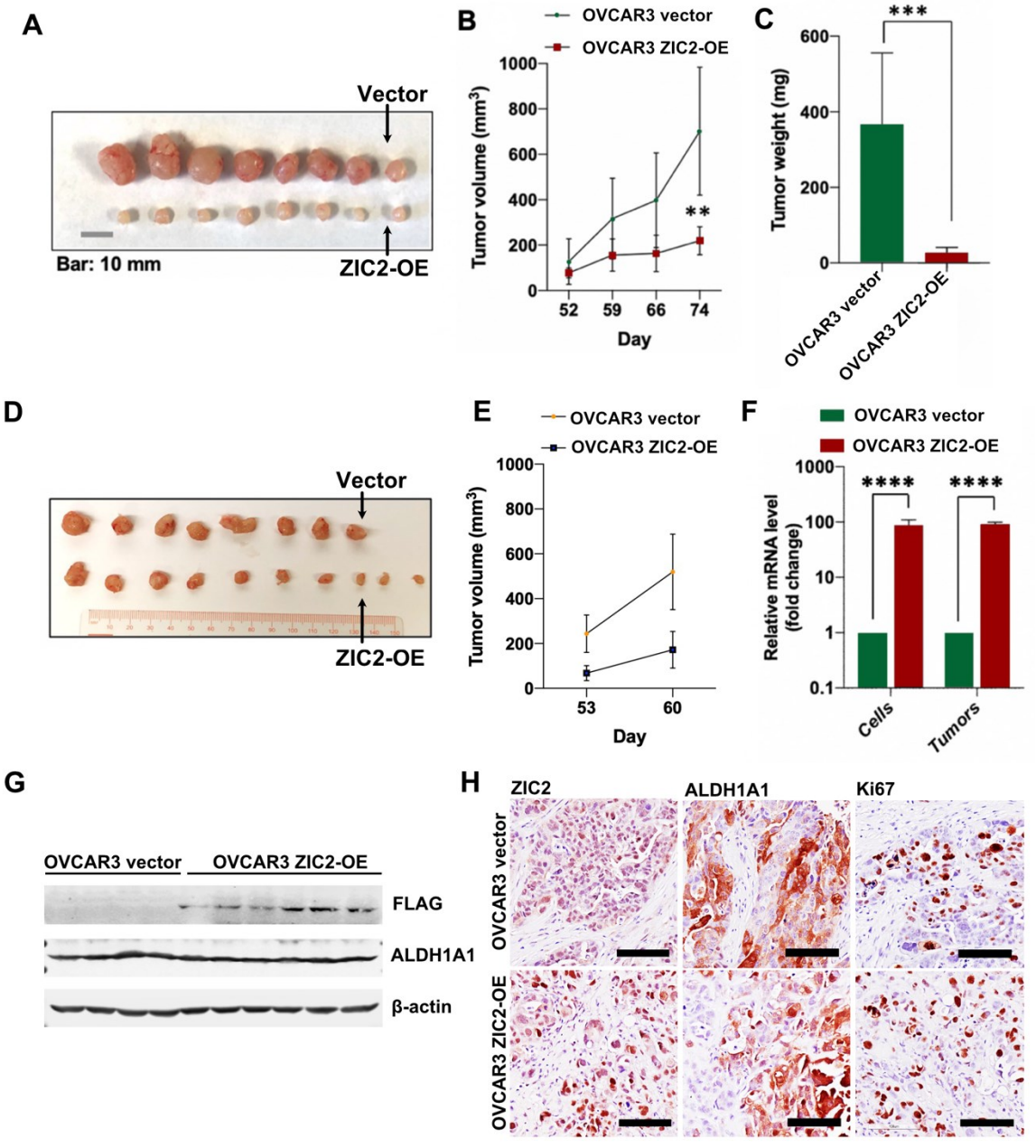

Figure 3.30 Overexpression of ZIC2 decreases tumor growth of OVCAR3 cells

(A) Image shows xenografted tumors formed by OVCAR3 vector (Vector) and OVCAR3 ZIC2-OE (ZIC2-OE) cells on day 74 in the first experiment. **(B)** Line chart shows tumor growth (tumor volume) of OVCAR3 vector and OVCAR3 ZIC2-OE cells at specific time points in the first experiment. Volumes of OVCAR3 vector tumors (n = 8) and OVCAR3 ZIC2-OE tumors (n = 8) are shown as mean ± SD. **(C)** Histogram shows the weight of OVCAR3 vector (n = 8) and OVCAR3 ZIC2-OE (n = 8) tumors. Tumor weights are shown as mean ± SD. **(D)** Image shows the xenografted tumors formed by OVCAR3 vector (Vector) and OVCAR3 ZIC2-OE (ZIC2-OE) cells on day 89 in the second experiment. **(E)** Line chart shows the volume of OVCAR3 vector and ZIC2-OE tumors at specific time points in the second experiment. **(F)** RT-qPCR showed ZIC2 expression in monolayer cultured cells and xenografted tumors. Relative mRNA expression is shown as mean ± SD. **(G)** Protein expression of ZIC2 (ZIC2-FLAG) and ALDH1A1 in OVCAR3 vector and OVCAR3 ZIC2-OE tumors was examined by immunoblotting with anti-FLAG and anti-ALDH1A1 antibodies, respectively. β-actin was used as a loading control. **(H)** ZIC2-positive, ALDH1A1-positive, and Ki-67-positive cells in sections from tumors formed by OVCAR3 vector and OVCAR3 ZIC2-OE cells were determined by IHC. Magnification: 20X. The scale bar is 100 μm. Statistical significance is determined using the one-way ANOVA (*: $p< 0.05$; **: $p< 0.01$; ***: $p< 0.001$; ****: $p< 0.0001$).

3.3 Discussion

In Chapter 3, we demonstrated that ZIC2 regulates the tumorigenic phenotypes in EOC cells, including cell growth, single-cell survival, anchorage-independent growth, cell migration, stemness, and tumor growth. Studies showed that upregulation of ZIC2 predicts poor survival in multiple human cancers, including EOC (163,165). Studies also showed that ZIC2 promotes tumorigenic phenotypes in human cancers (161,165,166,169,170). Expression of this gene in mouse ESC and liver CSCs is associated with maintaining the expression of CSC-related genes (169,171). We hypothesized that ZIC2 promotes tumorigenic phenotypes in EOC. To test this hypothesis, we first determined the relationship between ZIC2 expression and EOC patient survival, along with ZIC2 expression in EOC samples and cell lines. We found that high *ZIC2* expression is associated with poor overall and post-progression survival in EOC patients, and that *ZIC2* was expressed in a subset of EOC samples and in some EOC cell lines. To determine whether ZIC2 regulates the tumorigenic phenotypes, we establish ZIC2-KO and ZIC2-OE models using EOC cell lines that naturally express ZIC2 and EOC cell lines that naturally do not express ZIC2, respectively. Using these models, we performed *in vitro* functional assays and animal studies. In the ZIC2-KO models, knockout of ZIC2 inhibits almost all tested biological functions in SKOV3 cells, including cell growth, single-cell survival, anchorage-independent growth, cell migration, self-renewal ability, and tumor growth; knockout of ZIC2 also inhibits cell growth, cell migration, and self-renewal ability, but does not inhibit other tested biological functions in OVCAR8 cells. In the ZIC2-OE models, overexpression of

ZIC2 promotes single-cell survival, cell migration, and self-renewal ability, but inhibits cell growth, anchorage-independent growth, and tumor growth in OVCAR3 cells; overexpression of ZIC2 promotes cell migration and self-renewal ability but inhibits cell growth in A2780s cells. Our findings in this study suggest that ZIC2 is required for the tumorigenic phenotypes in EOC cell lines that naturally express ZIC2 (i.e., SKOV3 and OVCAR8). However, the effect of overexpressed ZIC2 in EOC cell lines that naturally do not express ZIC2 (i.e., A2780s and OVCAR3) is variable, depending on the pathobiological functions we examined. Therefore, we propose that the pathobiological functions of ZIC2 in EOC are cell-context dependent (**Table 3.2**).

Table 3.2 The cell-context dependent regulation of ZIC2 in the tumorigenic phenotypes of EOC cells

Models	**KO models**		**ZIC2-OE models**	
Functional assay and tumorigenic phenotypes	**SKOV3 ZIC2-KO**	**OVCAR8 ZIC2-KO**	**OVCAR3 ZIC2-OE**	**A2780s ZIC2-OE**
Neutral red uptake assay (cell growth)	Decreased	Decreased	Decreased	Decreased
Clonogenic assay (single-cell survival)	Decreased	Insignificant	Increased	Insignificant
Soft agar assay (anchorage-independent growth)	Decreased	Insignificant	Not available (no colonies)	Decreased
Transwell migration assay (cell migration)	Decreased	Decreased	Increased	Increased
Sphere formation assay (self-renewal ability)	Decreased	Insignificant	Increased	Increased
Subcutaneous injection (tumor growth)	Decreased	Not determined	Decreased	Not determined

*Insignificant: no significant change in the data. Not available (no colonies): OVCAR3 vector or OVCAR3 ZIC2-OE cells did not form colonies in the soft agar

assay and data were not available. Not determined: the indicated experiments were not performed with the model.

The regulatory effects of ZIC2 on the tumorigenic phenotypes of EOC might also be related to specific cell states. We suggest that ZIC2 promotes the self-renewal ability in all four EOC cell lines we examined. Immunoblotting showed that ZIC2 upregulates ALDH1A1 expression in SKOV3, OVCAR3, and A2780s cells. By performing ALDEFLUOR assay, we show that not all EOC cells expressing ZIC2 were $ALDH^{high}$ cells. ALDH1A1 expression might not be regulated by ZIC2 in all cell states, as cell states might be associated with different chromatin accessibility of cells, such as CSC and non-CSC (507-509). We sorted purified $ALDH^{high}$ cells from SKOV3 WT and SKOV3 ZIC2-KO cells and cultured them in a monolayer in normal medium for three days and found that SKOV3 WT cells maintain CSC-like cells, whereas $ALDH^{high}$ cells in SKOV3 ZIC2-KO cells rapidly differentiate into $ALDH^{low}$ cells (**Figure 3.17**). Similarly, overexpression of ZIC2 in A2780s cells helps maintain CSC-like cells ($ALDH^{high}$ cells) (**Figure 3.29**). ZIC2 activates the expression of the stem cell transcription factor *OCT4* in liver CSCs and is involved in the regulation of stem cell-related genes in mouse ESCs, in which these regulatory effects involve chromatin remodeling complexes (169,171). In this regard, we suggest that the regulation of self-renewal ability by ZIC2 may depend on the cell state. For instance, ZIC2 might specifically regulate genes that maintain self-renewal capacity through epigenetic modifications modifying chromatin accessibility in CSCs. Although we only tested the effect of ZIC2 on the

proportion of cells expressing CSC markers $CD133^{high}$ and $ALDH^{high}$, $ALDH^{high}$ cells in SKOV3, A2780, and OVCAR3 cells showed greater sphere-forming ability than $ALDH^{low}$ cells in these cell lines. Similarly, $CD133^{high}$ OVCAR3 cells showed greater sphere-forming capability than $CD133^{low}$ cells (**Figure 3.25**). In this study, no appropriate CSC markers were identified for OVCAR8 cells, but limiting dilution sphere formation assay indicated that ZIC2 promotes the sphere-forming ability in OVCAR8 cells.

The cell-context-dependent regulation of the tumorigenic phenotypes by ZIC2 could be attributed to the complexity of EOC. ZIC2 has been shown to be pro-tumorigenic in other human cancers (161,165,166,169,170). Until now, no report is available on the cell context-dependent regulation of the tumorigenic phenotype by ZIC2 in other human cancers. We suggest that this is partially due to the complexity of the EOC origins. There are four major subtypes of EOC that are thought to originate in different organs with different backgrounds for genetic mutations (55). In the cell models we explored, SKOV3 and A2780s are endometrioid cell lines, while OVCAR3 and OVCAR8 are HGSOC cell lines (55). We acknowledge that cell lines of different subtypes have distinct gene expression profiles and signaling pathway activities. Furthermore, unlike SKOV3 and OVCAR3 cells naturally expressing ZIC2, OVCAR3 and A2780s are EOC cells that naturally do not express ZIC2, suggesting that ZIC2 is not required to maintain the tumorigenic phenotypes in OVCAR3 and A2780s cells. Although we found that overexpression of ZIC2 in EOC cells that naturally do not express ZIC2 plays a role in promoting cell migration and self-renewal ability, it does not promote cell

growth, anchorage-independent growth, or tumor growth. Therefore, re-expression of ZIC2 in EOCs that naturally do not express ZIC2 might be of no benefit to cancer cells, as demonstrated by the ZIC2-OE models. One possibility is that overexpression of ZIC2 in these EOC cells might disrupt the balance in gene expression and signaling pathways, by which ZIC2 competes with other transcription factors or co-activators important for pathobiological functions in the cells.

The role of ZIC2 in regulating the tumorigenic phenotypes in EOC remains to be explored. In this chapter, we investigated the role of ZIC2 in the regulation of tumorigenic phenotypes in EOC. We suggest that ZIC2 promotes tumor growth in SKOV3 cells and reduces tumor growth in OVCAR3 cells, but how ZIC2 differentially regulates tumor growth in the SKOV3 ZIC2-KO and OVCAR3 ZIC2-OE models remains to be explored. *In vivo,* tumor growth is not only related to the gene expression in the cells themselves, but also to the tumor microenvironment (55,510,511). The tumor microenvironment is composed of non-cancer cells, chemokines, cytokines, and ECM-associated proteins, adding further complexity to tumor growth (510,511). Our current study is limited to exploring the pathobiological functions of ZIC2 regulating the tumorigenic phenotypes of EOC cells. Investigation of factors (e.g., non-cellular components of ECM, tumor cells, tumor stromal cells, immune cells, and endothelial cells) in the tumor microenvironment might benefit the understanding of the regulatory role of ZIC2 in the tumorigenic phenotypes *in vivo* (511-513).

Our research reveals for the first time that ZIC2 promotes tumorigenic phenotypes in EOC that naturally expresses ZIC2. In our study, we demonstrate a positive correlation between high *ZIC2* expression and poor survival in EOC patients, as well as upregulation of *ZIC2* in a subset of EOC samples and cell lines, along with regulatory effects of ZIC2 on tumorigenic phenotypes *in vitro* and *in vivo*. We suggest that the regulatory role of ZIC2 in promoting tumorigenic phenotypes in EOC is cell-context dependent. Research on ZIC2 in EOC is limited to one report published in 2012 (163). That report showed that EOC patients with high *ZIC2* expression are associated with poor overall survival. However, the survival data in that report were obtained from a limited number of EOC patients (n = 232) at an Italian institute, and their limited data on the regulation of tumorigenic phenotypes by ZIC2 do not suggest a regulatory role of ZIC2 in EOC. For instance, the authors showed biological functions of ZIC2 in ZIC2-overexpressed human embryonic kidney cell HEK293T, but their data only represent the role of ZIC2 in this cell line; the authors showed that knockdown of ZIC2 reduces the proliferation of OVCAR8 cells using the OVCAR8 ZIC2-knockdown model for EdU (5-ethynyl-2'-deoxyuridine) assay, but their data ignored the effect on the proliferation of EOCs that naturally do not express ZIC2.

Our findings highlight the biological importance of ZIC2 in EOC. ZIC2 might be a therapeutic target for EOCs that naturally express ZIC2, which might help improve the survival of EOC patients with ZIC2-positive tumors. EOC is considered the most lethal gynecological cancer (16). The lethality of EOC is due to the fact that most patients are diagnosed at advanced stages and these patients eventually

relapsed after treatment (97,98). The presence of CSCs and metastasis of EOC are considered important causes of chemoresistance and recurrence (282-285). Our data suggest that ZIC2 regulates the tumorigenic phenotypes in EOC, including promoting cell migration and maintaining the CSC-like cell population. The migration of tumor cells is related to the process of tumor metastasis. Thus, further exploration and development of ZIC2-targeted therapies and drugs might help overcome the recurrence and metastasis in EOC expressing ZIC2.

To conclude, we suggest that ZIC2 may promote tumorigenic phenotypes in EOCs that naturally express ZIC2 and that these regulatory effects are cell-context dependent.

CHAPTER 4: The role of ZIC2 in regulating the transcriptome in EOC

4.1 Introduction

Ovarian cancer is a disease that consists of various subtypes. Based on the clinical characteristics of ovarian cancer, it is divided into indolent Type I and highly aggressive Type II (2). Type I ovarian cancer includes low-grade serous, low-grade endometrioid, clear cell, and mucinous carcinomas (3,4). Type II ovarian cancer includes high-grade serous ovarian cancer, high-grade endometrioid carcinoma, and undifferentiated carcinoma (3,4). Type I and Type II ovarian cancers have unique gene mutations (55,56). For instance, Type II HGSOC usually has *TP53* mutations, which are uncommon in other EOC subtypes (55,56). In addition, EOC may be regulated by different tumor microenvironments and epigenetic modifications during tumor development (514,515).

ZIC2 has been reported to directly activate the expression of the stem cell transcription factor *OCT4* through interacting with the nuclear remodeling factor (NURF) complex (169). In mouse ESC, ZIC2 bound to gene enhancers and interacted with the nucleosome remodeling and deacetylase (Mbd3-NuRD) complex containing the core component MBD3, thereby regulating the expression of stem cell-associated genes (171). Similarly, in mouse ESC, ZIC2 directly regulated *Nodal* expression and heterozygous mutations in *Zic2* resulted in abnormal embryonic development (183). In zebrafish, the expression of *zic2a*, a homolog of ZIC2, can be activated by the growth factor Sonic hedgehog (Shh) and represses the expression of the transcription factor *six3b* (187). In human cervical cancer, ZIC2 directly interacts with GLI1 protein, a key transcription factor in the Sonic hedgehog pathway, promoting the activity of this pathway (186). In

hepatocellular carcinoma, ZIC2 upregulates *PAK4* expression and promotes tumor growth and metastasis in a mouse xenograft model (161). In Chapter 3, we suggest that ZIC2 promotes the tumorigenic phenotypes in EOC cells and that this regulation is cell-context dependent. As mentioned above, ZIC2 showed the ability to regulate genes and signaling pathways. Herein, we hypothesize that ZIC2 regulates tumorigenic phenotypes in EOC. There are no studies on the molecular mechanisms of ZIC2 in EOC. Herein, we show that ZIC2 regulates different transcriptomes in different EOCs and reveal potential underlying molecular mechanisms by which ZIC2 regulates tumorigenic phenotypes in EOC.

4.2 Results

4.2.1 The distinct transcriptome in the SKOV3 ZIC2-KO model

To understand how ZIC2 regulates the transcriptome in SKOV3 cells, we performed RNA-seq analysis. We obtained 28 GB of sequencing data from the SKOV3 ZIC2-KO model. The SKOV3 ZIC2-KO model was sequenced through the Illumina HiSeq system. The average reads per SKOV3 WT sample were 23.01 million, and the average reads per SKOV3 ZIC2-KO sample were 23.24 million. The average quality per read of the SKOV3 WT and SKOV3 ZIC2-KO samples was 38, indicating a base error rate of about 0.015%. The average read length was 100 bp (single-end sequencing).

By processing the RNA-seq data, we identified the list of differentially expressed genes in the SKOV3 ZIC2-KO model. Using the differentially expressed genes, we generated a multidimensional scaling (MDS) plot showing the low-dimensional expression distribution of the samples, a cluster heatmap showing the

upregulation and downregulation of genes, pie charts showing the upregulation and downregulation proportions of genes, a mean-difference (MD) plot showing the fold changes and counts of reads per million (CPM) of genes, and a volcano plot showing the *p*-value and fold changes of genes (**Figure 4.1**). The MDS plot showed that the fold changes were significantly different between control samples and ZIC2-KO samples for each model (y coordinate), while the fold changes were similar between samples of the same class (x coordinate) (**Figure 4.1A**). A total of 6,565 differentially expressed genes were identified (FDR< 0.05). The proportion of upregulated and downregulated genes was 48.01% (n = 3,413) and 51.99% (n = 3,152), respectively. Among the differentially expressed genes that were upregulated or downregulated more than 2-fold (n = 1,805), the proportion of downregulated and upregulated genes was 67.26% (n = 1,214) and 32.74% (n = 591), respectively (**Figure 4.1C**). In addition, the MD and volcano plots of the SKOV3 ZIC2-KO model showed more downregulated genes ($|\log_2 (\text{fold change})| > 1$) than upregulated genes **(Figure 4.1D and 4.1E).**

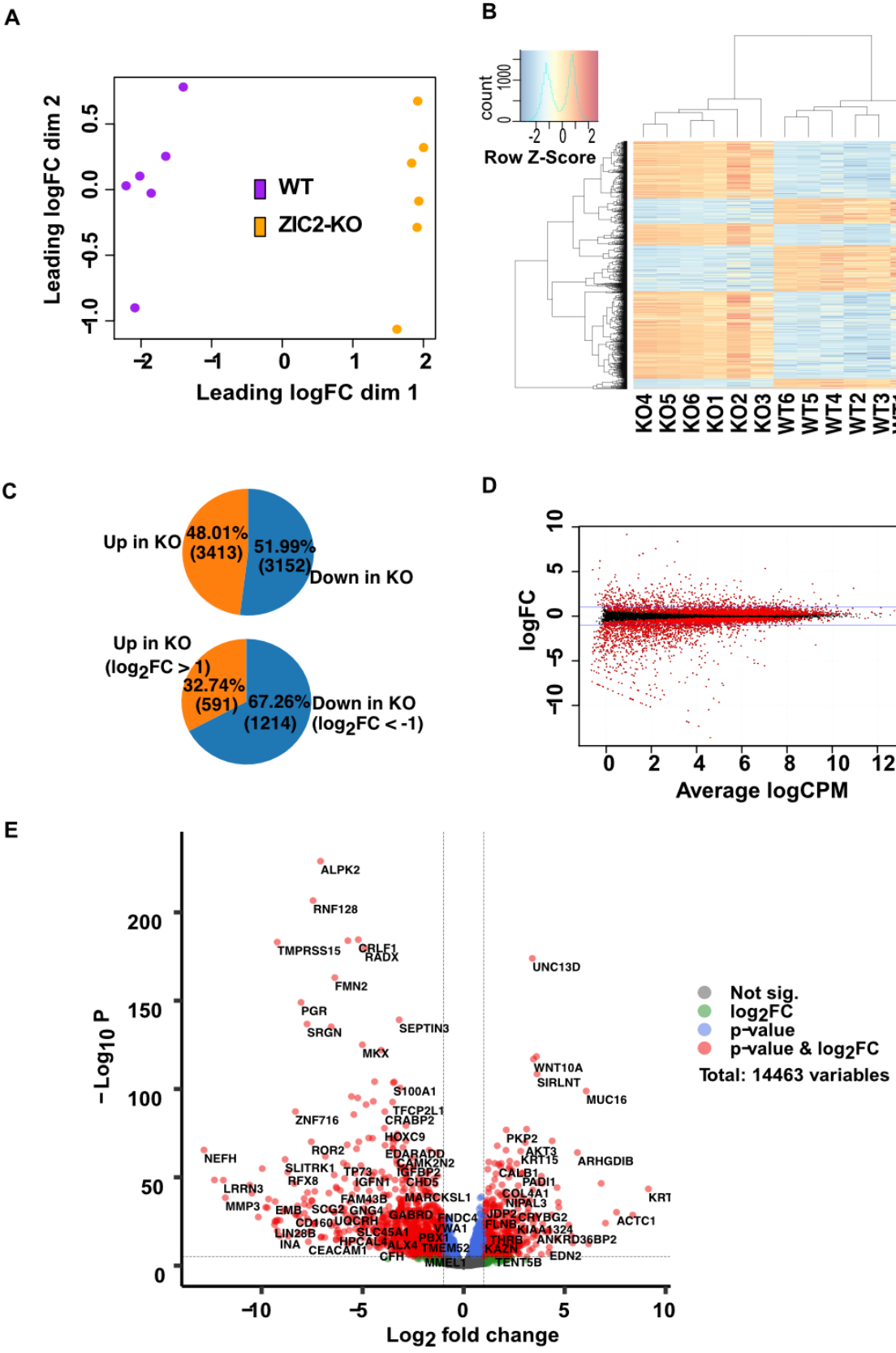
A
Leading logFC dim 2
Leading logFC dim 1
WT
ZIC2-KO
B
count
Row Z-Score
KO4
KO5
KO6
KO1
KO2
KO3
WT6
WT5
WT4
WT2
WT3
WT1
C
Up in KO
48.01%
(3413)
51.99%
(3152)
Down in KO
Up in KO
(log2FC > 1)
32.74%
(591)
67.26%
(1214)
Down in KO
(log2FC < -1)
D
logFC
Average logCPM
E
− Log10 P
Log2 fold change
Not sig.
log2FC
p-value
p-value & log2FC
Total: 14463 variables

Figure 4.1 The transcriptomes of the SKOV3 ZIC2-KO models

(A) Multidimensional scaling (MDS) plot shows the distribution of two-dimensional fold change (dim1 and dim2) of differentially expressed genes in the SKOV3 ZIC2-KO (ZIC2-KO) model. logFC = $\log_2$ (fold change). **(B)** Cluster heatmap shows the expression of all differentially expressed genes (FDR< 0.05) in SKOV3 WT (WT, n = 6) and SKOV3 ZIC2-KO (KO, n = 6). Row Z-Score shows the distribution and number of upregulated and downregulated genes. **(C)** Pie charts show the proportion of upregulated and downregulated for all differentially expressed genes (FDR< 0.05) and those with an absolute fold change greater than 2-fold (|$\log_2$ (fold change)| > 1) in the SKOV3 ZIC2-KO model. The number of genes is shown in parentheses. **(D)** Median-difference (MD) plot shows the relative fold change and relative abundance of reads for all differentially expressed genes (FDR< 0.05) in the SKOV3 ZIC2-KO model. Average logCPM: $\log_2$ (counts per million). **(E)** Volcano plot shows the relative fold change and significance (P-value) for all differentially expressed genes (FDR< 0.05) in the SKOV3 ZIC2-KO model. Not sig.: genes with FDR > 0.05; $\log_2$FC: genes with |$\log_2$ (foldchange)| > 1; P-value: genes with FDR< 0.05; P-value & $\log_2$FC: genes with FDR< 0.05 and |$\log_2$ (foldchange)| > 1.

Next, we explored the expression of the top 50 differentially expressed genes in ascending order of FDR (**Figure 4.2**). The majority of the transcripts were downregulated, accounting for 80% (n = 40), and 20% (n = 10) of these transcripts were upregulated.

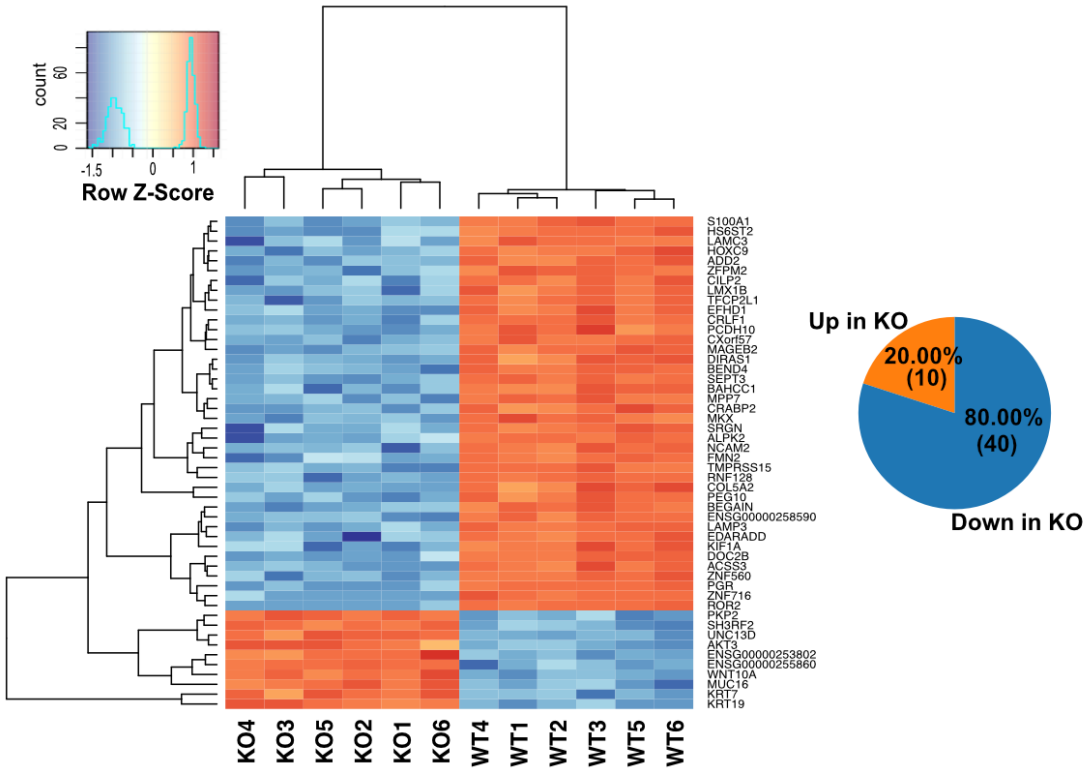

Figure 4.2 The top 50 differentially expressed genes regulated by ZIC2 in the SKOV3 ZIC2-KO model

Cluster heatmap shows the expression of the top 50 differentially expressed genes in the SKOV3 WT (WT, n = 6) and SKOV3 ZIC2-KO (KO, n = 6) samples. Pie chart shows the proportion of upregulated and downregulated genes in the top 50 differentially expressed genes in the SKOV3 ZIC2-KO (KO) model. The number of genes is shown in parentheses. Row Z-Score shows the distribution and number of upregulated and downregulated genes.

Studies showed that *CCND2* (cyclin D2), *MMP3*, *LIN28B*, *IGF2BP1* (IMP1), and *ROR2* are upregulated and promote tumorigenic phenotypes in various human cancers (160,516-520). These five genes were significantly downregulated in the

SKOV3 ZIC2-KO model (**Table 4.1**). To verify their expression at the mRNA and protein levels *in vitro* and *in vivo*, we performed RT-qPCR and immunoblotting assay with cell and tumor lysates. RT-qPCR showed significantly reduced mRNA expression of these genes in SKOV3 ZIC2-KO cells compared to SKOV3 WT cells, consistent with their expression in RNA-seq analysis (**Table 4.1 and Figure 4.3**). The mRNA levels of *CCND2*, *MMP3*, *LIN28B*, *IGF2BP1*, and *ROR2* in SKOV3 ZIC2-KO cells were decreased by 4,980, 3,249, 225, 164, and 119-fold ($p < 0.0001$), respectively, compared to SKOV3 WT cells.

Table 4.1 The expression profiles of selected differentially expressed genes of interest in the SKOV3 ZIC2-KO model

Name	log2 (fold change)	Fold change	logCPM	P Value	FDR
CCND2	-12.3327817	0.00019385	4.09139436	3.22×10^{-49}	4.05×10^{-47}
MMP3	-11.79230223	0.00028194	3.56662718	3.34×10^{-39}	2.67×10^{-37}
LIN28B	-9.358355259	0.00152354	1.1944465	6.72×10^{-24}	1.95×10^{-22}
IGF2BP1	-6.842734997	0.00871227	3.58296508	1.43×10^{-62}	3.40×10^{-60}
ROR2	-7.539836478	0.00537382	0.6955263	7.48×10^{-71}	2.52×10^{-68}

* logCPM = $\log_2$ (counts of reads per million).

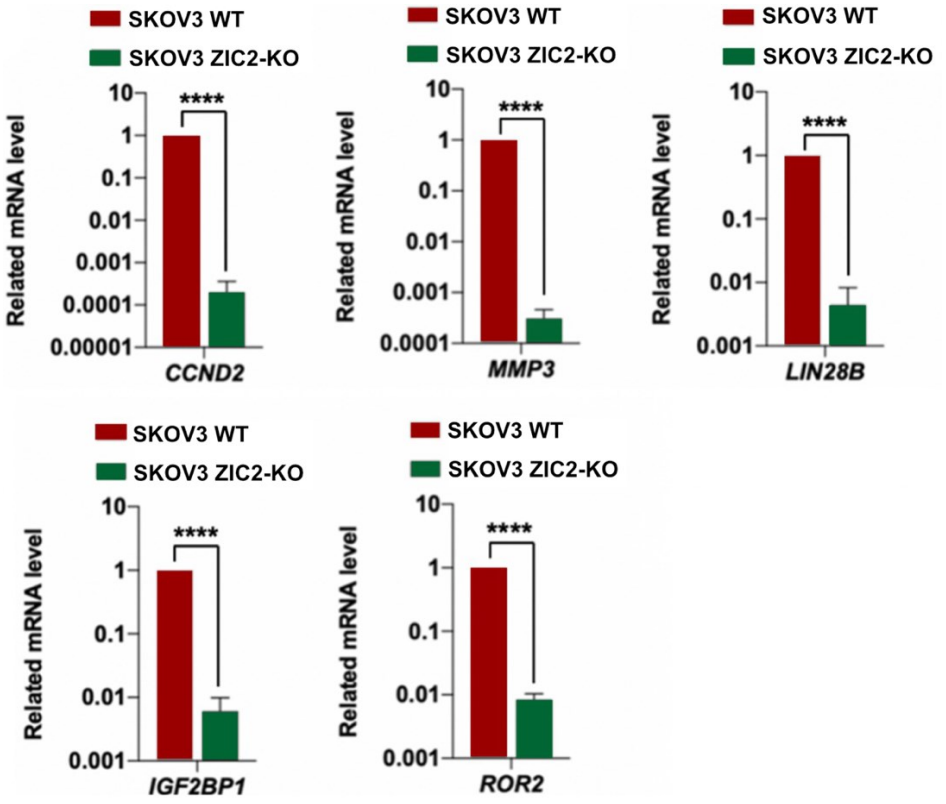

Figure 4.3 The mRNA expression of five differentially expressed genes

RT-qPCR showed mRNA expression of *CCND2*, *MMP3*, *LIN28B*, *IGF2BP1*, and *ROR2* in SKOV3 WT and SKOV3 ZIC2-KO cells. Relative mRNA level is shown as mean ± SD of three independent experiments. Statistical significance is determined using the one-way ANOVA (****: $p < 0.0001$).

Immunoblotting confirmed reduced protein levels of MMP3 and IMP1 in cell lysates and tumor lysates from the SKOV3 ZIC2-KO model, consistent with RT-qPCR results (**Figure 4.3 and 4.4**). Cyclin D2 protein levels were decreased in lysates from tumors formed by SKOV3 ZIC2-KO cells compared with SKOV3 WT cells but were not detected in lysates from SKOV3 ZIC2-KO cells cultured in a monolayer compared with SKOV3 WT cells. LIN28B was not detected by

immunoblotting in cell lysates and tumor lysates from the SKOV3 WT or SKOV3 ZIC2-KO cells. The expression of ROR2 protein was decreased in cell lysates from SKOV3 ZIC2-KO cells compared to SKOV3 WT cells but was elevated in lysates from tumors formed by SKOV3 ZIC2-KO cells compared to SKOV3 WT cells. Interestingly, the mRNA expression of all these genes was consistent with the RNA-seq expression data, but their protein expression in cell and tumor lysates was inconsistent. Therefore, we suggest that the effects of ZIC2 on the expression of these genes may be affected by post-transcriptional modifications and the tumor microenvironment in mice.

In summary, our data suggest that ZIC2 is associated with the mRNA transcription levels of various genes in the SKOV3 ZIC2-KO model.

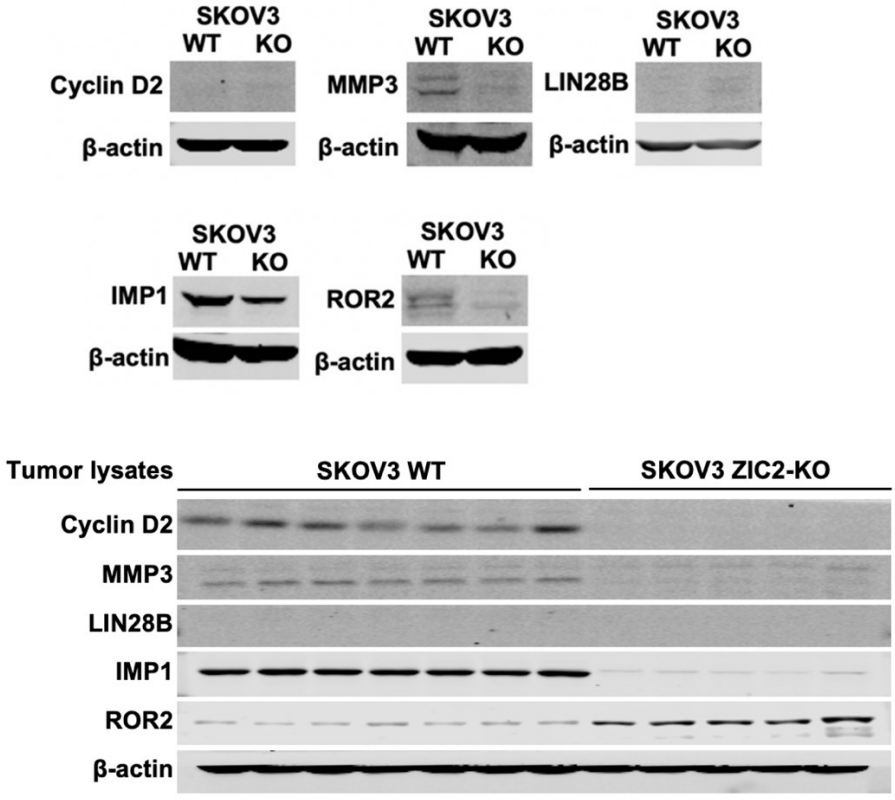

Figure 4.4 The protein expression of five differentially expressed genes in cell lysates and tumor lysates from the SKOV3 ZIC2-KO model

Protein levels of the five genes of interest in cell lysates and tumor lysates from the SKOV3 ZIC2-KO model were determined by immunoblotting. Data were obtained from one representative of three independent experiments.

4.2.2 Potential molecular mechanisms corresponding to differentially expressed genes regulated by ZIC2 in the SKOV3 ZIC2-KO model

Our data demonstrated that ZIC2 regulated the expression of numerous genes in SKOV3 cells. Emerging studies showed that ZIC2 is involved in the regulation of multiple signaling pathways, including Wnt/β-catenin, Sonic hedgehog, and PI3K/AKT pathways, which are associated with tumor progression in various human cancers (182,186,189,521-523). To better understand the potential underlying molecular mechanisms regulated by ZIC2 in SKOV3 cells, we performed Gene Set Enrichment Analysis (GSEA) using all differentially expressed genes (FDR< 0.05) identified in the SKOV3 ZIC2-KO model to enrich the gene sets of hallmarks, biological processes, signaling pathways, and oncogenic signatures, and determined the potential underlying molecular mechanisms regulated by ZIC2 (**Figure 4.5**).

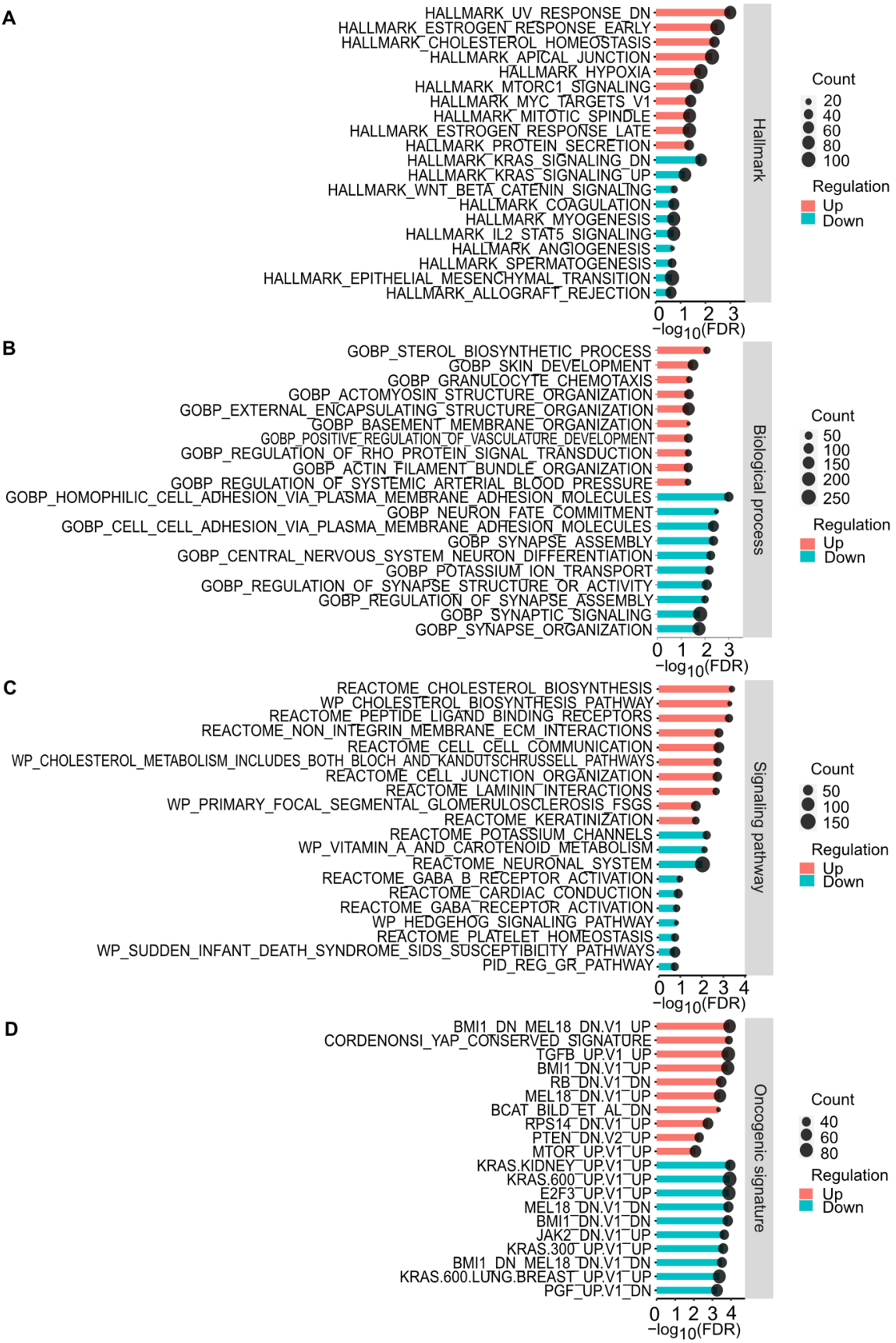
A
HALLMARK_UV_RESPONSE_DN
HALLMARK_ESTROGEN_RESPONSE_EARLY
HALLMARK_CHOLESTEROL_HOMEOSTASIS
HALLMARK_APICAL_JUNCTION
HALLMARK_HYPOXIA
HALLMARK_MTORC1_SIGNALING
HALLMARK_MYC_TARGETS_V1
HALLMARK_MITOTIC_SPINDLE
HALLMARK_ESTROGEN_RESPONSE_LATE
HALLMARK_PROTEIN_SECRETION
HALLMARK_KRAS_SIGNALING_DN
HALLMARK_KRAS_SIGNALING_UP
HALLMARK_WNT_BETA_CATENIN_SIGNALING
HALLMARK_COAGULATION
HALLMARK_MYOGENESIS
HALLMARK_IL2_STAT5_SIGNALING
HALLMARK_ANGIOGENESIS
HALLMARK_SPERMATOGENESIS
HALLMARK_EPITHELIAL_MESENCHYMAL_TRANSITION
HALLMARK_ALLOGRAFT_REJECTION
0 1 2 3
−log10(FDR)
Hallmark
Count
20
40
60
80
100
Regulation
Up
Down
B
GOBP_STEROL_BIOSYNTHETIC_PROCESS
GOBP_SKIN_DEVELOPMENT
GOBP_GRANULOCYTE_CHEMOTAXIS
GOBP_ACTOMYOSIN_STRUCTURE_ORGANIZATION
GOBP_EXTERNAL_ENCAPSULATING_STRUCTURE_ORGANIZATION
GOBP_BASEMENT_MEMBRANE_ORGANIZATION
GOBP_POSITIVE_REGULATION_OF_VASCULATURE_DEVELOPMENT
GOBP_REGULATION_OF_RHO_PROTEIN_SIGNAL_TRANSDUCTION
GOBP_ACTIN_FILAMENT_BUNDLE_ORGANIZATION
GOBP_REGULATION_OF_SYSTEMIC_ARTERIAL_BLOOD_PRESSURE
GOBP_HOMOPHILIC_CELL_ADHESION_VIA_PLASMA_MEMBRANE_ADHESION_MOLECULES
GOBP_NEURON_FATE_COMMITMENT
GOBP_CELL_CELL_ADHESION_VIA_PLASMA_MEMBRANE_ADHESION_MOLECULES
GOBP_SYNAPSE_ASSEMBLY
GOBP_CENTRAL_NERVOUS_SYSTEM_NEURON_DIFFERENTIATION
GOBP_POTASSIUM_ION_TRANSPORT
GOBP_REGULATION_OF_SYNAPSE_STRUCTURE_OR_ACTIVITY
GOBP_REGULATION_OF_SYNAPSE_ASSEMBLY
GOBP_SYNAPTIC_SIGNALING
GOBP_SYNAPSE_ORGANIZATION
0 1 2 3
−log10(FDR)
Biological process
Count
50
100
150
200
250
Regulation
Up
Down
C
REACTOME_CHOLESTEROL_BIOSYNTHESIS
WP_CHOLESTEROL_BIOSYNTHESIS_PATHWAY
REACTOME_PEPTIDE_LIGAND_BINDING_RECEPTORS
REACTOME_NON_INTEGRIN_MEMBRANE_ECM_INTERACTIONS
REACTOME_CELL_CELL_COMMUNICATION
WP_CHOLESTEROL_METABOLISM_INCLUDES_BOTH_BLOCH_AND_KANDUTSCHRUSSELL_PATHWAYS
REACTOME_CELL_JUNCTION_ORGANIZATION
REACTOME_LAMININ_INTERACTIONS
WP_PRIMARY_FOCAL_SEGMENTAL_GLOMERULOSCLEROSIS_FSGS
REACTOME_KERATINIZATION
REACTOME_POTASSIUM_CHANNELS
WP_VITAMIN_A_AND_CAROTENOID_METABOLISM
REACTOME_NEURONAL_SYSTEM
REACTOME_GABA_B_RECEPTOR_ACTIVATION
REACTOME_CARDIAC_CONDUCTION
REACTOME_GABA_RECEPTOR_ACTIVATION
WP_HEDGEHOG_SIGNALING_PATHWAY
REACTOME_PLATELET_HOMEOSTASIS
WP_SUDDEN_INFANT_DEATH_SYNDROME_SIDS_SUSCEPTIBILITY_PATHWAYS
PID_REG_GR_PATHWAY
0 1 2 3 4
−log10(FDR)
Signaling pathway
Count
50
100
150
Regulation
Up
Down
D
BMI1_DN_MEL18_DN.V1_UP
CORDENONSI_YAP_CONSERVED_SIGNATURE
TGFB_UP.V1_UP
BMI1_DN.V1_UP
RB_DN.V1_DN
MEL18_DN.V1_UP
BCAT_BILD_ET_AL_DN
RPS14_DN.V1_UP
PTEN_DN.V2_UP
MTOR_UP.V1_UP
KRAS.KIDNEY_UP.V1_UP
KRAS.600_UP.V1_UP
E2F3_UP.V1_UP
MEL18_DN.V1_DN
BMI1_DN.V1_DN
JAK2_DN.V1_UP
KRAS.300_UP.V1_UP
BMI1_DN_MEL18_DN.V1_DN
KRAS.600.LUNG.BREAST_UP.V1_UP
PGF_UP.V1_DN
0 1 2 3 4
−log10(FDR)
Oncogenic signature
Count
40
60
80
Regulation
Up
Down

Figure 4.5 The topmost enriched gene sets in the SKOV3 ZIC2-KO model

In the SKOV3 ZIC2-KO model, the upregulated (Up) and downregulated (Down) topmost enriched gene sets of hallmarks **(A)**, biological processes **(B)**, signaling pathways **(C)**, oncogenic signatures **(D)** from all differentially expressed genes (FDR< 0.05) regulated by ZIC2. Each bar plot shows the top 10 most enriched significant gene sets (FDR< 0.25) upregulated and the top 10 most enriched significant gene sets downregulated in each gene set category. It displays all gene sets if there are fewer than 10 significant gene sets. Count: number of genes in a specific gene set. NES: normalized enrichment score.

GSEA analyses revealed potential underlying molecular mechanisms regulated by ZIC2 in the SKOV3 ZIC2-KO model. The molecular mechanisms that might be involved in the regulation of tumorigenic phenotypes corresponding to the gene sets are listed in **Table 4.2**. The molecular mechanisms corresponding to these gene sets listed in the table have been shown to be associated with proliferation, cell survival, anchorage-independent growth, cell migration, invasion, CSC stemness, angiogenesis in human cancers (524-551).

In summary, these data suggest potential molecular mechanisms corresponding to the topmost enriched gene sets regulated by ZIC2 in the SKOV3 ZIC2-KO model.

Table 4.2 The topmost enriched gene sets in the SKOV3 ZIC2-KO model that might correspond to the regulation of tumorigenic phenotypes by ZIC2

Gene set	Category	Count	NES	FDR	Description
HALLMARK_KRAS_SIGNALING_UP	Hallmark	83	-1.95	1.51E-02	The hallmark of the upregulated KRAS signaling
HALLMARK_HYPOXIA	Hallmark	99	1.87	1.53E-02	The hallmark of hypoxia
HALLMARK_MYC_TAGETS_V1	Hallmark	61	1.69	3.93E-02	The hallmark of the targets regulated by *MYC* gene
HALLMARK_WNT_BETA_CATENIN_ SIGNALING	Hallmark	24	-1.53	1.81E-01	The hallmark of the Wnt/β-catenin signaling
HALLAMRK_ANGIOGENESIS	Hallmark	18	-1.39	2.13E-01	The hallmark of angiogenesis
HALLMARK_EPITHELIAL_MESENCHYMAL_ TRANSITION	Hallmark	114	-1.37	2.21E-01	The hallmark of the process of epithelial-mesenchymal transition
GOBP_CELL_CELL_ADHESION_VIA_ PLASMA_ MEMBRANE_ADHESION_ MOLECULES	Biological process	120	-2.35	4.40E-03	The biological process of cell-cell adhesion via plasma membrane molecules
GOBP_BASEMENT_MEMBRANE_ ORGANIZATION	Biological process	17	2.13	4.88E-02	The biological process of basement membrane organization
GOBP_REGULATION_OF_RHO_PROTEIN_ SIGNAL_ TRANSDUCTION	Biological process	35	2.12	5.01E-02	The biological process of regulation of Rho protein signal transduction (Rho-A signaling)
GOBP_ACTIN_FILAMENT_BUNDLE_ ORGANIZATION	Biological process	75	2.21	5.06E-02	The biological process of actin filament bundle organization
REACTOME_NON_INTEGRIN_MEMBRANE_ ECM_ INTERACTION	Signaling pathway	36	-2.56	1.61E-03	The pathways related to non-integrin membrane ECM interaction
REACTOME_CELL_CELL_ COMMUNICATION	Signaling pathway	58	-2.51	1.62E-03	The pathway related to cell-cell communication
WP_HEDGEHOG_SIGNALING_PATHWAY	Signaling pathway	15	1.96	1.50E-01	The pathway of Hedgehog signaling
KRAS.600_UP.V1 UP	Oncogenic signature	93	-2.63	0	The oncogenic signature of the upregulated genes upon overexpression of an oncogenic-form KRAS in multiple human lung cancer cell lines
BMI1_DN_MEL18_DN.V1_UP	Oncogenic signature	76	3.03	0	The oncogenic signature of the upregulated genes upon knockdown of *BMI1* and *MEL18* genes in human medulloblastoma cell line (DAOY)
E2F3_UP.V1_UP	Oncogenic signature	86	-2.61	0	The oncogenic signature of the upregulated genes upon overexpression of *E2F3* genes in human primary epithelial breast cancer cells
TGFB_UP.V1_UP	Oncogenic signature	88	2.45	0	The oncogenic signature of the upregulated genes upon the treatment of TGFB1 in human epithelial cell lines
CORDENONSI_YAP_CONSERVED_ SIGNATURE	Oncogenic signature	34	2.77	0	The oncogenic signature of the genes expressed in YAP-positive Grade 3 breast cancer
PTEN_DN.V2_UP	Oncogenic signature	44	1.99	5.16E-03	The oncogenic signature of the upregulated genes upon knockdown of *PTEN* gene in human colon cancer cell line (HCT116)
MTOR_UP.V1_UP	Oncogenic signature	63	1.91	8.13E-03	The oncogenic signature of the upregulated genes upon inhibition of mTOR signaling by a mTOR inhibitor RAD001 in mouse prostate tissue

*NES: normalized enrichment score.

4.2.3 The distinct transcriptome in the OVCAR3 ZIC2-OE model

To understand how ZIC2 regulates the transcriptome in OVCAR3 cells, we performed RNA-seq analysis. We obtained 52 GB of sequencing data from the OVCAR3 ZIC2-OE model. The OVCAR3 ZIC2-OE model was sequenced through the Illumina NOVAseq system. The average reads per OVCAR3 vector sample were 46.09 million, and the average reads per OVCAR3 ZIC2-OE sample were 41.52 million. The average quality per read for the OVCAR3 vector and OVCAR3 ZIC2-OE samples was 36, indicating a base error rate of about 0.025%. The average read length was 100 bp (single-end sequencing).

By processing the RNA-seq data, we identified the list of differentially expressed genes in the OVCAR3 ZIC2-OE model. Using all differentially expressed genes, we generated a multidimensional scaling (MDS) plot, a cluster heatmap, pie charts, a mean-difference (MD) plot, and a volcano plot to show the gene expression profiles in this model (**Figure 4.6**). 10,798 differentially expressed genes (FDR< 0.05) were identified. The proportion of upregulated and downregulated genes was similar at 49.80% (n = 5528) and 50.20% (n = 5270), respectively. Among the differentially expressed genes that were upregulated or downregulated more than 2-fold (n = 2169), we found that the proportion of upregulated and downregulated genes was 37.07% (n = 804) and 62.93% (n = 1365), respectively (**Figure 4.6C**). In addition, the MD and volcano plots of the OVCAR3 ZIC2-OE model showed more downregulated genes ($|\log_2$ (fold change)|> 1) than upregulated genes **(Figure 4.6D and 4.6E).**

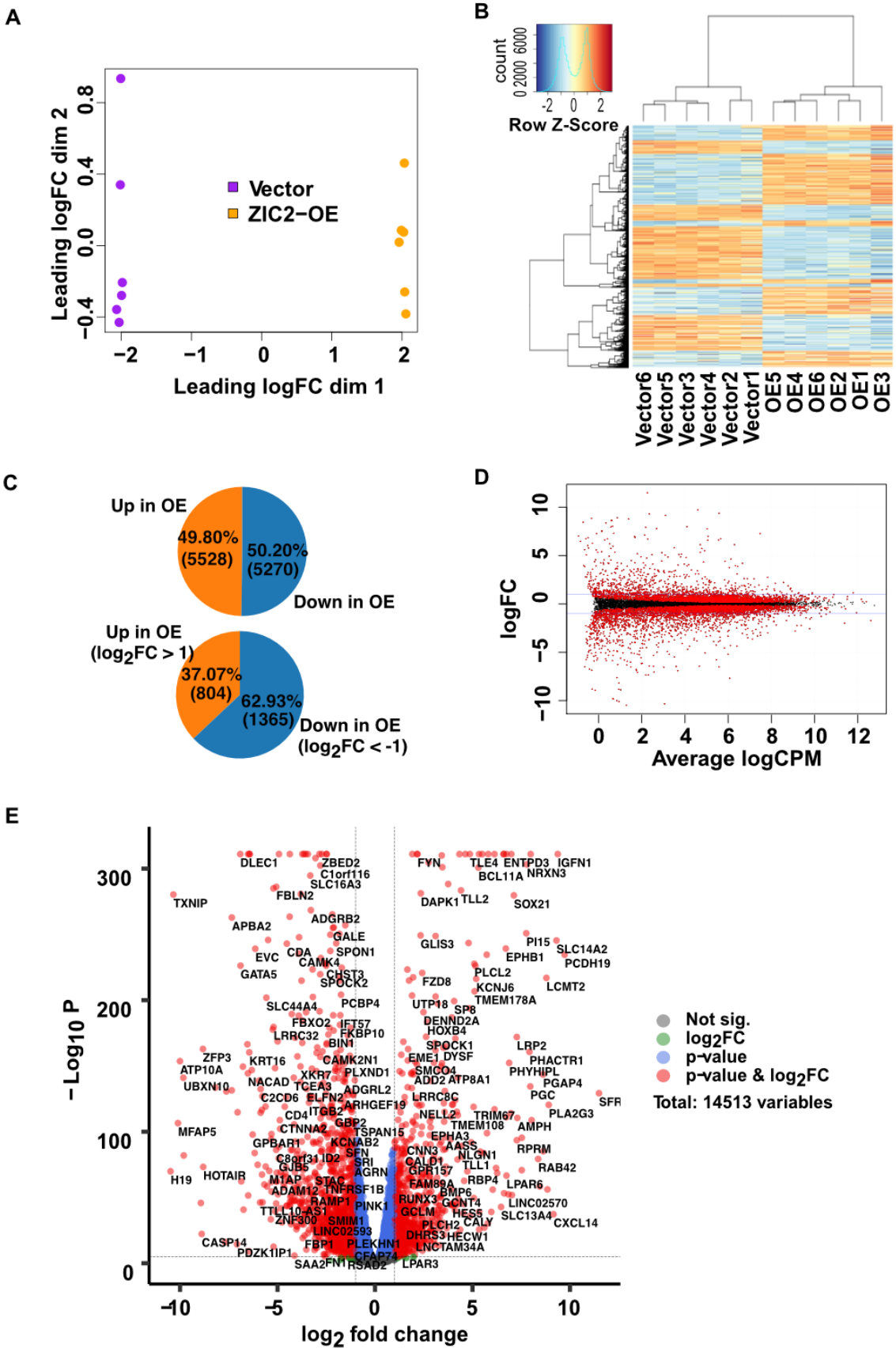
A
Leading logFC dim 2
Leading logFC dim 1
Vector
ZIC2−OE
B
count
Row Z-Score
Vector6
Vector5
Vector3
Vector4
Vector2
Vector1
OE5
OE4
OE6
OE2
OE1
OE3
C
Up in OE
49.80%
(5528)
50.20%
(5270)
Down in OE
Up in OE
(log2FC > 1)
37.07%
(804)
62.93%
(1365)
Down in OE
(log2FC < -1)
D
logFC
Average logCPM
E
−Log10 P
log2 fold change
Not sig.
log2FC
p-value
p-value & log2FC
Total: 14513 variables

Figure 4.6 The transcriptomes of the OVCAR3 ZIC2-OE models

(A) Multidimensional scaling (MDS) plot shows the distribution of two-dimensional fold change (dim1 and dim2) of differentially expressed genes in the OVCAR3 ZIC2-OE (ZIC2-OE) model. logFC = $\log_2$ (fold change). **(B)** Cluster heatmap shows the expression of all differentially expressed genes (FDR< 0.05) in OVCAR3 vector (Vector, n = 6) and OVCAR3 ZIC2-OE (OE, n = 6). Row Z-Score shows the distribution and number of upregulated and downregulated genes. **(C)** Pie charts show the upregulated and downregulated ratios for all differentially expressed genes (FDR< 0.05) and those with an absolute fold change greater than 2-fold (|$\log_2$ (fold change)| > 1) in the OVCAR3 ZIC2-OE samples. The number of genes is shown in parentheses. **(D)** Median-difference (MD) plot shows the relative fold change and relative abundance of reads for all differentially expressed genes (FDR< 0.05) in the OVCAR3 ZIC2-OE model. Average logCPM: $\log_2$ (counts per million). **(E)** Volcano plot shows the relative fold change and significance (P-value) for all differentially expressed genes (FDR< 0.05) in the OVCAR3 ZIC2-OE model. P-value ($\log_{10}$ P) of each differentially expressed gene. Not sig.: genes with FDR > 0.05; $\log_2$ FC: genes with |log2 (foldchange)| > 1; P-value: genes with FDR< 0.05; P-value & $\log_2$ FC: genes with FDR< 0.05 and |$\log_2$ (foldchange)| > 1.

Next, we explored the expression of the top 50 differentially expressed genes in ascending order of FDR (**Figure 4.7**). The upregulated and downregulated transcripts accounted for 58.00% (n = 29) and 42.00% (n = 21), respectively.

In summary, our data show that ZIC2 is associated with the mRNA transcript levels of various genes in the OVCAR3 ZIC2-OE model.

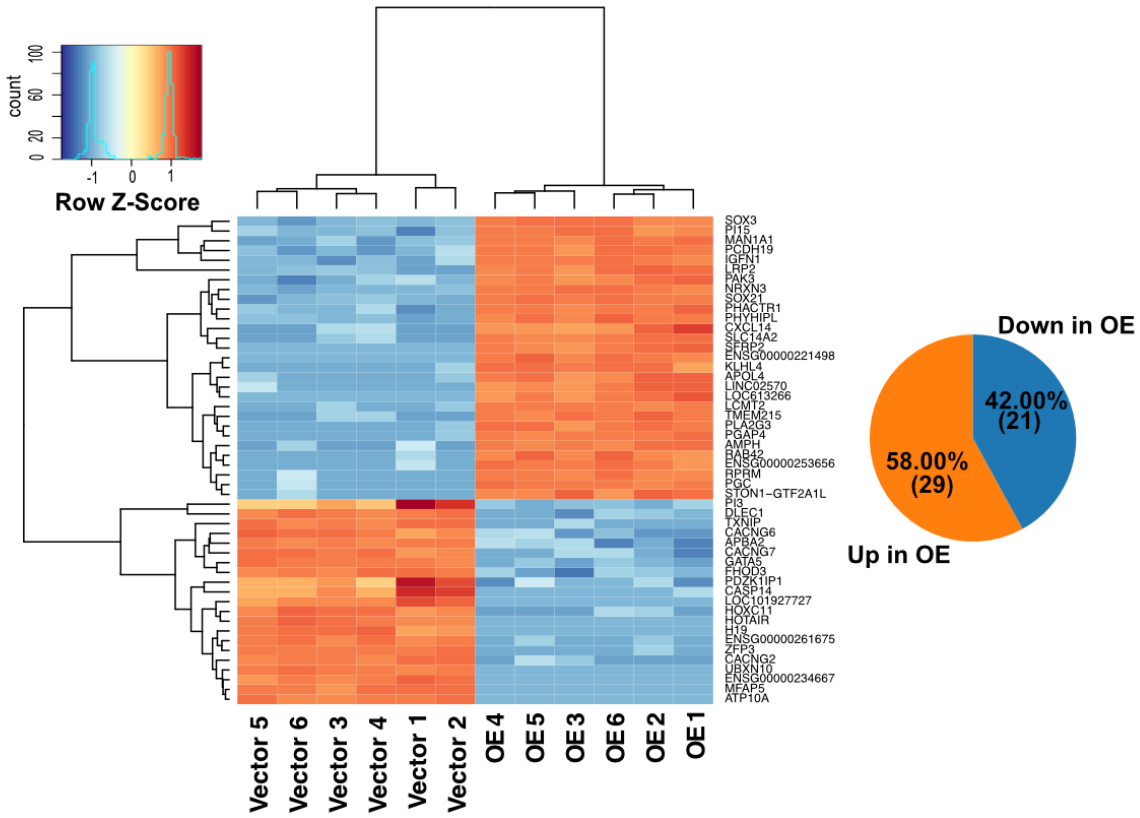

Figure 4.7 The top 50 differentially expressed genes regulated by ZIC2 in the OVCAR3 ZIC2-OE model

Cluster heatmap shows the expression of the top 50 differentially expressed genes in the OVCAR3 vector (Vector, n = 6) and ZIC2-OE (OE, n = 6) samples. Pie chart shows the proportion of upregulated and downregulated genes in the top 50 differentially expressed genes in the OVCAR3 ZIC2-OE (OE) model. The number of genes is shown in parentheses. Row Z-Score shows the distribution and number of upregulated and downregulated genes.

4.2.4 Potential molecular mechanisms corresponding to differentially expressed genes regulated by ZIC2 in the OVCAR3 ZIC2-OE model

To better understand the potential underlying molecular mechanisms regulated by ZIC2 in OVCAR3 cells, we performed GSEA analysis using all differentially expressed genes (FDR< 0.05) identified in the OVCAR3 ZIC2-OE model to enrich the gene sets of hallmarks, biological processes, signaling pathways, and oncogenic signatures (**Figure 4.8**).

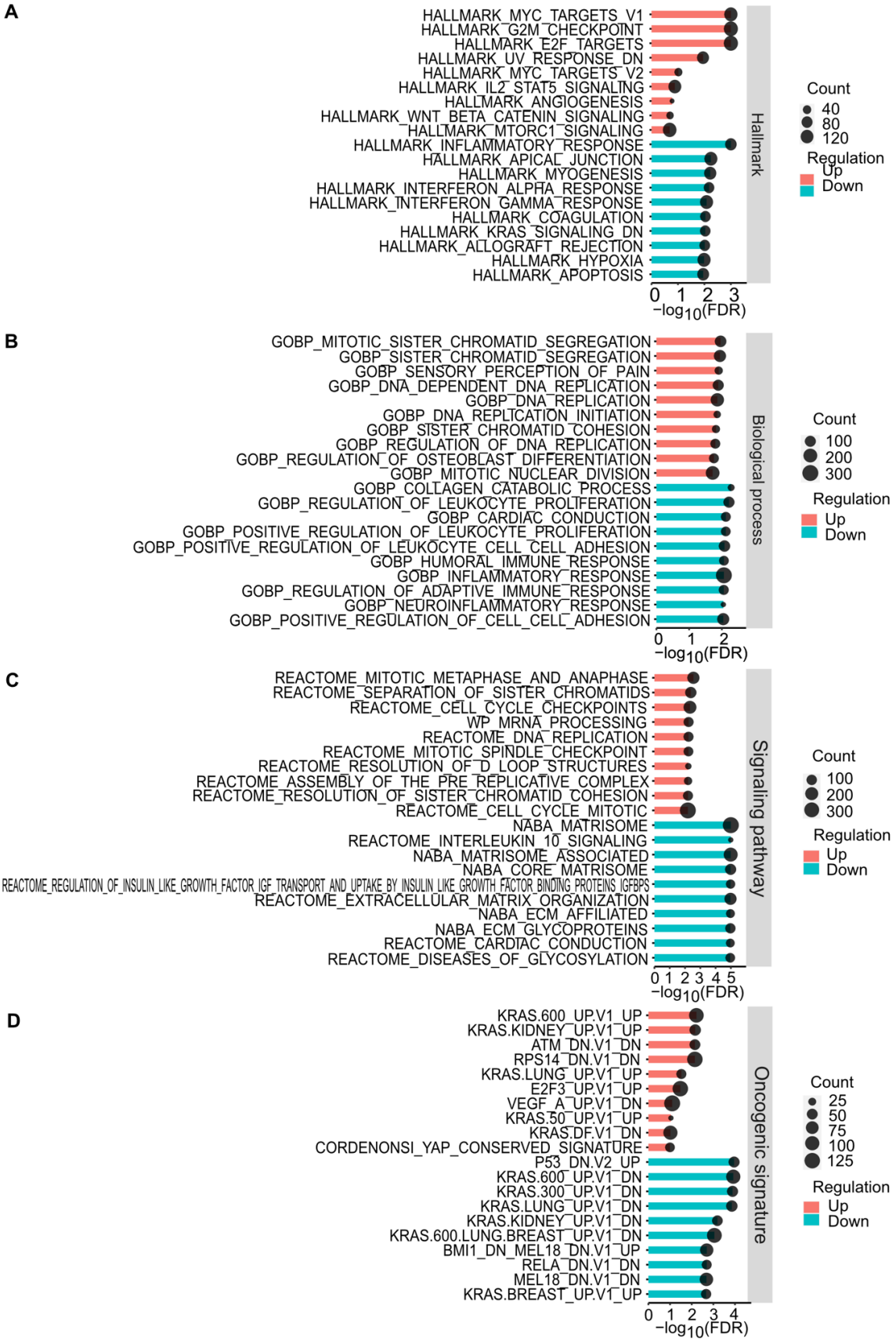
A
HALLMARK_MYC_TARGETS_V1
HALLMARK_G2M_CHECKPOINT
HALLMARK_E2F_TARGETS
HALLMARK_UV_RESPONSE_DN
HALLMARK_MYC_TARGETS_V2
HALLMARK_IL2_STAT5_SIGNALING
HALLMARK_ANGIOGENESIS
HALLMARK_WNT_BETA_CATENIN_SIGNALING
HALLMARK_MTORC1_SIGNALING
HALLMARK_INFLAMMATORY_RESPONSE
HALLMARK_APICAL_JUNCTION
HALLMARK_MYOGENESIS
HALLMARK_INTERFERON_ALPHA_RESPONSE
HALLMARK_INTERFERON_GAMMA_RESPONSE
HALLMARK_COAGULATION
HALLMARK_KRAS_SIGNALING_DN
HALLMARK_ALLOGRAFT_REJECTION
HALLMARK_HYPOXIA
HALLMARK_APOPTOSIS
0 1 2 3
−log10(FDR)
Hallmark
Count
40
80
120
Regulation
Up
Down
B
GOBP_MITOTIC_SISTER_CHROMATID_SEGREGATION
GOBP_SISTER_CHROMATID_SEGREGATION
GOBP_SENSORY_PERCEPTION_OF_PAIN
GOBP_DNA_DEPENDENT_DNA_REPLICATION
GOBP_DNA_REPLICATION
GOBP_DNA_REPLICATION_INITIATION
GOBP_SISTER_CHROMATID_COHESION
GOBP_REGULATION_OF_DNA_REPLICATION
GOBP_REGULATION_OF_OSTEOBLAST_DIFFERENTIATION
GOBP_MITOTIC_NUCLEAR_DIVISION
GOBP_COLLAGEN_CATABOLIC_PROCESS
GOBP_REGULATION_OF_LEUKOCYTE_PROLIFERATION
GOBP_CARDIAC_CONDUCTION
GOBP_POSITIVE_REGULATION_OF_LEUKOCYTE_PROLIFERATION
GOBP_POSITIVE_REGULATION_OF_LEUKOCYTE_CELL_CELL_ADHESION
GOBP_HUMORAL_IMMUNE_RESPONSE
GOBP_INFLAMMATORY_RESPONSE
GOBP_REGULATION_OF_ADAPTIVE_IMMUNE_RESPONSE
GOBP_NEUROINFLAMMATORY_RESPONSE
GOBP_POSITIVE_REGULATION_OF_CELL_CELL_ADHESION
0 1 2
−log10(FDR)
Biological process
Count
100
200
300
Regulation
Up
Down
C
REACTOME_MITOTIC_METAPHASE_AND_ANAPHASE
REACTOME_SEPARATION_OF_SISTER_CHROMATIDS
REACTOME_CELL_CYCLE_CHECKPOINTS
WP_MRNA_PROCESSING
REACTOME_DNA_REPLICATION
REACTOME_MITOTIC_SPINDLE_CHECKPOINT
REACTOME_RESOLUTION_OF_D_LOOP_STRUCTURES
REACTOME_ASSEMBLY_OF_THE_PRE_REPLICATIVE_COMPLEX
REACTOME_RESOLUTION_OF_SISTER_CHROMATID_COHESION
REACTOME_CELL_CYCLE_MITOTIC
NABA_MATRISOME
REACTOME_INTERLEUKIN_10_SIGNALING
NABA_MATRISOME_ASSOCIATED
NABA_CORE_MATRISOME
REACTOME_REGULATION_OF_INSULIN_LIKE_GROWTH_FACTOR_IGF_TRANSPORT_AND_UPTAKE_BY_INSULIN_LIKE_GROWTH_FACTOR_BINDING_PROTEINS_IGFBPS
REACTOME_EXTRACELLULAR_MATRIX_ORGANIZATION
NABA_ECM_AFFILIATED
NABA_ECM_GLYCOPROTEINS
REACTOME_CARDIAC_CONDUCTION
REACTOME_DISEASES_OF_GLYCOSYLATION
0 1 2 3 4 5
−log10(FDR)
Signaling pathway
Count
100
200
300
Regulation
Up
Down
D
KRAS.600_UP.V1_UP
KRAS.KIDNEY_UP.V1_UP
ATM_DN.V1_DN
RPS14_DN.V1_DN
KRAS.LUNG_UP.V1_UP
E2F3_UP.V1_UP
VEGF_A_UP.V1_DN
KRAS.50_UP.V1_UP
KRAS.DF.V1_DN
CORDENONSI_YAP_CONSERVED_SIGNATURE
P53_DN.V2_UP
KRAS.600_UP.V1_DN
KRAS.300_UP.V1_DN
KRAS.LUNG_UP.V1_DN
KRAS.KIDNEY_UP.V1_DN
KRAS.600.LUNG.BREAST_UP.V1_DN
BMI1_DN_MEL18_DN.V1_UP
RELA_DN.V1_DN
MEL18_DN.V1_DN
KRAS.BREAST_UP.V1_UP
0 1 2 3 4
−log10(FDR)
Oncogenic signature
Count
25
50
75
100
125
Regulation
Up
Down

Figure 4.8 The topmost enriched gene sets in the OVCAR3 ZIC2-OE model

In the OVCAR3 ZIC2-OE model, the upregulated (Up) and downregulated (Down) topmost enriched gene sets of hallmarks **(A)**, biological processes **(B)**, signaling pathways **(C)**, oncogenic signatures **(D)** from all differentially expressed genes (FDR< 0.05) regulated by ZIC2. Each bar plot shows the top 10 most enriched significant gene sets (FDR< 0.25) upregulated and the top 10 most enriched significant gene sets downregulated in each gene set category. It displays all the gene sets if there are fewer than 10 significant gene sets. Count: number of genes in a specific gene set. NES: normalized enrichment score.

GSEA analyses revealed the potential underlying molecular mechanisms regulated by ZIC2 in the OVCAR3 ZIC2-OE model. The molecular mechanisms that might be involved in the regulation of tumorigenic phenotypes by ZIC2 corresponding to the gene sets are listed in **Table 4.3**. The molecular mechanisms corresponding to these gene sets listed in the table have been shown to be associated with proliferation, cell survival, anchorage-independent growth, cell migration, invasion, CSC stemness, angiogenesis in human cancers (524-526,530-534,537-539,543-548,551-554). Notably, we found that the gene sets enriched in this model were also associated with the cell cycle, i.e., HALLMARK_G2M_CHECKPOINT and REACTOME_CELL_CYCLE_ CHECKPOINTS.

In summary, these data suggest the potential molecular mechanisms corresponding to the topmost enriched gene sets regulated by ZIC2 in the OVCAR3 ZIC2-OE model.

Table 4.3 The topmost enriched gene sets in the OVCAR3 ZIC2-OE model that might correspond to the regulation of tumorigenic phenotypes by ZIC2

Gene set	Category	Count	NES	FDR	Description
HALLMARK_HYPOXIA	Hallmark	129	-1.77	1.03E-02	The hallmark of hypoxia
HALLMARK_APOPTOSIS	Hallmark	98	-1.74	1.12E-02	The hallmark of apoptosis
HALLMARK_ANGIOGENESIS	Hallmark	19	1.38	1.67E-01	The hallmark of angiogenesis
HALLMARK_WNT_BETA_CATENIN_ SIGNALING	Hallmark	30	1.33	1.99E-01	The hallmark of the Wnt/β-catenin signaling
HALLMARK_MITORC1_SIGNALING	Hallmark	142	1.30	2.06E-01	The hallmark of mTORC1 signaling
GOBP_POSITIVE_REGULATION_OF_ LEUKOCYTE PROLIFERATION	Biological process	67	-2.30	7.58E-03	The biological process of positive regulation of leukoyocte proliferation
GOBP_INFLAMATORY_RESPONSE	Biological process	300	-2.26	8.66E-03	The biological process of inflammatory response
GOBP_POSITIVE_REGULATION_OF_ CELL_CELL_ADHESION	Biological process	133	-2.21	9.08E-03	The biological process of positive regulation of cell-cell adhesion
NABA_MATRISOME	Signaling pathway	371	2.61	0	The pathway related to extracellular matrix-associated proteins (matrisome)
REACTOME_EXTRACELLULAR_MATRIX_ ORGANIZATION	Signaling pathway	161	2.23	9.03E-03	The pathway related to extracellular matrix organization
P53_DN.V2_UP	Oncogenic signature	52	2.51	0	The oncogenic signature of the upregulated genes upon knockdown of *TP53* genes in human embryonic kidney cell line HEK293 cells
BMI1_DN_MEL18_DN.V1_UP	Oncogenic signature	84	2.00	2.02E-03	The oncogenic signature of the upregulated genes upon knockdown of *BMI1* and *MEL18* genes in human medulloblastoma cell line (DAOY)
KRAS.600_UP.V1_UP	Oncogenic signature	108	2.13	6.07E-03	The oncogenic signature of the upregulated genes upon overexpression of an oncogenic-form KRAS in multiple human lung cancer cell lines
E2F3_UP.V1_UP	Oncogenic signature	125	1.77	3.36E-02	The oncogenic signature of the upregulated genes upon overexpression of *E2F3* genes in human primary epithelial breast cancer cells
CORDENONSI_YAP_CONSERVED_ SIGNATURE	Oncogenic signature	39	1.57	1.01E-01	The oncogenic signature of the genes expressed in YAP-positive Grade 3 breast cancer

*NES: normalized enrichment score.

4.2.5 Potential underlying molecular mechanisms commonly regulated by ZIC2 in SKOV3 ZIC2-KO and OVCAR3 ZIC2-OE models

Our data showed that ZIC2 regulated the expression of a number of genes in OVCAR3 cells. To better understand the potential common molecular mechanisms regulated by ZIC2, we compared the topmost enriched gene sets in the SKOV3 ZIC2-KO and OVCAR3 ZIC2-OE models.

We identified four topmost enriched gene sets, including KRAS.600_ UP.V1_UP, E2F3_UP.V1_UP, BMI1_DN_MEL18_DN.V1_UP, and HALLMARK_ WNT_BETA_CATENIN_SIGNALING, which were the top enriched gene sets commonly regulated by ZIC2 in both models, and molecular mechanisms associated with these gene sets have been shown to be associated with tumor progression in human cancers (**Figure 4.9**) (527,530,544,546).

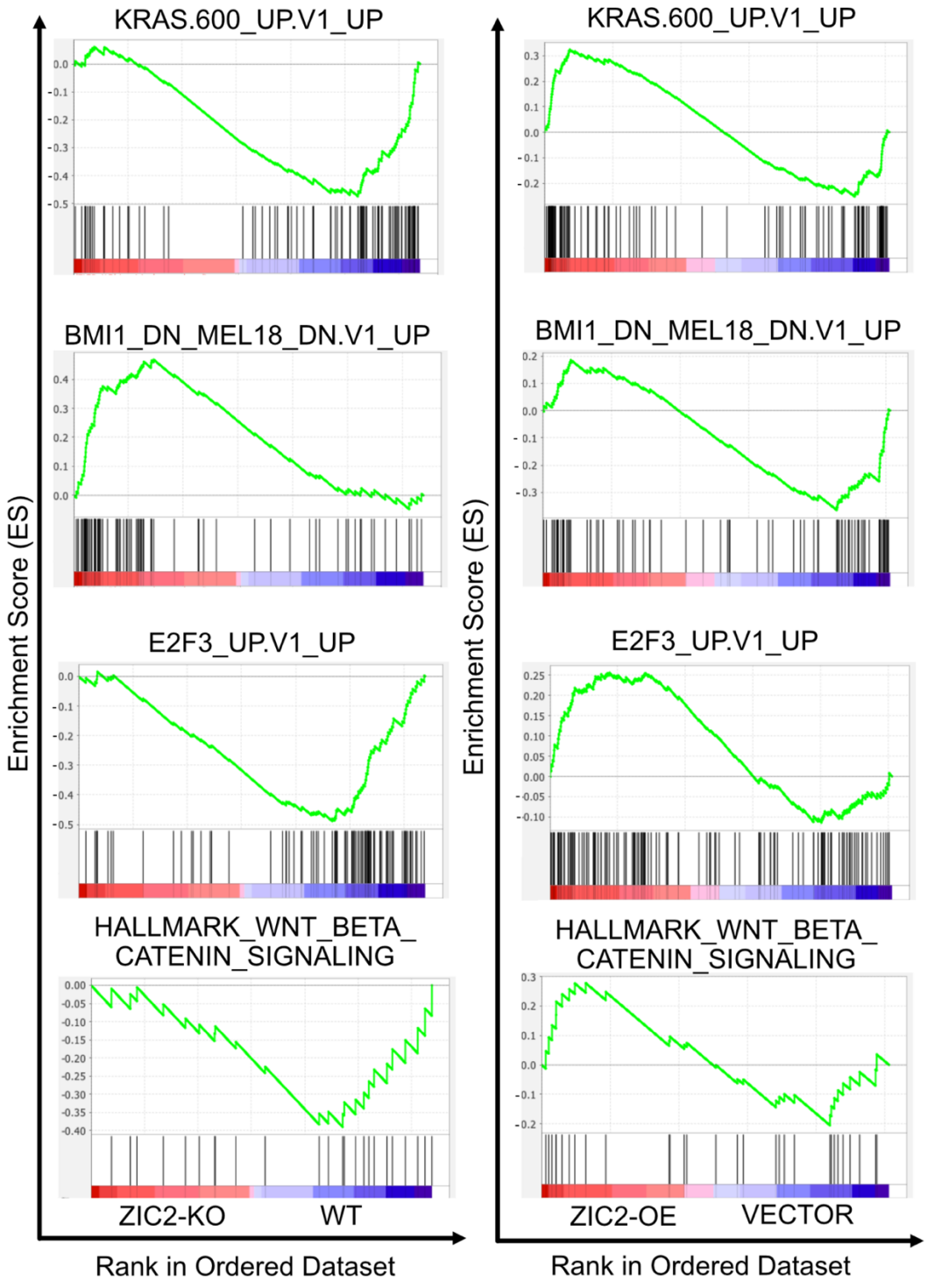
KRAS.600_UP.V1_UP
BMI1_DN_MEL18_DN.V1_UP
E2F3_UP.V1_UP
HALLMARK_WNT_BETA_
CATENIN_SIGNALING
Enrichment Score (ES)
ZIC2-KO
WT
Rank in Ordered Dataset
KRAS.600_UP.V1_UP
BMI1_DN_MEL18_DN.V1_UP
E2F3_UP.V1_UP
HALLMARK_WNT_BETA_
CATENIN_SIGNALING
Enrichment Score (ES)
ZIC2-OE
VECTOR
Rank in Ordered Dataset

Figure 4.9 The four gene sets commonly regulated by ZIC2 in the SKOV3 ZIC2-KO and OVCAR3 ZIC2-OE models

The enrichment plots show the four gene sets commonly regulated by ZIC2, belonging to the topmost gene sets enriched from all differentially expressed genes in the SKOV3 ZIC2-KO and OVCAR3 ZIC2-OE models.

We analyzed the proportions of common differentially expressed genes in the SKOV3 ZIC2-KO and OVCAR3 ZIC2-OE models (**Figure 4.10**). We defined the common differentially expressed genes that were upregulated in the SKOV3 ZIC2-KO model and downregulated in the OVCAR3 ZIC2-OE model, or the common differentially expressed genes that were downregulated in the SKOV3 ZIC2-KO models and upregulated in the OVCAR3 ZIC2-OE model as genes commonly regulated by ZIC2; we defined the common differentially expressed genes that were upregulated or the common differentially expressed genes that were downregulated in both models as genes oppositely regulated by ZIC2; we defined the genes that were independently regulated by ZIC2 in the SKOV3 ZIC2-KO model and OVCAR3 ZIC2-KO model as genes independently regulated by ZIC2 in their respective models. In transcriptome studies using the SKOV3 ZIC2-KO and OVCAR3 ZIC2-OE models, there were 4,335 common differentially expressed genes. In the SKOV3 ZIC2-KO model, genes commonly regulated by ZIC2 accounted for 37.38% (Commonly, n = 2,454), genes oppositely regulated by ZIC2 accounted for 28.65% (Oppositely, n = 1,881), and genes independently regulated by ZIC2 accounted for 33.97% (Independently, n = 2,230). In the OVCAR3 ZIC2-

OE model, genes commonly regulated by ZIC2 accounted for 23.38% (n = 2,454), genes oppositely regulated by ZIC2 accounted for 17.92% (n = 1,881), and genes independently regulated by ZIC2 accounted for 58.71% (n = 6,163). In addition, we listed the genes that were commonly regulated, oppositely regulated, and independently regulated in the four gene sets commonly regulated by ZIC2 in the two models, as shown in **Appendix I**.

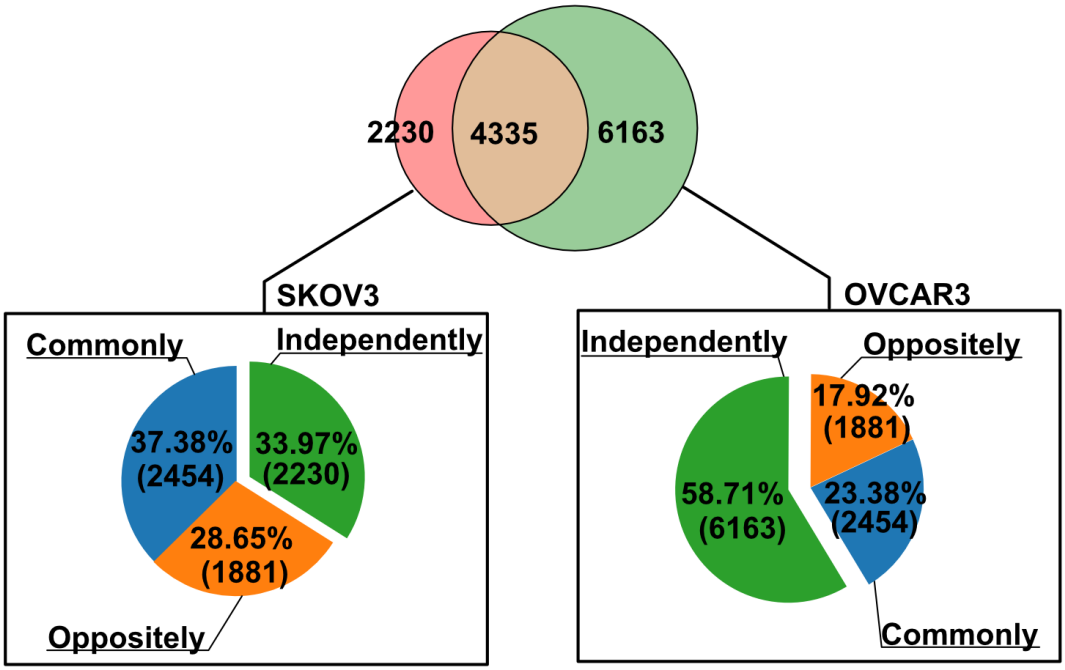

Figure 4.10 The differentially expressed gene composition in the SKOV3 ZIC2-KO and OVCAR3 ZIC2-OE models

Venn diagram shows the proportion of genes commonly regulated by ZIC2 (Commonly), genes oppositely regulated by ZIC2 (Oppositely), and genes independently regulated by ZIC2 (Independently) in all differentially expressed genes (FDR< 0.05) in the SKOV3 ZIC2-KO and OVCAR3 ZIC2-OE models. Genes commonly regulated by ZIC2 refer to genes upregulated in the SKOV3 ZIC2-KO

model and downregulated in the OVCAR3 ZIC2-OE model, or genes downregulated in the SKOV3 ZIC2-KO model and upregulated in the OVCAR3 ZIC2-OE model. Genes oppositely regulated by ZIC2 refer to genes upregulated or genes downregulated by ZIC2 in both models. Genes independently regulated by ZIC2 refer to differentially expressed genes that were not common among the two models.

Next, using these data, we analyzed the mRNA expression levels and the proportions of genes belonging to these three categories (i.e., genes commonly regulated by ZIC2, genes oppositely regulated by ZIC2, and genes independently regulated by ZIC2) in the four gene sets commonly regulated by ZIC2 in the two models (**Figure 4.11**). We found that in both models, the expression levels of genes belonging to their respective gene sets that were commonly regulated by ZIC2 were similar, while the expression levels of genes belonging to their respective gene sets that were oppositely regulated by ZIC2 and those that were independently regulated by ZIC2 were significantly different. In addition, the proportions of different categories of genes varied greatly across models, particularly the proportion of genes independently regulated by ZIC2 in their respective models.

In summary, we demonstrate that even among the molecular mechanisms commonly regulated by ZIC2 in the two models, ZIC2 might differentially regulate the corresponding gene expression through these molecular mechanisms in different cell-context conditions.

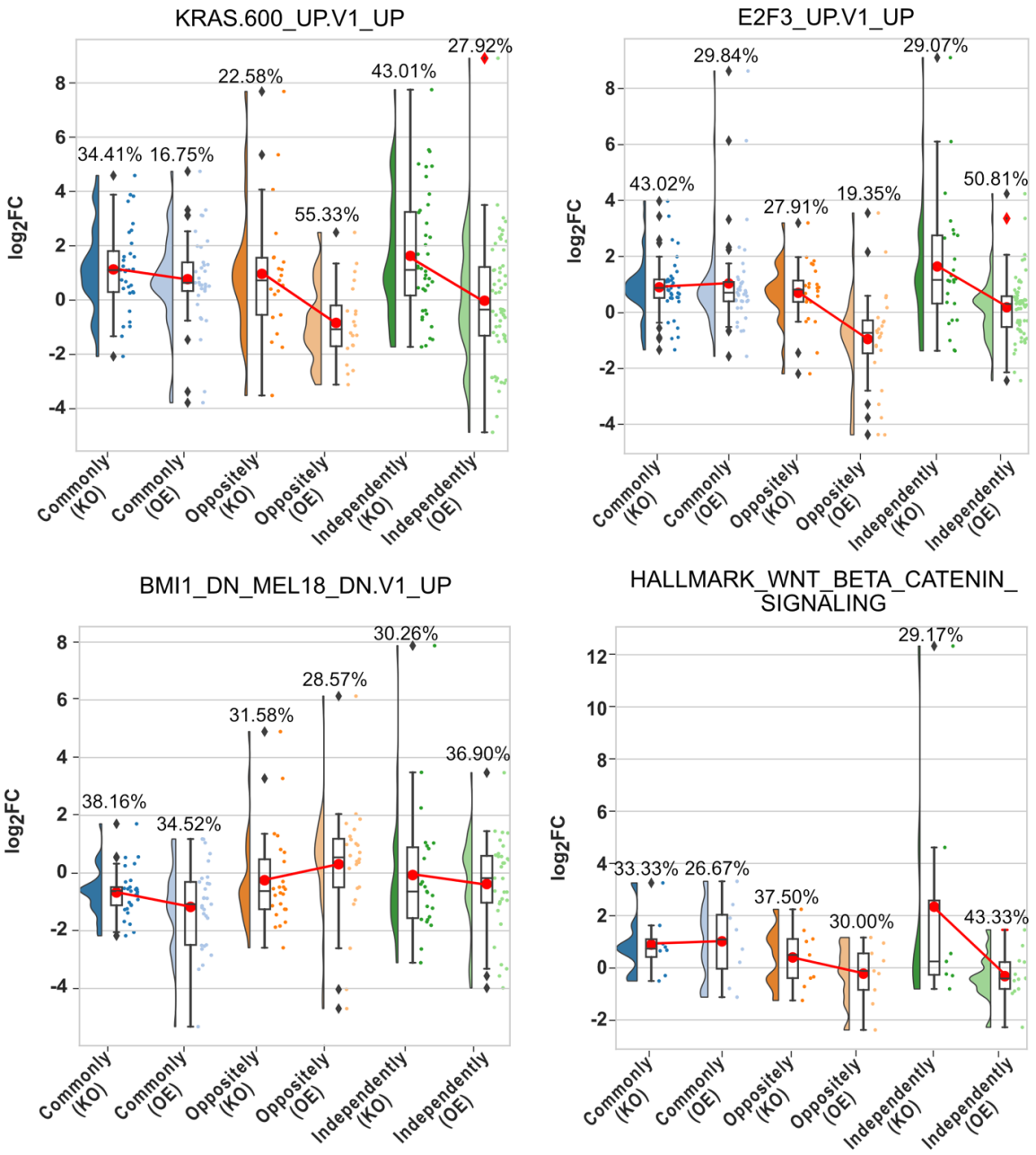

Figure 4.11 The expression and percentage of three categories of genes regulated by ZIC2 in the four common gene sets in the SKOV3 ZIC2-KO and OVCAR3 ZIC2-OE models

Rain-cloud plots show the expression of genes commonly regulated by ZIC2, genes oppositely regulated by ZIC2, and genes independently regulated by ZIC2 in their respective models, as well as their percentages in the specific models and

in the specific gene sets. The red line connects the mean value of boxplots between the two models. Expression data of the corresponding genes in the SKOV3 ZIC2-KO model were converted to $-\log_2$FC for comparison with expression data in the OVCAR3 ZIC2-OE model. The rain-cloud plot consists of a semi-violin plot, a box plot, and a scatter plot.

4.2.6 Preliminary study on the feasibility of identifying ZIC2-binding target genes in EOC using available ZIC2-ChIP-seq data

We showed that the molecular mechanism corresponding to KRAS.600_UP.V1_UP, E2F3_UP.V1_UP, BMI1_DN_MEL18_ DN.V1_UP, and HALLMARK_WNT_BETA_CATENIN_SIGNALING in the SKOV3 ZIC2-KO and OVCAR3 ZIC2-OE models might be potential molecular mechanisms commonly regulated by ZIC2. ZIC2 has been shown to be a transcription factor and co-activator (161,163,165,169,171,186,555,556). Herein, we explored genes that might be directly regulated by ZIC2 using the existing ZIC2-ChIP-seq datasets. The ChIP-seq datasets obtained by Luo *et al*. in the mouse ESC study on ZIC2 and histone modifications (accession number: Series GSE61188), the ZIC2-ChIP-seq datasets obtained by the ENCODE Project Consortium in the study of eGFP-ZIC2 HEK293 cells on ZIC2 (accession number: Series GSE105882), as well as the ChIP-seq datasets obtained by Zhao *et al*. in the study of human colon cancer cell line HCT116 on ZIC2 (accession number: Series GSE127960) were selected from the Gene Expression Omnibus (GEO) DataSets (171,557,558). In both models, all genes that were commonly regulated by ZIC2 and all genes that were

oppositely regulated by ZIC2 were selected from the four gene sets to show potential ZIC2 DNA-binding sites (ChIP-seq peaks). In addition, histone ChIP-seq datasets (e.g., H3K27me3, H3K27ac, H3K4me1, and H3K4me3) were also available in the mouse ESC study. Our analysis of the ZIC2-ChIP-seq datasets and histone ChIP-seq datasets in mouse ESC also revealed potential ZIC2 DNA-binding sites (ChIP-peaks) in eight genes and a correlation between their expression and histone modifications in mouse ESC.

Based on these data, we identified eight genes with ChIP-seq peaks in mouse ESC, eGFP-ZIC2 overexpressed HEK293T cells, and HCT116 cells with wild-type ZIC2 (**Figure 4.12**). Among these eight genes, *C1QTNF1*, *FADS3*, *FGFR3*, and *HEY1* are the genes commonly regulated by *ZIC2* in both models, and *CABLES2*, *KCNH2*, *MMP15*, and *SIX5* are the genes oppositely regulated by ZIC2 in both models. The ZIC2-ChIP-seq peaks in *Fads3*, *Fgfr*, *Kcnh2*, and *Six5* genes. partially overlap with the corresponding H3K27ac, H3K4me1, and H3K4me3 ChIP-seq peaks in these genes; the ZIC2-ChIP-seq peaks in *C1qtnf1*, *Cables2*, *Hey1*, and *Mmp15* genes partially overlap with the corresponding H3K27me3 and H3K4me1 ChIP-seq peaks in these genes. The data from the *Zic2*-ChIP-seq peaks and histone-ChIP-seq peaks suggest that ZIC2 may be a co-activator in the mouse ESC, recruiting chromatin remodeling complexes to modify histones corresponding to ZIC2-bound genes. Herein, we suggest that ZIC2 might act as a co-activator in EOC, recruiting chromatin remodeling complexes and participating in the regulation of gene expression through histone modifications of ZIC2-bound genes.

In summary, we demonstrate the feasibility of identifying ZIC2-binding target genes in the SKOV3 ZIC2-KO and OVCAR3 ZIC2-OE models that might be associated with tumor progression in the gene sets commonly regulated by ZIC2.


C1qtnf1
Cables2
Fads3
Fgfr3
Mouse genome M10
CACAGCAGG
CACAGCAGG Negative
GSM1499117-ZIC2
GSM1499122-H3K27me3-NonT
GSM1499124-H3K27me3-shZic2
GSM1499127-H3K27ac-NonT
GSM1499129-H3K27ac-shZic2
GSM1499131-H3K4me1-NonT
GSM1499133-H3K4me1-shZic2
GSM1499136-H3K4me3-NonT
GSM1499137-H3K4me3-shZic2
C1QTNF1
CABLES2
FADS3
FGFR3
Human genome Hg19
GSM2828565-HEK293-ZIC2
GSM3657706-HCT116-WT-ZIC2
Hey1
Kcnh2
Mmp15
Six5
HEY1
KCNH2
MMP15
SIX5

Figure 4.12 The ZIC2-ChIP-seq peaks and histone-ChIP-seq peaks of the eight genes in the four gene sets commonly regulated by ZIC2 in the SKOV3 ZIC2-KO and OVCAR3 ZIC2-OE models

The figures show the ZIC2-ChIP-seq peaks in the eight genes in the corresponding genomes in mouse ESC, a human embryonic kidney cell line HEK293, and a human colon cancer cell line HCT116. “CACAGCA” and “CACAGCA Negative” are a putative ZIC2 consensus sequence in the forward and reverse DNA strands in the mouse and human genomes, respectively. “GSM1499117-ZIC2” is a sample pulled down from mouse ESCs with anti-ZIC2 antibody. “NonT” are shRNA control samples pulled down from mouse ESC with anti-ZIC2 antibody. “sh*Zic2*” are samples with *Zic2* knocked down pulled downed from mouse ESC with specific histone modification antibodies. “HEK293T-ZIC2” is a sample pulled down from eGFP-ZIC2 overexpressed HEK293T cells with anti-ZIC2 antibody. “HCT116-WT-ZIC2” is a sample pulled down from HCT116 cells with wild-type ZIC2 with ZIC2 antibody.

4.3 Discussion

In Chapter 4, we identified differentially expressed genes and potential underlying mechanisms regulated by ZIC2 in the SKOV3 ZIC2-KO and OVCAR3 ZIC2-OE models. We demonstrate that ZIC2 has identical regulatory genes in both models, including genes that were commonly regulated and oppositely regulated by ZIC2 (**Figure 4.10 and Appendix I**). Each model also has its genes independently regulated by ZIC2 (**Figure 4.10 and Appendix I**). We show that in

the two models, genes that were commonly regulated by ZIC2, genes that were oppositely regulated by ZIC2, and genes that were independently regulated by ZIC2 were enriched into four gene sets that were commonly regulated by ZIC2. We suggest that these common mechanisms might also show different regulations due to the presence of genes oppositely regulated by ZIC2 and genes independently regulated by ZIC2 in the two models (**Figure 4.11 and Appendix I**). Studies showed that ZIC2 is associated with the activation of multiple signaling pathways, such as the Wnt/β-catenin, PI3K/AKT, and Hedgehog pathways (170,186,189). The role of these signaling pathways in promoting tumorigenic phenotypes in human cancers has been extensively studied (429,559,560). In this chapter, we hypothesized that ZIC2 promotes tumorigenic phenotypes in EOC. To test our hypothesis, we performed RNA-seq and GSEA analyses of the SKOV3 ZIC2-KO and OVCAR3 ZIC2-OE models. We show the differences in overall gene expression and the top 50 gene expression through heatmaps (**Figure 4.2 and 4.7**) and the differences in potential underlying mechanisms between the two models (**Figure 4.5 and 4.8**). The potential underlying molecular mechanisms commonly regulated by ZIC2 identified in both models were KRAS signaling, *E2F3*-related signaling, *BMI1*- and *MEL18*-relate signaling, and Wnt/β-catenin signaling, which are associated with pathobiological functions such as proliferation, survival, anchorage-independent growth, cell migration, invasion, self-renewal ability (527,530,544,546). In the OVCAR3 ZIC2-OE model, potential underlying molecular mechanisms regulated by ZIC2 are also involved in cell cycle phases, including cell cycle checkpoints and sister chromatid segregation and cohesion.

Regulation of proliferation, survival, anchorage-independent growth, cell migration, and invasion might be the major pathobiological functions of ZIC2 in regulating tumorigenic phenotypes. We suggest that the pathobiological functions involved in the molecular mechanisms corresponding to the topmost enriched gene sets in the two models include proliferation, survival, anchorage-independent growth, cell migration, invasion, metastasis, and stemness. These pathobiological functions are consistent with our findings in Chapter 3 regarding the role of ZIC2 in regulating the tumorigenic phenotypes. In Chapter 3, we suggest that ZIC2 promotes cell growth, single-cell survival, anchorage-independent growth, cell migration, self-renewal ability, and tumor growth in EOC and is cell-context dependent. The gene sets of KRAS.600_UP.V1_UP, E2F3_UP.V1_UP, BMI1_DN_MEL18_DN.V1_UP, and HALLMARK_WNT_BETA_CATENIN_ SIGNALING consist of genes that were commonly regulated, independently regulated, and independently regulated in the two models (**Figure 4.11**). We suggest that the molecular mechanisms corresponding to these gene sets might be regulated by the identical (i.e., genes commonly regulated by ZIC2 and genes oppositely regulated by ZIC2 in both models) or different (i.e., genes independently regulated by ZIC2 in their respective models) genes, with different expression patterns in different EOC cell lines. Signaling pathways involve multiple genes, and usually, the signaling pathways are not independent but interact with each other. Therefore, we suggest that differential regulation of common genes and regulation of different genes in different EOCs may be one of the reasons why ZIC2 mediates the differential regulation of tumorigenic phenotypes in EOC.

Overexpression of ZIC2 in OVCAR3 cells might be associated with cell cycle regulation. The top enriched gene sets in the OVCAR3 ZIC2-OE model involve cell cycle phases, including cell cycle checkpoints, as well as sister chromatid cohesion and segregation. In Chapter 3, our findings show decreased cell growth in the ZIC2-OE model of OVCAR3 and A2780s and decreased tumor growth in the OVCAR3 ZIC2-OE model. These tumorigenic phenotypes were opposite to those in the ZIC2-KO models of SKOV3 and OVCAR8 cells. The cell cycle plays an important role in cell proliferation and survival (561). Cell cycle checkpoints are a set of surveillance mechanisms that monitor DNA replication and chromosome allocation during the cell cycle (562). Cell cycle checkpoints are activated when cells undergo DNA damage or when DNA replication is blocked, causing cell cycle disruption (561). Thus, overexpression of ZIC2 in OVCAR3 cells might constitutively activate the cell cycle checkpoint mechanism, which might negatively affect cell proliferation and survival. This research suggests that ZIC2 might be involved in cell cycle regulation in EOC. How ZIC2 affects cell proliferation and survival by regulating the cell cycle in EOC warrants further investigation.

At the transcriptome level, we unveil for the first time genes regulated by ZIC2 in EOC cells and demonstrate potential mechanisms in the regulation of the tumorigenic phenotypes by ZIC2 through GSEA analyses. GSEA analyses suggest that these potential mechanisms are consistent with the role of ZIC2 in regulating the tumorigenic phenotypes of EOC, including cell growth, survival, anchorage-independent growth, cell migration, and self-renewal ability. Moreover, genes that were oppositely regulated by ZIC2 and genes that were independently

regulated by ZIC2 are present in the same molecular mechanisms in the two models, which might explain the cell-context dependent regulation of tumorigenic phenotypes by ZIC2. Only a few signaling pathway activations are known to be associated with ZIC2 promoting the tumorigenic phenotypes in human cancers (170,189,559). The molecular mechanisms by which ZIC2 regulates the tumorigenic phenotypes of EOC have not been studied. Our research explores for the first time the potential mechanisms regulated by ZIC2 in EOC. Our data suggest that these mechanisms might be involved in the regulation of the tumorigenic phenotypes by ZIC2. We demonstrate that mechanisms corresponding to the KRAS signaling, overexpression of E2F3, knockdown of BMI-1, or MEL-18, or both, and Wnt/β-catenin signaling are common in the SKOV3 ZIC2-KO and OVCAR3 ZIC2-OE models. These molecular mechanisms have been shown to promote tumorigenic phenotypes in various human cancers (524,525,527,530,559,563). Hedgehog signaling is also one of the top enriched gene sets that have been reported to be activated in human cancers (170,189,560). These findings suggest that ZIC2 might also have regulatory effects on these signaling pathways in EOC.

This study provides a new perspective for understanding the molecular mechanisms of ZIC2 in EOC. In this chapter, we present a big picture of the genes and potential underlying molecular mechanisms regulated by ZIC2 in EOC. These potential underlying molecular mechanisms regulated by ZIC2 corresponding to the two models require further validation to confirm their relationship with ZIC2. ZIC2 is a transcription factor and co-activator that has been shown to indirectly

regulate the expression of downstream genes by interacting with chromatin remodeling complexes (169,171). Using the existing ZIC2-ChIP-seq datasets, we conducted a preliminary study on the feasibility of identifying ZIC2-binding target genes in the four gene sets commonly regulated by ZIC2 in both models and found eight genes in the four gene sets that might be directly bound by ZIC2, and these genes might also be regulated by histone modifications (**Figure 4.12**). Thus, the research on the molecular mechanism of ZIC2 in EOC could be expanded in a variety of aspects. These include the study of genes directly bound by ZIC2 and protein factors interacting with ZIC2 in EOC. For instance, by performing ChIP-seq, we could identify a list of ZIC2-bound genes, corresponding ZIC2 DNA-binding sites, and a consensus sequence for ZIC2; by performing immunoprecipitation followed by liquid chromatography-mass spectrometry (IP LC-MS), we could identify a list of ZIC2-interacting proteins. After identifying the list of genes directly regulated by ZIC2 and the list of ZIC2-interacting proteins, we could select the genes and proteins of interest for subsequent experimental verification.

Our results further support ZIC2 as a promising therapeutic target for EOC. In this chapter, our data reveal the potential of ZIC2 to regulate tumorigenic phenotypes at the molecular level, including regulation of proliferation, survival, anchorage-independent growth, tumor metastasis, stemness, and angiogenesis. These pathobiological functions have been extensively studied and are considered cancer hallmarks in various human cancers (564). Thus, targeting ZIC2, a transcription factor that plays multifaceted functions in EOC, is important.

In conclusion, we suggest that ZIC2 is a key and multifaceted regulator in EOC. Our study highlights the importance of ZIC2 in regulating the tumorigenic phenotypes and that ZIC2 regulates distinct transcriptomes in different EOCs, which might explain why ZIC2 differentially regulates the tumorigenic phenotypes in different EOCs.

CHAPTER 5: The role of RUNX3 in granulosa cell tumor of the ovary

5.1 Introduction

Granulosa cell tumor of the ovary (GCT) is a rare malignant ovarian cancer that belongs to the sex cords-stromal (113). Although most GCT patients are diagnosed at an early stage and have a good prognosis, those with advanced and recurrent disease have a poor prognosis (116,118,126,128). GCT is divided into adult GCT (AGCT) and juvenile GCT (JGCT) (116,119). AGCT is the most common type of GCT, accounting for about 95% of all GCT cases (116,119). AGCT and JGCT have different pathobiological features, genetic mutations, and clinical presentations (116,119).

Runt-related transcription factors (RUNX) play an important role in normal tissue development and human cancers (565-567). The human RUNX family contains three members, including RUNX1, RUNX2, and RUNX3. RUNX proteins regulate the expression of target genes by binding to a molecular chaperone, the core-binding factor-β subunit/polyomavirus enhancer-binding protein 2β subunit (i.e., CBFβ) to form a heterodimer (223). RUNX3 is considered the most conserved gene in the evolution of the RUNX family (192,193). RUNX3 is involved in neurogenesis and T-lymphocyte development as well as in complex cell fate determination in the immune system (196-199). In human cancers, RUNX3 is considered a tumor suppressor or an oncogene, depending on the cancer types (207,208,210-212). For instance, in gastric cancer, RUNX3 expression is silenced due to methylation of promoter DNA, and silencing of this gene is associated with poor prognosis and promotion of tumorigenic phenotypes (212); in EOC, *RUNX3* is upregulated, resulting in enhanced cell proliferation, cell migration, and

carboplatin resistance (222,225,226). Ojima *et al.* showed that in mice RUNX3 is involved in follicle development and promoted the expression of Aromatase, a key enzyme associated with estrogen synthesis (228,229). As mentioned above, upregulation of *RUNX3* showed a role in promoting the tumorigenic phenotypes in EOC. There are no studies on the role of RUNX3 in regulating the tumorigenic phenotype in GCT. Herein, we hypothesize that RUNX3 promotes the tumorigenic phenotype in GCT. In this study, we show that RUNX proteins are expressed in human GCT cell lines and tumor samples and that RUNX3 promotes tumorigenic phenotypes in GCT cells.

5.2 Results

5.2.1 The expression of RUNX family members in GCT cell lines and tumor samples

To determine the protein expressions of RUNX1, RUNX2, and RUNX3 in GCT, we performed immunoblotting using the GCT cell lines KGN and COV434 (**Figure 5.1A**). There were only two available GCT cell lines. KGN and COV434 were derived from AGCT and JGCT, respectively. We included the immortalized non-tumorigenic granulosa cell line of the ovary SVOG as a normal control. Immunoblotting showed that the RUNX1 and CBFβ proteins were expressed in all cell lines, RUNX2 was expressed in cell lines other than COV434, while RUNX3 was expressed only in COV434. We showed that the RUNX3 protein had two bands, which may correspond to two isoforms of RUNX3 (i.e., RUNX3/p44 and RUNX3/p46). To determine the localization of RUNX proteins in the cell lines, their protein levels in the cytoplasmic and nuclear fractions of SVOG, KGN, and

COV434 cells were explored by immunoblotting (**Figure 5.1B**). Immunoblotting showed that all RUNX proteins were detected in the nuclear fractions, consistent with the function of the RUNX proteins as transcription factors.

Next, we confirmed the expression of RUNX proteins in human GCT samples. We examined the expression of RUNX proteins in 11 adult GCT (AGCT) samples from the Alberta Cancer Research Biobank, 6 AGCT samples, and 5 juvenile GCT (JGCT) samples from the Baylor College of Medicine Tissue Repository by immunoblotting. Immunoblotting indicated variable expression of all RUNX proteins in samples from the Alberta Cancer Research Biobank (**Figure 5.1C**). We found that the expression of RUNX3 protein was variable and lower than that of RUNX1 and RUNX2 proteins in these samples. In addition, we found that the expression of RUNX2 protein was variable and at high levels in AGCT samples and JGCT samples from the Baylor College of Medicine Tissue Repository, consistent with the expression of RUNX2 protein in samples from the Alberta Cancer Research Biobank. We noted that RUNX2 protein was detected in two normal ovarian tissue samples, but not in COV434 cells.

However, we did not detect RUNX3 protein expression in GCT samples from the Baylor College of Medicine Tissue Repository and in normal ovarian tissues (**Figure 5.1D**). We noted that two bands of RUNX3 were detected in COV434 cells. In immunoblotting, COV434 cells served as a RUNX2-negative control and a RUNX3-positive control. We further confirmed the mRNA expressions of *RUNX1*, *RUNX2*, and *RUNX3* in samples from the Baylor College of Medicine Tissue Repository. RNA samples from three normal ovarian tissues and KGN and

COV434 cells were included in RT-qPCR. We found that the mRNA expression levels of *RUNX1* and *RUNX2* were largely variable in all tumor samples and lower in KGN and COV434 cells than in normal ovarian tissues (**Figure 5.1E**). We found no significant changes in *RUNX3* mRNA expression in all samples from the Baylor College of Medicine Tissue Repository compared to normal ovarian tissues, consistent with previous immunoblotting results (**Figure 3.53D**). In addition, we found that *RUNX3* mRNA and protein expression was much higher in COV434 cells than in any samples from the Baylor College of Medicine Tissue Repository.

In summary, these data suggest that *RUNX* genes are expressed in some of the GCT cell lines and tumor samples.

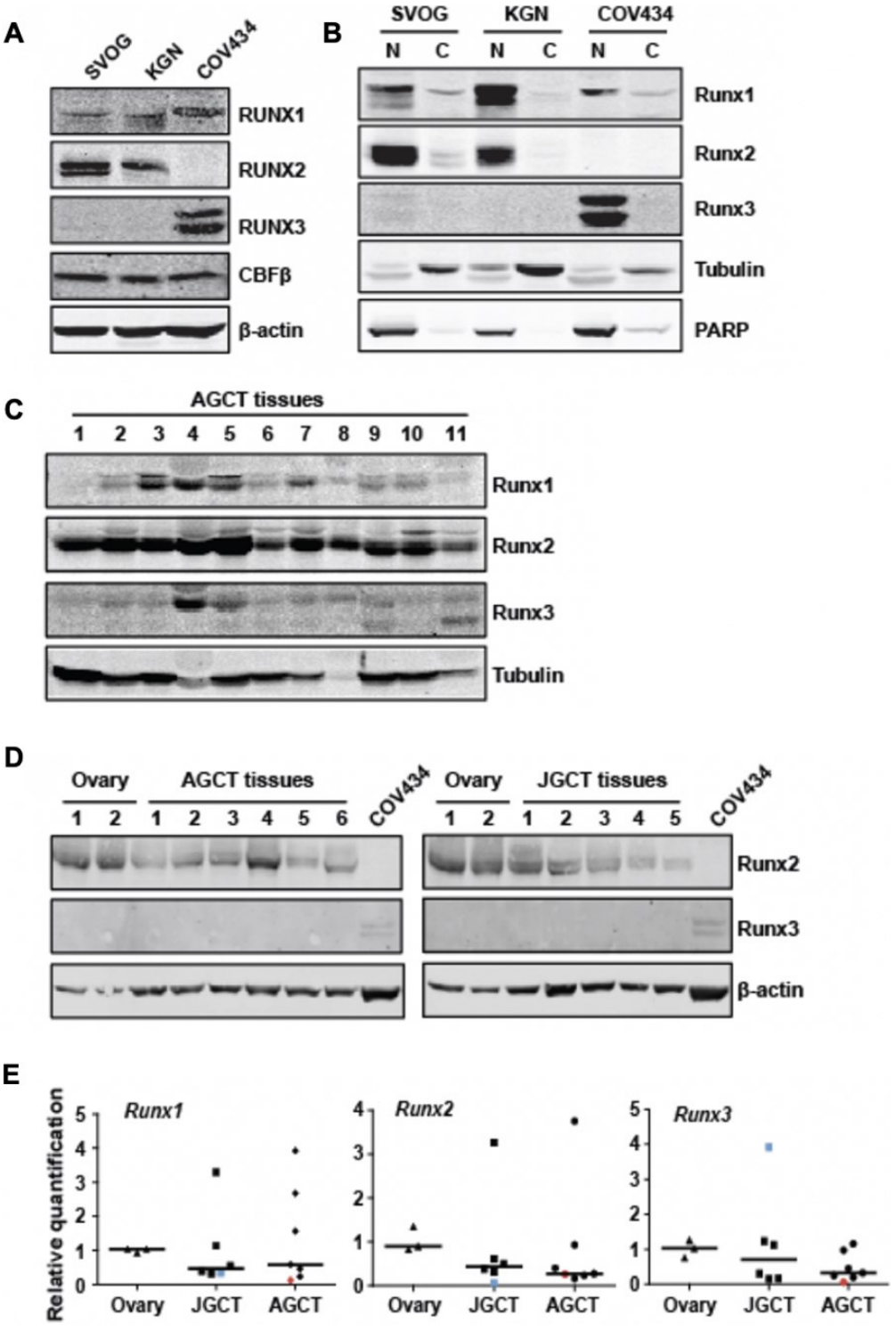
A
SVOG
KGN
COV434
RUNX1
RUNX2
RUNX3
CBFβ
β-actin
B
SVOG
KGN
COV434
N
C
N
C
N
C
Runx1
Runx2
Runx3
Tubulin
PARP
C
AGCT tissues
1 2 3 4 5 6 7 8 9 10 11
Runx1
Runx2
Runx3
Tubulin
D
Ovary
AGCT tissues
COV434
Ovary
JGCT tissues
COV434
1 2 1 2 3 4 5 6
1 2 1 2 3 4 5
Runx2
Runx3
β-actin
E
Relative quantification
Runx1
Runx2
Runx3
Ovary
JGCT
AGCT

Figure 5.1 The expression of *RUNX* genes in GCT cell lines and tumor samples

(A) Immunoblotting showed expression of RUNX proteins (i.e., RUNX1, RUNX2, and RUNX3) and CBFβ protein in the immortalized human ovarian granulosa cell line SVOG, the AGCT cell line KGN, and the JGCT cell line COV434. β-actin was used as a loading control. The two bands of RUNX3 correspond to two isoforms, RUNX3/p44 and RUNX3/p46, respectively. **(B)** Immunoblotting showed the expression of RUNX proteins in cytoplasmic and nuclear fractions of SVOG, KGN, and COV434. Tubulin and PARP were used as loading controls for cytoplasmic and nucleus fractions, respectively. **(C)** Immunoblotting showed expression of RUNX proteins in 11 AGCT samples from the Alberta Cancer Research Biobank. **(D)** Immunoblotting showed expression of RUNX2 and RUNX3 proteins in normal ovarian tissue samples, GCT samples from the Baylor College of Medicine Tissue Repository, and COV434 cells. β-actin was used as a loading control. **(E).** RT-qPCR showed mRNA expression of *RUNX1*, *RUNX2*, and *RUNX3* in normal ovarian tissue samples, GCT samples from the Baylor College of Medicine Tissue Repository, KGN cells, and COV434 cells. Data points for KGN cells are in red and for COV434 cells are in blue. The horizontal lines in the dot plots indicate the location of the average relative mRNA expression levels of genes in a specific sample.

5.2.2 Overexpression of RUNX3 promotes tumorigenic phenotypes in KGN cells *in vitro*

RUNX3 has been shown to promote proliferation and anchorage-independent growth in EOC cells (226). However, whether RUNX3 regulates the tumorigenic phenotypes in GCT is unclear. To fill this gap, we first generated a RUNX3-overexpressed (RUNX3 with FLAG-tag at the C-terminus) cell model (i.e., KGN vector and KGN RUNX3-OE) using KGN cells. Afterward, a series of experiments were performed using this cell model, including neutral red uptake assay, soft agar colony-formation assay, as well as scratch assay. We confirmed the expression of RUNX3 protein in KGN RUNX3-OE cells by immunoblotting (**Figure 5.2A**).

Neutral red uptake assay showed a 144.4% ($p< 0.05$) increase in cell growth on Day 3, 182.6% ($p< 0.05$) on day 5, and 170.4% ($p< 0.05$) on day 7 in KGN RUNX3-OE cells compared to KGN vector cells. Soft agar colony-formation assays showed a 246.5% increase ($p< 0.05$) in the size and number of colonies formed by KGN RUNX3-OE cells three weeks after seeding compared with KGN vector cells (**Figure 5.2C**). Scratch assay showed enhanced mobility of KGN RUNX3-OE cells compared to KGN vector cells (**Figure 5.2D**). We found that more KGN RUNX3 cells moved to the middle of the scratched area after 24 hours of scratching compared to KGN vector cells.

In summary, our data suggest that overexpression of RUNX3 in KGN cells enhances cell growth, anchorage-independent growth, and cell mobility.

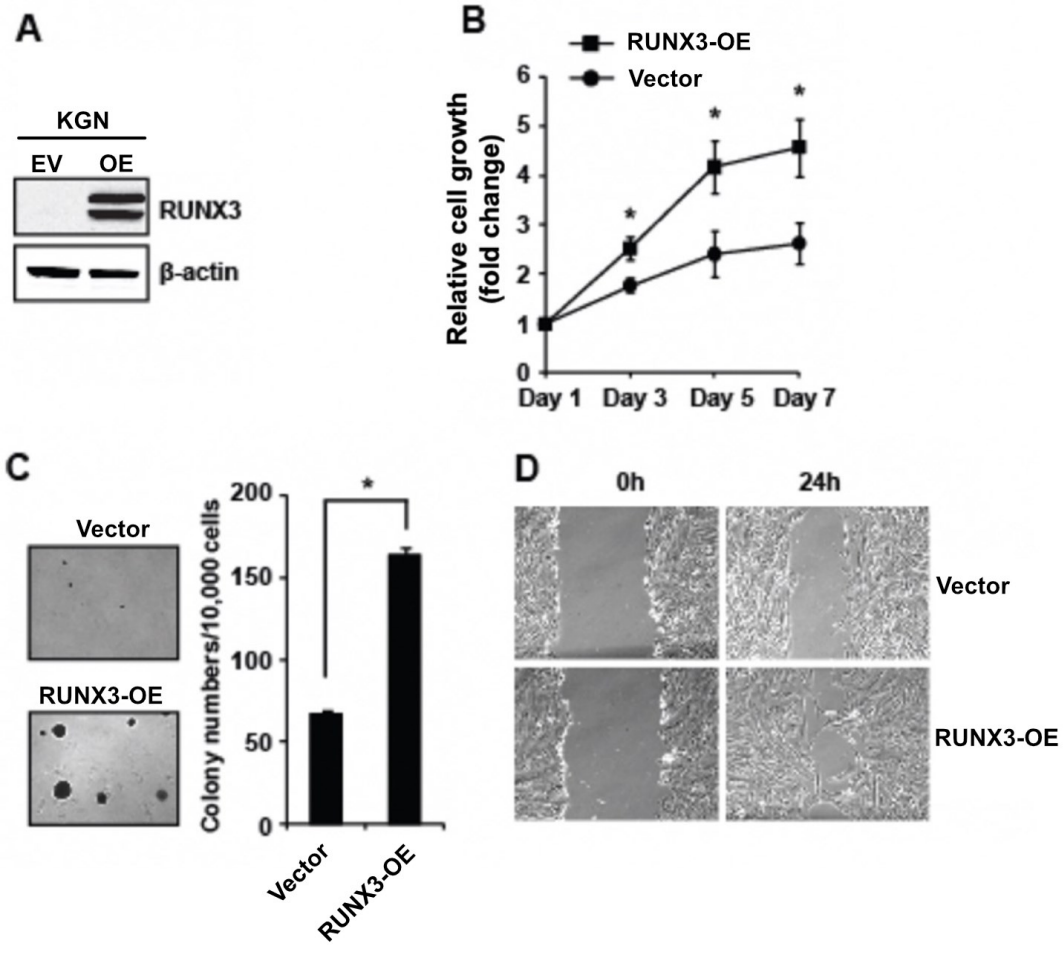

Figure 5.2 Overexpression of RUNX3 promotes tumorigenic phenotypes in KGN cells *in vitro*

(A) Immunoblotting showed expression of RUNX3 protein in KGN vector (EV) and KGN RUNX3-OE (OE) cells. β-actin was used as a loading control. **(B)** Neutral red uptake assay showed cell growth of KGN vector (Vector) and KGN RUNX3-OE (RUNX3-OE) cells. Relative cell growth (fold change) is shown as mean ± SD of three independent experiments. **(C)** Soft agar colony-formation assay showed anchorage-independent growth of KGN vector (Vector) and KGN RUNX3-OE (RUNX3-OE) cells. 10,000 cells per well were seeded in six-well plates. Colony

number per 10,000 cells showed the total number of colonies in the well of six-well plates. Data are shown as mean ± SD of three independent experiments. **(D).** Scratch assay showed mobility of KGN vector (Vector) and KGN RUNX3-OE (RUNX3-OE) cells. Images show the migration of KGN vector and KGN RUNX3-OE (RUNX3-OE) cells after 24 hours of scratching. Data were from one representative experiment of three independent experiments. Statistical significance is determined using the one-way ANOVA (*: $p < 0.05$).

5.2.3 Overexpression of RUNX3 promotes tumorigenic phenotypes in KGN cells *in vivo*

Next, we explored the effect of RUNX3 on the tumorigenic phenotypes of GCT cells *in vivo*. We examined whether KGN vector and RUNX3-OE cells form tumors in female NSG mice through subcutaneous injection. Only a few reports showed that KGN cells form small tumors in mice (486,568,569). We injected 2 x 10^7 KGN vector and KGN RUNX3-OE cells subcutaneously into the left and right flanks of mice (n = 6), respectively, twice over an interval of two weeks.

The results showed that no mice formed tumors subcutaneously on the left flank where KGN vector cells were injected, and four mice formed small tumors subcutaneously on the right flank where KGN RUNX3-OE cells were injected, 170 days after the first injection (**Figure 5.3A**). We confirmed the expression of RUNX3 protein in the tumor cells by immunoblotting. To collect sufficient cells for subsequent analysis, we disassociated the four collected tumors into single cells and expanded them in cell culture. We performed immunoblotting using these

tumor cells, KGN vector cells, and KGN RUNX3-OE cells cultured in a monolayer with anti-RUNX3 and anti-FLAG antibodies. Immunoblotting showed that RUNX3 protein (RUNX3-FLAG) was detected in normally cultured KGN RUNX3-OE cells and in tumor cells isolated from four tumors formed by KGN RUNX3-OE cells, but not in normally cultured KGN vector cells (**Figure 5.3B**).

In summary, these data suggest that RUNX3 may be a key factor supporting tumor formation by KGN cells in NSG mice.

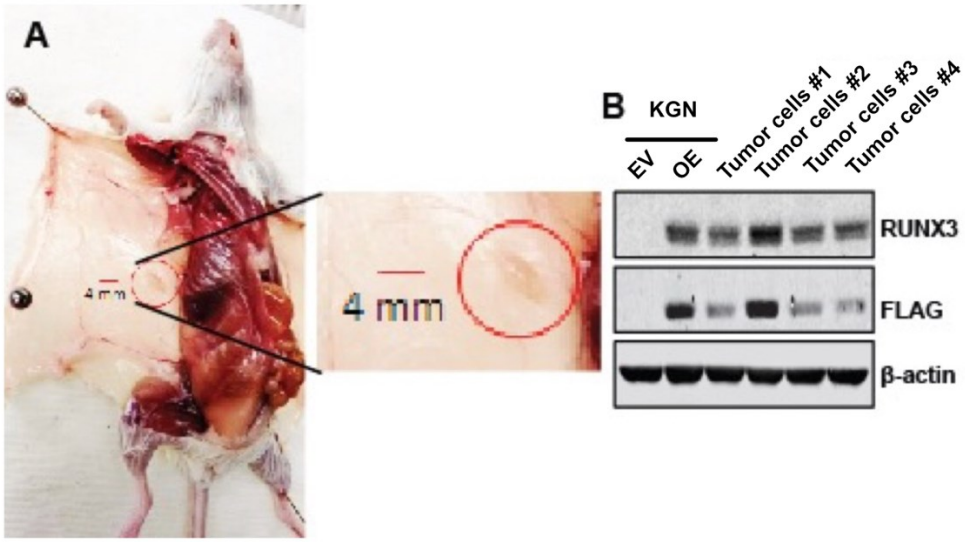

Figure 5.3 Overexpression of RUNX3 promotes tumor formation in KGN cells

(A) Images show that a small tumor was formed on the right flank of the NSG mouse, and the right flank was injected subcutaneously with KGN RUNX3-OE cells. The tumor was about 4 mm in diameter. **(B)** Immunoblotting showed that RUNX3 protein (RUNX3-FLAG) was expressed in normally cultured KGN RUNX3-OE (OE) cells and tumor cells from four collected tumors formed by KGN RUNX3-OE cells (Tumor cells #1-4), but not in KGN vector cells (EV). β-actin was used as a loading control.

5.2.4 Overexpression of dominant-negative RUNX3 (dnRUNX3) reduces cell growth in COV434

We showed that RUNX3 promoted tumorigenic phenotypes in KGN cells. Next, we investigated the role of RUNX3 in another GCT cell line, COV434. We generated a cell model (i.e., COV434 vector and COV434 dnRUNX3-OE) overexpressed a dominant-negative form of RUNX3 protein (FLAG-dnRUNX3, FLAG-tag at the N-terminus) using COV434 cells. DnRUNX3 is a truncated form of RUNX3 protein with 1-187 amino acid residues, including a conserved Runt homology domain (RHD) responsible for DNA binding and a nuclear localization signal (NLS), but lacking a transactivation domain (AD) and an inhibitory domain (ID) (570). Therefore, dnRUNX3 protein can localize in the nucleus, interact with CBFβ protein, and bind to DNA, but lacks transcriptional activity. In addition, the dnRUNX3 protein competes with the endogenous RUNX3 protein for binding to downstream targets, thereby inhibiting the transcriptional activity of endogenous RUNX3.

Immunoblotting confirmed that the expression of dnRUNX3 (FLAG-dnRUNX3) protein was detected in COV434 dnRUNX3-OE cells (**Figure 5.4A**). Next, we explored the effect of RUNX3 on the cell growth in COV434 cells using neutral red uptake assay. We found that the cell growth of COV434 dnRUNX3-OE cells was decreased by 53.7% ($p < 0.05$) on day 3, 41.8% ($p < 0.05$) on day 5, 34.8% ($p < 0.05$) on day 7 compared to COV434 vector cells.

Together, these data indicate that overexpression of dnRUNX3, which interferes with endogenous RUNX3, inhibits cell growth in COV434 cells, suggesting that endogenous RUNX3 may promote cell growth in COV434 cells.

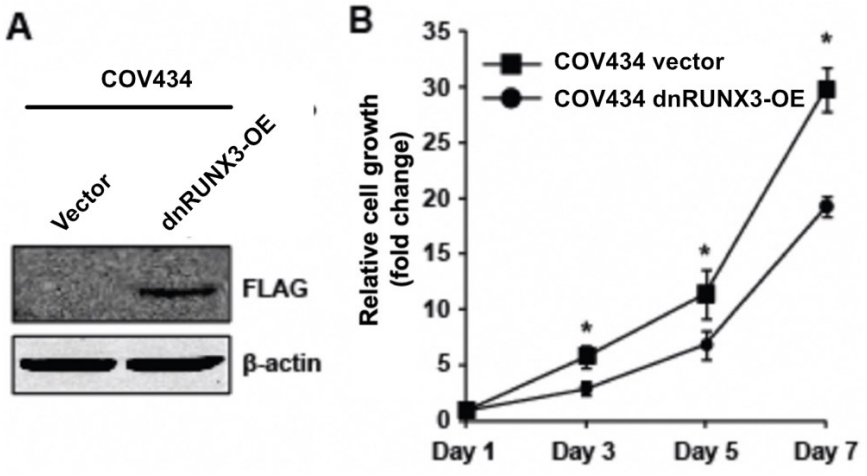

Figure 5.4 Overexpression of dominant-negative RUNX3 (dnRUNX3) inhibits cell growth in COV434 cells

(A) Immunoblotting showed that dnRUNX3 protein (FLAG-dnRUNX3) was expressed in COV434 dnRUNX3-OE cells but not in COV434 vector cells. β-actin was used as a loading control. **(B)** Neutral red uptake assay showed that cell growth was lower in COV434 vector cells than in COV434 dnRUNX3-OE cells. Relative cell growth (fold change) is shown as mean ± SD of three independent experiments. Statistical significance is determined using the one-way ANOVA (*: $p < 0.05$).

5.2.5 Overexpression of RUNX3 increases cyclin D2 (*CCND2*) mRNA and protein expression and inhibits $p27^{Kip}$ (*CDKN1B*) protein expression in KGN cells

Our data showed that overexpression of RUNX3 promoted cell growth in KGN cells, while inhibition of RUNX3 reduced cell growth in COV434 cells. One study showed that cell proliferation and cell survival in GCT depend on the balanced regulation of expression of the CDK inhibitor $p27^{Kip1}$ (*CDKN1B*) and the cyclin-dependent kinase cyclin D2 (*CCND2*) (484). To determine whether RUNX3 regulates the expression of these two genes in KGN cells, RT-qPCR and immunoblotting were performed using KGN vector and KGN RUNX3-OE cells (**Figure 5.5**). RT-qPCR showed a 2.7-fold increase ($p< 0.05$) in *CCND2* mRNA expression in KGN RUNX3-OE cells compared with KGN vector cells (**Figure 5.5A**). In addition, we found no difference in *CDKN1B* mRNA expression between KGN vector and KGN RUNX3-OE cells. Immunoblotting showed a significant upregulation of cyclin D2 expression in KGN RUNX3-OE cells compared to KGN vector cells. Interestingly, we found a 58% reduction in $p27^{Kip1}$ protein expression in KGN RUNX3-OE cells compared with KGN vector cells (**Figure 5.5B**).

In summary, our data indicate that overexpression of RUNX3 leads to inhibition of $p27^{Kip1}$ expression and promotion of cyclin D2 expression, which might be associated with increased cell growth in KGN cells.

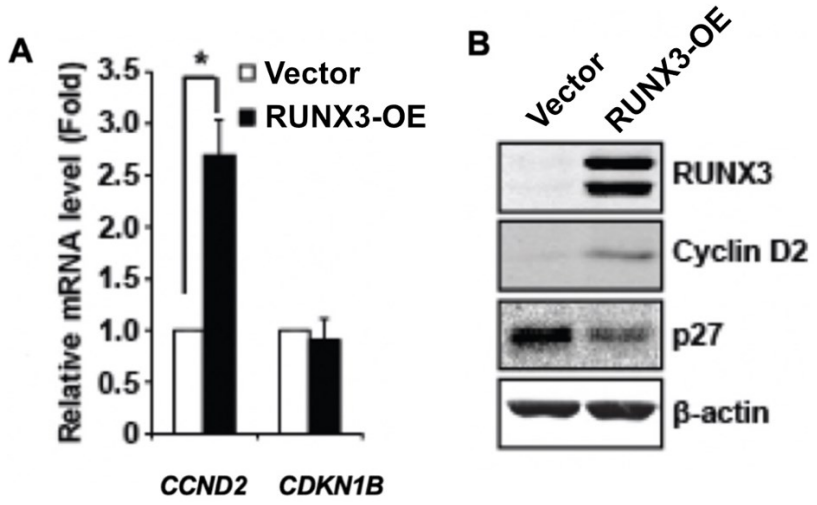

Figure 5.5 Overexpression of RUNX3 increases cyclin D2 (*CCND2*) mRNA and protein expression and inhibits the protein expression of $p27^{Kip1}$ (*CDKN1B*)

(A) RT-qPCR showed the relative mRNA expression of *CCND2* and *CDKN1B* in KGN vector (Vector) and KGN RUNX3-OE (RUNX3-OE) samples. **(B)** Immunoblotting showed protein levels of RUNX3, cyclin D2, and $p27^{Kip1}$ in KGN vector (Vector) and KGN RUNX3-OE (RUNX3-OE) cells. β-actin was used as a loading control. Relative mRNA level (Fold) is shown as mean ± SD of three independent experiments. Statistical significance is determined using the one-way ANOVA (*: $p < 0.05$).

5.3 Discussion

We demonstrated that RUNX3 promotes the tumorigenic phenotypes in GCT. *RUNX3* is both a tumor suppressor gene and an oncogene in human cancers (207,212,225,226). RUNX3 has been shown to promote tumorigenic phenotypes in EOC (225,226). At present, there are only studies on *RUNX3* gene promoter

methylation and no studies on tumorigenic phenotypes in GCT. We hypothesized that RUNX3 promotes the tumorigenic phenotypes in GCT. To test this hypothesis, we determined the expression of *RUNX3* in GCT samples and cell lines, established KGN RUNX3-OE and COV434 dnRUNX3-OE models, and performed *in vitro* functional assays and animal studies. We show that RUNX3 was expressed in a subset of GCT samples, that RUNX3 promoted cell growth, anchorage-independent growth, cell motility, and tumor formation in GCT cells, and that RUNX3 promoted mRNA and protein expression of cyclin D2 (*CCDN2*) and inhibited protein expression of $p27^{Kip1}$ (*CDKN1B*) in GCT cells (**Figure 5.6**).

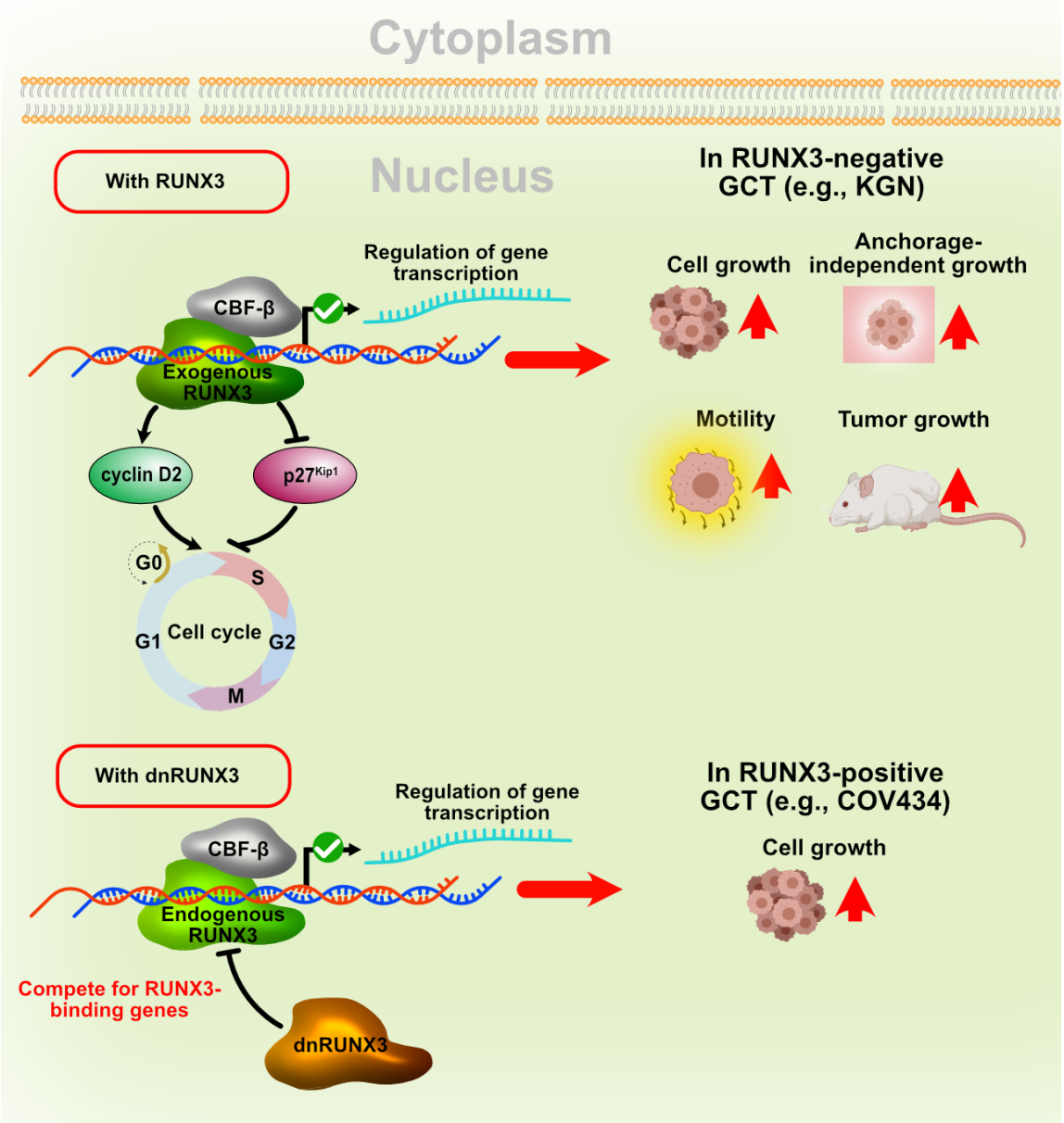

Figure 5.6 The role of RUNX3 in GCT cells.

RUNX3 promotes tumorigenic phenotypes (e.g., cell growth, anchorage-independent growth, motility, and tumor growth) in GCT cells (e.g., KGN cells) in which RUNX3 is not naturally expressed and promotes cyclin D2 expression and inhibits $p27^{Kip1}$ expression. The cell cycle regulators cyclin D2 and $p27^{Kip1}$ promote and inhibit the cell cycle progression, respectively.

RUNX3 promotes tumorigenic phenotypes (e.g., cell growth) in GCT cells (e.g., COV434 cells) that naturally express RUNX3.

RUNX3 is expressed in only a subset of GCT samples. By examining GCT samples from the Alberta Cancer Research Biobank and the Baylor College of Medicine Tissue Repository, we found that RUNX3 was expressed in only a few adult GCT samples from the Alberta Cancer Research Biobank. Next, we examined the GCT sample from the Baylor College of Medicine Tissue Repository and two GCT cell lines by RT-qPCR and finally confirmed that *RUNX3* was not expressed in these GCT samples. In the GCT cell lines, we found that KGN belonging to adult GCT did not express *RUNX3*, whereas COV434 belonging to juvenile GCT expressed this gene. The rarity of GCT and the availability of only two GCT cell lines limited our ability to detect RUNX3 expression in more GCT samples and cell lines. However, this does not preclude the fact that RUNX3 is expressed in a small number of GCTs.

The involvement of RUNX3 in GCT cell cycle regulation might be related to the promotion of cell growth. Our data suggest that RUNX3 promotes cell growth in KGN and COV434 cells. Studies showed that the growth of GCT cells is associated with increased expression of cyclin D2 and decreased expression of $p27^{Kip1}$ (484). Our data also demonstrate that RUNX3 promoted the expression of cyclin D2 and inhibited the expression of $p27^{Kip1}$ in KGN cells. Cyclin D2 is an important cell cycle regulator expressed in the G1 phase of the cell cycle. The main function of cyclin D2 is to bind to cyclin-dependent kinases (e.g., CDK 2) to form a

heterodimer, activating the enzymatic activity of CDKs and promoting the G1/S transition of the cell cycle (571). $P27^{Kip1}$ is a negative regulator of the cell cycle. $P27^{Kip1}$ is most expressed in the G1 phase and inhibits the enzymatic activity of CDKs, leading to cell cycle arrest in the G1 phase. Downregulation of $p27^{Kip1}$ results in a smooth G1/S transition (571). Increased expression of cyclin D2 (*CCND2*) and reduced expression of $p27^{Kip1}$ (*CDKN1B*) promote G1/S transition and cell cycle progression (572). Therefore, we suggest that the regulation of these cell cycle regulators by RUNX3 in KGN cells may be related to increased cell growth.

The role of RUNX3 in regulating the tumorigenic phenotypes in GCT remains to be explored. In this chapter, we investigated the role of RUNX3 in regulating the tumorigenic phenotypes in GCT, including cell growth, anchorage-independent growth, cell mobility, and tumor formation. As mentioned previously, the availability of only two GCT cell lines limited the cell models available to us. The tumorigenic phenotypes tested in this study represent the role of RUNX3 in the two GCT cell lines only. In terms of molecular mechanisms, we show that RUNX3 was involved in cell cycle regulation in the GCT cell line KGN by promoting the expression of cyclin D2 and inhibiting the expression of $p27^{Kip1}$. However, the expression regulation of cyclin D2 and $p27^{Kip1}$ by RUNX3 may be only a small part of the various mechanisms involved. To better understand the molecular mechanisms of RUNX3-mediated regulation in GCT, high-throughput sequencing is required. For instance, RNA-seq could be used to analyze RUNX3-regulated transcriptome and potential molecular mechanisms in GCT cells. By performing ChIP-seq, a list of

genes directly bound by RUNX3, the DNA-binding sites for RUNX3, and the consensus sequence for RUNX3 could be identified. Once the list of genes directly regulated by ZIC2 has been identified, genes of interest would be selected for subsequent experimental verification.

These findings highlight the biological importance of RUNX3 as a potential therapeutic target for GCT expressing RUNX3. GCT is a rare type of ovarian cancer that is prone to recurrence and has a recurrence mortality rate of 80% (116,128). Unlike EOC, GCT lacks cell and tumor models for research due to its rarity. Our research is the first to reveal that RUNX3 promotes cell growth, anchorage-independent growth, cell motility, and tumor formation in GCT cells. The KGN RUNX3-OE model provides a new cell model and a new tumor model for GCT research. Therefore, further study on the molecular mechanism of RUNX3 and development of drugs targeting RUNX3 might help overcome the recurrence of RUNX3-expressing GCT and improve the survival in GCT patients.

In conclusion, our study suggests that RUNX3 may promote the tumorigenic phenotypes in RUNX3-expressing GCT.

CHAPTER 6: DISCUSSION

6.1 Thesis overview

In this thesis, we explored the pathobiological role of ZIC2 and RUNX3 in regulating the tumorigenic phenotypes of EOC and GCT cells, respectively. In addition, we determined the ZIC2-regulated transcriptome in the SKOV3 ZIC2-KO and OVCAR3 ZIC2-OE models, aiming to explore the potential molecular mechanisms underlying ZIC2 functions in EOC. In the ZIC2 section (Chapter 3 and Chapter 4), we hypothesized that ZIC2 promotes tumorigenic phenotypes in EOC. In Chapter 3, we indicate that ZIC2 was highly expressed in a subset of EOC and that high ZIC2 expression in EOC was associated with the poor prognosis in patients based on the overall survival and post-progression survival in EOC patients with high and low ZIC2 expression. We show that the regulation of the tumorigenic phenotypes regulated by ZIC2 was cell-context dependent as determined by *in vitro* and *in vivo* functional assays. In Chapter 4, we show that ZIC2 was a pivotal regulator of gene expression and is associated with potential underlying molecular mechanisms related to EOC progression through RNA-seq and GSEA analyses. Our data indicate that ZIC2 regulated distinct transcriptomes in the SKOV3 ZIC2-KO and OVCAR3 ZIC2-OE models. The differentially expressed genes regulated by these models were enriched with various gene sets of hallmarks, biological processes, signaling pathways, and oncogenic signatures through GSEA analyses. We applied these topmost enriched gene sets to illustrate the potential underlying mechanisms behind the ZIC2-regulated tumorigenic phenotypes of the SKOV3 ZIC2-KO and OVCAR3 ZIC2-OE models and to

elucidate the discrepancies in tumorigenic phenotypes between these models in a broad sense.

In Chapter 5, we hypothesized that RUNX3 promotes the tumorigenic phenotypes of GCT. We demonstrate that RUNX3 expression was low and variable in GCT tumor samples and that its overexpression promoted the growth, anchorage-independent growth, cell mobility, and tumorigenicity of KGN cells, while inhibition of endogenous RUNX3 by overexpression of dnRUNX3 decreased cell growth in COV434 cells. We also demonstrate that the overexpression of RUNX3 was associated with an increase in cyclin D2 expression and a decrease in $p27^{Kip1}$ expression in KGN cells. Therefore, we suggest that RUNX3 might promote tumorigenic phenotypes by regulating the expression of the cell cycle regulators $p27^{Kip1}$ and cyclin D2.

6.2 Discussion

6.2.1 The regulation of tumorigenic phenotypes driven by ZIC2 in EOC is cell-context dependent

Our data show that knockout of ZIC2 attenuated the tumorigenic phenotypes in the SKOV3 ZIC2-KO and OVCAR8 ZIC2-KO models, consistent with reports that ZIC2 promotes tumorigenic phenotypes in multiple human cancers (165,167,169,186,556). We demonstrate that knockout of ZIC2 inhibited cell growth, cell migration, self-renewal ability, single-cell survival, anchorage-independent growth, $ALDH^{high}$ cell proportion, ALDH1A1 expression, and tumor growth in both ZIC2-KO models, and accelerated the reduction of the $ALDH^{high}$

population in the SKOV3 ZIC2-KO model. We indicate that knockout of ZIC2 did not consistently regulate the tumorigenic phenotypes in both ZIC2-KO models. For instance, in the SKOV3 ZIC2-KO model, knockout of ZIC2 inhibited single-cell survival and anchorage-independent growth, whereas in the OVCAR8 ZIC2-KO model, knockout of ZIC2 only reduced the size, not the number, of the colonies formed by OVCAR8 cells, which might be related to decreased proliferation (**Figure 3.9 and 3.10).** We suggest that ZIC2 promotes tumorigenic phenotypes in EOCs that naturally express ZIC2. According to reports, ZIC2 acts as a transcription factor or a co-factor (172,186). We hypothesize that ZIC2 promotes the tumorigenic phenotypes in EOCs that naturally express ZIC2 as a transcription factor that binds to DNA and recruits co-factors, directly regulating the expression of downstream target genes, or as a co-factor that interacts with other transcription factors, thereby participating the regulation of downstream target genes. We speculate that the regulatory effects of ZIC2 on these downstream genes contribute to diverse tumorigenic phenotypes in EOC (**Figure 6.1**).

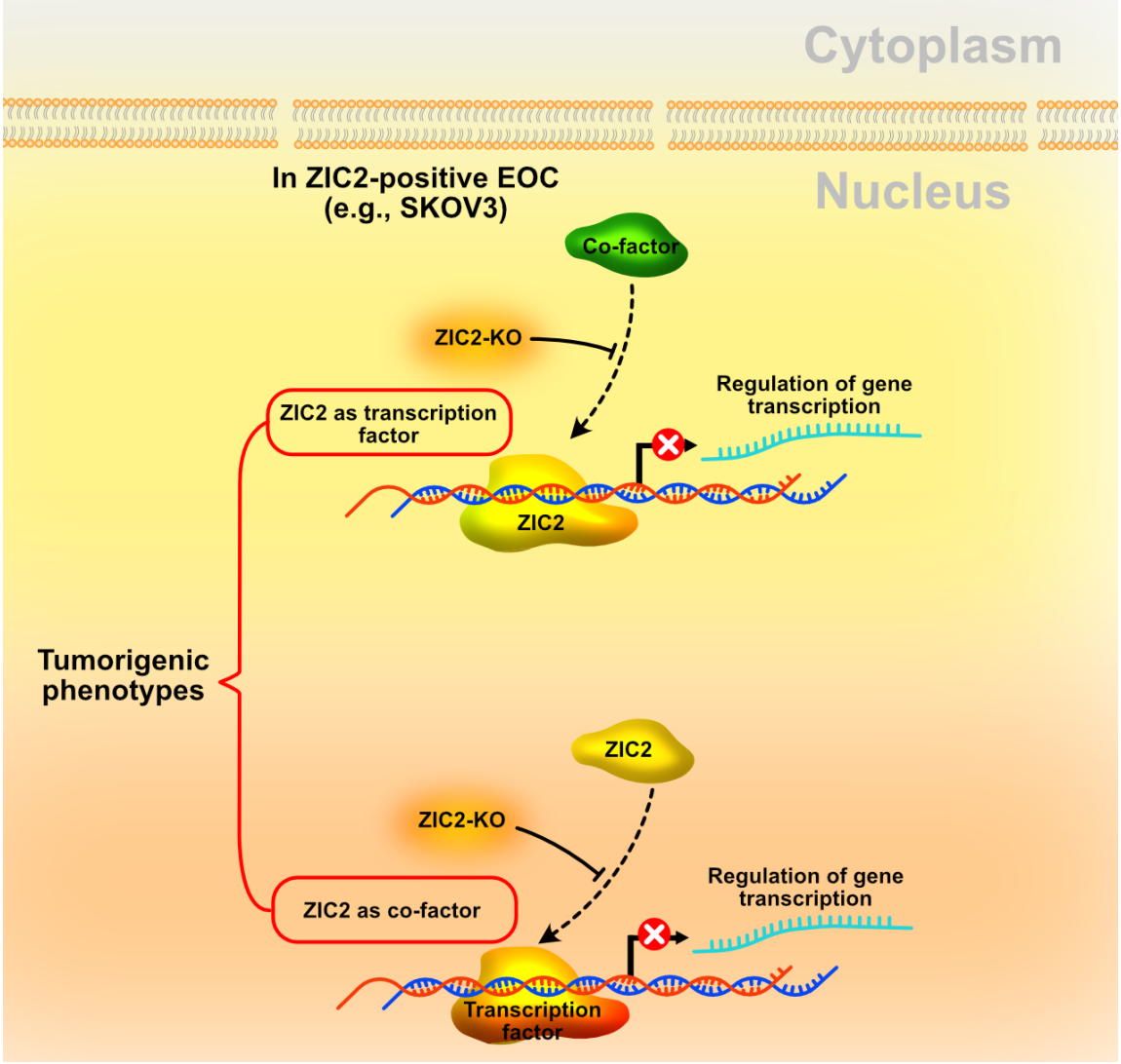

Figure 6.1 Proposed model for the ZIC2-regulated tumorigenic phenotypes in EOC naturally expressing ZIC2.

ZIC2 acts as a transcription factor or a co-factor in EOC cells that naturally express ZIC2 (e.g., SKOV3 cells) and regulates the expression of downstream genes. Knockout of ZIC2 in these EOC cells leads to inactivation of the genes regulated by ZIC2.

Overexpression of ZIC2 affected the tumorigenic phenotypes in the OVCAR3 ZIC2-OE and A2780s ZIC2-OE models, which was not completely consistent with the results in the ZIC2-KO models. Our data indicate that overexpression of ZIC2 promoted cell migration and self-renewal ability in both ZIC2-OE models, enhanced single-cell survival in the OVCAR3 ZIC2-OE model, increased the proportion of $ALDH^{high}$ cells and expression of ALDH1A1 in both ZIC2-OE models, and slowed the decline of the $ALDH^{high}$ population in A2780s cells. These functions of ZIC2 were consistent in both ZIC2-OE models and ZIC2-KO models. However, in the OVCAR3 ZIC2-OE or A2780s ZIC2-OE models, or both, the regulation of ZIC2 on cell growth, single-cell survival, anchorage-independent growth, and tumor growth was inconsistent with the ZIC2-KO models, as overexpression of ZIC2 inhibited these functions and reduces tumor growth. We show that overexpression of ZIC2 in EOC cells that do not express endogenous ZIC2 promotes self-renewal ability and cell migration, but not cell growth and tumor formation and growth. In EOC cells that do not express endogenous ZIC2, overexpression of ZIC2 might disrupt the cellular homeostasis already maintained by the EOC cells independent of ZIC2, thereby reducing certain tumorigenic phenotypes, such as cell growth. Because ZIC2 acts as both a transcription factor and a co-factor, we hypothesize that when ZIC2 is overexpressed as a transcription factor in these cells, it might compete with other transcription factors for co-factors, leading to dysregulation of the expression of the downstream genes regulated by these transcription factors. Similarly, when ZIC2 acts as a co-factor, it competes with other co-factors for their interacting transcription factors, which

might lead to alterations in the expression of downstream genes regulated by these transcription factors. Based on our data, we hypothesize that overexpression of ZIC2 in EOC cells that do not express endogenous ZIC2 disrupts the pre-existing cellular homeostasis, altering gene expression and signaling pathways, ultimately leading to the tumorigenic phenotypes (**Figure 6.2**).

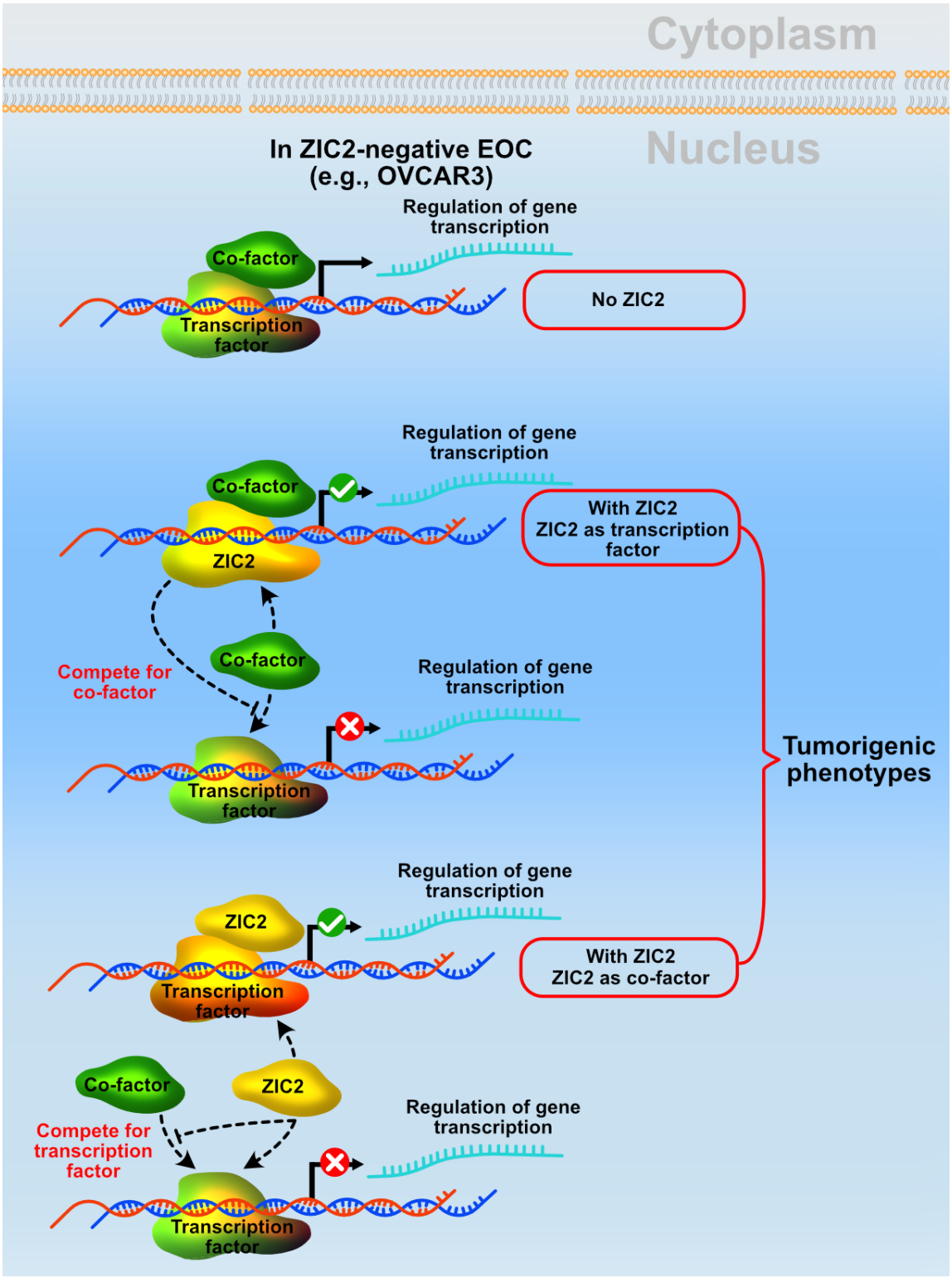
Cytoplasm
Nucleus
In ZIC2-negative EOC
(e.g., OVCAR3)
Regulation of gene transcription
Co-factor
Transcription factor
No ZIC2
Regulation of gene transcription
Co-factor
ZIC2
With ZIC2
ZIC2 as transcription factor
Compete for co-factor
Co-factor
Regulation of gene transcription
Transcription factor
Tumorigenic phenotypes
Regulation of gene transcription
ZIC2
Transcription factor
With ZIC2
ZIC2 as co-factor
Co-factor
ZIC2
Compete for transcription factor
Regulation of gene transcription
Transcription factor

Figure 6.2 Proposed model for the effects of overexpression ZIC2 on the tumorigenic phenotypes in EOC that EOC that does not express endogenous ZIC2.

In EOC cells that naturally do not express ZIC2, interactions between transcription factors and co-factors allow the expression of specific genes to maintain homeostasis and the tumorigenic phenotypes independent of ZIC2. Our hypothesis is that overexpression of ZIC2 in EOC cells that naturally do not express ZIC2 (e.g., OVCAR3 cells) disrupts cellular homeostasis and leads to altered tumorigenic phenotypes. For instance, ZIC2 as a transcription factor binds co-factors competitively with other transcription factors, or ZIC2 as a co-factor binds specific transcription factors competitively with other transcription factors.

RNA-seq analysis and the underlying molecular mechanisms from GSEA analysis in this study provide evidence that endogenous ZIC2 and overexpressed ZIC2 regulates different genes in EOC cells. We demonstrate that the SKOV3 ZIC2-KO and OVCAR3 ZIC2-OE models had distinct transcriptomes and might involve various potential molecular mechanisms. In terms of gene expression, the SKOV3 ZIC2-KO and OVCAR3 ZIC2-OE models showed different numbers of differentially expressed genes, especially genes upregulated over 2-fold and genes downregulated over 2-fold differed in these two cell models (**Figure 4.1C and 4.6C**). In the volcano plots with gene symbols listed, finding common genes between differentially expressed genes ($|\log_2 (\text{fold change})| > 1$, $P < 0.05$) in both models was challenging (**Figure 4.1E and 4.6E**). Similarly, no common genes

were found among the top 50 differentially expressed genes arranged in ascending order by FDR (**Figure 4.2 and 4.7**).

Regarding potential molecular mechanisms regulated by ZIC2, we show that in the SKOV3 ZIC2-KO and OVCAR3 ZIC2-OE models, the patterns of hallmarks, biological processes, signaling pathways, and oncogenic signatures corresponding to the topmost enriched gene sets were different. By performing GSEA analysis, we explored four gene sets that are potentially and commonly regulated by ZIC2 in both models, including those correlated with KRAS signaling, overexpression of E2F3, knockdown of BMI-1, or MEL-18, or both, and Wnt/β-catenin signaling. In addition, we show that in both models, all these gene sets consisted of genes commonly regulated by ZIC2, genes oppositely regulated by ZIC2, and genes independently regulated by ZIC2, and that by analyzing the ZIC2-ChIP-seq datasets of mouse ESC and two human cell lines, some genes in these gene sets might be the potential target genes of ZIC2 (**Figure 4.11 and 4.12**). Our hypothesis is that the differential expression of these three categories of genes in SKOV3 and OVCAR3 models in these four gene sets, particularly genes oppositely regulated by ZIC2 and genes independently regulated by ZIC2, might significantly affect the molecular mechanisms corresponding to these gene sets and lead to different tumorigenic phenotypes. Taking the gene set KRAS.600_UP.V1_UP as an example, the slope of the line between the mean values of genes commonly regulated by ZIC2 for SKOV3 ZIC2-KO and OVCAR3 ZIC2-OE models is significantly smaller than that of genes oppositely regulated by ZIC2 and genes independently regulated by ZIC2 (**Figure 4.11)**. Similarly, the scatter plot of

KRAS.600_UP.V1_UP shows that the distribution of mRNA expression from RNA-seq data for genes commonly regulated by ZIC2 is more consistent compared to the distribution of the other two categories of genes. Thus, even if ZIC2 regulates the tumorigenic phenotype by the same molecular mechanisms, different results might arise in the two models due to the presence of these genes, not to mention the molecular mechanisms corresponding to the gene sets oppositely regulated by ZIC2 in the two models, or gene sets independently regulated by ZIC2 in their respective models. Therefore, we suggest that the genes oppositely regulated by ZIC2 and the genes independently regulated by ZIC2 might result in unique ZIC2-mediated regulation of tumorigenic phenotypes in the two models.

Altogether, ZIC2 is pro-tumorigenic in EOC cells that naturally express ZIC2, while overexpressed ZIC2 might suppress certain tumorigenic phenotype in EOC cells that naturally do not express ZIC2. The regulation of tumorigenic phenotypes by ZIC2 in EOC is determined by the role of ZIC2 as a transcription factor or a co-factor, and the availability of the transcription factors and co-factors that interact with ZIC2 in the cell, and by the genomic background, such as gene mutations and epigenetic landscapes. In addition, different cell states also affect ZIC2 to exert its function in EOC cells. Even in the same EOC cell line, there are cells with different cell states, such as CSCs and non-CSCs. These different cell states might be associated with distinct chromatin accessibility, which determines the ability or inability of ZIC2 to bind to genome-specific DNA regulatory elements (e.g., promoters and enhancers) at specific time, leading to different gene regulation and manifestation of diverse tumorigenic effects.

In summary, we demonstrate that ZIC2 regulates the tumorigenic phenotypes of EOC cells in a cell-context dependent manner in terms of biological functions, differentially expressed genes, and potential molecular mechanisms in the SKOV3 ZIC2-KO and OVCAR3 ZIC2-OE models.

6.2.2 The potential underlying molecular mechanisms of ZIC2 regulating tumorigenic phenotypes of the SKOV3 ZIC2-KO model

Hitherto we explored the potential mechanisms by which ZIC2 regulates the tumorigenic phenotypes in the SKOV3 ZIC2-KO model. We show that the regulation of the tumorigenic phenotype by ZIC2 in the SKOV3 ZIC2-KO and OVCAR3 ZIC2-OE models is cell-context dependent. In the SKOV3 ZIC2-KO model, our data show that knockout of ZIC2 reduced cell growth, the number of colonies in clonogenic assay and soft agar colony-formation assay, cell migration, self-renewal ability, the proportion of $ALDH^{high}$ cells, and subcutaneous tumor growth.

In these attenuated tumorigenic phenotypes, cell growth, colony size in soft agar colony-formation assay, and tumor growth are related to proliferation. We indicate that the molecular mechanisms corresponding to the gene sets correlated with KRAS signaling, knockdown of *BMI1* or *MEL18*, or both, and overexpression of E2F3 were closely related to proliferation. In a variety of human cancers, upregulation of *KRAS*, *E2F3*, *BMI1*, and *MEL18* has been shown to promote proliferation (524-527,530-532,573). The signaling pathways downstream of KRAS, including the RAS/RAF/MEK/ERK, PI3K/AKT, and Ral-GEF pathways, play

an important role in tumor progression (574-577). Activation of the RAS/RAF/MEK/ERK pathway by KRAS ultimately leads to the translocation of activated ERK into the nucleus, which activates transcription factors required to promote cell cycle processes and plays an important role in promoting biosynthesis (e.g., pyrimidine, ribosomes, and proteins) and cell cycle transition in the G1/S and G2/M phases (578). In the PI3K/AKT pathway, activated RAS (e.g., KRAS) binds to the SH2 group of the PI3K regulatory subunit, enhancing the functional activity of PI3K itself, which then activates downstream Akt/PKB (Protein kinase B) (579). Moreover, Akt/PKB stimulates proliferation by inhibiting GSK-3β, promotes protein synthesis in the cell cycle, increases cell size by activating MTOR, and inhibits apoptosis through inhibiting BAD (579). Particularly, the gene sets correlated with KRAS signaling (e.g., KRAS.600_UP.V1_UP) were downregulated in the SKOV3 ZIC2-KO model, suggesting that knockout of ZIC2 might inhibit proliferation.

BMI-1 and MEL-18 are core components of the PRC1 complex (Polycomb Repressor Complex 1) and have overlapping functions in the proliferation of human medulloblastoma cells, i.e., knockdown of BMI-1 or MEL-18, or both, in these cells results in inhibition of proliferation, loss of colony formation, single-cell survival, and anchorage-independent growth, and inhibition of tumor growth in nude mice (527). Moreover, Akt phosphorylates BMI-1 protein at Ser316, and the phosphorylated BMI-1 protein segregates with an inhibitor of cyclin-dependent kinase 4-alternative reading frame (INK4a-ARF) locus, resulting in decreased tumor growth and self-renewal ability of hematopoietic stem and progenitor cells (580). Similarly, the gene sets correlated with the upregulated genes upon

knockdown of BMI-1 or MEL-18, or both, and those correlated with downregulated genes upon knockdown of BMI-1 or MEL-18, or both, were the downregulated and upregulated topmost enriched gene sets of oncogenic signatures, respectively, in the SKOV3 ZIC2-KO model, suggesting that knockout of ZIC2 and knockdown of BMI-1 or MEL-18, or both, might have similar effects.

Transcription factor E2F3 is a member of the pocket protein family and plays a key role in regulating the expression of cell cycle-dependent genes necessary for proliferation (581). In most human cancers, E2F3 activity is not repressed by pRB during the G1/S transition of the cell cycle due to dysfunction of retinoblastoma protein (pRB), which induces quiescent cells into the S phase, leading to increased proliferation (582). In the SKOV3 ZIC2-KO model, the enriched gene set correlated with upregulated genes upon overexpression of E2F3 was downregulated, suggesting that knockout of ZIC2 might play a role in inhibiting proliferation.

The number of colonies formed in clonogenic assay and soft agar colony-formation assay is associated with cell survival and anchorage-independent growth, respectively. In cancer cells, enhanced survival means that cells receive more pro-survival events (e.g., promotion of cell proliferation) and are more resistant to death-promoting events (e.g., apoptosis) (583). Therefore, the survival of cancer cells includes a balance between cell proliferation and apoptosis. We speculate that the reduced cell growth might be associated with a variety of molecular mechanisms, such as KRAS signaling, BMI-1 and MEL-18 related signaling, and E2F3 related signaling. We observed that knockout of ZIC2

increased the colony size formed by SKOV3 cells in clonogenic assay. Based on the hypothesis that the survival of cancer cells involves a balance between cell proliferation and apoptosis, knockout of ZIC2 might lead to more apoptosis and selection of those cells with better proliferative capacity. Anchorage-independent growth reflects the ability of EOC cells to resist anoikis during metastasis (584). In the metastatic process of ovarian cancer, exfoliated cells from the primary ovarian cancer are dispersed in the peritoneal fluid, survive as individual cells or spheres, and subsequently invade the mesothelium to form metastases in the peritoneum or omentum (585). Therefore, the ability of ovarian cancer cells in ascites to resist anoikis is crucial for successful metastasis. In addition, activation of the PI3K/AKT pathway downstream of KRAS and upregulation of *BMI1* or *MEL18*, or both, are associated with inhibition of apoptosis in cancer, and activation of the RAS/RAF/MEK/ERK and Gal-GEF pathways downstream of KRAS and upregulation of *BMI1* or *MEL18*, or both, are associated with the promotion of anchorage-independent growth (527,537,538). Thus, the molecular mechanisms corresponding to these gene sets in the SKOV3 ZIC2-KO model might also be potential underlying molecular mechanisms for ZIC2 to regulate cell survival and anchorage-independent growth.

In the SKOV3 ZIC2-KO model, cell migration was reduced. Metastasis of ovarian cancer involves cell migration (585). For instance, during the early development of ovarian cancer, serous tubal intraepithelial carcinoma (STIC), which is thought to be one of the origins of ovarian cancer, is stimulated by various hormones, including TGF-β and Activin-A present in the follicular fluid during

ovulation, leading to EMT of STIC cells and their migration from fallopian tubes to the ovary (585). Therefore, enhanced cell migration is related to the progression of ovarian cancer (586). Cell migration involves structural changes in cell adhesion (e.g., tight junctions, cadherin-based junctions, and desmosomes), cytoskeleton rearrangement, alteration in cell shape and motility, and perception of the surrounding environment (539). During cell migration, cells need to sense signals from their surrounding environment (e.g., cell-cell communication via focal adhesion and adhesion junctions) (539). When cells receive signals from the environment, this information causes cells to rapidly change through cytoskeletal rearrangements, cell shape, and motility, which macroscopically manifests as the occurrence of cell migration (587). Cell migration requires interactions between cells and the extracellular matrix. These interactions are the binding of fibrillar extracellular matrix proteins and integrins to focal adhesions or hemidesmosomes (539). For instance, cells use the adhesion site of the extracellular matrix at the anterior part of the cell as the cortical anchors for the polymerizing actin meshwork, pushing against the plasma membrane and contracting the cell body forward. In human cancers, cancer cells secrete protein factors (e.g., matrix metalloproteinases) to remodel the extracellular matrix and promote cell migration. In addition, chemotherapy promotes the migration of ovarian cancer cells by upregulating the expression of *GLI1*, a key transcription factor in Hedgehog signaling (588). Therefore, in terms of molecular mechanisms of cell migration, the molecular mechanisms corresponding to the gene sets correlated with cell adhesion, EMT, cytoskeleton organization, basement membrane organization,

cell-cell communication, and Hedgehog signaling might be potential molecular mechanisms of ZIC2 in regulating cell migration in the SKOV3 ZIC2-KO model.

In the SKOV3 ZIC2-KO model, self-renewal ability and the proportion of $ALDH^{high}$ cells were decreased, suggesting that ZIC2 might maintain the stemness of CSCs and inhibit their differentiation. We show that the molecular mechanisms corresponding to the gene sets correlated with Wnt/β-catenin signaling, Hedgehog signaling, and knockdown of BMI-1 (e.g., BMI1_DN.V1_UP) might be the potential mechanisms for ZIC2 to regulate self-renewal ability in the SKOV3 ZIC2-KO model. The activation of Wnt/β-catenin signaling, Hedgehog signaling concomitant with the upregulation of *BMI1* are closely related to the promotion of CSC stemness (543-546,550,589). Among them, BMI-1 is a core member of the PRC1 complex that modifies chromatin to repress transcription by epigenetic modifications, and BMI-1 is required to maintain stemness in mouse ESCs and a variety of somatic stem cells (590). Knockdown of BMI-1 inhibits the self-renewal ability of CSCs in human cancers (591). Among these gene sets, those downregulated in the SKOV3 ZIC2-KO model included those correlated with Wnt/β-catenin signaling, Hedgehog signaling, and downregulated genes upon knockdown of BMI-1; the upregulated topmost enriched gene set of oncogenic signatures in the SKOV3 ZIC2-KO model included those correlated with upregulated genes upon knockdown of BMI-1. The molecular mechanisms corresponding to these topmost enriched gene sets in the SKOV3 ZIC2-KO model reveal the potential underlying molecular mechanisms of ZIC2 in regulating the stemness of CSCs. In addition, knockout of ZIC2 reduced the expression of ALDH1A1 in the SKOV3 ZIC2-KO model and eliminated the

ALDH1A1-positive cells in SKOV3 ZIC2-KO tumor sections. Since CSCs are one of the important factors promoting tumor growth in the subcutaneous xenograft model, the decreased growth of SKOV3 ZIC2-KO tumors compared with SKOV3 WT tumors might be related to the decrease of self-renewal ability and CSC proportion.

Collectively, we reveal the potential underlying mechanisms of ZIC2 in regulating these tumorigenic phenotypes in the SKOV3 ZIC2-KO model. Further investigation of these molecular mechanisms might lead to a better understanding of the tumorigenic phenotypes regulated by ZIC2 in the SKOV3 ZIC2-KO model.

6.2.3 The potential underlying molecular mechanisms of ZIC2 regulating tumorigenic phenotypes of the OVCAR3 ZIC2-OE model

We explored the potential mechanism behind the tumorigenic phenotypes regulated by ZIC2 in the OVCAR3 ZIC2-OE model. We suggest that ZIC2 regulates the tumorigenic phenotypes in the OVCAR3 ZIC2-OE model differently from the SKOV3 ZIC2-KO model. For instance, overexpression of ZIC2 increased single-cell survival, cell migration, self-renewal ability, and the proportion of $ALDH^{high}$-enrich and $CD133^{high}$-enriched CSCs, but reduced cell growth and tumor growth.

In the OVCAR3 ZIC2-OE model, cell growth and tumor growth were reduced, suggesting that ZIC2 may inhibit the proliferation of OVCAR3 cells (**Figure 3.19, 3.30B, and 3.30E**). We show multiple gene sets correlated with the cell cycle (e.g., REACTOME_CELL_CYCLE_CHECKPOINTS) in the topmost

enriched gene sets, which might be related to the regulation of cell proliferation by ZIC2 in the OVCAR3 ZIC2-OE model. In the top hallmark gene sets, those correlated with the cell cycle were related to cell proliferation. These gene sets correlated with the cell cycle were mainly concentrated in those correlated with MYC-regulated target genes (i.e., HALLMARK_MYC_TARGETS_V1), E2F-regulated target (i.e., HALLMARK_ E2F_TARGETS), and G2/M checkpoint of the cell cycle (i.e., HALLMARK_G2M_CHECKPOINT), which were upregulated in the OVCAR3 ZIC2-OE model. E2F family members enhance cell proliferation by promoting the G1/S phase transition in the cell cycle (581,582). *MYC* is an oncogene in which the primary tumorigenic mechanism is inhibition of CDK inhibitors, promotion of cell cycle progression, and finally cell proliferation by activation or induction of cyclins and CDKs (528). Notably, overexpression of ZIC2 was also associated with the genes set correlated with the G2/M checkpoint. There are three important checkpoints in the cell cycle, the R (Restriction) point in the G1 phase, the checkpoint in the G2/M phase, and the spindle checkpoint in the M phase. The R point in the G1 phase is primarily responsible for checking whether the cells have sufficient growth (e.g., cell size, growth factors, and DNA damage) to undergo chromosome replication or enter the resting phase (i.e., G0 phase) (592). The G2/M checkpoint is a checkpoint at which the cells enter the M phase from the G2 phase and is mainly responsible for checking that all chromosomes have been replicated and for checking for damaged DNA (593). If a cell detects a DNA problem at this checkpoint, it halts the cell cycle until DNA repair is complete. The spindle checkpoint in the M phase is primarily responsible for checking

whether all spindles are attached to the chromosomes (594). Therefore, even though E2F and MYC play a role in promoting cell proliferation, activation or inhibition of genes related to the G2/M checkpoint might delay the G2/M transition in the cell cycle, which might be a factor contributing to slower cell growth and tumor growth in OVCAR3 ZIC2-OE cells compared with OVCAR3 vector cells.

Among the topmost enriched gene sets of biological processes, those associated with cell proliferation included those correlated with cell cycle and positive regulation of leukocyte proliferation (i.e., GOBP_POSITIVE _REGULATION_OF_LEUKOCYTE_PROLIFERATION). These gene sets correlated with the cell cycle were mainly concentrated in DNA replication in the S phase, cohesion and segregation of sister chromatids, and nuclear division in metaphase and anaphase of mitosis. Because the primary purpose of DNA replication is to replicate chromosomes and the primary purpose during the metaphase and anaphase of mitosis is to segregate sister chromatids, ZIC2 in the OVCAR3 ZIC2-OE model might regulate the cell cycle by mediating the replication and segregation of chromosomes (595). However, further studies are needed to determine whether this effect is associated with decreased proliferation. The gene set correlated with the positive regulation of leukocyte cell proliferation was also downregulated in the OVCAR3 ZIC2-OE model, suggesting that overexpression of ZIC2 might inhibit proliferation.

Among the topmost enriched gene sets of signaling pathways, those correlated with the cell cycle were related to proliferation. These gene sets were concentrated in those correlated with DNA replication in the S phase, sister

chromatid cohesion and segregation in metaphase and anaphase of mitosis, and cell cycle checkpoints. These gene sets correlated with DNA replication and sister chromatids were upregulated in the OVCAR3 ZIC2-OE model, consistent with the corresponding upregulated gene sets in the topmost enriched gene sets of biological processes. The topmost enriched signaling pathway gene sets upregulated in this model also included those correlated with cell cycle checkpoints. As mentioned, there are three important checkpoints in the cell cycle, and activation of genes related to these checkpoints might delay cell cycle progression, which might be one of the factors that reduce cell growth and tumor growth in the OVCAR3 ZIC2-OE model.

Among the topmost enriched gene sets of oncogenic signatures, those associated with proliferation included those correlated with overexpression of oncogenic KRAS, knockdown of BMI-1 or MEL-18, or both, and overexpression of E2F3. The gene sets upregulated in the OVCAR3 ZIC2-OE model included those correlated with upregulated genes upon overexpression of oncogenic KRAS (e.g., KRAS.600_UP.V1_UP) and upregulated genes upon overexpression of E2F3. The gene sets downregulated in this model were those correlated with genes downregulated upon overexpression of oncogenic KRAS (e.g., KRAS.600_UP.V1_DN). The molecular mechanisms corresponding to these gene sets are associated with enhanced proliferation, which has been previously deliberated in the SKOV3 ZIC2-KO model.

Herein, the analysis of potential underlying molecular mechanisms related to proliferation suggests that overexpression of ZIC2 in OVCAR3 cells might be

associated not only with the molecular mechanisms that promote proliferation but also with molecular mechanisms correlated with cell cycle checkpoints that might halt the cell cycle. Based on the reduced cell growth and tumor growth shown in the OVCAR3 ZIC2-OE model, we suggest that activated cell cycle checkpoints might have a negative effect on proliferation, although overexpression of ZIC2 might involve a range of molecular mechanisms that promote proliferation. Further studies are needed to determine whether the molecular mechanisms corresponding to the gene sets correlated with cell cycle checkpoints are associated with decreased cell growth and tumor growth.

The number of colonies formed in clonogenic assay is related to single-cell survival. Our data show that overexpression of ZIC2 increased the number of colonies formed in the OVCAR3 ZIC2-OE model. In terms of anchorage-independent growth, we could not determine which molecular mechanisms were involved in this biological function in the OVCAR3 ZIC2-OE model because neither the OVCAR3 vector nor the OVCAR3 ZIC2-OE cells formed colonies in soft agar colony-formation assay. Since cell survival also involves promotion of proliferation and resistance to apoptosis, molecular mechanisms corresponding to the upregulated gene sets correlated with proliferation and the downregulated gene sets correlated with apoptosis (i.e., HALLMARK_APOPTOSIS and P53_DN.V2_UP) might be the potential underlying molecular mechanisms by which ZIC2 regulates cell survival in the OVCAR3 ZIC2-OE model.

Cell migration was enhanced in the OVCAR3 ZIC2-OE model. Cell migration is associated with changes in cell adhesion structure, cytoskeleton

rearrangement, cell shape and motility, and perception of the surrounding environment (540). Based on the molecular mechanisms of cell migration, the molecular mechanisms corresponding to the gene sets correlated with cell adhesion, extracellular matrix (ECM), and ECM-associated proteins (e.g., matrisome) might be the potential underlying molecular mechanisms of ZIC2 regulating cell migration in the OVCAR3 ZIC2-OE model, suggesting that ZIC2 might enhance cell migration by modifying ECM, changing the composition of ECM-associated proteins and reducing cell adhesion.

In the OVCAR3 ZIC2-OE model, the self-renewal ability and proportion of $ALDH^{high}$ and $CD133^{high}$ cells were increased, suggesting that ZIC2 might maintain the stemness of CSCs and inhibit the differentiation of CSCs in OVCAR3 cells, consistent with the regulation of ZIC2 on CSC stemness in the SKOV3 ZIC2-KO model. This study suggests that the molecular mechanisms corresponding to the gene set correlated with Wnt/β-catenin signaling and KRAS signaling were closely related to self-renewal ability. Notably, the top gene sets related to self-renewal ability involved in the SKOV3 ZIC2-KO model also included those correlated with Wnt/β-catenin signaling and overexpression of oncogenic KRAS. Thus, the molecular mechanisms corresponding to these gene sets in the OVCAR3 ZIC2-OE model might be the potential underlying molecular mechanisms of ZIC2 in regulating self-renewal ability.

In the OVCAR3 ZIC2-OE model, the explanation for the attenuated tumor growth remains inconclusive because proliferation, the proportion of CSCs, and self-renewal ability are important, albeit not all, factors in regulating tumor growth.

For instance, in OVCAR3 cells, although overexpression of ZIC2 increased ALDH1A1 expression *in vitro*, it did not increase ALDH1A1 expression in tumor lysates, nor did it increase the proportion or intensity of ALDH1A1-positive cells in tumor sections. This might be due to the presence of cytokines, chemokines, tumor-associated macrophages, and tumor-associated fibroblasts in the tumor microenvironment, which also alters tumor growth. Moreover, the use of large numbers of cells (e.g., 10 million cells per injection) in the subcutaneous xenograft model is not appropriate model to determine tumorigenicity of CSCs in the OVCAR3 ZIC2-OE model. Further studies are needed to determine the effect of CSC stemness promoted by ZIC2 on tumorigenesis by limiting dilution assay *in vivo*.

Together, we reveal the potential underlying molecular mechanisms of ZIC2 in regulating these tumorigenic phenotypes in the OVCAR3 ZIC2-OE model, which might help better understand ZIC2-regulated tumorigenic phenotypes in the OVCAR3 ZIC2-OE model.

6.2.4 Overall explanations for the discrepancies in ZIC2's regulation of tumorigenic phenotypes by ZIC2 in the SKOV3 ZIC2-KO and OVCAR3 ZIC2-OE models

We showed that ZIC2 promotes the tumorigenic phenotypes in EOC cells that naturally express ZIC2 (e.g., SKOV3) and suppresses the tumorigenic phenotypes in EOC cells that naturally do not express ZIC2 (e.g., OVCAR3). In addition, by performing RNA-seq analysis and GSEA analysis, we determined the

transcriptome regulated by the endogenous and overexpressed ZIC2 and explored the potential molecular mechanisms underlying ZIC2 functions in EOC. Regarding cell growth, ZIC2 promotes this ability in SKOV3 and reduces it in OVCAR3 cells. We observed that in terms of potential molecular mechanisms, KRAS signaling, BMI-1 and MEL-18 related signaling, and E2F3 related signaling might be common potential molecular mechanisms in SKOV3 and OVCAR3 cells, but cell cycle checkpoint-related signaling might also be potential molecular mechanisms in OVCAR3 cells. In terms of cell survival, KRAS signaling, BMI-1 and MEL-18 related signaling, and E2F3 related pathways might be potential molecular mechanisms in SKOV3 cells, while apoptosis related signaling (e.g., HALLMARK_APOPTOSIS and P53_DN.V2_UP) might be potential molecular mechanisms in OVCAR3 cells. As for the cell migration, cell adhesion and extracellular matrix are common potential molecular mechanisms in SKOV3 and OVCAR3 cells. With respect to self-renewal capacity, knockdown of Wnt/β-catenin signaling, Hedgehog signaling and BMI-1 in SKOV3 (e.g., BMI1_DN.V1_UP) might be potential molecular mechanisms, while Wnt/β-catenin signaling and KRAS signaling are potential molecular mechanisms in OVCAR3 cells. Therefore, the pathobiological functions of ZIC2 in the development of EOC are cell-context dependent. We speculate that the discrepancies between the functions of the endogenous and overexpressed ZIC2 in EOC might be affected by the tumor microenvironment and might depend on the expression of ZIC2 at different stages of tumor development.

Among the intrinsic factors of EOC cells, the diversity of ZIC2 regulation on the tumorigenic phenotypes in EOC might be the result of a combination of genetic mutations, epigenetic modifications, and the diversity of ZIC2-interacting protein factors. In the SKOV3 ZIC2-KO and OVCAR3 ZIC2-OE models, multiple gene mutations in the genomes of different EOC cell lines might cause different responses to the ZIC2-regulated tumorigenic phenotypes. Different subtypes of EOC have different primary gene mutations. For instance, the primary mutation in HGSOC is *TP53*, whereas the primary mutations in endometrioid and clear cell carcinomas are *ARID1A*, *PIK3CA*, and *PTEN* (**Figure 1.3**) (55). These genes are associated with signaling pathways (e.g., PI3K/AKT pathway) related to cell proliferation and survival, and the roles of their mutations in promoting tumor progression in human cancers have been extensively investigated (55).

In particular, both the ZIC2-KO and ZIC2-OE models in the ZIC2 study included cell lines from both endometrioid and HGSOC subtypes. OVCAR8 and OVCAR3 are both HGSOC cell lines and have mutant *TP53* (562,596). SKOV3 and A2780s are endometrioid cell lines in which A2780s cells have *ARID1A*, *PIK3CA*, and *PTEN* mutations, while SKOV3 cells have *ARID1A* and *PIK3CA* mutations (597-601). Our data suggest that the regulation of tumorigenic phenotypes by ZIC2 is cell-context dependent. Meanwhile, we show that knockout of ZIC2 reduced cell growth in the SKOV3 ZIC2-KO and OVCAR8 ZIC2-KO models, while overexpression of ZIC2 attenuated cell growth in the OVCAR3 ZIC2-OE and A2780s ZIC2-OE models, suggesting that genomic mutations in these cell lines might affect the regulation of ZIC2 in some but not all the regulation of

tumorigenic phenotypes. Nevertheless, we suggest that dysfunction of these critical genes and changes in signaling pathways might lead to different presentations of ZIC2-regulated tumorigenic phenotypes in different EOCs.

Epigenetic modifications are closely related to tumor progression in that they regulate gene expression and biological functions through molecular mechanisms such as DNA methylation, histone modifications, non-coding RNA regulation, and chromatin remodeling (602-605). During tumorigenesis, promoter hypermethylation and overall gene hypomethylation lead to whole-genome instability and changes in gene expression profiles (606-608). Histone modifications include methylation, phosphorylation, acetylation, ubiquitination, and glycosylation (608). Together, histone modifications and the degree of DNA methylation determine specific chromatin structures, reversibly inhibit or promote gene transcription, and affect DNA replication, DNA repair, self-renewal, and stem cells differentiation (609,610). Non-coding RNA regulation refers to the regulation of specific gene expression at the transcription level by some functional RNAs that could be transcribed but not translated into proteins (e.g., microRNA and Circular RNA) and has been shown to be associated with cell proliferation, apoptosis, and metastasis (611-615). Chromatin remodeling refers to the transformation of chromatin from a tight supercoiled structure to an open, loose structure during DNA transcription. This process involves chromatin remodeling complexes, histone modifications, and DNA methylation and is closely related to tumorigenesis (615). The preliminary study on the feasibility of identifying ZIC2-binding target genes in four gene sets using ChIP-seq data from mouse ESC suggests that ZIC2 might

regulate gene expression through histone modifications (e.g., H3K27me3, H3K27ac, H3K4me1, and H3K27me3) (**Figure 4.12**) (171).

The differential regulation of gene expression by ZIC2 in different cell states might involve the regulation of epigenetic modifications. As a co-activator, ZIC2 has been shown to interact with chromatin remodeling complexes (e.g., NURF and NuRD complexes) in mouse ESC and liver CSCs, potentially regulating epigenetic modifications (170,171). We demonstrate that ZIC2 was expressed in SKOV3 WT and OVCAR3 ZIC2-OE cells, and that knockout of ZIC2 and overexpression of ZIC2 decreased and increased ALDH1A1 expression in the SKOV3 ZIC2-KO and OVCAR3 ZIC3-OE models, respectively. In contrast, ALDEFLUOR assay suggested that not all cells expressing ZIC2 were CSCs (**Figure 3.16 and 3.28**). The cell states of CSCs and non-CSCs might correspond to the differential regulatory effects of ZIC2 on epigenetic modifications in EOC. From the perspective of molecular mechanism, these regulatory effects are manifested as the ability or inability of ZIC2 to bind specific DNA sequences or specific protein factors in different cell states of EOC. The regulation of epigenetic modifications by ZIC2 might lead to changes in the expression levels of more genes indirectly regulated by ZIC2 than the number of genes directly bound by ZIC2. From the perspective of tumorigenic phenotypes, these regulatory effects are ultimately manifested in the ability or inability of ZIC2 to regulate specific pathobiological functions in different cell states.

Furthermore, RNA-seq analyses of both models showed that ZIC2 regulated a large number of genes, and GSEA analyses showed that some of the

differentially expressed genes were associated with the PRC1 complex (e.g., BMI1_DN_MEL18 _DN.V1_DN) (**Figure 4.5, 4.8, and 4.9, Table 4.2 and 4.3**), formed by Polycomb-group (PcG) proteins (616). The PRC1 complex is an important epigenetic regulator involved in maintaining the silencing of specific genes and plays a vital role in regulating the proliferation and differentiation of stem cells (616,617). We suggest that the regulation of the tumorigenic phenotypes by ZIC2 in EOC might involve epigenetic modifications and depend on the cell state. In the preliminary study on the feasibility of identifying ZIC2-binding target genes using existing ChIP-seq datasets from mouse ESC and human cell lines, we applied an existing ZIC2 consensus sequence (CACACAGG) shared by mice and humans in the JASPAR database (jaspar.genereg.net) to identify potential ZIC2 DNA-binding sites. However, it is important to identify genes directly regulated by ZIC2 in the EOC models by ChIP-seq and a consensus sequence in the populations of CSCs and non-CSCs, as the cell states of CSCs and EOC are different from mouse ESC and other human cell lines. It is also important to identify the ZIC2 interactomes (i.e., ZIC2-interacting proteins) in these cell populations by IP-MS (immunoprecipitation-mass spectrometry), which might help better understand the potential underlying molecular mechanisms of ZIC2 in regulating the tumorigenic phenotypes in different cell states of EOC.

The complexity of the tumor microenvironment relative to cell culture conditions might be a cause of the different pathobiological roles of ZIC2 *in vitro* and *in vivo*. *In vivo*, the tumor microenvironment in which cancer cells grow is more complex and uncertain. The tumor microenvironment consists of non-cellular

components of ECM, tumor cells, tumor stromal cells (e.g., stromal fibroblasts), immune cells, and endothelial cells (511-513). In the tumor microenvironment, tumor cells achieve tumor growth and metastasis by regulating complex signaling pathways and organizing non-cellular components such as ECM (618). Cell-cell communication is the main activity of the tumor microenvironment through a complex network formed by cytokines, chemokines, growth factors, matrix remodeling enzymes (e.g., matrix metalloproteinases), and inflammation mediators (513,619). Studies showed that ECM, non-tumor cells (e.g., immune cells), and genetically altered tumor cells in the tumor microenvironment affect most stages of tumorigenesis, including EMT, migration, invasion, metastasis, angiogenesis, and chemoresistance (513,620-624).

Our data show that knockout of ZIC2 in SKOV3 cells decreased the expression of ROR2 protein in monolayer cultured cells but increased its expression in tumors; cyclin D2 was detected in tumors formed by SKOV3 WT cells, but not in monolayer cultured cells (**Figure 4.3 and 4.4**). In particular, GSEA analyses revealed potential molecular mechanisms involved in both models, including ECM-associated proteins (i.e., matrisome), ECM organization, angiogenesis, and EMT. Thus, ZIC2 might be involved in the regulation of the tumor microenvironment, and the tumorigenic phenotypes regulated by ZIC2 might also be affected by the tumor microenvironment. Further studies are needed on whether and how ZIC2 participates in the regulation of the tumor microenvironment in EOC.

The diversity of ZIC2 regulation of tumorigenic phenotypes in the SKOV3 ZIC2-KO and OVCAR3 ZIC2-OE models might be related to ZIC2 expression in parental cells at different stages of tumor development. Our data show that ZIC2 expression was upregulated in a subset of clear cell, endometrioid, and HGSOC tumors, but not in mucinous tumors, and that ZIC2 upregulation was mainly concentrated in a small group of tumor samples from patients with advanced EOC (**Figure 3.1).** In addition, IHC staining showed ZIC2 expression in a subset of HGSOC and immunoblotting showed variable expression of ZIC2 in six of the nine EOC cell lines (**Figure 3.5A).** There could be two scenarios in terms of the lack of ZIC2 expression in EOCs that naturally do not express ZIC2: 1) ZIC2 might not be expressed throughout the tumor progression; 2) ZIC2 expression might be elevated at early stages and further decreased and lost during tumor progression. In the first scenario, EOCs that naturally do not express ZIC2 might not be chronically dependent on ZIC2-driven signaling pathways related to pathobiological functions, and ectopic expression of ZIC2 in these EOCs might result in variable degrees of suppression in tumorigenic phenotypes, such as decreased cell growth and tumor growth. In the second scenario, ectopic expression of ZIC2 might not result in a malignant tumorigenic phenotype of EOC if ZIC2 is not required for further tumor progression. Given these considerations, ZIC2 might not play a role in the pathobiological regulation of certain aspects (e.g., proliferation, survival, anchorage-independent growth, and tumor growth) in EOCs that naturally do not express ZIC2.

Conversely, for EOCs that naturally express ZIC2, ZIC2 might act as a transcription factor and co-activator in regulating pathobiological functions due to its upregulation and involvement in tumor progression. Thus, knockout of ZIC2 in EOCs that naturally express ZIC2 might alter the expression of specific genes and modify signaling pathways required for pathobiological function, thereby suppressing the tumorigenic phenotypes.

Overall, we suggest that multiple factors discussed above might account for the differential regulation of the tumorigenic phenotypes by ZIC2 in the SKOV3 ZIC2-KO and OVCAR3 ZIC2-OE models. Further exploration is needed to reveal the extensive tumor heterogeneity that leads to the diversity of ZIC2-mediated regulation of tumorigenic phenotypes in EOC.

6.2.5 RUNX3 is pro-tumorigenic in GCT

The pathogenesis of GCT is associated with a variety of signaling pathways in normal granulosa cells of the ovary, such as follicle-stimulating hormone (FSH)-mediated signaling pathways, the PI3K/AKT, the EGF, and the VEGF pathways (625-628). In normal ovaries, granulosa cells enter a peak of proliferation between the preantral and preovulatory stages of the follicle. At this time, the FSH receptor is expressed on the surface of preantral granulosa cells, and the presence of the FSH receptor promotes follicular growth (625). It is generally accepted that the development of GCT is the result of malignant transformation due to various genetic changes (e.g., *FOXL2* mutation) in granulosa cells (564). The gene expression profile of GCT is also consistent with FSH-stimulated granulosa cells,

such as the high expression of *CCND2* (cyclin D2) (629). RUNX proteins, together with the chaperone CBFβ, play a key role in regulating the biology of granulosa cells. For instance, the expression of *Runx1* in rat periovulatory granulosa cells is activated by luteinized hormone (LH), estrogen, and epidermal growth factor (EGF) (630,631). Estrogen and EGF also induce *Runx2* expression in rat preovulatory granulosa cells stimulated by hCG (human chorionic gonadotropin), while knockout of CBFβ results in decreased *Runx2* expression (632). Researchers showed that *Runx3* regulates folliculogenesis and steroidogenesis in immature mouse granulosa cells (228). Dinh *et al.* revealed that the inhibitory effect of PAX8 on *RUNX3* expression is attenuated in EOC cells compared to fallopian tube cells, suggesting that RUNX3 is a hypothetical regulator of the transformation of fallopian tube cells to HGSOC (633). Given that the *RUNX3* gene is upregulated and pro-tumorigenic in both EOC and GCT, dysregulation of *RUNX3* in granulosa cells might lead to GCT (222,225,226,633). Studies on the RUNX family in GCT are limited to the expression and DNA methylation of *RUNX* genes, and the role of these proteins in tumorigenesis remains unclear (484).

Our data indicate that RUNX1 and RUNX2 were expressed in GCT samples, the non-tumorigenic cell line SVOG, and the AGCT cell line KGN; RUNX2 was not expressed in the JGCT cell line COV434; RUNX3 was variably expressed in GCT samples and was highly expressed in COV434 cells but not in KGN cells. Regarding the expression of RUNX3, variable expression levels of this gene were low in samples from the Alberta Cancer Research Biobank, but not detected in samples from the Baylor College of Medicine Tissue Repository. Therefore, we

suggest that RUNX3 expression in GCT is not a common event. We noted that the expression patterns of RUNX2 and RUNX3 differ in COV434 cells and JGCT samples. For instance, the expression of RUNX2 and RUNX3 in KGN and COV434 cells was mutually exclusive. Nevertheless, both genes were expressed simultaneously in AGCT samples from the Alberta Cancer Research Biobank. Whether RUNX2 and RUNX3 negatively regulate each other in KGN and COV434 cells is worth exploring. Because COV434 is the only JGCT cell line, probably a misidentified small cell carcinoma of the ovary hypercalcemic type (SCCOHT) cell line, we could not interpret the role of RUNX proteins in JGCT development until further analysis of this cell line is confirmed (634).

Our research on GCT might fill the gap in the studies of the role of RUNX3 in GCT tumorigenesis. Published research on RUNX3 in GCT is limited to DNA methylation of the *RUNX3* promoter and post-translational modifications of the RUNX3 protein. For instance, Dhillon *et al.* showed that the promoter of the *RUNX3* gene was frequently methylated in GCT samples and GCT cell lines and that RUNX3 expression was detected in KGN cells only after treatment with 5-aza-2'-deoxycytidine (a demethylation reagent) (484). In our study, we show that overexpression of RUNX3 in KGN cells promoted cell growth, colony formation, and cell migration *in vitro*, as well as tumor formation in NSG mice. Moreover, we demonstrated that inhibition of endogenous RUNX3 by dnRUNX3 reduced cell growth in COV434 cells.

We also explored the potential underlying mechanism by which RUNX3 promotes KGN tumorigenesis. GCT proliferation and tumor formation have been

reported to be involved in the regulation of cell cycle-related genes, such as *CCND2* (cyclin D2) and *CDKN1B* ($p27^{Kip1}$) (635-637). We found that overexpression of RUNX3 in KGN cells increases the mRNA and protein expression of *CCND2*, while overexpression of RUNX3 results in a decrease in $p27^{Kip1}$ protein, suggesting that RUNX3 might regulate $p27^{Kip1}$ through post-translational modifications. According to Hnit *et al.,* although the expression of $p27^{Kip1}$ is regulated by transcription and post-translational modifications, post-translational modifications that alter E3 ubiquitin ligase-mediated protein degradation are the primary mechanism controlling $p27^{Kip1}$ protein levels (638). However, further studies are needed to explain how RUNX3 regulates protein expression of $p27^{Kip1}$ at the protein level rather than at the mRNA level.

Although most GCT patients are diagnosed at an early stage and the 10-year overall survival rate in GCT patients is about 96%, the prognosis for advanced GCT and recurrent GCT is poor (639-641). The recurrence rate of GCT ranges from 10% to 28%, and about 80% of patients die from recurrent GCT (130,625,641). Since GCT is a rare subtype of ovarian cancer, the treatment of GCT still relies on EOC regimens such as cytoreductive surgery and combination chemotherapy. However, current treatments are ineffective for recurrent GCT. One of the reasons for the slow progress in research on GCT tumor progression is the lack of preclinical *in vivo* GCT models, which hinders the development of new therapies. At present, there are few reports on mouse xenograft models of KGN cells, indicating that KGN cells formed small tumors in mice and that tumor growth was very slow (486,568,569). Herein, we demonstrated for the first time that

overexpression of RUNX3 in KGN cells in NSG mice is pro-tumorigenic. We suggest that repeated passage of these KGN RUNX3-OE tumors in mice to establish a KGN xenograft model might benefit the testing of therapeutic drugs.

Our research on RUNX3 was limited by the rarity of GCT samples. We only analyzed the expression of *RUNX1*, *RUNX2*, and *RUNX3* in a limited number of GCT samples. Nevertheless, our data suggest that RUNX3 may promote tumorigenic phenotypes of GCT *in vitro* and *in vivo*. RUNX3 is related to luteinizing hormone induction in normal granulosa cells of the ovary but was not detected in SVOG or KGN cells. Therefore, RUNX3 might be required for malignant transformation in granulosa cells of the ovary.

Similar to ZIC2, the RUNX3 protein is a transcription factor that pharmaceutical companies have long ignored as an undruggable target. Studies showed that *RUNX3* is both a tumor suppressor gene and an oncogene in various human cancers (207,212,216-218,220,222,227). Herein, our data suggest that RUNX3 may promote tumorigenesis in GCT. Since RUNX proteins rely on co-binding with CBFβ to form dimers to function as transcription factors, the interaction site between RUNX proteins and CBFβ has been used to develop targeted drugs (642-644). In chromosome invasion inv (16) leukemia, drugs have been developed to block the interaction between RUNX1 and CBFβ-SMMHC, a CBFβ protein fused with the *MYH11*-encoded smooth muscle myosin heavy chain (SMMHC) protein (642-644). Co-binding of RUNX1 to normal CBFβ is essential during hematopoiesis, but in this leukemia, RUNX1 is more likely to interact with CBFβ-SMMHC. For instance, 4-(2′-Chlorophenyl)-thiazol-2-yl- and 5-Ethyl-4-(4′-

methoxyphenyl)-thiazol-2-yl ammonium iodides, benzodiazepine Ro5-3335, and bivalent trifluoromethoxy-benzimidazole-pyridine compound (AI-10-49) have been reported to inhibit the binding of RUNX1 and CBFβ-SMMHC (642-644). Illendula *et al*. reported increased expression of *RUNX3* in the chromosome invasion inv (16) leukemia cell line ME-1 cells after treatment with AI-10-49 (644). Therefore, these three small-molecule drugs targeting CBFβ-SMMHC fusion protein might not be applicable to cancers with high RUNX3 expression.

In addition to the protein-protein interaction level, the mechanism involved in RUNX3 at the mRNA transcription level, the protein-DNA binding level, the DNA genome, and the protein degradation level might be used in the development of drugs against RUNX3. Therefore, the development of drugs targeting RUNX3 still relies on a better understanding of the molecular mechanisms of the pro-tumorigenic role of RUNX3.

In conclusion, in the RUNX3 section, we demonstrated that RUNX3 is expressed in some AGCT samples and COV434 cells and that RUNX3 may promote tumorigenic phenotypes in GCT.

6.3 Conclusion

In conclusion, our research demonstrates the roles of transcription factors ZIC2 and RUNX3 in regulating the tumorigenic phenotype in different subtypes of ovarian cancer. Studying the roles of ZIC2 and RUNX3 is of great importance for understanding the tumor progression and identifying therapeutic targets for ovarian cancer.

In Chapter 3 and Chapter 4, we hypothesized that ZIC2 promotes tumorigenic phenotypes. Briefly, this study builds on published findings and demonstrates that the regulation of tumorigenic phenotypes by ZIC2 is cell-context dependent. Knockout of ZIC2 in EOC cells (SKOV3 and OVCAR8) that naturally express ZIC2 attenuates tumorigenic phenotypes such as reduced cell growth, single-cell survival, anchorage-independent growth, cell migration, and tumor growth, while overexpression of ZIC2 in EOC cells (OVCAR3 and A2780s) that naturally do not express ZIC2 has variable effects on tumorigenic phenotypes such as increased cell migration and self-renewal ability, and decreased cell growth and tumor growth. In transcriptome studies, GSEA analyses and the preliminary study on the feasibility of identifying ZIC2-binding targets in the common gene sets in both models using the existing ChIP-seq datasets help us understand how ZIC2 potentially regulates tumorigenic phenotypes in EOC.

In Chapter 5, we hypothesized that RUNX3 promotes tumorigenic phenotypes in GCT. In brief, the study on RUNX3 demonstrates the expression of three RUNX family members in GCT samples and cell lines and suggests that RUNX3 promoted cell growth, anchorage-independent growth, cell mobility, and tumorigenesis in GCT, which may be associated with the regulation of the cell cycle regulators cyclin D2 and $p27^{Kip1}$. We suggest that the xenograft model of KGN RUNX3-OE cells could be further explored to generate a preclinical model for testing drugs against GCT *in vivo*.

6.4 Future directions

6.4.1 To determine the direct and indirect target genes of ZIC2

To identify genes directly or indirectly regulated by ZIC2, we will perform ChIP-seq once a ChIP-grade anti-ZIC2 antibody is available. Paired samples from SKOV3 WT and ZIC2-KO cells, and paired samples from OVCAR3 vector and ZIC2-OE cells, along with their respective input samples, will be analyzed by high-throughput sequencing and a list of genes directly regulated by ZIC2 will be identified. We will optimize the cross-linking and sonication of chromosomal fragments of the pair samples and perform immunoprecipitation using anti-ZIC2 antibody followed by DNA purification. By sequencing the collected ChIP-DNA samples, we will obtain the sequences of the DNA fragments bound by ZIC2 and a list of genes corresponding to the DNA fragments. Thus, ChIP-seq data from these paired samples will help distinguish genes that are directly or indirectly regulated by ZIC2. After obtaining the lists of directly regulated genes, we will design PCR primers based on the promoter sequences of target genes and the position of the ChIP-seq peaks, and then perform ChIP-PCR to verify the ZIC2 DNA-binding sites in these genes. We will perform GSEA analysis using the list of genes directly regulated by ZIC2 and expect to enrich the gene sets belonging to hallmarks, biological processes, signaling pathways, and oncogenic signatures.

6.4.2 To probe the differentially expressed genes and gene sets regulated by ZIC2 *in vivo*

To explore differentially expressed genes and gene sets regulated by ZIC2 *in vivo*, we will extract RNA samples from tumors formed by the SKOV3 ZIC2-KO and OVCAR3 ZIC2-OE models. RNA samples will be prepared for RNA-seq as we previously described. Once we obtain the list of differentially expressed genes, we will conduct RT-qPCR and immunoblotting to confirm their expression at the mRNA and protein levels. Since tumor growth in mice involves the tumor microenvironment, it more closely resembles the tumorigenesis conditions in humans. We found that knockout of ZIC2 decreased the protein expression of ROR2 in monolayer cultured SKOV3 cells but increased the protein expression of ROR2 in SKOV3 tumors (**Figure 4.3 and 4.4**). We expect to obtain a list of differentially expressed genes regulated by ZIC2 and perform GSEA analysis to enrich the top gene sets regulated by ZIC2 *in vivo*. We will also compare the expression of differentially expressed genes *in vitro* and *in vivo* (i.e., the genes commonly regulated by ZIC2, the genes oppositely regulated by ZIC2, genes downregulated by ZIC2, and genes upregulated by ZIC2, *in vivo* and *in vitro*).

6.4.3 To identify the interactomes regulated by ZIC2

To identify the interactomes regulated by ZIC2 in SKOV3 and OVCAR3 cells, cell lysates from paired samples of SKOV3 WT and SKOV3 ZIC2-KO cells and paired samples of OVCAR3 vector and OVCAR3 ZIC2-OE cells will be immunoprecipitated with IP (immunoprecipitation)-grade anti-ZIC2 antibody.

Studies showed that ZIC2 interacts with chromosome remodeling complexes in mouse ESCs and human liver CSCs and regulates gene expression by binding to gene promoters and enhancers (169,171,172). Herein, we hypothesize that ZIC2 acts as a transcription factor and a co-activator of transcriptional regulation in EOC. The ZIC2 protein and ZIC2-interacting partners in the cell lysate from SKOV3 WT and the OVCAR3 ZIC2-OE cells will be pulled down by anti-ZIC2 antibody. Any proteins pulled down by anti-ZIC2 antibody in cell lysate from SKOV3 ZIC2-KO and OVCAR3 vector cells are considered non-specific proteins. All these proteins will be analyzed by mass spectrometry to identify ZIC2-interacting proteins. We expect to obtain a list of proteins that directly interact with ZIC2 and further explore the role of proteins of interest in tumor progression. This study will help us understand the interactome of ZIC2 in SKOV3 and OVCAR3 cells and correlate it with the pathobiological functions we found.

6.4.4 To evaluate the role of ZIC2 in tumor metastasis

To assess whether ZIC2 plays a role in tumor metastasis, we will perform transwell assay and intraperitoneal injections in NSG mice to detect the ability of cancer cells to form metastatic tumors in the mouse peritoneal cavity using paired samples of SKOV3 WT and ZIC2-KO cells as well as paired samples of OVCAR3 vector and ZIC2-OE cells. GSEA analyses suggest that ZIC2 may be involved in tumor metastasis in EOC. Herein, we hypothesize that ZIC2 promotes tumor metastasis in EOC. The subcutaneous xenograft models of SKOV3 and OVCAR3 was convenient to assess tumor growth but did not evaluate the effect of ZIC2 on

tumor metastasis in EOC. Based on the characteristics of tumor metastasis in EOC that the metastasis mainly involves the exfoliation of tumor cells from the ovary surface into the abdominal cavity, and few EOC cells metastasize to the liver and lungs through the blood circulatory system, we will perform intraperitoneal injections to explore the role of ZIC2 in tumor metastasis in EOC. To visualize tumor growth, we will perform intraperitoneal injections using cells overexpressed luciferase and a fluorescent protein tdTomato. Following injections, tumor growth in mice injected with these samples will be regularly observed and compared using bioluminescence imaging. We expect that SKOV3 ZIC2-KO cells have fewer metastases in the abdominal cavity compared to SKOV3 WT cells and that OVCAR3 ZIC2-OE cells have more metastases in the abdominal cavity compared to OVCAR3 vector cells.

6.4.5 To examine the regulation of ZIC2 expression in EOC

To understand how *ZIC2* is regulated in EOC, we will investigate DNA amplification and DNA methylation**.** In terms of DNA amplification, we will use the TCGA-Ovarian Cancer dataset from the NIH Broad Institute to query the copy number variation of *ZIC2* in tumors of EOC patients. Copy number variation reflects the rearrangement of genome fragments larger than 1 kb in the genome. DNA amplification is defined as an increase in the expression of the specific gene involved when the copy number of a genome fragment increases. We hypothesize that upregulation of *ZIC2* expression in EOC is due to DNA amplification of the *ZIC2* gene. We expect to correlate the DNA amplification of *ZIC2* with *ZIC2*

expression in samples from the TGCA-Ovarian Cancer dataset. Next, we hypothesize that the inhibition of ZIC2 expression in EOC is due to DNA methylation of the *ZIC2* promoter. For *ZIC2* promoter methylation, we will use bisulfite sequencing PCR (BSP) to detect methylation of the *ZIC2* promoter in SKOV3 and OVCAR3 cells. We expect that the *ZIC2* promoter is methylated in OVCAR3 cells, but not in SKOV3 cells. This study will help us understand how *ZIC2* expression is regulated in different EOC cell lines.

6.4.6 To study the role of KRAS signaling in the tumorigenic functions of ZIC2

The PI3K/AKT and RAS/RAF/MEK/ERK pathways are downstream pathways activated by oncogenic *KRAS* in human cancers (645). PI3K (p110), AKT, and mTOR in the PI3K/AKT pathway, and RAF, MEK, and ERK in the RAS/RAF/MEK/ERK pathway are important kinases. To determine the role of KRAS signaling in the tumorigenic functions of ZIC2, we will use small molecule inhibitors of key proteins in the PI3K/AKT and RAS/RAF/MEK/ERK pathways (i.e., inhibitors of PI3K, AKT, mTOR, ARAF, BRAF, RAF1, MEK1, MEK2, ERK1, and ERK2) or specific siRNA or shRNA to inhibit their functions in these pathways in the ZIC2-KO and ZIC2-OE models. These signaling pathways play an important role in promoting proliferation, cell survival, and metastasis in human cancers (646-651). In GSEA analyses of the SKOV3 and OVCAR3 models, we found KRAS signaling as a potential pathway regulated by ZIC2 in SKOV3 and OVCAR3 cells. We hypothesize that KRAS signaling mediates the tumorigenic functions of ZIC2

in EOC. We expect that the use of kinase inhibitors in these pathways might attenuate phosphorylation of specific downstream protein factors and inhibit ZIC2-promoted tumorigenic phenotypes. The proposed study will help explore the role of KRAS signaling in mediating the tumorigenic functions of ZIC2 in EOC.

6.4.7 To explore the strategies of therapeutically targeting ZIC2 and RUNX3

To explore strategies to target *ZIC2* and *RUNX3*, we will design a variety of siRNAs and antisense oligonucleotides (ASOs) to target *ZIC2* and *RUNX3*, respectively, and test their effectiveness. Our data show that knockout of ZIC2 inhibits the tumorigenic phenotypes in SKOV3 and OVCAR8 cells and that overexpression of *RUNX3* promotes the tumorigenic phenotypes in KGN cells (**Figure 3.18 and 5.3**). Since studies targeting transcription factors are still in their initial stages and the PROTAC technologies for protein degradation rely on finding the degradation pathway for ZIC2, we will identify ubiquitination-related proteins in the list of ZIC2-interacting proteins (e.g., E3 ubiquitin ligases) in the mass-spectrometry proposed previously (**6.4.3**). Similarly, we will identify ubiquitination-related proteins in the list of RUNX3-interacting proteins in GCT cells. We expect to identify potent siRNAs and ASOs, as well as ubiquitination-associated proteins that interact with ZIC2 and RUNX3, respectively. This study will help explore strategies for therapeutically targeting ZIC2 in EOC and RUNX3 in GCT.

References

1. Lengyel E. Ovarian cancer development and metastasis. The American journal of pathology **2010**;177:1053-64
2. Toss A, Tomasello C, Razzaboni E, Contu G, Grandi G, Cagnacci A*, et al.* Hereditary ovarian cancer: not only BRCA 1 and 2 genes. BioMed research international **2015**;2015
3. Kurman RJ, Shih I-M. Pathogenesis of ovarian cancer. Lessons from morphology and molecular biology and their clinical implications. International journal of gynecological pathology: official journal of the International Society of Gynecological Pathologists **2008**;27:151
4. Kurman R. Origin and molecular pathogenesis of ovarian high-grade serous carcinoma. Annals of Oncology **2013**;24:x16-x21
5. Pecorelli S, Benedet J, Creasman W, Shepherd J, Oncology FCoG. FIGO staging of gynecologic cancer. International Journal of Gynecology & Obstetrics **1999**;65:243-9
6. Cormio G, Rossi C, Cazzolla A, Resta L, Loverro G, Greco P*, et al.* Distant metastases in ovarian carcinoma. International Journal of Gynecologic Cancer **2003**;13
7. King M-C, Marks JH, Mandell JB. Breast and ovarian cancer risks due to inherited mutations in BRCA1 and BRCA2. Science **2003**;302:643-6
8. Booth M, Beral V, Smith P. Risk factors for ovarian cancer: a case-control study. British journal of cancer **1989**;60:592-8
9. Salehi F, Dunfield L, Phillips KP, Krewski D, Vanderhyden BC. Risk factors for ovarian cancer: an overview with emphasis on hormonal factors. Journal of Toxicology and Environmental Health, Part B **2008**;11:301-21
10. Cramer DW, Hutchison GB, Welch WR, Scully RE, Ryan KJ. Determinants of ovarian cancer risk. I. Reproductive experiences and family History23. JNCI, Journal of the National Cancer Institute **1983**;71:711
11. Cramer DW, Welch WR. Determinants of ovarian cancer risk. II. Inferences regarding pathogenesis. Journal of the National Cancer Institute **1983**;71:717-21
12. Risch HA, Marrett LD, Howe GR. Parity, contraception, infertility, and the risk of epithelial ovarian cancer. American journal of epidemiology **1994**;140:585-97
13. Narod SA, Risch H, Moslehi R, Dørum A, Neuhausen S, Olsson H*, et al.* Oral contraceptives and the risk of hereditary ovarian cancer. New England Journal of Medicine **1998**;339:424-8
14. Goodman MT, Howe HL, Tung KH, Hotes J, Miller BA, Coughlin SS*, et al.* Incidence of ovarian cancer by race and ethnicity in the United States, 1992–1997. Cancer: Interdisciplinary International Journal of the American Cancer Society **2003**;97:2676-85
15. Bandera EV, Lee VS, Rodriguez-Rodriguez L, Powell CB, Kushi LH. Racial/ethnic disparities in ovarian cancer treatment and survival. Clinical Cancer Research **2016**;22:5909-14

16. Reid BM, Permuth JB, Sellers TA. Epidemiology of ovarian cancer: a review. Cancer biology & medicine **2017**;14:9
17. Gronwald J, Byrski T, Huzarski T, Cybulski C, Sun P, Tulman A*, et al.* Influence of selected lifestyle factors on breast and ovarian cancer risk in BRCA1 mutation carriers from Poland. Breast cancer research and treatment **2006**;95:105-9
18. Beesley VL, Price MA, Webb PM. Loss of lifestyle: health behaviour and weight changes after becoming a caregiver of a family member diagnosed with ovarian cancer. Supportive Care in Cancer **2011**;19:1949-56
19. Hedelin M, Löf M, Andersson TM-L, Adlercreutz H, Weiderpass E. Dietary phytoestrogens and the risk of ovarian cancer in the women's lifestyle and health cohort study. Cancer Epidemiology and Prevention Biomarkers **2011**;20:308-17
20. Song H, Cicek MS, Dicks E, Harrington P, Ramus SJ, Cunningham JM*, et al.* The contribution of deleterious germline mutations in BRCA1, BRCA2 and the mismatch repair genes to ovarian cancer in the population. Human molecular genetics **2014**;23:4703-9
21. Gayther SA, Russell P, Harrington P, Antoniou AC, Easton DF, Ponder BA. The contribution of Germline BRCA1 and BRCA2 mutations to familial ovarian cancer: no evidence for other ovarian cancer–susceptibility genes. The American Journal of Human Genetics **1999**;65:1021-9
22. Ramus SJ, Harrington PA, Pye C, DiCioccio RA, Cox MJ, Garlinghouse-Jones K*, et al.* Contribution of BRCA1 and BRCA2 mutations to inherited ovarian cancer. Human mutation **2007**;28:1207-15
23. Chan J, Urban R, Cheung M, Osann K, Husain A, Teng N*, et al.* Ovarian cancer in younger vs older women: a population-based analysis. British journal of cancer **2006**;95:1314-20
24. Arora N, Talhouk A, McAlpine JN, Law MR, Hanley GE. Long-term mortality among women with epithelial ovarian cancer: a population-based study in British Columbia, Canada. BMC cancer **2018**;18:1-9
25. Zheng G, Yu H, Kanerva A, Försti A, Sundquist K, Hemminki K. Familial risks of ovarian cancer by age at diagnosis, proband type and histology. PloS one **2018**;13:e0205000
26. Alsop K, Fereday S, Meldrum C, DeFazio A, Emmanuel C, George J*, et al.* BRCA mutation frequency and patterns of treatment response in BRCA mutation–positive women with ovarian cancer: a report from the Australian Ovarian Cancer Study Group. Journal of Clinical Oncology **2012**;30:2654
27. Fuh KC, Shin JY, Kapp DS, Brooks RA, Ueda S, Urban RR*, et al.* Survival differences of Asian and Caucasian epithelial ovarian cancer patients in the United States. Gynecologic oncology **2015**;136:491-7
28. Lee AW, Navajas EE, Liu L. Clear differences in ovarian cancer incidence and trends by ethnicity among Asian Americans. Cancer epidemiology **2019**;61:142-9
29. Chan JK, Teoh D, Hu JM, Shin JY, Osann K, Kapp DS. Do clear cell ovarian carcinomas have poorer prognosis compared to other epithelial cell types?

A study of 1411 clear cell ovarian cancers. Gynecologic oncology **2008**;109:370-6
30. Coburn S, Bray F, Sherman ME, Trabert B. International patterns and trends in ovarian cancer incidence, overall and by histologic subtype. International journal of cancer **2017**;140:2451-60
31. Mørch LS, Løkkegaard E, Andreasen AH, Krüger-Kjær S, Lidegaard Ø. Hormone therapy and ovarian cancer. Jama **2009**;302:298-305
32. Zhou B, Sun Q, Cong R, Gu H, Tang N, Yang L*, et al.* Hormone replacement therapy and ovarian cancer risk: a meta-analysis. Gynecologic oncology **2008**;108:641-51
33. Lacey Jr JV, Mink PJ, Lubin JH, Sherman ME, Troisi R, Hartge P*, et al.* Menopausal hormone replacement therapy and risk of ovarian cancer. Jama **2002**;288:334-41
34. Faber MT, Kjær SK, Dehlendorff C, Chang-Claude J, Andersen KK, Høgdall E*, et al.* Cigarette smoking and risk of ovarian cancer: a pooled analysis of 21 case–control studies. Cancer Causes & Control **2013**;24:989-1004
35. Terry P, Miller A, Jones J, Rohan T. Cigarette smoking and the risk of invasive epithelial ovarian cancer in a prospective cohort study. European journal of cancer **2003**;39:1157-64
36. Kushi LH, Mink PJ, Folsom AR, Anderson KE, Zheng W, Lazovich D*, et al.* Prospective study of diet and ovarian cancer. American journal of epidemiology **1999**;149:21-31
37. Pan SY, Ugnat A-M, Mao Y, Wen SW, Johnson KC, Group CCRER. A case-control study of diet and the risk of ovarian cancer. Cancer Epidemiology and Prevention Biomarkers **2004**;13:1521-7
38. Fairfield KM, Willett WC, Rosner BA, Manson JE, Speizer FE, Hankinson SE. Obesity, weight gain, and ovarian cancer. Obstetrics & Gynecology **2002**;100:288-96
39. Olsen CM, Green AC, Whiteman DC, Sadeghi S, Kolahdooz F, Webb PM. Obesity and the risk of epithelial ovarian cancer: a systematic review and meta-analysis. European journal of cancer **2007**;43:690-709
40. Kurman RJ, Shih I-M. The Origin and pathogenesis of epithelial ovarian cancer-a proposed unifying theory. The American journal of surgical pathology **2010**;34:433
41. Malpica A, Deavers MT, Lu K, Bodurka DC, Atkinson EN, Gershenson DM*, et al.* Grading ovarian serous carcinoma using a two-tier system. The American journal of surgical pathology **2004**;28:496-504
42. Gilks CB. Subclassification of ovarian surface epithelial tumors based on correlation of histologic and molecular pathologic data. International journal of gynecological pathology **2004**;23:200-5
43. Bowtell DD, Böhm S, Ahmed AA, Aspuria P-J, Bast RC, Beral V*, et al.* Rethinking ovarian cancer II: reducing mortality from high-grade serous ovarian cancer. Nature reviews Cancer **2015**;15:668-79
44. Li J, Abushahin N, Pang S, Xiang L, Chambers SK, Fadare O*, et al.* Tubal origin of 'ovarian'low-grade serous carcinoma. Modern Pathology **2011**;24:1488-99

45. Kim J, Coffey DM, Creighton CJ, Yu Z, Hawkins SM, Matzuk MM. High-grade serous ovarian cancer arises from fallopian tube in a mouse model. Proceedings of the National Academy of Sciences **2012**;109:3921-6
46. Reade CJ, McVey RM, Tone AA, Finlayson SJ, McAlpine JN, Fung-Kee-Fung M*, et al.* The fallopian tube as the origin of high grade serous ovarian cancer: review of a paradigm shift. Journal of obstetrics and gynaecology Canada **2014**;36:133-40
47. Kessler M, Fotopoulou C, Meyer T. The molecular fingerprint of high grade serous ovarian cancer reflects its fallopian tube origin. International journal of molecular sciences **2013**;14:6571-96
48. Wang Y, Mang M, Wang Y, Wang L, Klein R, Kong B*, et al.* Tubal origin of ovarian endometriosis and clear cell and endometrioid carcinoma. American journal of cancer research **2015**;5:869
49. Cochrane DR, Tessier-Cloutier B, Lawrence KM, Nazeran T, Karnezis AN, Salamanca C*, et al.* Clear cell and endometrioid carcinomas: are their differences attributable to distinct cells of origin? The Journal of pathology **2017**;243:26-36
50. Cheasley D, Wakefield MJ, Ryland GL, Allan PE, Alsop K, Amarasinghe KC*, et al.* The molecular origin and taxonomy of mucinous ovarian carcinoma. Nature communications **2019**;10:1-11
51. Prat J. New insights into ovarian cancer pathology. Annals of oncology **2012**;23:x111-x7
52. Lisio M-A, Fu L, Goyeneche A, Gao Z-h, Telleria C. High-grade serous ovarian cancer: basic sciences, clinical and therapeutic standpoints. International journal of molecular sciences **2019**;20:952
53. Kaku T, Ogawa S, Kawano Y, Ohishi Y, Kobayashi H, Hirakawa T*, et al.* Histological classification of ovarian cancer. Medical electron microscopy **2003**;36:9-17
54. Cho KR, Shih I-M. Ovarian cancer. Annual review of pathology: mechanisms of disease **2009**;4:287-313
55. Banerjee S, Kaye SB. New strategies in the treatment of ovarian cancer: current clinical perspectives and future potential. Clinical cancer research **2013**;19:961-8
56. Kurman RJ, Shih I-M. Molecular pathogenesis and extraovarian origin of epithelial ovarian cancer—shifting the paradigm. Human pathology **2011**;42:918-31
57. Sung H, Ferlay J, Siegel RL, Laversanne M, Soerjomataram I, Jemal A*, et al.* Global cancer statistics 2020: GLOBOCAN estimates of incidence and mortality worldwide for 36 cancers in 185 countries. CA: a cancer journal for clinicians **2021**;71:209-49
58. Doubeni CA, Doubeni AR, Myers AE. Diagnosis and management of ovarian cancer. American family physician **2016**;93:937-44
59. Rost AD, Wilson K, Buchanan E, Hildebrandt MJ, Mutch D. Improving psychological adjustment among late-stage ovarian cancer patients: examining the role of avoidance in treatment. Cognitive and Behavioral Practice **2012**;19:508-17

60. Colombo N, Van Gorp T, Parma G, Amant F, Gatta G, Sessa C*, et al.* Ovarian cancer. Critical reviews in oncology/hematology **2006**;60:159-79
61. Gockley A, Melamed A, Bregar AJ, Clemmer JT, Birrer M, Schorge JO*, et al.* Outcomes of women with high-grade and low-grade advanced-stage serous epithelial ovarian cancer. Obstetrics and gynecology **2017**;129:439
62. Tingulstad S, Skjeldestad FE, Halvorsen TB, jørn Hagen B. Survival and prognostic factors in patients with ovarian cancer. Obstetrics & Gynecology **2003**;101:885-91
63. Storey DJ, Rush R, Stewart M, Rye T, Al-Nafussi A, Williams AR*, et al.* Endometrioid epithelial ovarian cancer: 20 years of prospectively collected data from a single center. Cancer **2008**;112:2211-20
64. Shu CA, Zhou Q, Jotwani AR, Iasonos A, Leitao Jr MM, Konner JA*, et al.* Ovarian clear cell carcinoma, outcomes by stage: the MSK experience. Gynecologic oncology **2015**;139:236-41
65. van Nagell Jr J, DePriest P, Reedy M, Gallion H, Ueland F, Pavlik E*, et al.* The efficacy of transvaginal sonographic screening in asymptomatic women at risk for ovarian cancer. Gynecologic oncology **2000**;77:350-6
66. Adonakis GL, Paraskevaidis E, Tsiga S, Seferiadis K, Lolis DE. A combined approach for the early detection of ovarian cancer in asymptomatic women. European Journal of Obstetrics & Gynecology and Reproductive Biology **1996**;65:221-5
67. Reade CJ, Riva JJ, Busse JW, Goldsmith CH, Elit L. Risks and benefits of screening asymptomatic women for ovarian cancer: a systematic review and meta-analysis. Gynecologic oncology **2013**;130:674-81
68. Kipps E, Tan DS, Kaye SB. Meeting the challenge of ascites in ovarian cancer: new avenues for therapy and research. Nature Reviews Cancer **2013**;13:273-82
69. Olson SH, Mignone L, Nakraseive C, Caputo T, Barakat R, Harlap S. Symptoms of ovarian cancer. Obstetrics & Gynecology **2001**;98:212-7
70. Bankhead CR, Kehoe ST, Austoker J. Symptoms associated with diagnosis of ovarian cancer: a systematic review. BJOG: An International Journal of Obstetrics & Gynaecology **2005**;112:857-65
71. Goff BA, Mandel LS, Melancon CH, Muntz HG. Frequency of symptoms of ovarian cancer in women presenting to primary care clinics. Jama **2004**;291:2705-12
72. Friedman GD, Skilling JS, Udaltsova NV, Smith LH. Early symptoms of ovarian cancer: a case–control study without recall bias. Family practice **2005**;22:548-53
73. Visintin I, Feng Z, Longton G, Ward DC, Alvero AB, Lai Y*, et al.* Diagnostic markers for early detection of ovarian cancer. Clinical cancer research **2008**;14:1065-72
74. Jacobs IJ, Menon U. Progress and challenges in screening for early detection of ovarian cancer. Molecular & Cellular Proteomics **2004**;3:355-66
75. Scholler N, Urban N. CA125 in ovarian cancer. **2007**

76. Havrilesky LJ, Whitehead CM, Rubatt JM, Cheek RL, Groelke J, He Q*, et al.* Evaluation of biomarker panels for early stage ovarian cancer detection and monitoring for disease recurrence. Gynecologic oncology **2008**;110:374-82
77. van Nagell Jr JR, Higgins RV, Donaldson ES, Gallion HH, Powell DE, Pavlik EJ*, et al.* Transvaginal sonography as a screening method for ovarian cancer a report of the first 1000 cases screened. Cancer **1990**;65:573-7
78. Van Nagell JR, Gallion HH, Pavlik EJ, Depriest PD. Ovarian cancer screening. Cancer **1995**;76:2086-91
79. Elias KM, Guo J, Bast RC. Early detection of ovarian cancer. Hematology/Oncology Clinics **2018**;32:903-14
80. Slomski A. Screening women for ovarian cancer still does more harm than good. Jama **2012**;307:2474-5
81. George SH, Garcia R, Slomovitz BM. Ovarian cancer: the fallopian tube as the site of origin and opportunities for prevention. Frontiers in oncology **2016**;6:108
82. Walker M, Jacobson M, Sobel M. Management of ovarian cancer risk in women with BRCA1/2 pathogenic variants. CMAJ **2019**;191:E886-E93
83. Griffiths CT, Parker LM, Fuller A. Role of cytoreductive surgical treatment in the management of advanced ovarian cancer. Cancer Treat Rep **1979**;63:235-40
84. Eisenkop SM, Friedman RL, Spirtos NM. The role of secondary cytoreductive surgery in the treatment of patients with recurrent epithelial ovarian carcinoma. Cancer **2000**;88:144-53
85. Bristow RE, Puri I, Chi DS. Cytoreductive surgery for recurrent ovarian cancer: a meta-analysis. Gynecologic oncology **2009**;112:265-74
86. Spiliotis J, Halkia E, Lianos E, Kalantzi N, Grivas A, Efstathiou E*, et al.* Cytoreductive surgery and HIPEC in recurrent epithelial ovarian cancer: a prospective randomized phase III study. Annals of surgical oncology **2015**;22:1570-5
87. Hoskins WJ. Surgical staging and cytoreductive surgery of epithelial ovarian cancer. Cancer **1993**;71:1534-40
88. Ghezzi F, Cromi A, Uccella S, Bergamini V, Tomera S, Franchi M*, et al.* Laparoscopy versus laparotomy for the surgical management of apparent early stage ovarian cancer. Gynecologic oncology **2007**;105:409-13
89. Bae JH, Lee JM, Ryu KS, Lee YS, Park YG, Hur SY*, et al.* Treatment of ovarian cancer with paclitaxel-or carboplatin-based intraperitoneal hyperthermic chemotherapy during secondary surgery. Gynecologic oncology **2007**;106:193-200
90. da Costa Miranda V, de Souza Fêde ÂB, Dos Anjos CH, da Silva JR, Sanchez FB, da Silva Bessa LR*, et al.* Neoadjuvant chemotherapy with six cycles of carboplatin and paclitaxel in advanced ovarian cancer patients unsuitable for primary surgery: safety and effectiveness. Gynecologic oncology **2014**;132:287-91
91. Eisenkop SM, Friedman RL, Wang HJ. Secondary cytoreductive surgery for recurrent ovarian cancer. A prospective study. Cancer **1995**;76:1606-14

92. Güngör M, Ortaç F, Arvas M, Kösebay D, Sönmezer M, Köse K. The role of secondary cytoreductive surgery for recurrent ovarian cancer. Gynecologic oncology **2005**;97:74-9
93. Donovan KA, Greene PG, Shuster Jr JL, Partridge EE, Tucker DC. Treatment preferences in recurrent ovarian cancer. Gynecologic oncology **2002**;86:200-11
94. Mangili G, Aletti G, Frigerio L, Franchi M, Panacci N, Vigano R*, et al.* Palliative care for intestinal obstruction in recurrent ovarian cancer: a multivariate analysis. International Journal of Gynecologic Cancer **2005**;15
95. Gotlieb WH, Feldman B, Feldman-Moran O, Zmira N, Kreizer D, Segal Y*, et al.* Intraperitoneal pressures and clinical parameters of total paracentesis for palliation of symptomatic ascites in ovarian cancer. Gynecologic oncology **1998**;71:381-5
96. Lim MC, Lee H-S, Jung DC, Choi JY, Seo S-S, Park S-Y. Pathological diagnosis and cytoreduction of cardiophrenic lymph node and pleural metastasis in ovarian cancer patients using video-assisted thoracic surgery. Annals of surgical oncology **2009**;16:1990-6
97. Harter P, Du Bois A, Hahmann M, Hasenburg A, Burges A, Loibl S*, et al.* Surgery in recurrent ovarian cancer: the Arbeitsgemeinschaft Gynaekologische Onkologie (AGO) DESKTOP OVAR trial. Annals of surgical oncology **2006**;13:1702-10
98. Jayson GC, Kohn EC, Kitchener HC, Ledermann JA. Ovarian cancer. The Lancet **2014**;384:1376-88
99. Kim S, Han Y, Kim SI, Kim H-S, Kim SJ, Song YS. Tumor evolution and chemoresistance in ovarian cancer. NPJ precision oncology **2018**;2:1-9
100. Steg AD, Bevis KS, Katre AA, Ziebarth A, Dobbin ZC, Alvarez RD*, et al.* Stem cell pathways contribute to clinical chemoresistance in ovarian cancer. Clinical cancer research **2012**;18:869-81
101. Rizzuto I, Stavraka C, Chatterjee J, Borley J, Hopkins TG, Gabra H*, et al.* Risk of ovarian cancer relapse score: a prognostic algorithm to predict relapse following treatment for advanced ovarian cancer. International Journal of Gynecologic Cancer **2015**;25
102. Pfisterer J, Ledermann JA. Management of platinum-sensitive recurrent ovarian cancer. 2006. Elsevier. p 12-6.
103. Soyama H, Takano M, Miyamoto M, Yoshikawa T, Aoyama T, Goto T*, et al.* Factors favouring long-term survival following recurrence in ovarian cancer. Molecular and clinical oncology **2017**;7:42-6
104. Ozols R. Challenges for chemotherapy in ovarian cancer. Annals of Oncology **2006**;17:v181-v7
105. Azaïs H, Estevez JP, Foucher P, Kerbage Y, Mordon S, Collinet P. Dealing with microscopic peritoneal metastases of epithelial ovarian cancer. A surgical challenge. Surgical oncology **2017**;26:46-52
106. Moore K, Colombo N, Scambia G, Kim B-G, Oaknin A, Friedlander M*, et al.* Maintenance olaparib in patients with newly diagnosed advanced ovarian cancer. New England Journal of Medicine **2018**;379:2495-505

107. Audeh MW, Carmichael J, Penson RT, Friedlander M, Powell B, Bell-McGuinn KM*, et al.* Oral poly (ADP-ribose) polymerase inhibitor olaparib in patients with BRCA1 or BRCA2 mutations and recurrent ovarian cancer: a proof-of-concept trial. The lancet **2010**;376:245-51
108. Pujade-Lauraine E, Ledermann JA, Selle F, Gebski V, Penson RT, Oza AM*, et al.* Olaparib tablets as maintenance therapy in patients with platinum-sensitive, relapsed ovarian cancer and a BRCA1/2 mutation (SOLO2/ENGOT-Ov21): a double-blind, randomised, placebo-controlled, phase 3 trial. The lancet oncology **2017**;18:1274-84
109. Ledermann J, Harter P, Gourley C, Friedlander M, Vergote I, Rustin G*, et al.* Olaparib maintenance therapy in patients with platinum-sensitive relapsed serous ovarian cancer: a preplanned retrospective analysis of outcomes by BRCA status in a randomised phase 2 trial. The lancet oncology **2014**;15:852-61
110. Mirza MR, Monk BJ, Herrstedt J, Oza AM, Mahner S, Redondo A*, et al.* Niraparib maintenance therapy in platinum-sensitive, recurrent ovarian cancer. New England Journal of Medicine **2016**;375:2154-64
111. González-Martín A, Pothuri B, Vergote I, DePont Christensen R, Graybill W, Mirza MR*, et al.* Niraparib in patients with newly diagnosed advanced ovarian cancer. New England Journal of Medicine **2019**;381:2391-402
112. Zamarin D, Burger RA, Sill MW, Powell Jr DJ, Lankes HA, Feldman MD*, et al.* Randomized phase II trial of nivolumab versus nivolumab and ipilimumab for recurrent or persistent ovarian cancer: an NRG oncology study. Journal of Clinical Oncology **2020**;38:1814
113. Outwater EK, Wagner BJ, Mannion C, McLarney JK, Kim B. Sex cord-stromal and steroid cell tumors of the ovary. Radiographics **1998**;18:1523-46
114. Schumer ST, Cannistra SA. Granulosa cell tumor of the ovary. Journal of clinical oncology **2003**;21:1180-9
115. Inada Y, Nakai G, Yamamoto K, Yamada T, Hirose Y, Terai Y*, et al.* Rapidly growing juvenile granulosa cell tumor of the ovary arising in adult: a case report and review of the literature. Journal of ovarian research **2018**;11:1-5
116. Kottarathil VD, Antony MA, Nair IR, Pavithran K. Recent advances in granulosa cell tumor ovary: a review. Indian journal of surgical oncology **2013**;4:37-47
117. Li J, Bao R, Peng S, Zhang C. The molecular mechanism of ovarian granulosa cell tumors. Journal of ovarian research **2018**;11:1-8
118. Fox H, Agrawal K, Langley F. A clinicopathologic study of 92 cases of granulosa cell tumor of the ovary with special reference to the factors influencing prognosis. Cancer **1975**;35:231-41
119. Pectasides D, Pectasides E, Psyrri A. Granulosa cell tumor of the ovary. Cancer treatment reviews **2008**;34:1-12
120. Fletcher J, Gibas Z, Donovan K, Perez-Atayde A, Genest D, Morton C*, et al.* Ovarian granulosa-stromal cell tumors are characterized by trisomy 12. The American journal of pathology **1991**;138:515

121. Schofield D, Fletcher J. Trisomy 12 in pediatric granulosa-stromal cell tumors. Demonstration by a modified method of fluorescence in situ hybridization on paraffin-embedded material. The American journal of pathology **1992**;141:1265
122. Jamieson S, Butzow R, Andersson N, Alexiadis M, Unkila-Kallio L, Heikinheimo M*, et al.* The FOXL2 C134W mutation is characteristic of adult granulosa cell tumors of the ovary. Modern pathology **2010**;23:1477-85
123. Miller BE, Barron BA, Wan JY, Delmore JE, Silva EG, Gershenson DM. Prognostic factors in adult granulosa cell tumor of the ovary. Cancer: Interdisciplinary International Journal of the American Cancer Society **1997**;79:1951-5
124. Shah SP, Köbel M, Senz J, Morin RD, Clarke BA, Wiegand KC*, et al.* Mutation of FOXL2 in granulosa-cell tumors of the ovary. New England Journal of Medicine **2009**;360:2719-29
125. Sehouli J, Drescher FS, Mustea A, Elling D, Friedmann W, Kühn W*, et al.* Granulosa cell tumor of the ovary: 10 years follow-up data of 65 patients. Anticancer research **2004**;24:1223-30
126. Björkholm E, Silfverswärd C. Prognostic factors in granulosa-cell tumors. Gynecologic oncology **1981**;11:261-74
127. Hines JF, Khalifa MA, Moore JL, Fine KP, Lage JM, Barnes WA. Recurrent granulosa cell tumor of the ovary 37 years after initial diagnosis: a case report and review of the literature. Gynecologic oncology **1996**;60:484-8
128. Park J-Y, Jin KL, Kim D-Y, Kim J-H, Kim Y-M, Kim K-R*, et al.* Surgical staging and adjuvant chemotherapy in the management of patients with adult granulosa cell tumors of the ovary. Gynecologic Oncology **2012**;125:80-6
129. Sun H-D, Lin H, Jao M-S, Wang K-L, Liou W-S, Hung Y-C*, et al.* A long-term follow-up study of 176 cases with adult-type ovarian granulosa cell tumors. Gynecologic oncology **2012**;124:244-9
130. Mangili G, Ottolina J, Gadducci A, Giorda G, Breda E, Savarese A*, et al.* Long-term follow-up is crucial after treatment for granulosa cell tumours of the ovary. British journal of cancer **2013**;109:29-34
131. Malmström H, Högberg T, Risberg B, Simonsen E. Granulosa cell tumors of the ovary: prognostic factors and outcome. Gynecologic oncology **1994**;52:50-5
132. Fujimoto T, Sakuragi N, Okuyama K, Fujino T, Yamashita K, Yamashiro S*, et al.* Histopathological prognostic factors of adult granulosa cell tumors of the ovary. Acta obstetricia et gynecologica Scandinavica **2001**;80:1069-74
133. Sommers S, Gates O, Goodof I. Late recurrence of granulosa cell tumors: report of two cases. Obstetrics & Gynecology **1955**;6:395-8
134. Grinberg I, Millen K. The ZIC gene family in development and disease. Clinical genetics **2005**;67:290-6
135. Ishiguro A, Inoue T, Mikoshiba K, Aruga J. Molecular properties of Zic4 and Zic5 proteins: functional diversity within Zic family. Biochemical and biophysical research communications **2004**;324:302-7

136. Han W, Zhang C, Gao X-j, Wang H-b, Chen F, Cao F*, et al.* Clinicopathologic and prognostic significance of the zinc finger of the cerebellum family in invasive breast cancer. Journal of breast cancer **2018**;21:51
137. Ali RG, Bellchambers HM, Arkell RM. Zinc fingers of the cerebellum (Zic): transcription factors and co-factors. The international journal of biochemistry & cell biology **2012**;44:2065-8
138. Fujimi TJ, Mikoshiba K, Aruga J. Xenopus Zic4: conservation and diversification of expression profiles and protein function among the Xenopus Zic family. Developmental dynamics: an official publication of the American Association of Anatomists **2006**;235:3379-86
139. Hatayama M, Aruga J. Characterization of the tandem CWCH2 sequence motif: a hallmark of inter-zinc finger interactions. BMC evolutionary biology **2010**;10:1-18
140. Hatayama M, Aruga J. Role of Zic family proteins in transcriptional regulation and chromatin remodeling. Zic family **2018**:353-80
141. Mizugishi K, Hatayama M, Tohmonda T, Ogawa M, Inoue T, Mikoshiba K*, et al.* Myogenic repressor I-mfa interferes with the function of Zic family proteins. Biochemical and biophysical research communications **2004**;320:233-40
142. Himeda CL, Barro MV, Emerson Jr CP. Pax3 synergizes with Gli2 and Zic1 in transactivating the Myf5 epaxial somite enhancer. Developmental biology **2013**;383:7-14
143. Chervenak AP, Hakim IS, Barald KF. Spatiotemporal expression of zic genes during vertebrate inner ear development. Developmental Dynamics **2013**;242:897-908
144. Brown SA, Warburton D, Brown LY, Yu C-y, Roeder ER, Stengel-Rutkowski S*, et al.* Holoprosencephaly due to mutations in ZIC2, a homologue of Drosophila odd-paired. Nature genetics **1998**;20:180-3
145. Solomon BD, Lacbawan F, Mercier S, Clegg NJ, Delgado MR, Rosenbaum K*, et al.* Mutations in ZIC2 in human holoprosencephaly: description of a novel ZIC2 specific phenotype and comprehensive analysis of 157 individuals. Journal of medical genetics **2010**;47:513-24
146. Barratt KS, Arkell RM. ZIC2 in Holoprosencephaly. Zic family **2018**:269-99
147. Aruga J, Inoue T, Hoshino J, Mikoshiba K. Zic2 controls cerebellar development in cooperation with Zic1. Journal of Neuroscience **2002**;22:218-25
148. Nagai T, Aruga J, Minowa O, Sugimoto T, Ohno Y, Noda T*, et al.* Zic2 regulates the kinetics of neurulation. Proceedings of the National Academy of Sciences **2000**;97:1618-23
149. Elms P, Siggers P, Napper D, Greenfield A, Arkell R. Zic2 is required for neural crest formation and hindbrain patterning during mouse development. Developmental biology **2003**;264:391-406
150. Nagai T, Aruga J, Takada S, Günther T, Spörle R, Schughart K*, et al.* The expression of the MouseZic1, Zic2, andZic3Gene suggests an essential

role forZicGenes in body pattern formation. Developmental biology **1997**;182:299-313
151. Elms P, Scurry A, Davies J, Willoughby C, Hacker T, Bogani D*, et al.* Overlapping and distinct expression domains of Zic2 and Zic3 during mouse gastrulation. Gene Expression Patterns **2004**;4:505-11
152. Brown LY, Kottmann AH, Brown S. Immunolocalization of Zic2 expression in the developing mouse forebrain. Gene Expression Patterns **2003**;3:361-7
153. Herrera Es, Brown L, Aruga J, Rachel RA, Dolen G, Mikoshiba K*, et al.* Zic2 patterns binocular vision by specifying the uncrossed retinal projection. Cell **2003**;114:545-57
154. Pan H, Gustafsson MK, Aruga J, Tiedken JJ, Chen JC, Emerson Jr CP. A role for Zic1 and Zic2 in Myf5 regulation and somite myogenesis. Developmental biology **2011**;351:120-7
155. Orriss IR, Lanham S, Savery D, Greene ND, Stanier P, Oreffo R*, et al.* Spina bifida-predisposing heterozygous mutations in Planar Cell Polarity genes and Zic2 reduce bone mass in young mice. Scientific reports **2018**;8:1-14
156. Inoue T, Ota M, Mikoshiba K, Aruga J. Zic2 and Zic3 synergistically control neurulation and segmentation of paraxial mesoderm in mouse embryo. Developmental biology **2007**;306:669-84
157. Hatayama M, Ishiguro A, Iwayama Y, Takashima N, Sakoori K, Toyota T*, et al.* Zic2 hypomorphic mutant mice as a schizophrenia model and ZIC2 mutations identified in schizophrenia patients. Scientific reports **2011**;1:1-11
158. Ogura H, Aruga J, Mikoshiba K. Behavioral abnormalities of Zic1 and Zic2 mutant mice: implications as models for human neurological disorders. Behavior genetics **2001**;31:317-24
159. Maria BL, Zinreich J, Carson BC, Rosenbaum AE, Freeman JM. Dandy-Walker syndrome revisited. Pediatric Neurosurgery **1987**;13:45-51
160. Li Y-L, Wang J, Zhang C-Y, Shen Y-Q, Wang H-M, Ding L*, et al.* MiR-146a-5p inhibits cell proliferation and cell cycle progression in NSCLC cell lines by targeting CCND1 and CCND2. Oncotarget **2016**;7:59287
161. Lu S-X, Zhang CZ, Luo R-Z, Wang C-H, Liu L-L, Fu J*, et al.* Zic2 promotes tumor growth and metastasis via PAK4 in hepatocellular carcinoma. Cancer letters **2017**;402:71-80
162. Kong Q, Li W, Hu P, Zeng H, Pan Y, Zhou T*, et al.* The expression status of ZIC2 is an independent prognostic marker of hepatocellular carcinoma. Liver Research **2020**;4:40-6
163. Marchini S, Poynor E, Barakat RR, Clivio L, Cinquini M, Fruscio R*, et al.* The zinc finger gene ZIC2 has features of an oncogene and its overexpression correlates strongly with the clinical course of epithelial ovarian cancer. Clinical Cancer Research **2012**;18:4313-24
164. Jiang Z, Zhang Y, Chen X, Wu P, Chen D. Inactivation of the Wnt/β-catenin signaling pathway underlies inhibitory role of microRNA-129-5p in epithelial–mesenchymal transition and angiogenesis of prostate cancer by targeting ZIC2. Cancer cell international **2019**;19:1-15

165. Davis KC. Characterization of Zic2 as an Oncoprotein in Prostate Cancer. **2017**
166. Shen Z, Zhao K, Du T. Du T. HOXA10 promotes nasopharyngeal carcinoma cell proliferation and invasion via inducing the expression of ZIC2. Eur Rev Med Pharmacol Sci **2017**;21:945-52
167. Yi W, Wang J, Yao Z, Kong Q, Zhang N, Mo W*, et al.* The expression status of ZIC2 as a prognostic marker for nasopharyngeal carcinoma. International journal of clinical and experimental pathology **2018**;11:4446
168. Yu D, Han G-H, Zhao X, Liu X, Xue K, Wang D*, et al.* MicroRNA-129-5p suppresses nasopharyngeal carcinoma lymphangiogenesis and lymph node metastasis by targeting ZIC2. Cellular Oncology **2020**;43:249-61
169. Zhu P, Wang Y, He L, Huang G, Du Y, Zhang G*, et al.* ZIC2-dependent OCT4 activation drives self-renewal of human liver cancer stem cells. The Journal of clinical investigation **2015**;125:3795-808
170. Wang Y-F, Yang H-Y, Shi X-Q, Wang Y. Upregulation of microRNA-129-5p inhibits cell invasion, migration and tumor angiogenesis by inhibiting ZIC2 via downregulation of the Hedgehog signaling pathway in cervical cancer. Cancer biology & therapy **2018**;19:1162-73
171. Luo Z, Gao X, Lin C, Smith ER, Marshall SA, Swanson SK*, et al.* Zic2 is an enhancer-binding factor required for embryonic stem cell specification. Molecular cell **2015**;57:685-94
172. Ishiguro A, Ideta M, Mikoshiba K, Chen DJ, Aruga J. ZIC2-dependent transcriptional regulation is mediated by DNA-dependent protein kinase, poly (ADP-ribose) polymerase, and RNA helicase A. Journal of biological chemistry **2007**;282:9983-95
173. Collis SJ, DeWeese TL, Jeggo PA, Parker AR. The life and death of DNA-PK. Oncogene **2005**;24:949-61
174. Pellizzoni L, Charroux B, Rappsilber J, Mann M, Dreyfuss G. A functional interaction between the survival motor neuron complex and RNA polymerase II. The Journal of cell biology **2001**;152:75-86
175. Schlegel BP, Starita LM, Parvin JD. Overexpression of a protein fragment of RNA helicase A causes inhibition of endogenous BRCA1 function and defects in ploidy and cytokinesis in mammary epithelial cells. Oncogene **2003**;22:983-91
176. Tetsuka T, Uranishi H, Sanda T, Asamitsu K, Yang JP, Wong-Staal F*, et al.* RNA helicase A interacts with nuclear factor κB p65 and functions as a transcriptional coactivator. European journal of biochemistry **2004**;271:3741-51
177. Nussenzweig A, Chen C, da Costa Soares V, Sanchez M, Sokol K, Nussenzweig MC*, et al.* Requirement for Ku80 in growth and immunoglobulin V (D) J recombination. Nature **1996**;382:551-5
178. Henrie MS, Kurimasa A, Burma S, Ménissier-de Murcia J, De Murcia G, Li GC*, et al.* Lethality in PARP-1/Ku80 double mutant mice reveals physiological synergy during early embryogenesis. DNA repair **2003**;2:151-8

179. Lee C-G, da Costa Soares V, Newberger C, Manova K, Lacy E, Hurwitz J. RNA helicase A is essential for normal gastrulation. Proceedings of the National Academy of Sciences **1998**;95:13709-13
180. Aruga J, Tohmonda T, Homma S, Mikoshiba K. Zic1 promotes the expansion of dorsal neural progenitors in spinal cord by inhibiting neuronal differentiation. Developmental biology **2002**;244:329-41
181. Inoue T, Hatayama M, Tohmonda T, Itohara S, Aruga J, Mikoshiba K. Mouse Zic5 deficiency results in neural tube defects and hypoplasia of cephalic neural crest derivatives. Developmental biology **2004**;270:146-62
182. Pourebrahim R, Houtmeyers R, Ghogomu S, Janssens S, Thelie A, Tran HT*, et al.* Transcription factor Zic2 inhibits Wnt/β-catenin protein signaling. Journal of Biological Chemistry **2011**;286:37732-40
183. Houtmeyers R, Tchouate Gainkam O, Glanville-Jones HA, Van den Bosch B, Chappell A, Barratt KS*, et al.* Zic2 mutation causes holoprosencephaly via disruption of NODAL signalling. Human molecular genetics **2016**;25:3946-59
184. Houston DW, Wylie C. Maternal Xenopus Zic2 negatively regulates Nodal-related gene expression during anteroposterior patterning. Development **2005**;132:4845-55
185. Dykes IM, Szumska D, Kuncheria L, Puliyadi R, Chen C-m, Papanayotou C*, et al.* A requirement for Zic2 in the regulation of Nodal expression underlies the establishment of left-sided identity. Scientific reports **2018**;8:1-16
186. Chan DW, Liu VW, Leung LY, Yao KM, Chan KK, Cheung AN*, et al.* Zic2 synergistically enhances Hedgehog signalling through nuclear retention of Gli1 in cervical cancer cells. The Journal of pathology **2011**;225:525-34
187. Sanek NA, Taylor AA, Nyholm MK, Grinblat Y. Zebrafish zic2a patterns the forebrain through modulation of Hedgehog-activated gene expression. Development **2009**;136:3791-800
188. Mercier S, Odent S, Collignon J, Bhattacharya S. A REQUIREMENT FOR ZIC2 IN THE REGULATION OF NODAL EXPRESSION UNDERLIES THE ESTABLISHMENT OF LEFT-SIDED IDENTITY.
189. Lv B, Li F, Liu X, Lin L. The tumor-suppressive role of microRNA-873 in nasopharyngeal carcinoma correlates with downregulation of ZIC2 and inhibition of AKT signaling pathway. Cancer gene therapy **2021**;28:74-88
190. Geoffroy V, Corral D, Zhou L, Lee B, Karsenty G. Genomic organization, expression of the human CBFA1 gene, and evidence for an alternative splicing event affecting protein function. Mammalian genome **1998**;9:54-7
191. Xiao Z, Thomas R, Hinson T, Quarles L. Genomic structure and isoform expression of the mouse, rat and human Cbfa1/Osf2 transcription factor. Gene **1998**;214:187-97
192. Levanon D, Glusman G, Bangsow T, Ben-Asher E, Male DA, Avidan N*, et al.* Architecture and anatomy of the genomic locus encoding the human leukemia-associated transcription factor RUNX1/AML1. Gene **2001**;262:23-33

193. Bangsow C, Rubins N, Glusman G, Bernstein Y, Negreanu V, Goldenberg D*, et al.* The RUNX3 gene–sequence, structure and regulated expression. Gene **2001**;279:221-32
194. Mevel R, Draper JE, Lie-a-Ling M, Kouskoff V, Lacaud G. RUNX transcription factors: orchestrators of development. Development **2019**;146
195. Camilleri S, McDonald F. Runx2 and dental development. European journal of oral sciences **2006**;114:361-73
196. Hassan H, Sakaguchi S, Tenno M, Kopf A, Boucheron N, Carpenter AC*, et al.* Cd8 enhancer E8I and Runx factors regulate CD8α expression in activated CD8+ T cells. Proceedings of the National Academy of Sciences **2011**;108:18330-5
197. Kohu K, Sato T, Ohno S-i, Hayashi K, Uchino R, Abe N*, et al.* Overexpression of the Runx3 transcription factor increases the proportion of mature thymocytes of the CD8 single-positive lineage. The Journal of Immunology **2005**;174:2627-36
198. Inoue K-i, Ozaki S, Shiga T, Ito K, Masuda T, Okado N*, et al.* Runx3 controls the axonal projection of proprioceptive dorsal root ganglion neurons. Nature neuroscience **2002**;5:946-54
199. Levanon D, Bettoun D, Harris-Cerruti C, Woolf E, Negreanu V, Eilam R*, et al.* The Runx3 transcription factor regulates development and survival of TrkC dorsal root ganglia neurons. The EMBO journal **2002**;21:3454-63
200. Raveh E, Cohen S, Levanon D, Negreanu V, Groner Y, Gat U. Dynamic expression of Runx1 in skin affects hair structure. Mechanisms of development **2006**;123:842-50
201. Fainaru O, Woolf E, Lotem J, Yarmus M, Brenner O, Goldenberg D*, et al.* Runx3 regulates mouse TGF-β-mediated dendritic cell function and its absence results in airway inflammation. The EMBO journal **2004**;23:969-79
202. Fainaru O, Shseyov D, Hantisteanu S, Groner Y. Accelerated chemokine receptor 7-mediated dendritic cell migration in Runx3 knockout mice and the spontaneous development of asthma-like disease. Proceedings of the National Academy of Sciences **2005**;102:10598-603
203. Yoshida CA, Yamamoto H, Fujita T, Furuichi T, Ito K, Inoue K-i*, et al.* Runx2 and Runx3 are essential for chondrocyte maturation, and Runx2 regulates limb growth through induction of Indian hedgehog. Genes & development **2004**;18:952-63
204. de Bruijn M, Dzierzak E. Runx transcription factors in the development and function of the definitive hematopoietic system. Blood **2017**;129:2061-9
205. Collins A, Hewitt SL, Chaumeil J, Sellars M, Micsinai M, Allinne J*, et al.* RUNX transcription factor-mediated association of Cd4 and Cd8 enables coordinate gene regulation. Immunity **2011**;34:303-14
206. Steinke FC, Yu S, Zhou X, He B, Yang W, Zhou B*, et al.* TCF-1 and LEF-1 act upstream of Th-POK to promote the CD4+ T cell fate and interact with Runx3 to silence Cd4 in CD8+ T cells. Nature immunology **2014**;15:646-56
207. Kim W-J, Kim E-J, Jeong P, Quan C, Kim J, Li Q-L*, et al.* RUNX3 inactivation by point mutations and aberrant DNA methylation in bladder tumors. Cancer research **2005**;65:9347-54

208. Lee Y-S, Lee J-W, Jang J-W, Chi X-Z, Kim J-H, Li Y-H*, et al.* Runx3 inactivation is a crucial early event in the development of lung adenocarcinoma. Cancer cell **2013**;24:603-16
209. Wada M, Yazumi S, Takaishi S, Hasegawa K, Sawada M, Tanaka H*, et al.* Frequent loss of RUNX3 gene expression in human bile duct and pancreatic cancer cell lines. Oncogene **2004**;23:2401-7
210. Li Q-L, Ito K, Sakakura C, Fukamachi H, Inoue K-i, Chi X-Z*, et al.* Causal relationship between the loss of RUNX3 expression and gastric cancer. Cell **2002**;109:113-24
211. Ito K, Chuang LSH, Ito T, Chang TL, Fukamachi H, Salto–Tellez M*, et al.* Loss of Runx3 is a key event in inducing precancerous state of the stomach. Gastroenterology **2011**;140:1536-46. e8
212. Ito K, Liu Q, Salto-Tellez M, Yano T, Tada K, Ida H*, et al.* RUNX3, a novel tumor suppressor, is frequently inactivated in gastric cancer by protein mislocalization. Cancer research **2005**;65:7743-50
213. Dachrut S, Banthaisong S, Sripa M, Paeyao A, Ho C, Lee S*, et al.* DNA copy-number loss on 1p36. 1 harboring RUNX3 with promoter hypermethylation and associated loss of RUNX3 expression in liver fluke-associated intrahepatic cholangiocarcinoma. Asian Pac J Cancer Prev **2009**;10:575-82
214. Li J, Kleeff J, Guweidhi A, Esposito I, Berberat P, Giese T*, et al.* RUNX3 expression in primary and metastatic pancreatic cancer. Journal of clinical pathology **2004**;57:294-9
215. Nomoto S, Kinoshita T, Mori T, Kato K, Sugimoto H, Kanazumi N*, et al.* Adverse prognosis of epigenetic inactivation in RUNX3 gene at 1p36 in human pancreatic cancer. British journal of cancer **2008**;98:1690-5
216. Ku J-L, Kang S-B, Shin Y-K, Kang HC, Hong S-H, Kim I-J*, et al.* Promoter hypermethylation downregulates RUNX3 gene expression in colorectal cancer cell lines. Oncogene **2004**;23:6736-42
217. Wang Y, Qin X, Wu J, Qi B, Tao Y, Wang W*, et al.* Association of promoter methylation of RUNX3 gene with the development of esophageal cancer: a meta analysis. PLoS One **2014**;9:e107598
218. Lau QC, Raja E, Salto-Tellez M, Liu Q, Ito K, Inoue M*, et al.* RUNX3 is frequently inactivated by dual mechanisms of protein mislocalization and promoter hypermethylation in breast cancer. Cancer research **2006**;66:6512-20
219. Wolff EM, Liang G, Cortez CC, Tsai YC, Castelao JE, Cortessis VK*, et al.* RUNX3 methylation reveals that bladder tumors are older in patients with a history of smoking. Cancer research **2008**;68:6208-14
220. Park WS, Cho YG, Kim CJ, Song JH, Lee YS, Kim SY*, et al.* Hypermethylation of the RUNX3 gene in hepatocellular carcinoma. Experimental & molecular medicine **2005**;37:276-81
221. Subramaniam MM, Chan JY, Yeoh KG, Quek T, Ito K, Salto-Tellez M. Molecular pathology of RUNX3 in human carcinogenesis. Biochimica et Biophysica Acta (BBA)-Reviews on Cancer **2009**;1796:315-31

222. Nevadunsky NS, Barbieri JS, Kwong J, Merritt MA, Welch WR, Berkowitz RS*, et al.* RUNX3 protein is overexpressed in human epithelial ovarian cancer. Gynecologic oncology **2009**;112:325-30
223. Ogawa E, Inuzuka M, Maruyama M, Satake M, Naito-Fujimoto M, Ito Y*, et al.* Molecular cloning and characterization of PEBP2β, the heterodimeric partner of a novel Drosophila runt-related DNA binding protein PEBP2α. Virology **1993**;194:314-31
224. Salto-Tellez M, Peh BK, Ito K, Tan SH, Chong P, Han H*, et al.* RUNX3 protein is overexpressed in human basal cell carcinomas. Oncogene **2006**;25:7646-9
225. Lee CWL, Chuang LSH, Kimura S, Lai SK, Ong CW, Yan B*, et al.* RUNX3 functions as an oncogene in ovarian cancer. Gynecologic oncology **2011**;122:410-7
226. Barghout SH, Zepeda N, Vincent K, Azad AK, Xu Z, Yang C*, et al.* RUNX3 contributes to carboplatin resistance in epithelial ovarian cancer cells. Gynecologic oncology **2015**;138:647-55
227. Zhang S, Wei L, Zhang A, Zhang L, Yu H. RUNX3 gene methylation in epithelial ovarian cancer tissues and ovarian cancer cell lines. OMICS A Journal of Integrative Biology **2009**;13:307-11
228. Ojima F, Saito Y, Tsuchiya Y, Ogoshi M, Fukamachi H, Inagaki K*, et al.* Runx3 regulates folliculogenesis and steroidogenesis in granulosa cells of immature mice. Cell and tissue research **2019**;375:743-54
229. Ojima F, Saito Y, Tsuchiya Y, Kayo D, Taniuchi S, Ogoshi M*, et al.* Runx3 transcription factor regulates ovarian functions and ovulation in female mice. Journal of Reproduction and Development **2016**
230. Dierich A, Sairam MR, Monaco L, Fimia GM, Gansmuller A, LeMeur M*, et al.* Impairing follicle-stimulating hormone (FSH) signaling in vivo: targeted disruption of the FSH receptor leads to aberrant gametogenesis and hormonal imbalance. Proceedings of the National Academy of Sciences **1998**;95:13612-7
231. Kumar TR, Wang Y, Lu N, Matzuk MM. Follicle stimulating hormone is required for ovarian follicle maturation but not male fertility. Nature genetics **1997**;15:201-4
232. Lei Z, Mishra S, Zou W, Xu B, Foltz M, Li X*, et al.* Targeted disruption of luteinizing hormone/human chorionic gonadotropin receptor gene. Molecular endocrinology **2001**;15:184-200
233. Orisaka M, Tajima K, Tsang BK, Kotsuji F. Oocyte-granulosa-theca cell interactions during preantral follicular development. Journal of ovarian research **2009**;2:1-7
234. Nowell PC. The clonal evolution of tumor cell populations. Science **1976**;194:23-8
235. Greaves M, Maley CC. Clonal evolution in cancer. Nature **2012**;481:306-13
236. Kreso A, Dick JE. Evolution of the cancer stem cell model. Cell stem cell **2014**;14:275-91
237. Pardal R, Clarke MF, Morrison SJ. Applying the principles of stem-cell biology to cancer. Nature Reviews Cancer **2003**;3:895-902

238. Shackleton M, Quintana E, Fearon ER, Morrison SJ. Heterogeneity in cancer: cancer stem cells versus clonal evolution. Cell **2009**;138:822-9
239. Polyak K. Breast cancer: origins and evolution. The Journal of clinical investigation **2007**;117:3155-63
240. Chaffer CL, San Juan BP, Lim E, Weinberg RA. EMT, cell plasticity and metastasis. Cancer and Metastasis Reviews **2016**;35:645-54
241. Meacham CE, Morrison SJ. Tumour heterogeneity and cancer cell plasticity. Nature **2013**;501:328-37
242. Mani SA, Guo W, Liao M-J, Eaton EN, Ayyanan A, Zhou AY*, et al.* The epithelial-mesenchymal transition generates cells with properties of stem cells. Cell **2008**;133:704-15
243. Roesch A, Fukunaga-Kalabis M, Schmidt EC, Zabierowski SE, Brafford PA, Vultur A*, et al.* A temporarily distinct subpopulation of slow-cycling melanoma cells is required for continuous tumor growth. Cell **2010**;141:583-94
244. Castracani CC, Longhitano L, Distefano A, Di Rosa M, Pittalà V, Lupo G*, et al.* Heme oxygenase-1 and carbon monoxide regulate growth and progression in glioblastoma cells. Molecular neurobiology **2020**;57:2436-46
245. Bao S, Wu Q, McLendon RE, Hao Y, Shi Q, Hjelmeland AB*, et al.* Glioma stem cells promote radioresistance by preferential activation of the DNA damage response. nature **2006**;444:756-60
246. Diehn M, Cho RW, Lobo NA, Kalisky T, Dorie MJ, Kulp AN*, et al.* Association of reactive oxygen species levels and radioresistance in cancer stem cells. nature **2009**;458:780-3
247. Oravecz-Wilson KI, Philips ST, Yilmaz ÖH, Ames HM, Li L, Crawford BD*, et al.* Persistence of leukemia-initiating cells in a conditional knockin model of an imatinib-responsive myeloproliferative disorder. Cancer cell **2009**;16:137-48
248. Nguyen GH, Murph MM, Chang JY. Cancer stem cell radioresistance and enrichment: where frontline radiation therapy may fail in lung and esophageal cancers. Cancers **2011**;3:1232-52
249. Clarke MF, Hass AT. Cancer stem cells. Reviews in Cell Biology and Molecular Medicine **2006**
250. Doherty MR, Smigiel JM, Junk DJ, Jackson MW. Cancer stem cell plasticity drives therapeutic resistance. Cancers **2016**;8:8
251. Dingli D, Michor F. Successful therapy must eradicate cancer stem cells. Stem cells **2006**;24:2603-10
252. Batlle E, Clevers H. Cancer stem cells revisited. Nature medicine **2017**;23:1124
253. Chen W, Dong J, Haiech J, Kilhoffer M-C, Zeniou M. Cancer stem cell quiescence and plasticity as major challenges in cancer therapy. Stem cells international **2016**;2016
254. Li L, Bhatia R. Stem cell quiescence. Clinical cancer research **2011**;17:4936-41
255. Clevers H. The cancer stem cell: premises, promises and challenges. Nature medicine **2011**;17:313-9

256. Kurtova AV, Xiao J, Mo Q, Pazhanisamy S, Krasnow R, Lerner SP*, et al.* Blocking PGE 2-induced tumour repopulation abrogates bladder cancer chemoresistance. Nature **2015**;517:209-13
257. Jordan CT. The leukemic stem cell. Best practice & research Clinical haematology **2007**;20:13-8
258. Schepers K, Campbell TB, Passegué E. Normal and leukemic stem cell niches: insights and therapeutic opportunities. Cell stem cell **2015**;16:254-67
259. Soltysova A, Altanerova V, Altaner C. Cancer stem cells. Neoplasma **2005**;52:435
260. Biddle A, Liang X, Gammon L, Fazil B, Harper LJ, Emich H*, et al.* Cancer stem cells in squamous cell carcinoma switch between two distinct phenotypes that are preferentially migratory or proliferative. Cancer research **2011**;71:5317-26
261. Wang D, Plukker JTM, Coppes R. Cancer stem cells with increased metastatic potential as a therapeutic target for esophageal cancer. 2017. Elsevier. p 60-6.
262. Davis SJ, Divi V, Owen JH, Bradford CR, Carey TE, Papagerakis S*, et al.* Metastatic potential of cancer stem cells in head and neck squamous cell carcinoma. Archives of Otolaryngology–Head & Neck Surgery **2010**;136:1260-6
263. Charafe-Jauffret E, Ginestier C, Iovino F, Wicinski J, Cervera N, Finetti P*, et al.* Breast cancer cell lines contain functional cancer stem cells with metastatic capacity and a distinct molecular signature. Cancer research **2009**;69:1302-13
264. Hill RP, Marie-Egyptienne DT, Hedley DW. Cancer stem cells, hypoxia and metastasis. 2009. Elsevier. p 106-11.
265. Singh A, Settleman J. EMT, cancer stem cells and drug resistance: an emerging axis of evil in the war on cancer. Oncogene **2010**;29:4741-51
266. Scheel C, Weinberg RA. Cancer stem cells and epithelial–mesenchymal transition: concepts and molecular links. 2012. Elsevier. p 396-403.
267. May CD, Sphyris N, Evans KW, Werden SJ, Guo W, Mani SA. Epithelial-mesenchymal transition and cancer stem cells: a dangerously dynamic duo in breast cancer progression. Breast Cancer Research **2011**;13:1-10
268. Brabletz T. EMT and MET in metastasis: where are the cancer stem cells? Cancer cell **2012**;22:699-701
269. Boccaccio C, Comoglio PM. Invasive growth: a MET-driven genetic programme for cancer and stem cells. Nature Reviews Cancer **2006**;6:637-45
270. Nieto MA, Huang RY-J, Jackson RA, Thiery JP. EMT: 2016. Cell **2016**;166:21-45
271. da Silva-Diz V, Lorenzo-Sanz L, Bernat-Peguera A, Lopez-Cerda M, Muñoz P. Cancer cell plasticity: Impact on tumor progression and therapy response. 2018. Elsevier. p 48-58.

272. Diepenbruck M, Christofori G. Epithelial–mesenchymal transition (EMT) and metastasis: yes, no, maybe? Current opinion in cell biology **2016**;43:7-13
273. Ji J, Wang XW. Clinical implications of cancer stem cell biology in hepatocellular carcinoma. 2012. Elsevier. p 461-72.
274. Matsumura Y, Maeda H. A new concept for macromolecular therapeutics in cancer chemotherapy: mechanism of tumoritropic accumulation of proteins and the antitumor agent smancs. Cancer research **1986**;46:6387-92
275. Herskovic A, Martz K, Al-Sarraf M, Leichman L, Brindle J, Vaitkevicius V*, et al.* Combined chemotherapy and radiotherapy compared with radiotherapy alone in patients with cancer of the esophagus. New England Journal of Medicine **1992**;326:1593-8
276. Morrison R, Schleicher SM, Sun Y, Niermann KJ, Kim S, Spratt DE*, et al.* Targeting the mechanisms of resistance to chemotherapy and radiotherapy with the cancer stem cell hypothesis. Journal of oncology **2011**;2011
277. Lagadec C, Vlashi E, Della Donna L, Dekmezian C, Pajonk F. Radiation-induced reprogramming of breast cancer cells. Stem cells **2012**;30:833-44
278. Dean M. ABC transporters, drug resistance, and cancer stem cells. Journal of mammary gland biology and neoplasia **2009**;14:3-9
279. Wang Q-E. DNA damage responses in cancer stem cells: Implications for cancer therapeutic strategies. World journal of biological chemistry **2015**;6:57
280. Signore M, Ricci-Vitiani L, De Maria R. Targeting apoptosis pathways in cancer stem cells. Cancer letters **2013**;332:374-82
281. Moitra K, Lou H, Dean M. Multidrug efflux pumps and cancer stem cells: insights into multidrug resistance and therapeutic development. Clinical Pharmacology & Therapeutics **2011**;89:491-502
282. Alvero AB, Chen R, Fu H-H, Montagna M, Schwartz PE, Rutherford T*, et al.* Molecular phenotyping of human ovarian cancer stem cells unravels the mechanisms for repair and chemoresistance. Cell cycle **2009**;8:158-66
283. Cioffi M, D'Alterio C, Camerlingo R, Tirino V, Consales C, Riccio A*, et al.* Identification of a distinct population of CD133+ CXCR4+ cancer stem cells in ovarian cancer. Scientific reports **2015**;5:1-11
284. Nuti SV, Mor G, Li P, Yin G. TWIST and ovarian cancer stem cells: implications for chemoresistance and metastasis. Oncotarget **2014**;5:7260
285. Zong X, Nephew KP. Ovarian cancer stem cells: role in metastasis and opportunity for therapeutic targeting. Cancers **2019**;11:934
286. Boesch M, Sopper S, Zeimet AG, Reimer D, Gastl G, Ludewig B*, et al.* Heterogeneity of cancer stem cells: rationale for targeting the stem cell niche. Biochimica et Biophysica Acta (BBA)-Reviews on Cancer **2016**;1866:276-89
287. Plaks V, Kong N, Werb Z. The cancer stem cell niche: how essential is the niche in regulating stemness of tumor cells? Cell stem cell **2015**;16:225-38
288. Melzer C, von der Ohe J, Lehnert H, Ungefroren H, Hass R. Cancer stem cell niche models and contribution by mesenchymal stroma/stem cells. Molecular cancer **2017**;16:1-15

289. Condello S, Morgan CA, Nagdas S, Cao L, Turek J, Hurley TD*, et al.* β-Catenin-regulated ALDH1A1 is a target in ovarian cancer spheroids. Oncogene **2015**;34:2297-308
290. Sneha S, Nagare RP, Sidhanth C, Krishnapriya S, Garg M, Ramachandran B*, et al.* The hedgehog pathway regulates cancer stem cells in serous adenocarcinoma of the ovary. Cellular Oncology **2020**;43:601-16
291. McAuliffe SM, Morgan SL, Wyant GA, Tran LT, Muto KW, Chen YS*, et al.* Targeting Notch, a key pathway for ovarian cancer stem cells, sensitizes tumors to platinum therapy. Proceedings of the National Academy of Sciences **2012**;109:E2939-E48
292. Abubaker K, Luwor RB, Zhu H, McNally O, Quinn MA, Burns CJ*, et al.* Inhibition of the JAK2/STAT3 pathway in ovarian cancer results in the loss of cancer stem cell-like characteristics and a reduced tumor burden. BMC cancer **2014**;14:1-22
293. Ray A, Meng E, Reed E, Shevde LA, Rocconi RP. Hedgehog signaling pathway regulates the growth of ovarian cancer spheroid forming cells. International journal of oncology **2011**;39:797-804
294. Leizer AL, Alvero AB, Fu HH, Holmberg JC, Cheng YC, Silasi DA*, et al.* Regulation of Inflammation by the NF-κB Pathway in Ovarian Cancer Stem Cells. American journal of reproductive immunology **2011**;65:438-47
295. Zhang T, Xu J, Deng S, Zhou F, Li J, Zhang L*, et al.* Core signaling pathways in ovarian cancer stem cell revealed by integrative analysis of multi-marker genomics data. PLoS One **2018**;13:e0196351
296. Wang Y, Cardenas H, Fang F, Condello S, Taverna P, Segar M*, et al.* Epigenetic targeting of ovarian cancer stem cells. Cancer research **2014**;74:4922-36
297. Mazzoldi EL, Pastò A, Pilotto G, Minuzzo S, Piga I, Palumbo P*, et al.* Comparison of the genomic profile of cancer stem cells and their non-stem counterpart: the case of ovarian cancer. Journal of clinical medicine **2020**;9:368
298. Xiang T, Long H, He L, Han X, Lin K, Liang Z*, et al.* Interleukin-17 produced by tumor microenvironment promotes self-renewal of CD133+ cancer stem-like cells in ovarian cancer. Oncogene **2015**;34:165-76
299. Gao X, Lin J, Li Y, Gao L, Wang X, Wang W*, et al.* MicroRNA-193a represses c-kit expression and functions as a methylation-silenced tumor suppressor in acute myeloid leukemia. Oncogene **2011**;30:3416-28
300. Koinuma K, Kaneda R, Toyota M, Yamashita Y, Takada S, Choi YL*, et al.* Screening for genomic fragments that are methylated specifically in colorectal carcinoma with a methylated MLH1 promoter. Carcinogenesis **2005**;26:2078-85
301. Baba T, Convery P, Matsumura N, Whitaker R, Kondoh E, Perry T*, et al.* Epigenetic regulation of CD133 and tumorigenicity of CD133+ ovarian cancer cells. Oncogene **2009**;28:209-18
302. Abelson S, Shamai Y, Berger L, Skorecki K, Tzukerman M. Niche-dependent gene expression profile of intratumoral heterogeneous ovarian cancer stem cell populations. PloS one **2013**;8:e83651

303. Borovski T, Felipe De Sousa EM, Vermeulen L, Medema JP. Cancer stem cell niche: the place to be. Cancer research **2011**;71:634-9
304. Li L, Neaves WB. Normal stem cells and cancer stem cells: the niche matters. Cancer research **2006**;66:4553-7
305. Gattazzo F, Urciuolo A, Bonaldo P. Extracellular matrix: a dynamic microenvironment for stem cell niche. Biochimica et Biophysica Acta (BBA)-General Subjects **2014**;1840:2506-19
306. Mukherjee S, Kong J, Brat DJ. Cancer stem cell division: when the rules of asymmetry are broken. Stem cells and development **2015**;24:405-16
307. Flesken-Nikitin A, Hwang C-I, Cheng C-Y, Michurina TV, Enikolopov G, Nikitin AY. Ovarian surface epithelium at the junction area contains a cancer-prone stem cell niche. Nature **2013**;495:241-5
308. Wang Y, Sacchetti A, van Dijk MR, van der Zee M, van der Horst PH, Joosten R*, et al.* Identification of quiescent, stem-like cells in the distal female reproductive tract. PLoS One **2012**;7:e40691
309. Ng A, Tan S, Singh G, Rizk P, Swathi Y, Tan TZ*, et al.* Lgr5 marks stem/progenitor cells in ovary and tubal epithelia. Nature cell biology **2014**;16:745-57
310. Snegovskikh V, Mutlu L, Massasa E, Taylor HS. Identification of putative fallopian tube stem cells. Reproductive sciences **2014**;21:1460-4
311. Paik DY, Janzen DM, Schafenacker AM, Velasco VS, Shung MS, Cheng D*, et al.* Stem-like epithelial cells are concentrated in the distal end of the fallopian tube: A site for injury and serous cancer initiation. Stem cells **2012**;30:2487-97
312. Szotek PP, Chang HL, Brennand K, Fujino A, Pieretti-Vanmarcke R, Celso CL*, et al.* Normal ovarian surface epithelial label-retaining cells exhibit stem/progenitor cell characteristics. Proceedings of the National Academy of Sciences **2008**;105:12469-73
313. Ng A, Barker N. Ovary and fimbrial stem cells: biology, niche and cancer origins. Nature reviews Molecular cell biology **2015**;16:625-38
314. Lupia M, Cavallaro U. Ovarian cancer stem cells: still an elusive entity? Molecular cancer **2017**;16:1-17
315. Kim S, Kim B, Song YS. Ascites modulates cancer cell behavior, contributing to tumor heterogeneity in ovarian cancer. Cancer science **2016**;107:1173-8
316. Kenny HA, Chiang C-Y, White EA, Schryver EM, Habis M, Romero IL*, et al.* Mesothelial cells promote early ovarian cancer metastasis through fibronectin secretion. The Journal of clinical investigation **2014**;124:4614-28
317. Guo Y, Li B, Yan X, Shen X, Ma J, Liu S*, et al.* Bisphenol A and polychlorinated biphenyls enhance the cancer stem cell properties of human ovarian cancer cells by activating the WNT signaling pathway. Chemosphere **2020**;246:125775
318. Van Camp J, Beckers S, Zegers D, Van Hul W. Wnt signaling and the control of human stem cell fate. Stem cell reviews and reports **2014**;10:207-29

319. Teo J-L, Kahn M. The Wnt signaling pathway in cellular proliferation and differentiation: a tale of two coactivators. Advanced drug delivery reviews **2010**;62:1149-55
320. Karamboulas C, Ailles L. Developmental signaling pathways in cancer stem cells of solid tumors. Biochimica et Biophysica Acta (BBA)-General Subjects **2013**;1830:2481-95
321. Takebe N, Miele L, Harris PJ, Jeong W, Bando H, Kahn M*, et al.* Targeting Notch, Hedgehog, and Wnt pathways in cancer stem cells: clinical update. Nature reviews Clinical oncology **2015**;12:445
322. Chiba S. Concise review: Notch signaling in stem cell systems. Stem cells **2006**;24:2437-47
323. Stine RR, Matunis EL. JAK-STAT signaling in stem cells. Transcriptional and Translational Regulation of Stem Cells: Springer; 2013. p 247-67.
324. Chambers I. The molecular basis of pluripotency in mouse embryonic stem cells. Cloning and stem cells **2004**;6:386-91
325. Merchant AA, Matsui W. Targeting Hedgehog—a cancer stem cell pathway. Clinical cancer research **2010**;16:3130-40
326. Petrova R, Joyner AL. Roles for Hedgehog signaling in adult organ homeostasis and repair. Development **2014**;141:3445-57
327. Hayden MS, Ghosh S. Shared principles in NF-κB signaling. Cell **2008**;132:344-62
328. Su D, Deng H, Zhao X, Zhang X, Chen L, Chen X*, et al.* Targeting CD24 for treatment of ovarian cancer by short hairpin RNA. Cytotherapy **2009**;11:642-52
329. Gao M, Choi Y, Kang S, Youn J, Cho N. CD24+ cells from hierarchically organized ovarian cancer are enriched in cancer stem cells. Oncogene **2010**;29:2672-80
330. Meirelles K, Benedict LA, Dombkowski D, Pepin D, Preffer FI, Teixeira J*, et al.* Human ovarian cancer stem/progenitor cells are stimulated by doxorubicin but inhibited by Mullerian inhibiting substance. Proceedings of the National Academy of Sciences **2012**;109:2358-63
331. Nakamura K, Terai Y, Tanabe A, Ono YJ, Hayashi M, Maeda K*, et al.* CD24 expression is a marker for predicting clinical outcome and regulates the epithelial-mesenchymal transition in ovarian cancer via both the Akt and ERK pathways. Oncology reports **2017**;37:3189-200
332. Jaggupilli A, Elkord E. Significance of CD44 and CD24 as cancer stem cell markers: an enduring ambiguity. Clinical and Developmental Immunology **2012**;2012
333. Choi Y-L, Kim S-H, Shin YK, Hong Y-C, Lee S-J, Kang SY*, et al.* Cytoplasmic CD24 expression in advanced ovarian serous borderline tumors. Gynecologic oncology **2005**;97:379-86
334. Zhang S, Balch C, Chan MW, Lai H-C, Matei D, Schilder JM*, et al.* Identification and characterization of ovarian cancer-initiating cells from primary human tumors. Cancer research **2008**;68:4311-20
335. Casagrande F, Cocco E, Bellone S, Richter CE, Bellone M, Todeschini P*, et al.* Eradication of chemotherapy-resistant CD44+ human ovarian cancer

stem cells in mice by intraperitoneal administration of clostridium perfringens enterotoxin. Cancer **2011**;117:5519-28
336. Meng E, Long B, Sullivan P, McClellan S, Finan MA, Reed E*, et al.* CD44+/CD24− ovarian cancer cells demonstrate cancer stem cell properties and correlate to survival. Clinical & experimental metastasis **2012**;29:939-48
337. Štemberger-Papić S, Vrdoljak-Mozetič D, Verša Ostojić D, Rubeša-Mihaljević R, Krištofić I, Brnčić-Fischer A*, et al.* Expression of CD133 and CD117 in 64 serous ovarian cancer cases. Collegium antropologicum **2015**;39:745-53
338. Zheng J, Zhao S, Yu X, Huang S, Liu HY. Simultaneous targeting of CD44 and EpCAM with a bispecific aptamer effectively inhibits intraperitoneal ovarian cancer growth. Theranostics **2017**;7:1373
339. Tayama S, Motohara T, Narantuya D, Li C, Fujimoto K, Sakaguchi I*, et al.* The impact of EpCAM expression on response to chemotherapy and clinical outcomes in patients with epithelial ovarian cancer. Oncotarget **2017**;8:44312
340. Zhang S, Cui B, Lai H, Liu G, Ghia EM, Widhopf GF*, et al.* Ovarian cancer stem cells express ROR1, which can be targeted for anti–cancer-stem-cell therapy. Proceedings of the National Academy of Sciences **2014**;111:17266-71
341. Zhang H, Qiu J, Ye C, Yang D, Gao L, Su Y*, et al.* ROR1 expression correlated with poor clinical outcome in human ovarian cancer. Scientific reports **2014**;4:1-7
342. Wang Y, Shao F, Chen L. ALDH1A2 suppresses epithelial ovarian cancer cell proliferation and migration by downregulating STAT3. OncoTargets and therapy **2018**;11:599
343. Wang Y-C, Yo Y-T, Lee H-Y, Liao Y-P, Chao T-K, Su P-H*, et al.* ALDH1-bright epithelial ovarian cancer cells are associated with CD44 expression, drug resistance, and poor clinical outcome. The American journal of pathology **2012**;180:1159-69
344. Landen CN, Goodman B, Katre AA, Steg AD, Nick AM, Stone RL*, et al.* Targeting aldehyde dehydrogenase cancer stem cells in ovarian cancer. Molecular cancer therapeutics **2010**;9:3186-99
345. Miang-Lon Ng P, Lufkin T. Embryonic stem cells: protein interaction networks. **2011**
346. Yu Z, Pestell TG, Lisanti MP, Pestell RG. Cancer stem cells. The international journal of biochemistry & cell biology **2012**;44:2144-51
347. Wen Y, Hou Y, Huang Z, Cai J, Wang Z. SOX 2 is required to maintain cancer stem cells in ovarian cancer. Cancer science **2017**;108:719-31
348. Ruan Z, Yang X, Cheng W. OCT4 accelerates tumorigenesis through activating JAK/STAT signaling in ovarian cancer side population cells. Cancer management and research **2019**;11:389
349. Siu MK, Wong ES, Kong DS, Chan HY, Jiang L, Wong OG*, et al.* Stem cell transcription factor NANOG controls cell migration and invasion via

dysregulation of E-cadherin and FoxJ1 and contributes to adverse clinical outcome in ovarian cancers. Oncogene **2013**;32:3500-9
350. Pan Y, Jiao J, Zhou C, Cheng Q, Hu Y, Chen H. Nanog is highly expressed in ovarian serous cystadenocarcinoma and correlated with clinical stage and pathological grade. Pathobiology **2010**;77:283-8
351. Qin S, Li Y, Cao X, Du J, Huang X. NANOG regulates epithelial–mesenchymal transition and chemoresistance in ovarian cancer. Bioscience reports **2017**;37
352. Di J, Duiveman-de Boer T, Zusterzeel PL, Figdor CG, Massuger LFG, Torensma R. The stem cell markers Oct4A, Nanog and c-Myc are expressed in ascites cells and tumor tissue of ovarian cancer patients. Cellular oncology **2013**;36:363-74
353. Ning Y-X, Luo X, Xu M, Feng X, Wang J. Let-7d increases ovarian cancer cell sensitivity to a genistein analog by targeting c-Myc. Oncotarget **2017**;8:74836
354. Garson K, Vanderhyden BC. Epithelial ovarian cancer stem cells: underlying complexity of a simple paradigm. Reproduction **2015**;149:R59-70
355. Hu L, McArthur C, Jaffe R. Ovarian cancer stem-like side-population cells are tumourigenic and chemoresistant. British journal of cancer **2010**;102:1276-83
356. Dou J, Jiang C, Wang J, Zhang X, Zhao F, Hu W*, et al.* Using ABCG2-molecule-expressing side population cells to identify cancer stem-like cells in a human ovarian cell line. Cell biology international **2011**;35:227-34
357. Kobayashi Y, Seino K-i, Hosonuma S, Ohara T, Itamochi H, Isonishi S*, et al.* Side population is increased in paclitaxel-resistant ovarian cancer cell lines regardless of resistance to cisplatin. Gynecologic oncology **2011**;121:390-4
358. Januchowski R, Wojtowicz K, Sterzyńska K, Sosińska P, Andrzejewska M, Zawierucha P*, et al.* Inhibition of ALDH1A1 activity decreases expression of drug transporters and reduces chemotherapy resistance in ovarian cancer cell lines. The international journal of biochemistry & cell biology **2016**;78:248-59
359. Lee M, Nam EJ, Kim SW, Kim S, Kim JH, Kim YT. Prognostic impact of the cancer stem cell–related marker NANOG in ovarian serous carcinoma. International Journal of Gynecologic Cancer **2012**;22
360. Wang J, Wang H, Li Z, Wu Q, Lathia JD, McLendon RE*, et al.* c-Myc is required for maintenance of glioma cancer stem cells. PloS one **2008**;3:e3769
361. Luo L, Zeng J, Liang B, Zhao Z, Sun L, Cao D*, et al.* Ovarian cancer cells with the CD117 phenotype are highly tumorigenic and are related to chemotherapy outcome. Experimental and molecular pathology **2011**;91:596-602
362. Conic I, Stanojevic Z, Jankovic Velickovic L, Stojnev S, Ristic Petrovic A, Krstic M*, et al.* Epithelial ovarian cancer with CD117 phenotype is highly

aggressive and resistant to chemotherapy. Journal of Obstetrics and Gynaecology Research **2015**;41:1630-7
363. Curley MD, Therrien VA, Cummings CL, Sergent PA, Koulouris CR, Friel AM*, et al.* CD133 expression defines a tumor initiating cell population in primary human ovarian cancer. Stem cells **2009**;27:2875-83
364. Skubitz AP, Taras EP, Boylan KL, Waldron NN, Oh S, Panoskaltsis-Mortari A*, et al.* Targeting CD133 in an in vivo ovarian cancer model reduces ovarian cancer progression. Gynecologic oncology **2013**;130:579-87
365. Zhang J, Guo X, Chang DY, Rosen DG, Mercado-Uribe I, Liu J. CD133 expression associated with poor prognosis in ovarian cancer. Modern pathology **2012**;25:456-64
366. Suster NK, Virant-Klun I. Presence and role of stem cells in ovarian cancer. World journal of stem cells **2019**;11:383
367. Lambert M, Jambon S, Depauw S, David-Cordonnier M-H. Targeting transcription factors for cancer treatment. Molecules **2018**;23:1479
368. Network T. institution.)(Participants are arranged by area of contribution and then by, Sites D, Bell D, Berchuck A, Birrer M, Chien J, Cramer DW, Dao F, Dhir R, et al. 2011. Integrated genomic analyses of ovarian carcinoma. Nature;474:609-15
369. Hardy LR, Pergande MR, Esparza K, Heath KN, Önyüksel H, Cologna SM*, et al.* Proteomic analysis reveals a role for PAX8 in peritoneal colonization of high grade serous ovarian cancer that can be targeted with micelle encapsulated thiostrepton. Oncogene **2019**;38:6003-16
370. Ahmed AA, Etemadmoghadam D, Temple J, Lynch AG, Riad M, Sharma R*, et al.* Driver mutations in TP53 are ubiquitous in high grade serous carcinoma of the ovary. The Journal of pathology **2010**;221:49-56
371. Network CGAR. Integrated genomic analyses of ovarian carcinoma. Nature **2011**;474:609
372. Ghannam-Shahbari D, Jacob E, Kakun RR, Wasserman T, Korsensky L, Sternfeld O*, et al.* PAX8 activates a p53-p21-dependent pro-proliferative effect in high grade serous ovarian carcinoma. Oncogene **2018**;37:2213-24
373. Manchana T, Phoolcharoen N, Tantbirojn P. BRCA mutation in high grade epithelial ovarian cancers. Gynecologic oncology reports **2019**;29:102-5
374. Tassi RA, Todeschini P, Siegel ER, Calza S, Cappella P, Ardighieri L*, et al.* FOXM1 expression is significantly associated with chemotherapy resistance and adverse prognosis in non-serous epithelial ovarian cancer patients. Journal of Experimental & Clinical Cancer Research **2017**;36:1-18
375. Zhao F, Siu MK, Jiang L, Tam KF, Ngan HY, Le XF*, et al.* Overexpression of forkhead box protein M1 (FOXM1) in ovarian cancer correlates with poor patient survival and contributes to paclitaxel resistance. PloS one **2014**;9:e113478
376. Tung CS, Mok SC, Tsang YT, Zu Z, Song H, Liu J*, et al.* PAX2 expression in low malignant potential ovarian tumors and low-grade ovarian serous carcinomas. Modern Pathology **2009**;22:1243-50
377. Palacios J, Gamallo C. Mutations in the β-catenin gene (CTNNB1) in endometrioid ovarian carcinomas. Cancer research **1998**;58:1344-7

378. Lee S, Garner EI, Welch WR, Berkowitz RS, Mok SC. Over-expression of hypoxia-inducible factor 1 alpha in ovarian clear cell carcinoma. Gynecologic oncology **2007**;106:311-7
379. Tsuchiya A, Sakamoto M, Yasuda J, Chuma M, Ohta T, Ohki M*, et al.* Expression profiling in ovarian clear cell carcinoma: identification of hepatocyte nuclear factor-1β as a molecular marker and a possible molecular target for therapy of ovarian clear cell carcinoma. The American journal of pathology **2003**;163:2503-12
380. Shen H, Fridley BL, Song H, Lawrenson K, Cunningham JM, Ramus SJ*, et al.* Epigenetic analysis leads to identification of HNF1B as a subtype-specific susceptibility gene for ovarian cancer. Nature communications **2013**;4:1-10
381. Kato N, Sasou S-i, Motoyama T. Expression of hepatocyte nuclear factor-1beta (HNF-1beta) in clear cell tumors and endometriosis of the ovary. Modern pathology **2006**;19:83-9
382. Li Q, Cheng X, Ji J, Zhang J, Huang W. The application value of HNF-1β transcription factor in the diagnosis of ovarian clear cell carcinoma. International Journal of Gynecological Pathology **2016**;35:66-71
383. Kim MJ. The usefulness of CDX-2 for differentiating primary and metastatic ovarian carcinoma: an immunohistochemical study using a tissue microarray. Journal of Korean medical science **2005**;20:643
384. Morice P, Gouy S, Leary A. Mucinous ovarian carcinoma. New England Journal of Medicine **2019**;380:1256-66
385. Nonaka D, Chiriboga L, Soslow RA. Expression of pax8 as a useful marker in distinguishing ovarian carcinomas from mammary carcinomas. The American journal of surgical pathology **2008**;32:1566-71
386. Tong GX, Devaraj K, Hamele-Bena D, Yu WM, Turk A, Chen X*, et al.* Pax8: a marker for carcinoma of Müllerian origin in serous effusions. Diagnostic cytopathology **2011**;39:562-6
387. Chai HJ, Ren Q, Fan Q, Ye L, Du GY, Du HW*, et al.* PAX8 is a potential marker for the diagnosis of primary epithelial ovarian cancer. Oncology letters **2017**;14:5871-5
388. Köbel M, Kalloger SE, Boyd N, McKinney S, Mehl E, Palmer C*, et al.* Ovarian carcinoma subtypes are different diseases: implications for biomarker studies. PLoS medicine **2008**;5:e232
389. Reddy J, Fonseca MA, Corona RI, Nameki R, Dezem FS, Klein IA*, et al.* Predicting master transcription factors from pan-cancer expression data. bioRxiv **2019**:839142
390. Adler EK, Corona RI, Lee JM, Rodriguez-Malave N, Mhawech-Fauceglia P, Sowter H*, et al.* The PAX8 cistrome in epithelial ovarian cancer. Oncotarget **2017**;8:108316
391. Di Palma T, Lucci V, de Cristofaro T, Filippone MG, Zannini M. A role for PAX8 in the tumorigenic phenotype of ovarian cancer cells. BMC cancer **2014**;14:1-8

392. Rodgers LH, Eoghainín Ó, Burdette JE. Loss of PAX8 in high-grade serous ovarian cancer reduces cell survival despite unique modes of action in the fallopian tube and ovarian surface epithelium. Oncotarget **2016**;7:32785
393. Cheung HW, Cowley GS, Weir BA, Boehm JS, Rusin S, Scott JA*, et al.* Systematic investigation of genetic vulnerabilities across cancer cell lines reveals lineage-specific dependencies in ovarian cancer. Proceedings of the National Academy of Sciences **2011**;108:12372-7
394. Høgdall EV, Christensen L, Kjaer SK, Blaakaer J, Christensen IJ, Gayther S*, et al.* Expression level of Wilms tumor 1 (WT1) protein has limited prognostic value in epithelial ovarian cancer From the Danish "MALOVA" Ovarian Cancer Study. Gynecologic oncology **2007**;106:318-24
395. Köbel M, Luo L, Grevers X, Lee S, Brooks-Wilson A, Gilks CB*, et al.* Ovarian carcinoma histotype: strengths and limitations of integrating morphology with immunohistochemical predictions. International journal of gynecological pathology: official journal of the International Society of Gynecological Pathologists **2019**;38:353
396. Shimizu M, Toki T, Takagi Y, Konishi I, Fujii S. Immunohistochemical detection of the Wilms' tumor gene (WT1) in epithelial ovarian tumors. International journal of gynecological pathology **2000**;19:158-63
397. Mitra AK, Davis DA, Tomar S, Roy L, Gurler H, Xie J*, et al.* In vivo tumor growth of high-grade serous ovarian cancer cell lines. Gynecologic oncology **2015**;138:372-7
398. Yang L, Han Y, Saiz FS, Minden M. A tumor suppressor and oncogene: the WT1 story. Leukemia **2007**;21:868-76
399. Karlan BY, Dering J, Walsh C, Orsulic S, Lester J, Anderson LA*, et al.* POSTN/TGFBI-associated stromal signature predicts poor prognosis in serous epithelial ovarian cancer. Gynecologic oncology **2014**;132:334-42
400. Taube ET, Denkert C, Sehouli J, Kunze CA, Dietel M, Braicu I*, et al.* Wilms tumor protein 1 (WT1)—not only a diagnostic but also a prognostic marker in high-grade serous ovarian carcinoma. Gynecologic oncology **2016**;140:494-502
401. Yoh M, Honda T, Miwatani T, Tsunasawa S, Sakiyama F. Comparative amino acid sequence analysis of hemolysins produced by Vibrio hollisae and Vibrio parahaemolyticus. Journal of bacteriology **1989**;171:6859
402. Kandoth C, McLellan MD, Vandin F, Ye K, Niu B, Lu C*, et al.* Mutational landscape and significance across 12 major cancer types. Nature **2013**;502:333-9
403. Brachova P, Thiel KW, Leslie KK. The consequence of oncomorphic TP53 mutations in ovarian cancer. International journal of molecular sciences **2013**;14:19257-75
404. Seagle B-LL, Yang C-PH, Eng KH, Dandapani M, Odunsi-Akanji O, Goldberg GL*, et al.* TP53 hot spot mutations in ovarian cancer: selective resistance to microtubule stabilizers in vitro and differential survival outcomes from The Cancer Genome Atlas. Gynecologic oncology **2015**;138:159-64

405. ST Wong A, Maines-Bandiera SL, Rosen B, Wheelock MJ, Johnson KR, Leung PC*, et al.* Constitutive and conditional cadherin expression in cultured human ovarian surface epithelium: influence of family history of ovarian cancer. International journal of cancer **1999**;81:180-8
406. Joerger AC, Rajagopalan S, Natan E, Veprintsev DB, Robinson CV, Fersht AR. Structural evolution of p53, p63, and p73: implication for heterotetramer formation. Proceedings of the National Academy of Sciences **2009**;106:17705-10
407. Song H, Hollstein M, Xu Y. p53 gain-of-function cancer mutants induce genetic instability by inactivating ATM. Nature cell biology **2007**;9:573-80
408. Girardini JE, Napoli M, Piazza S, Rustighi A, Marotta C, Radaelli E*, et al.* A Pin1/mutant p53 axis promotes aggressiveness in breast cancer. Cancer cell **2011**;20:79-91
409. Farmer H, McCabe N, Lord CJ, Tutt AN, Johnson DA, Richardson TB*, et al.* Targeting the DNA repair defect in BRCA mutant cells as a therapeutic strategy. Nature **2005**;434:917-21
410. Yeh S, Hu Y-C, Rahman M, Lin H-K, Hsu C-L, Ting H-J*, et al.* Increase of androgen-induced cell death and androgen receptor transactivation by BRCA1 in prostate cancer cells. Proceedings of the National Academy of Sciences **2000**;97:11256-61
411. Takaoka M, Miki Y. BRCA1 gene: function and deficiency. International journal of clinical oncology **2018**;23:36-44
412. Mullan P, Quinn J, Harkin D. The role of BRCA1 in transcriptional regulation and cell cycle control. Oncogene **2006**;25:5854-63
413. Helleday T. The underlying mechanism for the PARP and BRCA synthetic lethality: clearing up the misunderstandings. Molecular oncology **2011**;5:387-93
414. Tutt A, Robson M, Garber J, Domchek S, Audeh M, Weitzel J*, et al.* Phase II trial of the oral PARP inhibitor olaparib in BRCA-deficient advanced breast cancer. Journal of clinical oncology **2009**;27:CRA501-CRA
415. Kim G, Ison G, McKee AE, Zhang H, Tang S, Gwise T*, et al.* FDA approval summary: olaparib monotherapy in patients with deleterious germline BRCA-mutated advanced ovarian cancer treated with three or more lines of chemotherapy. Clinical cancer research **2015**;21:4257-61
416. Fan Q, Cai Q, Xu Y. FOXM1 is a downstream target of LPA and YAP oncogenic signaling pathways in high grade serous ovarian cancer. Oncotarget **2015**;6:27688
417. Fang P, Madden JA, Neums L, Moulder RK, Forrest ML, Chien J. Olaparib-induced adaptive response is disrupted by FOXM1 targeting that enhances sensitivity to PARP inhibition. Molecular Cancer Research **2018**;16:961-73
418. Zeng M, Kwiatkowski NP, Zhang T, Nabet B, Xu M, Liang Y*, et al.* Targeting MYC dependency in ovarian cancer through inhibition of CDK7 and CDK12/13. Elife **2018**;7:e39030
419. Reyes-González JM, Armaiz-Peña GN, Mangala LS, Valiyeva F, Ivan C, Pradeep S*, et al.* Targeting c-MYC in platinum-resistant ovarian cancer. Molecular cancer therapeutics **2015**;14:2260-9

420. Papp E, Hallberg D, Konecny GE, Bruhm DC, Adleff V, Noë M*, et al.* Integrated genomic, epigenomic, and expression analyses of ovarian cancer cell lines. Cell reports **2018**;25:2617-33
421. Goode EL, Chenevix-Trench G, Song H, Ramus SJ, Notaridou M, Lawrenson K*, et al.* A genome-wide association study identifies susceptibility loci for ovarian cancer at 2q31 and 8q24. Nature genetics **2010**;42:874-9
422. Li C, Bonazzoli E, Bellone S, Choi J, Dong W, Menderes G*, et al.* Mutational landscape of primary, metastatic, and recurrent ovarian cancer reveals c-MYC gains as potential target for BET inhibitors. Proceedings of the National Academy of Sciences **2019**;116:619-24
423. Trop-Steinberg S, Azar Y. Is Myc an important biomarker? Myc expression in immune disorders and cancer. The American journal of the medical sciences **2018**;355:67-75
424. Karst AM, Levanon K, Drapkin R. Modeling high-grade serous ovarian carcinogenesis from the fallopian tube. Proceedings of the National Academy of Sciences **2011**;108:7547-52
425. Lawrenson K, Sproul D, Grun B, Notaridou M, Benjamin E, Jacobs IJ*, et al.* Modelling genetic and clinical heterogeneity in epithelial ovarian cancers. Carcinogenesis **2011**;32:1540-9
426. Al-Hujaily EM, Tang Y, Yao D-S, Carmona E, Garson K, Vanderhyden BC. Divergent roles of PAX2 in the etiology and progression of ovarian cancer. Cancer Prevention Research **2015**;8:1163-73
427. Polakis P. Wnt signaling and cancer. Genes & development **2000**;14:1837-51
428. Wodarz A, Nusse R. Mechanisms of Wnt signaling in development. Annual review of cell and developmental biology **1998**;14:59-88
429. Zhan T, Rindtorff N, Boutros M. Wnt signaling in cancer. Oncogene **2017**;36:1461-73
430. Jung Y-S, Park J-I. Wnt signaling in cancer: therapeutic targeting of Wnt signaling beyond β-catenin and the destruction complex. Experimental & molecular medicine **2020**;52:183-91
431. McConechy MK, Ding J, Senz J, Yang W, Melnyk N, Tone AA*, et al.* Ovarian and endometrial endometrioid carcinomas have distinct CTNNB1 and PTEN mutation profiles. Modern pathology **2014**;27:128-34
432. Semenza GL. HIF-1 and tumor progression: pathophysiology and therapeutics. Trends in molecular medicine **2002**;8:S62-S7
433. Yang J, Nie J, Ma X, Wei Y, Peng Y, Wei X. Targeting PI3K in cancer: mechanisms and advances in clinical trials. Molecular cancer **2019**;18:1-28
434. Cuff J, Salari K, Clarke N, Esheba GE, Forster AD, Huang S*, et al.* Integrative bioinformatics links HNF1B with clear cell carcinoma and tumor-associated thrombosis. PLoS One **2013**;8:e74562
435. Hanley KZ, Cohen C, Osunkoya AO. Hepatocyte Nuclear Factor-1β Expression in Clear Cell Renal Cell Carcinoma and Urothelial Carcinoma With Clear Cell Features: A Potential Diagnostic Pitfall. Applied immunohistochemistry & molecular morphology **2017**;25:134-8

436. Pearce CL, Templeman C, Rossing MA, Lee A, Near AM, Webb PM*, et al.* Association between endometriosis and risk of histological subtypes of ovarian cancer: a pooled analysis of case–control studies. The lancet oncology **2012**;13:385-94
437. Takakura Y, Hinoi T, Oue N, Sasada T, Kawaguchi Y, Okajima M*, et al.* CDX2 regulates multidrug resistance 1 gene expression in malignant intestinal epithelium. Cancer research **2010**;70:6767-78
438. Bareiss PM, Paczulla A, Wang H, Schairer R, Wiehr S, Kohlhofer U*, et al.* SOX2 expression associates with stem cell state in human ovarian carcinoma. Cancer research **2013**;73:5544-55
439. Bushweller JH. Targeting transcription factors in cancer—from undruggable to reality. Nature Reviews Cancer **2019**;19:611-24
440. Lebedeva I, Stein C. Antisense oligonucleotides: promise and reality. Annual Review of Pharmacology and Toxicology **2001**;41:403-19
441. Wernert N, Stanjek A, Kiriakidis S, Hügel A, Jha HC, Mazitschek R*, et al.* Inhibition of angiogenesis in vivo by Ets-1 antisense oligonucleotides—inhibition of Ets-1 transcription factor expression by the antibiotic fumagillin. Angewandte Chemie International Edition **1999**;38:3228-31
442. Hong D, Kurzrock R, Kim Y, Woessner R, Younes A, Nemunaitis J*, et al.* AZD9150, a next-generation antisense oligonucleotide inhibitor of STAT3 with early evidence of clinical activity in lymphoma and lung cancer. Science translational medicine **2015**;7:314ra185-314ra185
443. Leong PL, Andrews GA, Johnson DE, Dyer KF, Xi S, Mai JC*, et al.* Targeted inhibition of Stat3 with a decoy oligonucleotide abrogates head and neck cancer cell growth. Proceedings of the National Academy of Sciences **2003**;100:4138-43
444. Mann MJ, Dzau VJ. Therapeutic applications of transcription factor decoy oligonucleotides. The Journal of clinical investigation **2000**;106:1071-5
445. Higgins KA, Perez JR, Coleman TA, Dorshkind K, McComas WA, Sarmiento UM*, et al.* Antisense inhibition of the p65 subunit of NF-kappa B blocks tumorigenicity and causes tumor regression. Proceedings of the National Academy of Sciences **1993**;90:9901-5
446. Agami R. RNAi and related mechanisms and their potential use for therapy. Current opinion in chemical biology **2002**;6:829-34
447. Sachdeva M, Sachdeva N, Pal M, Gupta N, Khan I, Majumdar M*, et al.* CRISPR/Cas9: molecular tool for gene therapy to target genome and epigenome in the treatment of lung cancer. Cancer gene therapy **2015**;22:509-17
448. Lee M, Kim H. Therapeutic application of the CRISPR system: current issues and new prospects. Human genetics **2019**;138:563-90
449. Chen M, Mao A, Xu M, Weng Q, Mao J, Ji J. CRISPR-Cas9 for cancer therapy: Opportunities and challenges. Cancer letters **2019**;447:48-55
450. Gagnon KT, Pendergraff HM, Deleavey GF, Swayze EE, Potier P, Randolph J*, et al.* Allele-selective inhibition of mutant huntingtin expression with antisense oligonucleotides targeting the expanded CAG repeat. Biochemistry **2010**;49:10166-78

451. Shu Y, Pi F, Sharma A, Rajabi M, Haque F, Shu D*, et al.* Stable RNA nanoparticles as potential new generation drugs for cancer therapy. Advanced drug delivery reviews **2014**;66:74-89
452. Howard KA. Delivery of RNA interference therapeutics using polycation-based nanoparticles. Advanced drug delivery reviews **2009**;61:710-20
453. Miele E, Spinelli GP, Miele E, Di Fabrizio E, Ferretti E, Tomao S*, et al.* Nanoparticle-based delivery of small interfering RNA: challenges for cancer therapy. International journal of nanomedicine **2012**;7:3637
454. Stellas D, Szabolcs M, Koul S, Li Z, Polyzos A, Anagnostopoulos C*, et al.* Therapeutic effects of an anti-Myc drug on mouse pancreatic cancer. JNCI: Journal of the National Cancer Institute **2014**;106
455. Beaulieu M-E, Jauset T, Massó-Vallés D, Martínez-Martín S, Rahl P, Maltais L*, et al.* Intrinsic cell-penetrating activity propels Omomyc from proof of concept to viable anti-MYC therapy. Science translational medicine **2019**;11
456. Aziz MH, Shen H, Maki CG. Acquisition of p53 mutations in response to the non-genotoxic p53 activator Nutlin-3. Oncogene **2011**;30:4678-86
457. Villalonga-Planells R, Coll-Mulet L, Martínez-Soler F, Castaño E, Acebes J-J, Giménez-Bonafé P*, et al.* Activation of p53 by nutlin-3a induces apoptosis and cellular senescence in human glioblastoma multiforme. PloS one **2011**;6:e18588
458. Van Maerken T, Rihani A, Van Goethem A, De Paepe A, Speleman F, Vandesompele J. Pharmacologic activation of wild-type p53 by nutlin therapy in childhood cancer. Cancer letters **2014**;344:157-65
459. An S, Fu L. Small-molecule PROTACs: An emerging and promising approach for the development of targeted therapy drugs. EBioMedicine **2018**;36:553-62
460. Schneekloth AR, Pucheault M, Tae HS, Crews CM. Targeted intracellular protein degradation induced by a small molecule: En route to chemical proteomics. Bioorganic & medicinal chemistry letters **2008**;18:5904-8
461. Tang Y-Q, Han B-M, Yao X-Q, Hong Y, Wang Y, Zhao F-J*, et al.* Chimeric molecules facilitate the degradation of androgen receptors and repress the growth of LNCaP cells. Asian journal of andrology **2009**;11:119
462. Dias N, Stein C. Antisense oligonucleotides: basic concepts and mechanisms. Molecular cancer therapeutics **2002**;1:347-55
463. Murano M, Maemura K, Hirata I, Toshina K, Nishikawa T, Hamamoto N*, et al.* Therapeutic effect of intracolonically administered nuclear factor κB (p65) antisense oligonucleotide on mouse dextran sulphate sodium (DSS)-induced colitis. Clinical & Experimental Immunology **2000**;120:51-8
464. Zou Y, Ma D, Wang Y. The PROTAC technology in drug development. Cell biochemistry and function **2019**;37:21-30
465. Gulei D, Raduly L, Berindan-Neagoe I, Calin GA. CRISPR-based RNA editing: diagnostic applications and therapeutic options. Expert review of molecular diagnostics **2019**;19:83-8

466. Chio IIC, Yordanov G, Tuveson D. MAX-ing out MYC: a novel small molecule inhibitor against MYC-dependent tumors. JNCI: Journal of the National Cancer Institute **2014**;106
467. Taniguchi J, Pandian GN, Hidaka T, Hashiya K, Bando T, Kim KK*, et al.* A synthetic DNA-binding inhibitor of SOX2 guides human induced pluripotent stem cells to differentiate into mesoderm. Nucleic acids research **2017**;45:9219-28
468. Paiva S-L, Crews CM. Targeted protein degradation: elements of PROTAC design. Current opinion in chemical biology **2019**;50:111-9
469. Konstantinidou M, Li J, Zhang B, Wang Z, Shaabani S, Ter Brake F*, et al.* PROTACs–a game-changing technology. Expert opinion on drug discovery **2019**;14:1255-68
470. Schneekloth JS, Fonseca FN, Koldobskiy M, Mandal A, Deshaies R, Sakamoto K*, et al.* Chemical genetic control of protein levels: selective in vivo targeted degradation. Journal of the American Chemical Society **2004**;126:3748-54
471. Itoh Y. Chemical protein degradation approach and its application to epigenetic targets. The Chemical Record **2018**;18:1681-700
472. Samarasinghe K, Jaime-Figueroa S, Dai K, Hu Z, Crews CM. Targeted Degradation of Transcription Factors by TRAFTACs: Transcription Factor Targeting Chimeras. bioRxiv **2020**
473. Gao H, Sun X, Rao Y. PROTAC technology: opportunities and challenges. ACS medicinal chemistry letters **2020**;11:237-40
474. Harper SQ. Progress and challenges in RNA interference therapy for Huntington disease. Archives of neurology **2009**;66:933-8
475. Frazier KS. Antisense oligonucleotide therapies: the promise and the challenges from a toxicologic pathologist's perspective. Toxicologic pathology **2015**;43:78-89
476. Deng Y, Wang CC, Choy KW, Du Q, Chen J, Wang Q*, et al.* Therapeutic potentials of gene silencing by RNA interference: principles, challenges, and new strategies. Gene **2014**;538:217-27
477. Mout R, Ray M, Lee Y-W, Scaletti F, Rotello VM. In vivo delivery of CRISPR/Cas9 for therapeutic gene editing: progress and challenges. Bioconjugate chemistry **2017**;28:880-4
478. Lino CA, Harper JC, Carney JP, Timlin JA. Delivering CRISPR: a review of the challenges and approaches. Drug delivery **2018**;25:1234-57
479. Secchiero P, Bosco R, Celeghini C, Zauli G. Recent advances in the therapeutic perspectives of Nutlin-3. Current pharmaceutical design **2011**;17:569-77
480. Rusiecki R, Witkowski J, Joanna J-A. MDM2-p53 interaction inhibitors: The current state-of-art and updated patent review (2010-Present). Recent patents on anti-cancer drug discovery **2019**;14:324-69
481. Hedvat M, Huszar D, Herrmann A, Gozgit JM, Schroeder A, Sheehy A*, et al.* The JAK2 inhibitor AZD1480 potently blocks Stat3 signaling and oncogenesis in solid tumors. Cancer cell **2009**;16:487-97

482. Hollenhorst PC, Chandler KJ, Poulsen RL, Johnson WE, Speck NA, Graves BJ. DNA specificity determinants associate with distinct transcription factor functions. PLoS Genet **2009**;5:e1000778
483. Riching KM, Mahan S, Corona CR, McDougall M, Vasta JD, Robers MB*, et al.* Quantitative live-cell kinetic degradation and mechanistic profiling of PROTAC mode of action. ACS chemical biology **2018**;13:2758-70
484. Dhillon VS, Shahid M, Husain SA. CpG methylation of the FHIT, FANCF, cyclin-D2, BRCA2 and RUNX3 genes in Granulosa cell tumors (GCTs) of ovarian origin. Molecular cancer **2004**;3:1-8
485. Repetto G, Del Peso A, Zurita JL. Neutral red uptake assay for the estimation of cell viability/cytotoxicity. Nature protocols **2008**;3:1125
486. Kim J-H, Kim Y-H, Kim H-M, Park H-O, Ha N-C, Kim TH*, et al.* FOXL2 posttranslational modifications mediated by GSK3β determine the growth of granulosa cell tumours. Nature communications **2014**;5:1-13
487. Schmittgen TD, Livak KJ. Analyzing real-time PCR data by the comparative C T method. Nature protocols **2008**;3:1101
488. Győrffy B. Survival analysis across the entire transcriptome identifies biomarkers with the highest prognostic power in breast cancer. Computational and Structural Biotechnology Journal **2021**;19:4101-9
489. Jelovac D, Armstrong DK. Recent progress in the diagnosis and treatment of ovarian cancer. CA: a cancer journal for clinicians **2011**;61:183-203
490. Zhang S, Dolgalev I, Zhang T, Ran H, Levine DA, Neel BG. Both fallopian tube and ovarian surface epithelium are cells-of-origin for high-grade serous ovarian carcinoma. Nature communications **2019**;10:1-16
491. Marquez RT, Baggerly KA, Patterson AP, Liu J, Broaddus R, Frumovitz M*, et al.* Patterns of gene expression in different histotypes of epithelial ovarian cancer correlate with those in normal fallopian tube, endometrium, and colon. Clinical cancer research **2005**;11:6116-26
492. Erickson BK, Conner MG, Landen Jr CN. The role of the fallopian tube in the origin of ovarian cancer. American journal of obstetrics and gynecology **2013**;209:409-14
493. Domcke S, Sinha R, Levine DA, Sander C, Schultz N. Evaluating cell lines as tumour models by comparison of genomic profiles. Nature communications **2013**;4:1-10
494. Beaufort CM, Helmijr JC, Piskorz AM, Hoogstraat M, Ruigrok-Ritstier K, Besselink N*, et al.* Ovarian cancer cell line panel (OCCP): clinical importance of in vitro morphological subtypes. PloS one **2014**;9:e103988
495. Chen S-F, Chang Y-C, Nieh S, Liu C-L, Yang C-Y, Lin Y-S. Nonadhesive culture system as a model of rapid sphere formation with cancer stem cell properties. PloS one **2012**;7:e31864
496. O'Brien CA, Kreso A, Jamieson CH. Cancer stem cells and self-renewal. Clinical cancer research **2010**;16:3113-20
497. Nam EJ, Lee M, Yim GW, Kim JH, Kim S, Kim SW*, et al.* MicroRNA profiling of a CD133+ spheroid-forming subpopulation of the OVCAR3 human ovarian cancer cell line. BMC medical genomics **2012**;5:1-9

498. Deng S, Yang X, Lassus H, Liang S, Kaur S, Ye Q*, et al.* Distinct expression levels and patterns of stem cell marker, aldehyde dehydrogenase isoform 1 (ALDH1), in human epithelial cancers. PloS one **2010**;5:e10277
499. Silva IA, Bai S, McLean K, Yang K, Griffith K, Thomas D*, et al.* Aldehyde dehydrogenase in combination with CD133 defines angiogenic ovarian cancer stem cells that portend poor patient survival. Cancer research **2011**;71:3991-4001
500. Burgos-Ojeda D, Rueda BR, Buckanovich RJ. Ovarian cancer stem cell markers: prognostic and therapeutic implications. Cancer letters **2012**;322:1-7
501. Meng E, Mitra A, Tripathi K, Finan MA, Scalici J, McClellan S*, et al.* ALDH1A1 maintains ovarian cancer stem cell-like properties by altered regulation of cell cycle checkpoint and DNA repair network signaling. PloS one **2014**;9:e107142
502. Li T, Su Y, Mei Y, Leng Q, Leng B, Liu Z*, et al.* ALDH1A1 is a marker for malignant prostate stem cells and predictor of prostate cancer patients' outcome. Laboratory investigation **2010**;90:234-44
503. Qian X, Wagner S, Ma C, Coordes A, Gekeler J, Klussmann JP*, et al.* Prognostic significance of ALDH1A1-positive cancer stem cells in patients with locally advanced, metastasized head and neck squamous cell carcinoma. Journal of cancer research and clinical oncology **2014**;140:1151-8
504. Yang L, Ren Y, Yu X, Qian F, Xiao H-l, Wang W-g*, et al.* ALDH1A1 defines invasive cancer stem-like cells and predicts poor prognosis in patients with esophageal squamous cell carcinoma. Modern Pathology **2014**;27:775-83
505. Guo R, Wu Q, Liu F, Wang Y. Description of the CD133+ subpopulation of the human ovarian cancer cell line OVCAR3. Oncology reports **2011**;25:141-6
506. Mi Y, Huang Y, Deng J. The enhanced delivery of salinomycin to CD133+ ovarian cancer stem cells through CD133 antibody conjugation with poly (lactic-co-glycolic acid)-poly (ethylene glycol) nanoparticles. Oncology letters **2018**;15:6611-21
507. Guilhamon P, Chesnelong C, Kushida MM, Nikolic A, Singhal D, MacLeod G*, et al.* Single-cell chromatin accessibility profiling of glioblastoma identifies an invasive cancer stem cell population associated with lower survival. Elife **2021**;10:e64090
508. Buenrostro JD, Wu B, Litzenburger UM, Ruff D, Gonzales ML, Snyder MP*, et al.* Single-cell chromatin accessibility reveals principles of regulatory variation. Nature **2015**;523:486-90
509. Corces MR, Granja JM, Shams S, Louie BH, Seoane JA, Zhou W*, et al.* The chromatin accessibility landscape of primary human cancers. Science **2018**;362:eaav1898
510. Balkwill FR, Capasso M, Hagemann T. The tumor microenvironment at a glance. The Company of Biologists Ltd; 2012.
511. Wang M, Zhao J, Zhang L, Wei F, Lian Y, Wu Y*, et al.* Role of tumor microenvironment in tumorigenesis. Journal of Cancer **2017**;8:761

512. Fang M, Yuan J, Peng C, Li Y. Collagen as a double-edged sword in tumor progression. Tumor Biology **2014**;35:2871-82
513. Balkwill FR, Capasso M, Hagemann T. The tumor microenvironment at a glance. Journal of cell science **2012**;125:5591-6
514. Seeber L, Van Diest P. Epigenetics in ovarian cancer. Cancer Epigenetics **2012**:253-69
515. Ghoneum A, Afify H, Salih Z, Kelly M, Said N. Role of tumor microenvironment in ovarian cancer pathobiology. Oncotarget **2018**;9:22832
516. Dong Q, Meng P, Wang T, Qin W, Qin W, Wang F*, et al.* MicroRNA let-7a inhibits proliferation of human prostate cancer cells in vitro and in vivo by targeting E2F2 and CCND2. PloS one **2010**;5:e10147
517. Zhu C, Shao P, Bao M, Li P, Zhou H, Cai H*, et al.* miR-154 inhibits prostate cancer cell proliferation by targeting CCND2. 2014. Elsevier. p 31. e9-. e16.
518. Xie R, Wang Y, Nie W, Huang W, Song W, Wang Z*, et al.* Lin28B expression correlates with aggressive clinicopathological characteristics in breast invasive ductal carcinoma. Cancer Biotherapy and Radiopharmaceuticals **2014**;29:215-20
519. Chu C, Liu X, Bai X, Zhao T, Wang M, Xu R*, et al.* MiR-519d suppresses breast cancer tumorigenesis and metastasis via targeting MMP3. International journal of biological sciences **2018**;14:228
520. Henry C, Hacker N, Ford C. Silencing ROR1 and ROR2 inhibits invasion and adhesion in an organotypic model of ovarian cancer metastasis. Oncotarget **2017**;8:112727
521. Arend RC, Londoño-Joshi AI, Straughn Jr JM, Buchsbaum DJ. The Wnt/β-catenin pathway in ovarian cancer: a review. Gynecologic oncology **2013**;131:772-9
522. Mabuchi S, Kuroda H, Takahashi R, Sasano T. The PI3K/AKT/mTOR pathway as a therapeutic target in ovarian cancer. Gynecologic oncology **2015**;137:173-9
523. Liao X, Siu MK, Au CW, Wong ES, Chan HY, Ip PP*, et al.* Aberrant activation of hedgehog signaling pathway in ovarian cancers: effect on prognosis, cell invasion and differentiation. Carcinogenesis **2009**;30:131-40
524. Bryant KL, Mancias JD, Kimmelman AC, Der CJ. KRAS: feeding pancreatic cancer proliferation. Trends in biochemical sciences **2014**;39:91-100
525. Liu X, Jakubowski M, Hunt JL. KRAS gene mutation in colorectal cancer is correlated with increased proliferation and spontaneous apoptosis. American journal of clinical pathology **2011**;135:245-52
526. Jiang Y, Duan Y, Zhou H. MicroRNA-27a directly targets KRAS to inhibit cell proliferation in esophageal squamous cell carcinoma. Oncology letters **2015**;9:471-7
527. Wiederschain D, Chen L, Johnson B, Bettano K, Jackson D, Taraszka J*, et al.* Contribution of polycomb homologues Bmi-1 and Mel-18 to medulloblastoma pathogenesis. Molecular and cellular biology **2007**;27:4968-79

528. García-Gutiérrez L, Delgado MD, León J. MYC oncogene contributions to release of cell cycle brakes. Genes **2019**;10:244
529. Cappellen D, Schlange T, Bauer M, Maurer F, Hynes NE. Novel c-MYC target genes mediate differential effects on cell proliferation and migration. EMBO reports **2007**;8:70-6
530. Olsson A, Feber A, Edwards S, Te Poele R, Giddings I, Merson S*, et al.* Role of E2F3 expression in modulating cellular proliferation rate in human bladder and prostate cancer cells. Oncogene **2007**;26:1028-37
531. Li X, Li H, Zhang R, Liu J, Liu J. MicroRNA-449a inhibits proliferation and induces apoptosis by directly repressing E2F3 in gastric cancer. Cellular physiology and biochemistry **2015**;35:2033-42
532. Oeggerli M, Tomovska S, Schraml P, Calvano-Forte D, Schafroth S, Simon R*, et al.* E2F3 amplification and overexpression is associated with invasive tumor growth and rapid tumor cell proliferation in urinary bladder cancer. Oncogene **2004**;23:5616-23
533. Carnero A, Blanco-Aparicio C, Renner O, Link W, Leal JF. The PTEN/PI3K/AKT signalling pathway in cancer, therapeutic implications. Current cancer drug targets **2008**;8:187-98
534. Hickman ES, Moroni MC, Helin K. The role of p53 and pRB in apoptosis and cancer. Current opinion in genetics & development **2002**;12:60-6
535. Huang SS, Huang JS. TGF-β control of cell proliferation. Journal of cellular biochemistry **2005**;96:447-62
536. Wu H, Huang M, Cao P, Wang T, Shu Y, Liu P. MiR-135a targets JAK2 and inhibits gastric cancer cell proliferation. Cancer biology & therapy **2012**;13:281-8
537. Yamazaki Y, Kaziro Y, Koide H. Ral Promotes Anchorage-Independent Growth of a Human Fibrosarcoma, HT10801. Biochemical and biophysical research communications **2001**;280:868-73
538. Qiu R-G, Abo A, McCormick F, Symons M. Cdc42 regulates anchorage-independent growth and is necessary for Ras transformation. Molecular and cellular biology **1997**;17:3449-58
539. De Pascalis C, Etienne-Manneville S. Single and collective cell migration: the mechanics of adhesions. Molecular biology of the cell **2017**;28:1833-46
540. Xie F, Ling L, van Dam H, Zhou F, Zhang L. TGF-β signaling in cancer metastasis. Acta biochimica et biophysica Sinica **2018**;50:121-32
541. Heerboth S, Housman G, Leary M, Longacre M, Byler S, Lapinska K*, et al.* EMT and tumor metastasis. Clinical and translational medicine **2015**;4:1-13
542. Nair PR, Wirtz D. Enabling migration by moderation: YAP/TAZ are essential for persistent migration. The Journal of cell biology **2019**;218:1092
543. Zacharek SJ, Fillmore CM, Lau AN, Gludish DW, Chou A, Ho JW*, et al.* Lung stem cell self-renewal relies on BMI1-dependent control of expression at imprinted loci. Cell stem cell **2011**;9:272-81
544. Paranjape AN, Balaji SA, Mandal T, Krushik EV, Nagaraj P, Mukherjee G*, et al.* Bmi1 regulates self-renewal and epithelial to mesenchymal transition in breast cancer cells through Nanog. BMC cancer **2014**;14:1-14

545. Gil J, Bernard D, Peters G. Role of polycomb group proteins in stem cell self-renewal and cancer. DNA and cell biology **2005**;24:117-25
546. Fodde R, Brabletz T. Wnt/β-catenin signaling in cancer stemness and malignant behavior. Current opinion in cell biology **2007**;19:150-8
547. Cordenonsi M, Zanconato F, Azzolin L, Forcato M, Rosato A, Frasson C*, et al.* The Hippo transducer TAZ confers cancer stem cell-related traits on breast cancer cells. Cell **2011**;147:759-72
548. Lian I, Kim J, Okazawa H, Zhao J, Zhao B, Yu J*, et al.* The role of YAP transcription coactivator in regulating stem cell self-renewal and differentiation. Genes & development **2010**;24:1106-18
549. Xia P, Xu X-Y. PI3K/Akt/mTOR signaling pathway in cancer stem cells: from basic research to clinical application. American journal of cancer research **2015**;5:1602
550. Islam S, Mokhtari R, Noman A, Uddin M, Rahman M, Azadi M*, et al.* Sonic hedgehog (Shh) signaling promotes tumorigenicity and stemness via activation of epithelial-to-mesenchymal transition (EMT) in bladder cancer. Molecular carcinogenesis **2016**;55:537-51
551. Pugh CW, Ratcliffe PJ. Regulation of angiogenesis by hypoxia: role of the HIF system. Nature medicine **2003**;9:677-84
552. Nagy JA, Dvorak AM, Dvorak HF. VEGF-A and the induction of pathological angiogenesis. Annu Rev Pathol Mech Dis **2007**;2:251-75
553. Cargnello M, Tcherkezian J, Roux PP. The expanding role of mTOR in cancer cell growth and proliferation. Mutagenesis **2015**;30:169-76
554. Zheng H, Högberg J, Stenius U. ATM-activated autotaxin (ATX) propagates inflammation and DNA damage in lung epithelial cells: a new mode of action for silica-induced DNA damage? Carcinogenesis **2017**;38:1196-206
555. Liu ZH, Chen ML, Zhang Q, Zhang Y, An X, Luo YL*, et al.* ZIC2 is downregulated and represses tumor growth via the regulation of STAT3 in breast cancer. International journal of cancer **2020**;147:505-18
556. Wei-Hua W, Ning Z, Qian C, Dao-Wen J. ZIC2 promotes cancer stem cell traits via up-regulating OCT4 expression in lung adenocarcinoma cells. Journal of Cancer **2020**;11:6070
557. Consortium EP. An integrated encyclopedia of DNA elements in the human genome. Nature **2012**;489:57
558. Zhao Z, Wang L, Bartom E, Marshall S, Rendleman E, Ryan C*, et al.* β-Catenin/Tcf7l2–dependent transcriptional regulation of GLUT1 gene expression by Zic family proteins in colon cancer. Science advances **2019**;5:eaax0698
559. Lu P, Weaver VM, Werb Z. The extracellular matrix: a dynamic niche in cancer progression. Journal of cell biology **2012**;196:395-406
560. Xu Z, Zheng J, Chen Z, Guo J, Li X, Wang X*, et al.* Multilevel regulation of Wnt signaling by Zic2 in colon cancer due to mutation of β-catenin. Cell death & disease **2021**;12:1-13
561. Evan GI, Vousden KH. Proliferation, cell cycle and apoptosis in cancer. nature **2001**;411:342-8

562. Ghosh-Choudhury T, Loomans HA, Wan Y-W, Liu Z, Hawkins SM, Anderson ML. Hyperactivation of FOXM1 drives ovarian cancer growth and metastasis independent of the G2-M cell cycle checkpoint. AACR; 2013.
563. Makrilia N, Kollias A, Manolopoulos L, Syrigos K. Cell adhesion molecules: role and clinical significance in cancer. Cancer investigation **2009**;27:1023-37
564. Hanahan D, Weinberg RA. Hallmarks of cancer: the next generation. cell **2011**;144:646-74
565. Goyama S, Schibler J, Cunningham L, Zhang Y, Rao Y, Nishimoto N*, et al.* Transcription factor RUNX1 promotes survival of acute myeloid leukemia cells. The Journal of clinical investigation **2013**;123:3876-88
566. Akech J, Wixted JJ, Bedard K, Van der Deen M, Hussain S, Guise TA*, et al.* Runx2 association with progression of prostate cancer in patients: mechanisms mediating bone osteolysis and osteoblastic metastatic lesions. Oncogene **2010**;29:811-21
567. Huang B, Qu Z, Ong CW, Tsang YN, Xiao G, Shapiro D*, et al.* RUNX3 acts as a tumor suppressor in breast cancer by targeting estrogen receptor α. Oncogene **2012**;31:527-34
568. Imai M, Muraki M, Takamatsu K, Saito H, Seiki M, Takahashi Y. Spontaneous transformation of human granulosa cell tumours into an aggressive phenotype: a metastasis model cell line. BMC cancer **2008**;8:1-10
569. Bilandzic M, Wang Y, Ahmed N, Luwor RB, Zhu HJ, Findlay JK*, et al.* Betaglycan blocks metastatic behaviors in human granulosa cell tumors by suppressing NFκB-mediated induction of MMP2. Cancer letters **2014**;354:107-14
570. Ito Y. Oncogenic potential of the RUNX gene family:'overview'. Oncogene **2004**;23:4198-208
571. Sweeney KJ, Sarcevic B, Sutherland RL, Musgrove EA. Cyclin D2 activates Cdk2 in preference to Cdk4 in human breast epithelial cells. Oncogene **1997**;14:1329-40
572. Bouchard C, Thieke K, Maier A, Saffrich R, Hanley-Hyde J, Ansorge W*, et al.* Direct induction of cyclin D2 by Myc contributes to cell cycle progression and sequestration of p27. The EMBO journal **1999**;18:5321-33
573. Lu X, Sun S, Qi J, Li W, Liu L, Zhang Y*, et al.* Bmi1 regulates the proliferation of cochlear supporting cells via the canonical Wnt signaling pathway. Molecular neurobiology **2017**;54:1326-39
574. De Luca A, Maiello MR, D'Alessio A, Pergameno M, Normanno N. The RAS/RAF/MEK/ERK and the PI3K/AKT signalling pathways: role in cancer pathogenesis and implications for therapeutic approaches. Expert opinion on therapeutic targets **2012**;16:S17-S27
575. Feig LA. Ral-GTPases: approaching their 15 minutes of fame. Trends in cell biology **2003**;13:419-25
576. Ward AF, Braun BS, Shannon KM. Targeting oncogenic Ras signaling in hematologic malignancies. Blood, The Journal of the American Society of Hematology **2012**;120:3397-406

577. Cherfils J, Zeghouf M. Regulation of small gtpases by gefs, gaps, and gdis. Physiological reviews **2013**;93:269-309
578. Chambard J-C, Lefloch R, Pouysségur J, Lenormand P. ERK implication in cell cycle regulation. Biochimica et Biophysica Acta (BBA)-Molecular Cell Research **2007**;1773:1299-310
579. Weinberg RA. The biology of cancer. Garland science; 2013.
580. Liu Y, Liu F, Yu H, Zhao X, Sashida G, Deblasio A*, et al.* Akt phosphorylates the transcriptional repressor bmi1 to block its effects on the tumor-suppressing ink4a-arf locus. Science signaling **2012**;5:ra77-ra
581. Dyson N. The regulation of E2F by pRB-family proteins. Genes & development **1998**;12:2245-62
582. Weinberg RA. Tumor suppressor genes. Science **1991**;254:1138-46
583. Maddika S, Ande SR, Panigrahi S, Paranjothy T, Weglarczyk K, Zuse A*, et al.* Cell survival, cell death and cell cycle pathways are interconnected: implications for cancer therapy. Drug Resistance Updates **2007**;10:13-29
584. Guadamillas MC, Cerezo A, Del Pozo MA. Overcoming anoikis–pathways to anchorage-independent growth in cancer. Journal of cell science **2011**;124:3189-97
585. Loret N, Denys H, Tummers P, Berx G. The role of epithelial-to-mesenchymal plasticity in ovarian cancer progression and therapy resistance. Cancers **2019**;11:838
586. Naora H, Montell DJ. Ovarian cancer metastasis: integrating insights from disparate model organisms. Nature reviews cancer **2005**;5:355-66
587. Takahashi M, Ishida T, Traub O, Corson MA, Berk BC. Mechanotransduction in endothelial cells: temporal signaling events in response to shear stress. Journal of vascular research **1997**;34:212-9
588. Zhao Y, He M, Cui L, Gao M, Zhang M, Yue F*, et al.* Chemotherapy exacerbates ovarian cancer cell migration and cancer stem cell-like characteristics through GLI1. British journal of cancer **2020**;122:1638-48
589. Pannuti A, Foreman K, Rizzo P, Osipo C, Golde T, Osborne B*, et al.* Targeting Notch to target cancer stem cells. Clinical cancer research **2010**;16:3141-52
590. Ma R-g, Zhang Y, Sun T-t, Cheng B. Epigenetic regulation by polycomb group complexes: focus on roles of CBX proteins. Journal of Zhejiang University Science B **2014**;15:412-28
591. Zhu D, Wan X, Huang H, Chen X, Liang W, Zhao F*, et al.* Knockdown of Bmi1 inhibits the stemness properties and tumorigenicity of human bladder cancer stem cell-like side population cells. Oncology Reports **2014**;31:727-36
592. Blagosklonny MV, Pardee AB. The restriction point of the cell cycle. Cell cycle **2002**;1:102-9
593. Stark GR, Taylor WR. Analyzing the G2/M checkpoint. Checkpoint Controls and Cancer **2004**:51-82
594. Amon A. The spindle checkpoint. Current opinion in genetics & development **1999**;9:69-75

595. Noguchi E. The DNA replication checkpoint and preserving genomic integrity during DNA synthesis. Nature Education **2010**;3:46
596. Stewart A, Pickard L, Hallsworth AE, Sauvaigo S, Muggiolu G, Raynaud F*, et al.* A study of combinatorial growth inhibition, cell death and DNA damage repair caused by CHK1 inhibitor SRA737 and WEE1 inhibitor adavosertib in TP53 mutated cell lines. AACR; 2021.
597. Wang D, Wang M, Jiang N, Zhang Y, Bian X, Wang X*, et al.* Effective use of PI3K inhibitor BKM120 and PARP inhibitor Olaparib to treat PIK3CA mutant ovarian cancer. Oncotarget **2016**;7:13153
598. Stubbs F, Birnie M, Biddie S, Lightman S, Conway-Campbell B. SKOV3 cells containing a truncated ARID1a protein have a restricted genome-wide response to glucocorticoids. Molecular and cellular endocrinology **2018**;461:226-35
599. Bitler BG, Fatkhutdinov N, Zhang R. Potential therapeutic targets in ARID1A-mutated cancers. Expert opinion on therapeutic targets **2015**;19:1419-22
600. Hu X, Xia M, Wang J, Yu H, Chai J, Zhang Z*, et al.* Dual PI3K/mTOR inhibitor PKI-402 suppresses the growth of ovarian cancer cells by degradation of Mcl-1 through autophagy. Biomedicine & Pharmacotherapy **2020**;129:110397
601. Saito M, Okamoto A, Kohno T, Takakura S, Shinozaki H, Isonishi S*, et al.* Allelic imbalance and mutations of the PTEN gene in ovarian cancer. International journal of cancer **2000**;85:160-5
602. Portela A, Esteller M. Epigenetic modifications and human disease. Nature biotechnology **2010**;28:1057-68
603. Chen YG, Satpathy AT, Chang HY. Gene regulation in the immune system by long noncoding RNAs. Nature immunology **2017**;18:962-72
604. Ponting CP, Oliver PL, Reik W. Evolution and functions of long noncoding RNAs. Cell **2009**;136:629-41
605. Goldberg AD, Allis CD, Bernstein E. Epigenetics: a landscape takes shape. Cell **2007**;128:635-8
606. Baer C, Claus R, Plass C. Genome-wide epigenetic regulation of miRNAs in cancer. Cancer research **2013**;73:473-7
607. Baylin SB, Jones PA. A decade of exploring the cancer epigenome—biological and translational implications. Nature Reviews Cancer **2011**;11:726-34
608. Kouzarides T. Chromatin modifications and their function. Cell **2007**;128:693-705
609. Misri S, Pandita S, Kumar R, Pandita T. Telomeres, histone code, and DNA damage response. Cytogenetic and genome research **2008**;122:297-307
610. Lawrence M, Daujat S, Schneider R. Lateral thinking: how histone modifications regulate gene expression. Trends in Genetics **2016**;32:42-56
611. Pu M, Li C, Qi X, Chen J, Wang Y, Gao L*, et al.* MiR-1254 suppresses HO-1 expression through seed region-dependent silencing and non-seed interaction with TFAP2A transcript to attenuate NSCLC growth. PLoS genetics **2017**;13:e1006896

612. Zhang M, Huang N, Yang X, Luo J, Yan S, Xiao F*, et al.* A novel protein encoded by the circular form of the SHPRH gene suppresses glioma tumorigenesis. Oncogene **2018**;37:1805-14
613. Huang J-Z, Chen M, Chen D, Gao X-C, Zhu S, Huang H*, et al.* A peptide encoded by a putative lncRNA HOXB-AS3 suppresses colon cancer growth. Molecular cell **2017**;68:171-84. e6
614. Dimitrova N, Zamudio JR, Jong RM, Soukup D, Resnick R, Sarma K*, et al.* LincRNA-p21 activates p21 in cis to promote Polycomb target gene expression and to enforce the G1/S checkpoint. Molecular cell **2014**;54:777-90
615. Lin A, Li C, Xing Z, Hu Q, Liang K, Han L*, et al.* The LINK-A lncRNA activates normoxic HIF1α signalling in triple-negative breast cancer. Nature cell biology **2016**;18:213-24
616. Lessard J, Schumacher A, Thorsteinsdottir U, van Lohuizen M, Magnuson T, Sauvageau G. Functional antagonism of the Polycomb-Group genes eed and Bmi1 in hemopoietic cell proliferation. Genes & development **1999**;13:2691-703
617. Grossniklaus U, Paro R. Transcriptional silencing by polycomb-group proteins. Cold Spring Harbor perspectives in biology **2014**;6:a019331
618. Roma-Rodrigues C, Mendes R, Baptista PV, Fernandes AR. Targeting tumor microenvironment for cancer therapy. International journal of molecular sciences **2019**;20:840
619. Brücher BL, Jamall IS. Cell-cell communication in the tumor microenvironment, carcinogenesis, and anticancer treatment. Cellular Physiology and Biochemistry **2014**;34:213-43
620. Quail DF, Joyce JA. Microenvironmental regulation of tumor progression and metastasis. Nature medicine **2013**;19:1423-37
621. Levental KR, Yu H, Kass L, Lakins JN, Egeblad M, Erler JT*, et al.* Matrix crosslinking forces tumor progression by enhancing integrin signaling. Cell **2009**;139:891-906
622. Jing Y, Han Z, Zhang S, Liu Y, Wei L. Epithelial-Mesenchymal Transition in tumor microenvironment. Cell & bioscience **2011**;1:1-7
623. Nyberg P, Salo T, Kalluri R. Tumor microenvironment and angiogenesis. Front Biosci **2008**;13:6537-53
624. Castells M, Thibault B, Delord J-P, Couderc B. Implication of tumor microenvironment in chemoresistance: tumor-associated stromal cells protect tumor cells from cell death. International journal of molecular sciences **2012**;13:9545-71
625. Jamieson S, Fuller PJ. Molecular pathogenesis of granulosa cell tumors of the ovary. Endocrine reviews **2012**;33:109-44
626. Schmidt M, Kammerer U, Segerer S, Cramer A, Kohrenhagen N, Dietl J*, et al.* Glucose metabolism and angiogenesis in granulosa cell tumors of the ovary: activation of Akt, expression of M2PK, TKTL1 and VEGF. European Journal of Obstetrics & Gynecology and Reproductive Biology **2008**;139:72-8

627. Tao X, Sood AK, Deavers MT, Schmeler KM, Nick AM, Coleman RL*, et al.* Anti-angiogenesis therapy with bevacizumab for patients with ovarian granulosa cell tumors. Gynecologic oncology **2009**;114:431-6
628. Färkkilä A, Anttonen M, Pociuviene J, Leminen A, Butzow R, Heikinheimo M*, et al.* Vascular endothelial growth factor (VEGF) and its receptor VEGFR-2 are highly expressed in ovarian granulosa cell tumors. European journal of endocrinology **2011**;164:115
629. Chu S, Rushdi S, Zumpe ET, Mamers P, Healy D, Jobling T*, et al.* FSH-regulated gene expression profiles in ovarian tumours and normal ovaries. Molecular human reproduction **2002**;8:426-33
630. Liu J, Park E-S, Jo M. Runt-related transcription factor 1 regulates luteinized hormone-induced prostaglandin-endoperoxide synthase 2 expression in rat periovulatory granulosa cells. Endocrinology **2009**;150:3291-300
631. Jo M, Curry Jr TE. Luteinizing hormone-induced RUNX1 regulates the expression of genes in granulosa cells of rat periovulatory follicles. Molecular endocrinology **2006**;20:2156-72
632. Park E-S, Lind A-K, Dahm-Kähler P, Brännström M, Carletti MZ, Christenson LK*, et al.* RUNX2 transcription factor regulates gene expression in luteinizing granulosa cells of rat ovaries. Molecular endocrinology **2010**;24:846-58
633. Dinh HQ, Lin X, Abbasi F, Nameki R, Haro M, Olingy CE*, et al.* Single-cell transcriptomics identifies gene expression networks driving differentiation and tumorigenesis in the human fallopian tube. Cell Reports **2021**;35:108978
634. Chan-Penebre E, Armstrong K, Drew A, Grassian AR, Feldman I, Knutson SK*, et al.* Selective killing of SMARCA2-and SMARCA4-deficient small cell carcinoma of the ovary, hypercalcemic type cells by inhibition of EZH2: in vitro and in vivo preclinical models. Molecular cancer therapeutics **2017**;16:850-60
635. Anttonen M, Pihlajoki M, Andersson N, Georges A, l'Hôte D, Vattulainen S*, et al.* FOXL2, GATA4, and SMAD3 co-operatively modulate gene expression, cell viability and apoptosis in ovarian granulosa cell tumor cells. PLoS One **2014**;9:e85545
636. Cheng J-C, Chang H-M, Qiu X, Fang L, Leung PC. FOXL2-induced follistatin attenuates activin A-stimulated cell proliferation in human granulosa cell tumors. Biochemical and biophysical research communications **2014**;443:537-42
637. Wang C, Lv X, Jiang C, Cordes CM, Fu L, Lele SM*, et al.* Transforming growth factor alpha (TGFα) regulates granulosa cell tumor (GCT) cell proliferation and migration through activation of multiple pathways. PloS one **2012**;7:e48299
638. Hnit SST, Xie C, Yao M, Holst J, Bensoussan A, De Souza P*, et al.* p27Kip1 signaling: Transcriptional and post-translational regulation. The international journal of biochemistry & cell biology **2015**;68:9-14
639. Colombo N, Parma G, Zanagnolo V, Insinga A. Management of ovarian stromal cell tumors. Journal of Clinical Oncology **2007**;25:2944-51

640. Sekkate S, Kairouani M, Serji B, M'Rabti H, El Ghissassi I, Errihani H. Granulosa cell tumors of the ovary. Bulletin du cancer **2014**;101:93-101
641. Levin G, Zigron R, Haj-Yahya R, Matan LS, Rottenstreich A. Granulosa cell tumor of ovary: A systematic review of recent evidence. European Journal of Obstetrics and Gynecology and Reproductive Biology **2018**;225:57-61
642. Gorczynski MJ, Grembecka J, Zhou Y, Kong Y, Roudaiya L, Douvas MG*, et al.* Supplemental Data Allosteric Inhibition of the Protein-Protein Interaction between the Leukemia-Associated.
643. Cunningham L, Finckbeiner S, Hyde RK, Southall N, Marugan J, Yedavalli VR*, et al.* Identification of benzodiazepine Ro5-3335 as an inhibitor of CBF leukemia through quantitative high throughput screen against RUNX1–CBFβ interaction. Proceedings of the National Academy of Sciences **2012**;109:14592-7
644. Illendula A, Pulikkan JA, Zong H, Grembecka J, Xue L, Sen S*, et al.* A small-molecule inhibitor of the aberrant transcription factor CBFβ-SMMHC delays leukemia in mice. Science **2015**;347:779-84
645. Rajalingam K, Schreck R, Rapp UR, Albert Š. Ras oncogenes and their downstream targets. Biochimica et Biophysica Acta (BBA)-Molecular Cell Research **2007**;1773:1177-95
646. McCubrey J, Steelman L, Abrams S, Bertrand F, Ludwig D, Bäsecke J*, et al.* Targeting survival cascades induced by activation of Ras/Raf/MEK/ERK, PI3K/PTEN/Akt/mTOR and Jak/STAT pathways for effective leukemia therapy. Leukemia **2008**;22:708-22
647. Bonni A, Brunet A, West AE, Datta SR, Takasu MA, Greenberg ME. Cell survival promoted by the Ras-MAPK signaling pathway by transcription-dependent and-independent mechanisms. Science **1999**;286:1358-62
648. Zhang W, Liu HT. MAPK signal pathways in the regulation of cell proliferation in mammalian cells. Cell research **2002**;12:9-18
649. Qu J-L, Qu X-J, Zhao M-F, Teng Y-E, Zhang Y, Hou K-Z*, et al.* Gastric cancer exosomes promote tumour cell proliferation through PI3K/Akt and MAPK/ERK activation. Digestive and liver disease **2009**;41:875-80
650. Drosten M, Dhawahir A, Sum EY, Urosevic J, Lechuga CG, Esteban LM*, et al.* Genetic analysis of Ras signalling pathways in cell proliferation, migration and survival. The EMBO journal **2010**;29:1091-104
651. Sun Y, Liu W-Z, Liu T, Feng X, Yang N, Zhou H-F. Signaling pathway of MAPK/ERK in cell proliferation, differentiation, migration, senescence and apoptosis. Journal of Receptors and Signal Transduction **2015**;35:600-4

Appendix I: Gene lists of selected GSEA gene sets

Notes:
1, The genes are ranked as FDR value from small to large by each category of genes.
2, Symbol: Gene symbol; Ensembl: Ensembl Gene ID; Entrez: Entrez Gene ID; logFC: $\log_2$ (fold change); logCPM: $\log_2$ (count per million); FDR: false discovery rate.

Table S1 Gene list of KRAS.600_UP.V1_UP in SKOV3 ZIC2-KO model

	Category	Symbol	EntrezGene	Ensembl	logFC	logCPM	Pvalue	FDR
1	Commonly	PCDH9	5101	ENSG00000184226	-4.59	6.25	4.59E-49	5.53E-47
2	Commonly	NMNAT2	23057	ENSG00000157064	-1.70	3.76	1.63E-33	9.38E-32
3	Commonly	REEP2	51308	ENSG00000132563	-2.08	5.54	2.14E-32	1.15E-30
4	Commonly	FLT4	2324	ENSG00000037280	-3.88	1.78	5.91E-32	3.09E-30
5	Commonly	KIAA1549L	25758	ENSG00000110427	-1.13	4.32	6.76E-32	3.52E-30
6	Commonly	ETV1	2115	ENSG00000006468	-3.63	2.03	3.16E-29	1.36E-27
7	Commonly	ITPKA	3706	ENSG00000137825	-1.59	2.76	8.70E-28	3.36E-26
8	Commonly	KIF5C	3800	ENSG00000168280	-2.81	1.18	9.42E-28	3.62E-26
9	Commonly	ITGB2	3689	ENSG00000160255	2.08	2.32	1.05E-26	3.73E-25
10	Commonly	RBP4	5950	ENSG00000138207	-3.82	1.60	1.31E-24	3.96E-23
11	Commonly	RRAGD	58528	ENSG00000025039	-1.10	4.91	3.10E-22	7.97E-21
12	Commonly	WNT7A	7476	ENSG00000154764	1.34	6.27	5.28E-16	8.49E-15
13	Commonly	ZNF529	57711	ENSG00000186020	-0.73	4.31	1.57E-14	2.22E-13
14	Commonly	RCAN2	10231	ENSG00000172348	-2.57	0.66	1.58E-14	2.23E-13
15	Commonly	C1QTNF1	114897	ENSG00000173918	-2.49	1.36	4.46E-10	4.05E-09
16	Commonly	FAM174B	400451	ENSG00000185442	0.99	4.17	1.39E-09	1.19E-08
17	Commonly	SORL1	6653	ENSG00000137642	0.98	5.46	2.32E-09	1.94E-08
18	Commonly	ANK3	288	ENSG00000151150	-1.59	2.46	1.32E-08	1.01E-07
19	Commonly	FMNL2	114793	ENSG00000157827	0.42	7.33	6.94E-07	4.10E-06
20	Commonly	DOCK4	9732	ENSG00000128512	0.82	3.39	1.40E-06	7.82E-06
21	Commonly	NAP1L2	4674	ENSG00000186462	-1.46	0.60	2.05E-06	1.11E-05
22	Commonly	UGT8	7368	ENSG00000174607	-1.04	3.38	1.44E-05	6.70E-05
23	Commonly	ETV5	2119	ENSG00000244405	-1.24	4.79	2.75E-05	1.22E-04
24	Commonly	MKRN3	7681	ENSG00000179455	-1.10	1.16	6.67E-05	2.73E-04
25	Commonly	GLRX	2745	ENSG00000173221	-1.09	2.60	4.11E-04	1.44E-03
26	Commonly	DNMBP	23268	ENSG00000107554	-0.48	3.93	4.59E-04	1.59E-03
27	Commonly	HEY1	23462	ENSG00000164683	-0.67	1.95	1.46E-03	4.50E-03
28	Commonly	ADAM19	8728	ENSG00000135074	-0.54	5.37	4.20E-03	1.15E-02
29	Commonly	TRIM45	80263	ENSG00000134253	-0.42	2.03	5.69E-03	1.50E-02
30	Commonly	RREB1	6239	ENSG00000124782	-0.25	5.30	5.74E-03	1.51E-02
31	Commonly	TRIM36	55521	ENSG00000152503	-0.30	4.21	6.62E-03	1.72E-02
32	Commonly	NRP1	8829	ENSG00000099250	-0.26	7.78	1.96E-02	4.39E-02
33	Oppositely	SCN1B	6324	ENSG00000105711	-1.55	3.77	5.95E-35	3.79E-33
34	Oppositely	TRIB2	28951	ENSG00000071575	1.75	5.15	9.39E-35	5.96E-33
35	Oppositely	KCNH2	3757	ENSG00000055118	-5.35	0.63	1.84E-21	4.56E-20
36	Oppositely	SOX9	6662	ENSG00000125398	3.53	2.03	1.04E-20	2.40E-19
37	Oppositely	CEACAM1	634	ENSG00000079385	-7.68	-0.35	2.89E-14	3.98E-13
38	Oppositely	CEND1	51286	ENSG00000184524	-4.07	0.95	3.62E-14	4.94E-13
39	Oppositely	SPP1	6696	ENSG00000118785	1.56	7.05	4.71E-12	5.24E-11
40	Oppositely	VEGFC	7424	ENSG00000150630	-0.72	4.07	1.37E-09	1.18E-08
41	Oppositely	SPRY2	10253	ENSG00000136158	-1.12	3.25	3.55E-09	2.92E-08
42	Oppositely	PTX3	5806	ENSG00000163661	-2.45	-0.22	7.52E-06	3.69E-05
43	Oppositely	MMP17	4326	ENSG00000198598	-0.90	1.11	1.05E-05	4.99E-05
44	Oppositely	MGAT4A	11320	ENSG00000071073	-0.54	4.84	1.26E-05	5.94E-05
45	Oppositely	KIF5A	3798	ENSG00000155980	-1.57	-0.14	4.77E-05	2.01E-04
46	Oppositely	GNG11	2791	ENSG00000127920	-0.33	6.60	1.87E-04	7.04E-04
47	Oppositely	PMS2P4	5382	ENSG00000067601	0.65	0.68	1.47E-03	4.53E-03
48	Oppositely	MTMR8	55613	ENSG00000102043	1.25	-0.35	1.82E-03	5.47E-03
49	Oppositely	ZNF528	84436	ENSG00000167555	-0.20	5.51	2.48E-03	7.21E-03
50	Oppositely	IL1R2	7850	ENSG00000115590	-1.39	0.37	3.05E-03	8.65E-03
51	Oppositely	MMP11	4320	ENSG00000099953	-1.15	1.72	6.34E-03	1.65E-02
52	Oppositely	STX1A	6804	ENSG00000106089	-0.40	2.26	8.03E-03	2.03E-02
53	Oppositely	CYP27B1	1594	ENSG00000111012	0.55	0.35	1.76E-02	4.00E-02
54	Independently	SRGN	5552	ENSG00000122862	-7.75	5.19	1.64E-137	2.15E-134
55	Independently	RTN1	6252	ENSG00000139970	-3.51	3.10	4.16E-67	1.18E-64

	Category	Symbol	EntrezGene	Ensembl	logFC	logCPM	Pvalue	FDR
56	Independently	CALB1	793	ENSG00000104327	1.73	8.73	4.62E-58	9.28E-56
57	Independently	CHRNA3	1136	ENSG00000080644	-2.83	1.48	4.38E-39	3.48E-37
58	Independently	FAM155B	27112	ENSG00000130054	-2.38	1.31	1.55E-30	7.19E-29
59	Independently	BMP7	655	ENSG00000101144	-5.47	0.61	7.99E-30	3.58E-28
60	Independently	KIT	3815	ENSG00000157404	-3.30	2.17	4.85E-29	2.04E-27
61	Independently	SLC6A15	55117	ENSG00000072041	-5.53	1.59	2.48E-27	9.15E-26
62	Independently	MMP1	4312	ENSG00000196611	-4.91	6.54	4.50E-27	1.63E-25
63	Independently	KCNJ8	3764	ENSG00000121361	-4.93	-0.32	1.98E-26	6.94E-25
64	Independently	PTGS2	5743	ENSG00000073756	-5.01	2.16	6.10E-24	1.77E-22
65	Independently	MMP10	4319	ENSG00000166670	-4.55	4.13	8.38E-23	2.24E-21
66	Independently	PLAU	5328	ENSG00000122861	1.42	7.72	1.40E-17	2.53E-16
67	Independently	HTR7	3363	ENSG00000148680	-3.90	-0.52	8.21E-17	1.41E-15
68	Independently	ITGBL1	9358	ENSG00000198542	-2.03	0.70	1.02E-15	1.59E-14
69	Independently	NRCAM	4897	ENSG00000091129	0.99	5.95	2.32E-13	2.95E-12
70	Independently	SYNE3	161176	ENSG00000176438	-1.18	2.36	1.21E-11	1.28E-10
71	Independently	MLXIPL	51085	ENSG00000009950	-3.22	1.16	2.91E-10	2.69E-09
72	Independently	SIGLEC15	284266	ENSG00000197046	-1.69	1.09	3.03E-09	2.51E-08
73	Independently	CDK5R1	8851	ENSG00000176749	-0.67	4.36	2.43E-08	1.80E-07
74	Independently	SNAP91	9892	ENSG00000065609	-2.31	2.00	9.00E-08	6.11E-07
75	Independently	DUSP6	1848	ENSG00000139318	-1.68	1.87	2.30E-07	1.47E-06
76	Independently	TMEM158	25907	ENSG00000249992	-1.15	3.37	2.06E-06	1.12E-05
77	Independently	DDX6	1656	ENSG00000110367	-0.34	7.53	4.09E-06	2.10E-05
78	Independently	GLDC	2731	ENSG00000178445	1.46	4.89	7.16E-06	3.52E-05
79	Independently	HAS2	3037	ENSG00000170961	1.69	0.89	2.70E-05	1.20E-04
80	Independently	ANPEP	290	ENSG00000166825	-0.78	6.81	3.61E-05	1.56E-04
81	Independently	LPAR1	1902	ENSG00000198121	-0.44	4.38	9.34E-05	3.75E-04
82	Independently	PNMA2	10687	ENSG00000240694	0.73	5.18	5.19E-04	1.78E-03
83	Independently	SCN2A	6326	ENSG00000136531	0.64	4.44	5.25E-04	1.80E-03
84	Independently	LIMCH1	22998	ENSG00000064042	0.40	6.96	6.45E-04	2.16E-03
85	Independently	CTNND2	1501	ENSG00000169862	-1.24	0.62	1.46E-03	4.49E-03
86	Independently	ANGPTL4	51129	ENSG00000167772	-0.79	3.04	3.98E-03	1.10E-02
87	Independently	TEC	7006	ENSG00000135605	-0.35	3.49	4.09E-03	1.12E-02
88	Independently	INHBA	3624	ENSG00000122641	-1.06	4.59	6.18E-03	1.61E-02
89	Independently	ETV4	2118	ENSG00000175832	-0.91	3.64	6.18E-03	1.61E-02
90	Independently	HS3ST3B1	9953	ENSG00000125430	0.39	5.58	1.03E-02	2.51E-02
91	Independently	EN2	2020	ENSG00000164778	-0.53	1.52	1.15E-02	2.78E-02
92	Independently	ADGRA2	25960	ENSG00000020181	-0.40	5.86	1.99E-02	4.45E-02
93	Independently	G0S2	50486	ENSG00000123689	0.52	3.90	2.13E-02	4.73E-02

Table S2 Gene list of KRAS.600_UP.V1_UP in OVCAR3 ZIC2-OE model

	Category	Symbol	EntrezGene	Ensembl	logFC	logCPM	Pvalue	FDR
1	Commonly	RCAN2	10231	ENSG00000172348	3.10	6.42	1.28E-162	1.37E-160
2	Commonly	HEY1	23462	ENSG00000164683	3.31	3.25	1.57E-147	1.36E-145
3	Commonly	KIF5C	3800	ENSG00000168280	1.98	4.61	2.16E-144	1.75E-142
4	Commonly	ITGB2	3689	ENSG00000160255	-3.38	3.41	8.11E-123	5.21E-121
5	Commonly	TRIM36	55521	ENSG00000152503	3.12	2.58	5.20E-96	2.22E-94
6	Commonly	WNT7A	7476	ENSG00000154764	-3.79	2.98	5.51E-80	1.76E-78
7	Commonly	RBP4	5950	ENSG00000138207	4.74	2.23	1.39E-70	3.68E-69
8	Commonly	ADAM19	8728	ENSG00000135074	1.18	5.66	1.70E-70	4.47E-69
9	Commonly	FAM174B	400451	ENSG00000185442	-1.47	4.59	4.28E-51	7.12E-50
10	Commonly	NAP1L2	4674	ENSG00000186462	2.53	1.43	6.59E-40	7.66E-39
11	Commonly	TRIM45	80263	ENSG00000134253	1.28	4.34	1.45E-35	1.45E-34
12	Commonly	NMNAT2	23057	ENSG00000157064	1.30	3.85	3.58E-33	3.30E-32
13	Commonly	KIAA1549L	25758	ENSG00000110427	1.38	6.25	1.08E-32	9.77E-32
14	Commonly	C1QTNF1	114897	ENSG00000173918	1.06	3.65	9.69E-30	7.73E-29
15	Commonly	NRP1	8829	ENSG00000099250	1.95	0.58	6.62E-26	4.58E-25
16	Commonly	DOCK4	9732	ENSG00000128512	-0.71	4.29	2.13E-20	1.14E-19
17	Commonly	ANK3	288	ENSG00000151150	0.55	6.80	2.58E-18	1.25E-17
18	Commonly	MKRN3	7681	ENSG00000179455	0.63	3.46	2.38E-17	1.10E-16
19	Commonly	PCDH9	5101	ENSG00000184226	2.17	0.70	2.14E-16	9.39E-16
20	Commonly	UGT8	7368	ENSG00000174607	0.39	5.27	6.63E-15	2.67E-14
21	Commonly	DNMBP	23268	ENSG00000107554	0.80	4.67	7.78E-12	2.61E-11
22	Commonly	RREB1	6239	ENSG00000124782	0.42	6.42	5.30E-11	1.68E-10
23	Commonly	ETV5	2119	ENSG00000244405	0.64	4.86	9.82E-11	3.05E-10
24	Commonly	RRAGD	58528	ENSG00000025039	0.58	3.81	3.96E-08	1.01E-07
25	Commonly	GLRX	2745	ENSG00000173221	0.48	2.35	1.02E-07	2.54E-07
26	Commonly	PMS2P4	5382	ENSG00000067601	-0.66	0.98	6.35E-07	1.48E-06
27	Commonly	SORL1	6653	ENSG00000137642	-0.77	5.87	8.55E-07	1.98E-06
28	Commonly	ETV1	2115	ENSG00000006468	1.04	0.80	1.80E-05	3.66E-05
29	Commonly	FLT4	2324	ENSG00000037280	0.55	0.08	1.09E-03	1.85E-03
30	Commonly	REEP2	51308	ENSG00000132563	0.51	2.67	2.20E-03	3.59E-03
31	Commonly	FMNL2	114793	ENSG00000157827	-0.17	6.68	2.39E-03	3.89E-03
32	Commonly	ZNF529	57711	ENSG00000186020	0.17	4.23	4.41E-03	6.95E-03
33	Commonly	ITPKA	3706	ENSG00000137825	0.33	1.98	1.98E-02	2.85E-02
34	Oppositely	TRIB2	28951	ENSG00000071575	1.34	5.55	5.71E-81	1.86E-79
35	Oppositely	KCNH2	3757	ENSG00000055118	-3.13	2.36	7.56E-67	1.83E-65
36	Oppositely	CEND1	51286	ENSG00000184524	-2.73	1.24	1.21E-56	2.29E-55
37	Oppositely	MMP11	4320	ENSG00000099953	-2.40	2.43	2.14E-49	3.41E-48
38	Oppositely	SPP1	6696	ENSG00000118785	2.49	1.36	1.46E-45	2.04E-44
39	Oppositely	VEGFC	7424	ENSG00000150630	-2.61	0.66	2.97E-28	2.25E-27
40	Oppositely	SCN1B	6324	ENSG00000105711	-1.68	1.07	1.14E-26	8.08E-26
41	Oppositely	IL1R2	7850	ENSG00000115590	-1.31	2.92	2.12E-20	1.14E-19
42	Oppositely	SOX9	6662	ENSG00000125398	1.04	5.12	2.48E-19	1.26E-18
43	Oppositely	ZNF528	84436	ENSG00000167555	-1.32	0.45	1.92E-18	9.39E-18
44	Oppositely	MGAT4A	11320	ENSG00000071073	-1.22	4.52	8.46E-16	3.59E-15
45	Oppositely	CEACAM1	634	ENSG00000079385	-1.67	0.02	9.25E-14	3.50E-13
46	Oppositely	GNG11	2791	ENSG00000127920	-0.80	2.34	7.75E-13	2.77E-12
47	Oppositely	PTX3	5806	ENSG00000163661	-1.79	3.82	1.10E-10	3.42E-10
48	Oppositely	MMP17	4326	ENSG00000198598	-0.95	1.29	5.45E-08	1.38E-07
49	Oppositely	STX1A	6804	ENSG00000106089	-0.53	2.37	1.15E-06	2.63E-06
50	Oppositely	MTMR8	55613	ENSG00000102043	0.72	1.21	3.13E-06	6.85E-06
51	Oppositely	SPRY2	10253	ENSG00000136158	-0.41	3.06	1.59E-04	2.93E-04
52	Oppositely	KIF5A	3798	ENSG00000155980	-0.41	2.43	7.26E-04	1.25E-03
53	Oppositely	CYP27B1	1594	ENSG00000111012	0.40	0.94	4.98E-03	7.78E-03
54	Independently	MMD	23531	ENSG00000108960	2.16	5.99	1.66E-126	1.10E-124
55	Independently	PLA2G3	50487	ENSG00000100078	8.91	0.87	3.94E-121	2.45E-119

	Category	Symbol	EntrezGene	Ensembl	logFC	logCPM	Pvalue	FDR
56	Independently	CTNNA2	1496	ENSG00000066032	-4.88	1.90	1.60E-109	8.42E-108
57	Independently	DNM3	26052	ENSG00000197959	-1.53	4.75	8.23E-106	4.06E-104
58	Independently	ITGA2	3673	ENSG00000164171	1.26	4.30	1.73E-71	4.66E-70
59	Independently	SLCO5A1	81796	ENSG00000137571	2.41	2.49	2.65E-66	6.33E-65
60	Independently	DUSP4	1846	ENSG00000120875	2.57	5.02	5.70E-61	1.20E-59
61	Independently	RELN	5649	ENSG00000189056	2.89	1.45	2.32E-55	4.31E-54
62	Independently	TGM2	7052	ENSG00000198959	-4.30	6.10	3.27E-52	5.62E-51
63	Independently	FOXG1	2290	ENSG00000176165	1.11	5.78	6.04E-47	9.03E-46
64	Independently	CXCR4	7852	ENSG00000121966	2.64	1.11	7.52E-47	1.12E-45
65	Independently	SYT1	6857	ENSG00000067715	-3.07	3.29	2.51E-46	3.65E-45
66	Independently	SLCO4A1	28231	ENSG00000101187	-3.37	2.09	5.47E-43	7.08E-42
67	Independently	CLSTN2	64084	ENSG00000158258	2.32	3.06	7.33E-42	9.12E-41
68	Independently	GRIN2A	2903	ENSG00000183454	3.02	1.85	4.40E-41	5.35E-40
69	Independently	LGALS14	56891	ENSG00000006659	-2.84	1.74	6.59E-35	6.43E-34
70	Independently	GRM1	2911	ENSG00000152822	3.50	2.75	2.26E-31	1.94E-30
71	Independently	PDE2A	5138	ENSG00000186642	-2.96	0.78	1.27E-26	9.05E-26
72	Independently	EMP1	2012	ENSG00000134531	-2.86	5.58	1.25E-25	8.53E-25
73	Independently	GPR37	2861	ENSG00000170775	1.85	0.52	2.24E-25	1.51E-24
74	Independently	DIRAS2	54769	ENSG00000165023	1.01	6.44	4.22E-24	2.69E-23
75	Independently	LDB3	11155	ENSG00000122367	2.08	0.02	3.58E-21	2.00E-20
76	Independently	ADAM8	101	ENSG00000151651	-1.32	1.65	5.86E-21	3.23E-20
77	Independently	SATB1	6304	ENSG00000182568	2.24	1.58	8.88E-20	4.61E-19
78	Independently	KCNK3	3777	ENSG00000171303	-2.89	0.24	1.30E-18	6.39E-18
79	Independently	EFCAB6	64800	ENSG00000186976	-1.20	0.94	3.93E-17	1.80E-16
80	Independently	SH2D2A	9047	ENSG00000027869	-1.55	-0.03	5.64E-16	2.41E-15
81	Independently	ARHGAP24	83478	ENSG00000138639	1.09	3.96	6.15E-16	2.63E-15
82	Independently	GFI1	2672	ENSG00000162676	1.84	-0.40	1.63E-15	6.81E-15
83	Independently	DHRS9	10170	ENSG00000073737	-3.04	2.59	2.30E-15	9.51E-15
84	Independently	TERT	7015	ENSG00000164362	-1.28	0.78	7.00E-15	2.82E-14
85	Independently	MMP9	4318	ENSG00000100985	-1.32	0.34	1.81E-12	6.31E-12
86	Independently	CXCL3	2921	ENSG00000163734	-2.98	2.68	1.81E-12	6.33E-12
87	Independently	ZDHHC11	79844	ENSG00000188818	1.17	2.09	1.87E-10	5.69E-10
88	Independently	TRIM2	23321	ENSG00000109654	0.58	6.42	3.90E-10	1.17E-09
89	Independently	LRCH1	23143	ENSG00000136141	-0.34	4.00	5.11E-10	1.52E-09
90	Independently	MAGEH1	28986	ENSG00000187601	-0.99	0.68	6.39E-10	1.88E-09
91	Independently	SEMA3A	10371	ENSG00000075213	-0.46	5.64	1.14E-09	3.29E-09
92	Independently	MAPK10	5602	ENSG00000109339	-1.42	-0.21	6.41E-08	1.62E-07
93	Independently	BEX1	55859	ENSG00000133169	0.89	1.06	1.05E-07	2.62E-07
94	Independently	LMO3	55885	ENSG00000048540	-0.77	6.65	2.34E-07	5.64E-07
95	Independently	ERC2	26059	ENSG00000187672	0.71	0.85	4.56E-06	9.83E-06
96	Independently	CHGA	1113	ENSG00000100604	-0.56	1.03	1.59E-05	3.24E-05
97	Independently	EXOC6B	23233	ENSG00000144036	0.28	4.51	2.20E-05	4.42E-05
98	Independently	MAP4K1	11184	ENSG00000104814	-0.97	2.36	2.88E-05	5.72E-05
99	Independently	CFAP69	79846	ENSG00000105792	-0.54	0.97	9.01E-05	1.71E-04
100	Independently	PLAT	5327	ENSG00000104368	0.57	5.51	1.00E-04	1.90E-04
101	Independently	DCBLD2	131566	ENSG00000057019	-0.42	9.84	1.08E-04	2.03E-04
102	Independently	LPXN	9404	ENSG00000110031	-0.56	0.74	5.76E-04	1.00E-03
103	Independently	RUBCNL	80183	ENSG00000102445	-0.65	0.30	2.96E-03	4.76E-03
104	Independently	FGF9	2254	ENSG00000102678	0.34	1.99	4.91E-03	7.68E-03
105	Independently	ANO1	55107	ENSG00000131620	-0.36	1.67	1.11E-02	1.66E-02
106	Independently	COL26A1	136227	ENSG00000160963	0.25	6.88	1.12E-02	1.67E-02
107	Independently	CEL	1056	ENSG00000170835	-0.40	0.27	2.48E-02	3.52E-02
108	Independently	ETV2	2116	ENSG00000105672	0.44	0.07	3.48E-02	4.83E-02

Table S3 Gene list of E2F3_UP.V1_UP in SKOV3 ZIC2-KO model

	Category	Symbol	EntrezGene	Ensembl	logFC	logCPM	Pvalue	FDR
1	Commonly	PEG10	23089	ENSG00000242265	-3.43	5.21	1.04E-104	7.95E-102
2	Commonly	CEBPA	1050	ENSG00000245848	-2.47	3.20	2.68E-57	5.16E-55
3	Commonly	NPTX1	4884	ENSG00000171246	-3.97	1.30	9.22E-50	1.20E-47
4	Commonly	REEP1	65055	ENSG00000068615	-1.17	4.41	3.31E-31	1.63E-29
5	Commonly	MICB	4277	ENSG00000204516	-1.45	3.34	6.28E-26	2.11E-24
6	Commonly	SLC27A2	11001	ENSG00000140284	-2.59	2.94	1.42E-22	3.76E-21
7	Commonly	RRAGD	58528	ENSG00000025039	-1.10	4.91	3.10E-22	7.97E-21
8	Commonly	CBX2	84733	ENSG00000173894	-1.21	3.75	7.88E-21	1.86E-19
9	Commonly	PLXND1	23129	ENSG00000004399	0.90	6.95	1.52E-19	3.20E-18
10	Commonly	ZIC2	7546	ENSG00000043355	-1.15	5.91	3.73E-18	7.02E-17
11	Commonly	CHST2	9435	ENSG00000175040	1.34	7.67	2.26E-13	2.87E-12
12	Commonly	CD83	9308	ENSG00000112149	-1.14	2.30	7.26E-12	7.89E-11
13	Commonly	ZDHHC23	254887	ENSG00000184307	-0.69	4.06	1.66E-10	1.58E-09
14	Commonly	JPH1	56704	ENSG00000104369	-1.67	1.63	4.92E-10	4.45E-09
15	Commonly	IL17RB	55540	ENSG00000056736	-1.99	0.74	7.63E-09	6.02E-08
16	Commonly	PGAP4	84302	ENSG00000165152	-0.90	3.83	1.39E-07	9.24E-07
17	Commonly	GCH1	2643	ENSG00000131979	-0.65	2.94	1.42E-07	9.43E-07
18	Commonly	TIAM1	7074	ENSG00000156299	-0.95	3.74	2.17E-07	1.39E-06
19	Commonly	MSRB1	51734	ENSG00000198736	-0.63	4.09	4.67E-07	2.84E-06
20	Commonly	LIN7B	64130	ENSG00000104863	-0.87	2.01	7.32E-07	4.30E-06
21	Commonly	CSPG5	10675	ENSG00000114646	-0.79	3.90	4.23E-06	2.16E-05
22	Commonly	PTCH1	5727	ENSG00000185920	-0.92	2.57	5.31E-06	2.68E-05
23	Commonly	SMAD6	4091	ENSG00000137834	0.57	5.20	6.77E-06	3.35E-05
24	Commonly	CDKN2C	1031	ENSG00000123080	-0.78	6.11	7.22E-06	3.55E-05
25	Commonly	ZNF483	158399	ENSG00000173258	-1.09	0.29	8.74E-06	4.23E-05
26	Commonly	FGFR3	2261	ENSG00000068078	-0.50	4.08	1.14E-05	5.41E-05
27	Commonly	UGT8	7368	ENSG00000174607	-1.04	3.38	1.44E-05	6.70E-05
28	Commonly	CHST7	56548	ENSG00000147119	-0.40	4.07	3.02E-05	1.32E-04
29	Commonly	LMO2	4005	ENSG00000135363	-1.29	1.78	3.23E-05	1.41E-04
30	Commonly	RIPPLY3	53820	ENSG00000183145	0.94	1.92	4.88E-05	2.05E-04
31	Commonly	FAM222A	84915	ENSG00000139438	-0.53	3.57	2.36E-04	8.70E-04
32	Commonly	NGEF	25791	ENSG00000066248	0.37	6.24	1.30E-03	4.06E-03
33	Commonly	CCNE1	898	ENSG00000105173	-0.51	4.43	1.32E-03	4.12E-03
34	Commonly	HEY1	23462	ENSG00000164683	-0.67	1.95	1.46E-03	4.50E-03
35	Commonly	FAXC	84553	ENSG00000146267	-0.38	3.26	2.13E-03	6.30E-03
36	Commonly	TSHZ1	10194	ENSG00000179981	0.31	4.88	1.52E-02	3.53E-02
37	Commonly	GPR137C	283554	ENSG00000180998	-0.54	2.70	1.78E-02	4.03E-02
38	Oppositely	SEPTIN3	55964	ENSG00000100167	-3.19	3.84	6.62E-140	9.58E-137
39	Oppositely	EEF1A2	1917	ENSG00000101210	-1.71	6.99	4.06E-66	1.07E-63
40	Oppositely	TLE2	7089	ENSG00000065717	-1.97	4.70	1.04E-43	1.02E-41
41	Oppositely	ARRDC2	27106	ENSG00000105643	-0.86	4.10	7.56E-17	1.30E-15
42	Oppositely	ZNF703	80139	ENSG00000183779	1.45	5.28	4.98E-14	6.70E-13
43	Oppositely	RASGRP1	10125	ENSG00000172575	2.20	3.39	9.79E-13	1.18E-11
44	Oppositely	TMEM121	80757	ENSG00000184986	-1.02	3.27	1.51E-11	1.58E-10
45	Oppositely	ENO2	2026	ENSG00000111674	-0.89	5.31	3.51E-09	2.89E-08
46	Oppositely	CABLES2	81928	ENSG00000149679	-0.67	3.33	4.41E-08	3.14E-07
47	Oppositely	HOXA9	3205	ENSG00000078399	-1.74	-0.53	5.81E-07	3.49E-06
48	Oppositely	TLCD1	116238	ENSG00000160606	-0.75	2.78	7.06E-07	4.16E-06
49	Oppositely	MMP15	4324	ENSG00000102996	-0.95	4.90	2.81E-06	1.49E-05
50	Oppositely	MAFG-DT	92659	ENSG00000265688	-0.57	3.03	7.61E-06	3.72E-05
51	Oppositely	TMOD2	29767	ENSG00000128872	-0.44	5.54	3.35E-05	1.46E-04
52	Oppositely	RAB26	25837	ENSG00000167964	-1.47	2.55	5.62E-05	2.33E-04
53	Oppositely	INHBB	3625	ENSG00000163083	-0.89	1.83	1.11E-04	4.39E-04
54	Oppositely	SAMD11	148398	ENSG00000187634	-1.83	4.70	1.96E-04	7.37E-04

	Category	Symbol	EntrezGene	Ensembl	logFC	logCPM	Pvalue	FDR
55	Oppositely	DHRS13	147015	ENSG00000167536	-0.37	4.46	1.93E-03	5.75E-03
56	Oppositely	CRY1	1407	ENSG00000008405	0.34	5.75	3.24E-03	9.13E-03
57	Oppositely	ATRNL1	26033	ENSG00000107518	-0.99	2.77	3.86E-03	1.06E-02
58	Oppositely	PIN1	5300	ENSG00000127445	0.23	6.23	4.57E-03	1.24E-02
59	Oppositely	ADGRB2	576	ENSG00000121753	-0.44	4.06	7.60E-03	1.94E-02
60	Oppositely	KHDRBS3	10656	ENSG00000131773	0.33	4.42	1.11E-02	2.69E-02
61	Oppositely	SIX5	147912	ENSG00000177045	-0.37	5.16	1.52E-02	3.54E-02
62	Independently	FAM43B	163933	ENSG00000183114	-6.10	0.39	2.53E-43	2.44E-41
63	Independently	NR2F1	7025	ENSG00000175745	-3.26	1.96	4.07E-28	1.60E-26
64	Independently	SOWAHA	134548	ENSG00000198944	-2.75	1.45	4.38E-26	1.49E-24
65	Independently	NPAS1	4861	ENSG00000130751	-1.19	3.64	8.05E-24	2.33E-22
66	Independently	NAT8L	339983	ENSG00000185818	-1.10	5.00	5.13E-23	1.39E-21
67	Independently	FAM78A	286336	ENSG00000126882	-1.90	3.54	1.84E-20	4.18E-19
68	Independently	KCNS3	3790	ENSG00000170745	1.38	3.47	2.44E-19	5.06E-18
69	Independently	INA	9118	ENSG00000148798	-9.10	2.14	1.23E-17	2.24E-16
70	Independently	SBK1	388228	ENSG00000188322	-2.80	1.73	2.22E-16	3.69E-15
71	Independently	UBE2QL1	134111	ENSG00000215218	-2.65	-0.01	2.64E-14	3.66E-13
72	Independently	LRP4	4038	ENSG00000134569	-1.08	4.43	1.53E-12	1.80E-11
73	Independently	SYN1	6853	ENSG00000008056	-2.94	-0.02	2.46E-12	2.82E-11
74	Independently	CYP26A1	1592	ENSG00000095596	-4.25	1.17	4.50E-11	4.49E-10
75	Independently	CDK5R1	8851	ENSG00000176749	-0.67	4.36	2.43E-08	1.80E-07
76	Independently	TPPP	11076	ENSG00000171368	-1.31	3.21	7.01E-08	4.84E-07
77	Independently	MBOAT1	154141	ENSG00000172197	1.01	3.54	1.08E-06	6.16E-06
78	Independently	TMEM158	25907	ENSG00000249992	-1.15	3.37	2.06E-06	1.12E-05
79	Independently	EML6	400954	ENSG00000214595	-1.13	0.83	1.05E-05	5.01E-05
80	Independently	PDIA2	64714	ENSG00000185615	-1.51	0.46	2.53E-05	1.13E-04
81	Independently	ABCG2	9429	ENSG00000118777	1.35	0.52	1.30E-04	5.04E-04
82	Independently	LRRC45	201255	ENSG00000169683	0.28	4.91	2.12E-03	6.27E-03
83	Independently	EGLN1	54583	ENSG00000135766	-0.31	5.23	2.61E-03	7.52E-03
84	Independently	TP53I13	90313	ENSG00000167543	0.28	5.36	5.08E-03	1.36E-02
85	Independently	ANKRD18A	253650	ENSG00000180071	0.40	2.75	6.35E-03	1.65E-02
86	Independently	SHISA8	440829	ENSG00000234965	-0.35	2.47	6.99E-03	1.80E-02

Table S4 Gene list of E2F3_UP.V1_UP in OVCAR3 ZIC2-OE model

	Category	Symbol	EntrezGene	Ensembl	logFC	logCPM	Pvalue	FDR
1	Commonly	ZIC2	7546	ENSG00000043355	6.13	6.29	0.00E+00	0.00E+00
2	Commonly	PLXND1	23129	ENSG00000004399	-1.57	7.57	2.10E-152	1.95E-150
3	Commonly	HEY1	23462	ENSG00000164683	3.31	3.25	1.57E-147	1.36E-145
4	Commonly	PGAP4	84302	ENSG00000165152	8.62	0.59	3.31E-144	2.67E-142
5	Commonly	REEP1	65055	ENSG00000068615	2.32	1.51	3.15E-60	6.53E-59
6	Commonly	PTCH1	5727	ENSG00000185920	1.46	3.96	5.43E-54	9.74E-53
7	Commonly	NPTX1	4884	ENSG00000171246	2.23	1.75	5.73E-52	9.79E-51
8	Commonly	GCH1	2643	ENSG00000131979	1.26	4.35	6.60E-47	9.83E-46
9	Commonly	FGFR3	2261	ENSG00000068078	1.08	4.85	3.57E-42	4.52E-41
10	Commonly	TIAM1	7074	ENSG00000156299	0.71	6.70	6.10E-36	6.17E-35
11	Commonly	MSRB1	51734	ENSG00000198736	0.64	5.51	1.03E-33	9.78E-33
12	Commonly	ZNF483	158399	ENSG00000173258	1.74	1.86	3.37E-31	2.87E-30
13	Commonly	JPH1	56704	ENSG00000104369	0.70	4.48	4.55E-26	3.16E-25
14	Commonly	MICB	4277	ENSG00000204516	0.83	3.66	2.56E-18	1.24E-17
15	Commonly	FAXC	84553	ENSG00000146267	0.91	2.36	7.79E-18	3.69E-17
16	Commonly	LMO2	4005	ENSG00000135363	1.17	2.94	2.22E-16	9.76E-16
17	Commonly	UGT8	7368	ENSG00000174607	0.39	5.27	6.63E-15	2.67E-14
18	Commonly	CD83	9308	ENSG00000112149	0.72	2.83	1.86E-14	7.31E-14
19	Commonly	CHST7	56548	ENSG00000147119	1.04	1.17	2.62E-13	9.65E-13
20	Commonly	TSHZ1	10194	ENSG00000179981	-0.67	3.98	4.03E-13	1.46E-12
21	Commonly	CBX2	84733	ENSG00000173894	0.42	5.95	4.85E-10	1.44E-09
22	Commonly	GPR137C	283554	ENSG00000180998	0.61	2.62	2.59E-08	6.74E-08
23	Commonly	CDKN2C	1031	ENSG00000123080	1.03	2.36	3.48E-08	8.97E-08
24	Commonly	RRAGD	58528	ENSG00000025039	0.58	3.81	3.96E-08	1.01E-07
25	Commonly	CCNE1	898	ENSG00000105173	0.44	7.15	1.88E-07	4.56E-07
26	Commonly	SMAD6	4091	ENSG00000137834	-0.52	5.76	5.91E-07	1.38E-06
27	Commonly	IL17RB	55540	ENSG00000056736	0.77	2.28	6.94E-07	1.62E-06
28	Commonly	CEBPA	1050	ENSG00000245848	0.80	0.85	2.01E-06	4.48E-06
29	Commonly	NGEF	25791	ENSG00000066248	-0.36	4.33	9.31E-05	1.76E-04
30	Commonly	RIPPLY3	53820	ENSG00000183145	-0.66	0.54	2.80E-04	5.05E-04
31	Commonly	CSPG5	10675	ENSG00000114646	0.42	5.37	3.69E-04	6.56E-04
32	Commonly	FAM222A	84915	ENSG00000139438	0.39	3.84	1.48E-03	2.47E-03
33	Commonly	SLC27A2	11001	ENSG00000140284	0.64	0.59	3.04E-03	4.89E-03
34	Commonly	CHST2	9435	ENSG00000175040	-0.21	6.29	4.13E-03	6.53E-03
35	Commonly	ZDHHC23	254887	ENSG00000184307	0.15	4.98	1.60E-02	2.34E-02
36	Commonly	PEG10	23089	ENSG00000242265	0.15	7.38	1.90E-02	2.75E-02
37	Commonly	LIN7B	64130	ENSG00000104863	0.40	0.58	1.96E-02	2.82E-02
38	Oppositely	EEF1A2	1917	ENSG00000101210	-4.37	6.41	0.00E+00	0.00E+00
39	Oppositely	ADGRB2	576	ENSG00000121753	-3.29	5.18	3.75E-269	1.16E-266
40	Oppositely	HOXA9	3205	ENSG00000078399	-4.38	4.21	3.57E-264	1.06E-261
41	Oppositely	ATRNL1	26033	ENSG00000107518	-3.77	2.05	1.49E-215	2.46E-213
42	Oppositely	ZNF703	80139	ENSG00000183779	2.15	6.34	1.00E-151	9.26E-150
43	Oppositely	KHDRBS3	10656	ENSG00000131773	3.55	1.97	2.05E-108	1.05E-106
44	Oppositely	TLCD1	116238	ENSG00000160606	-0.86	4.25	1.54E-42	1.98E-41
45	Oppositely	SAMD11	148398	ENSG00000187634	-2.80	2.21	2.02E-35	2.01E-34
46	Oppositely	TMEM121	80757	ENSG00000184986	-1.79	2.39	2.52E-35	2.49E-34
47	Oppositely	MMP15	4324	ENSG00000102996	-0.72	6.77	3.73E-33	3.44E-32
48	Oppositely	CABLES2	81928	ENSG00000149679	-0.67	5.44	1.14E-31	9.92E-31
49	Oppositely	ARRDC2	27106	ENSG00000105643	-0.90	3.44	6.13E-30	4.93E-29
50	Oppositely	SEPTIN3	55964	ENSG00000100167	-1.22	3.87	2.15E-28	1.65E-27
51	Oppositely	TMOD2	29767	ENSG00000128872	-1.18	1.92	3.73E-23	2.28E-22
52	Oppositely	RAB26	25837	ENSG00000167964	-1.36	3.34	5.81E-21	3.20E-20
53	Oppositely	DHRS13	147015	ENSG00000167536	-0.49	4.47	3.57E-15	1.46E-14
54	Oppositely	MAFG-DT	92659	ENSG00000265688	-0.60	3.19	2.55E-14	9.95E-14
55	Oppositely	CRY1	1407	ENSG00000008405	0.59	4.35	1.22E-12	4.31E-12

	Category	Symbol	EntrezGene	Ensembl	logFC	logCPM	Pvalue	FDR
56	Oppositely	INHBB	3625	ENSG00000163083	-0.35	6.93	1.51E-06	3.41E-06
57	Oppositely	RASGRP1	10125	ENSG00000172575	0.52	2.11	7.14E-06	1.51E-05
58	Oppositely	TLE2	7089	ENSG00000065717	-0.75	3.61	8.90E-06	1.86E-05
59	Oppositely	SIX5	147912	ENSG00000177045	-0.32	4.52	1.07E-04	2.02E-04
60	Oppositely	PIN1	5300	ENSG00000127445	0.16	5.58	7.65E-03	1.17E-02
61	Oppositely	ENO2	2026	ENSG00000111674	-0.19	4.30	2.74E-02	3.86E-02
62	Independently	SMCO4	56935	ENSG00000166002	2.05	3.85	8.30E-154	8.03E-152
63	Independently	FOXD1	2297	ENSG00000251493	1.86	5.89	1.39E-144	1.14E-142
64	Independently	SHANK3	85358	ENSG00000251322	-1.14	4.34	1.69E-102	7.97E-101
65	Independently	CDKN1C	1028	ENSG00000129757	-2.44	5.31	1.35E-96	5.86E-95
66	Independently	HPGD	3248	ENSG00000164120	4.23	0.44	1.16E-79	3.69E-78
67	Independently	ZNF367	195828	ENSG00000165244	1.14	4.51	1.19E-54	2.16E-53
68	Independently	RTN4RL1	146760	ENSG00000185924	3.35	1.51	1.46E-51	2.48E-50
69	Independently	DDAH1	23576	ENSG00000153904	1.10	6.58	4.32E-50	7.00E-49
70	Independently	RYR1	6261	ENSG00000196218	-2.15	4.15	6.48E-50	1.05E-48
71	Independently	POLE2	5427	ENSG00000100479	1.08	3.92	3.27E-48	5.08E-47
72	Independently	SYNGR3	9143	ENSG00000127561	-1.09	5.68	2.36E-43	3.09E-42
73	Independently	TSPAN5	10098	ENSG00000168785	1.51	1.93	4.46E-40	5.21E-39
74	Independently	CHML	1122	ENSG00000203668	0.69	6.11	5.95E-35	5.81E-34
75	Independently	RTN4R	65078	ENSG00000040608	-0.94	4.06	1.29E-34	1.25E-33
76	Independently	SLC4A3	6508	ENSG00000114923	-0.91	4.45	8.12E-30	6.50E-29
77	Independently	NOL4L	140688	ENSG00000197183	-0.68	6.16	5.95E-25	3.93E-24
78	Independently	CCP110	9738	ENSG00000103540	0.49	5.09	5.03E-22	2.91E-21
79	Independently	MANEAL	149175	ENSG00000185090	-1.35	2.59	8.54E-22	4.91E-21
80	Independently	FBXL16	146330	ENSG00000127585	-1.48	3.77	2.24E-21	1.26E-20
81	Independently	HRK	8739	ENSG00000135116	0.86	2.86	3.61E-21	2.01E-20
82	Independently	BRI3BP	140707	ENSG00000184992	0.66	6.02	7.33E-20	3.82E-19
83	Independently	TMEM106C	79022	ENSG00000134291	-0.46	6.51	2.40E-19	1.22E-18
84	Independently	HSPA2	3306	ENSG00000126803	-1.05	3.73	6.70E-19	3.34E-18
85	Independently	PLSCR4	57088	ENSG00000114698	1.90	0.59	8.86E-19	4.39E-18
86	Independently	DTL	51514	ENSG00000143476	0.72	5.00	4.18E-17	1.91E-16
87	Independently	DCK	1633	ENSG00000156136	0.41	5.35	1.49E-16	6.59E-16
88	Independently	ZDHHC12	84885	ENSG00000160446	0.39	5.16	7.29E-16	3.10E-15
89	Independently	ATP6V1E1	529	ENSG00000131100	-0.35	6.34	3.34E-15	1.36E-14
90	Independently	ZFP30	22835	ENSG00000120784	0.55	3.99	4.63E-15	1.88E-14
91	Independently	UNG	7374	ENSG00000076248	0.48	6.38	1.58E-13	5.88E-13
92	Independently	MYB	4602	ENSG00000118513	0.80	2.13	2.44E-13	8.99E-13
93	Independently	GINS1	9837	ENSG00000101003	0.44	4.95	1.45E-12	5.08E-12
94	Independently	E2F7	144455	ENSG00000165891	0.60	4.00	6.69E-12	2.25E-11
95	Independently	PCNA	5111	ENSG00000132646	0.48	6.64	7.31E-12	2.46E-11
96	Independently	RECQL4	9401	ENSG00000160957	0.36	6.02	1.80E-11	5.87E-11
97	Independently	APOLD1	81575	ENSG00000178878	-0.76	2.31	7.56E-11	2.37E-10
98	Independently	RASD1	51655	ENSG00000108551	-0.69	2.30	3.84E-10	1.15E-09
99	Independently	WNT9A	7483	ENSG00000143816	-1.03	2.96	9.71E-10	2.82E-09
100	Independently	SNRNP25	79622	ENSG00000161981	0.43	4.30	1.82E-09	5.15E-09
101	Independently	GAD1	2571	ENSG00000128683	-0.63	1.84	1.17E-07	2.90E-07
102	Independently	SNX10	29887	ENSG00000086300	-0.38	3.59	1.87E-07	4.54E-07
103	Independently	MEX3B	84206	ENSG00000183496	1.24	-0.08	3.22E-07	7.67E-07
104	Independently	LEF1	51176	ENSG00000138795	-0.98	1.45	3.94E-07	9.34E-07
105	Independently	EMC9	51016	ENSG00000100908	0.37	4.68	4.36E-07	1.03E-06
106	Independently	ATAD2	29028	ENSG00000156802	0.30	7.55	5.36E-07	1.26E-06
107	Independently	ABHD15	116236	ENSG00000168792	-0.37	3.83	9.03E-07	2.08E-06
108	Independently	NUDT22	84304	ENSG00000149761	-0.31	5.74	2.72E-06	6.01E-06
109	Independently	EPHX4	253152	ENSG00000172031	-0.30	3.79	4.66E-06	1.01E-05
110	Independently	ZDHHC14	79683	ENSG00000175048	-0.60	0.91	5.51E-06	1.18E-05
111	Independently	PXMP2	5827	ENSG00000176894	0.40	3.09	1.06E-05	2.21E-05

	Category	Symbol	EntrezGene	Ensembl	logFC	logCPM	Pvalue	FDR
112	Independently	TIFA	92610	ENSG00000145365	0.30	4.46	1.28E-05	2.63E-05
113	Independently	DCLRE1B	64858	ENSG00000118655	0.30	3.93	1.54E-05	3.16E-05
114	Independently	TAF5	6877	ENSG00000148835	0.26	4.23	2.68E-05	5.35E-05
115	Independently	SAC3D1	29901	ENSG00000168061	-0.30	4.65	4.47E-05	8.75E-05
116	Independently	PCOLCE2	26577	ENSG00000163710	0.45	1.96	1.03E-04	1.94E-04
117	Independently	GKAP1	80318	ENSG00000165113	0.53	1.35	2.90E-04	5.22E-04
118	Independently	CCNE2	9134	ENSG00000175305	0.26	4.36	9.02E-04	1.54E-03
119	Independently	MFHAS1	9258	ENSG00000147324	0.13	6.82	4.31E-03	6.80E-03
120	Independently	FGF9	2254	ENSG00000102678	0.34	1.99	4.91E-03	7.68E-03
121	Independently	CDK19	23097	ENSG00000155111	-0.30	5.26	5.49E-03	8.54E-03
122	Independently	TMEM97	27346	ENSG00000109084	0.13	5.72	1.22E-02	1.80E-02
123	Independently	MAP3K21	84451	ENSG00000143674	0.19	4.36	1.29E-02	1.90E-02
124	Independently	SAMD1	90378	ENSG00000141858	0.10	6.17	3.33E-02	4.63E-02

Table S5 Gene list of BMI1_DN_MEL_18_DN.V1_UP in SKOV3 ZIC2-KO model

	Category	Symbol	EntrezGene	Ensembl	logFC	logCPM	Pvalue	FDR
1	Commonly	EHD1	10938	ENSG00000110047	1.02	6.62	5.28E-29	2.21E-27
2	Commonly	ABLIM3	22885	ENSG00000173210	2.05	4.09	1.90E-25	6.15E-24
3	Commonly	ADGRE5	976	ENSG00000123146	1.24	5.55	5.75E-25	1.81E-23
4	Commonly	ITGB6	3694	ENSG00000115221	2.17	4.79	1.92E-24	5.75E-23
5	Commonly	LAMB3	3914	ENSG00000196878	1.77	7.84	1.26E-15	1.95E-14
6	Commonly	FADS3	3995	ENSG00000221968	0.92	6.55	2.24E-15	3.40E-14
7	Commonly	F3	2152	ENSG00000117525	1.38	9.27	2.70E-11	2.76E-10
8	Commonly	KCNN4	3783	ENSG00000104783	0.57	4.76	1.47E-10	1.41E-09
9	Commonly	TNFSF9	8744	ENSG00000125657	0.59	6.72	1.97E-09	1.66E-08
10	Commonly	MT1F	4494	ENSG00000198417	-1.70	0.98	1.80E-08	1.36E-07
11	Commonly	MICA	100507436	ENSG00000204520	-0.56	5.12	1.44E-07	9.52E-07
12	Commonly	NAV2	89797	ENSG00000166833	1.68	2.88	1.25E-06	7.05E-06
13	Commonly	PSAT1	29968	ENSG00000135069	-0.32	7.48	4.15E-06	2.13E-05
14	Commonly	ASPH	444	ENSG00000198363	0.49	9.46	2.42E-05	1.08E-04
15	Commonly	VLDLR	7436	ENSG00000147852	0.53	5.16	4.02E-05	1.72E-04
16	Commonly	GADD45A	1647	ENSG00000116717	1.27	6.00	4.59E-05	1.94E-04
17	Commonly	PIEZO1	9780	ENSG00000103335	0.55	7.43	1.01E-04	4.01E-04
18	Commonly	PMEPA1	56937	ENSG00000124225	0.76	8.22	1.33E-04	5.17E-04
19	Commonly	MAP3K7CL	56911	ENSG00000156265	1.10	-0.08	2.73E-04	9.94E-04
20	Commonly	ZC3H12A	80149	ENSG00000163874	0.66	3.46	2.83E-04	1.03E-03
21	Commonly	CHST3	9469	ENSG00000122863	0.74	7.10	3.97E-04	1.40E-03
22	Commonly	DUSP10	11221	ENSG00000143507	0.31	4.98	6.96E-04	2.32E-03
23	Commonly	ITGB8	3696	ENSG00000105855	0.53	5.77	2.33E-03	6.80E-03
24	Commonly	CXCL1	2919	ENSG00000163739	1.12	4.93	4.16E-03	1.14E-02
25	Commonly	ADAM19	8728	ENSG00000135074	-0.54	5.37	4.20E-03	1.15E-02
26	Commonly	RREB1	6239	ENSG00000124782	-0.25	5.30	5.74E-03	1.51E-02
27	Commonly	ADAM12	8038	ENSG00000148848	0.63	4.62	1.27E-02	3.01E-02
28	Commonly	NRP2	8828	ENSG00000118257	0.25	7.45	1.35E-02	3.18E-02
29	Commonly	CPA4	51200	ENSG00000128510	0.58	2.41	1.51E-02	3.51E-02
30	Oppositely	ANXA3	306	ENSG00000138772	1.84	7.59	8.38E-57	1.59E-54
31	Oppositely	CSPG4	1464	ENSG00000173546	-4.90	1.79	3.78E-20	8.31E-19
32	Oppositely	PODXL	5420	ENSG00000128567	1.07	8.34	6.65E-18	1.23E-16
33	Oppositely	KIF21B	23046	ENSG00000116852	-1.29	2.80	4.41E-15	6.55E-14
34	Oppositely	KLF7	8609	ENSG00000118263	1.13	6.25	1.54E-14	2.19E-13
35	Oppositely	ADRB2	154	ENSG00000169252	2.59	2.88	1.30E-13	1.70E-12
36	Oppositely	EDN1	1906	ENSG00000078401	1.88	5.43	1.70E-13	2.18E-12
37	Oppositely	JAG1	182	ENSG00000101384	1.25	5.83	1.20E-12	1.43E-11
38	Oppositely	VEGFC	7424	ENSG00000150630	-0.72	4.07	1.37E-09	1.18E-08
39	Oppositely	TIMP3	7078	ENSG00000100234	-3.28	0.34	5.05E-09	4.08E-08
40	Oppositely	TRIO	7204	ENSG00000038382	0.69	7.74	5.17E-09	4.16E-08
41	Oppositely	CLDN1	9076	ENSG00000163347	1.26	6.58	2.46E-07	1.56E-06
42	Oppositely	TAGLN	6876	ENSG00000149591	1.70	8.00	5.70E-07	3.43E-06
43	Oppositely	RUSC2	9853	ENSG00000198853	0.49	6.77	6.44E-06	3.20E-05
44	Oppositely	GAB2	9846	ENSG00000033327	0.77	4.15	1.43E-05	6.67E-05
45	Oppositely	PLAUR	5329	ENSG00000011422	-0.82	4.35	5.13E-05	2.15E-04
46	Oppositely	PTHLH	5744	ENSG00000087494	1.45	1.72	2.16E-04	8.01E-04
47	Oppositely	TRIB3	57761	ENSG00000101255	0.56	4.78	3.32E-04	1.19E-03
48	Oppositely	TUFT1	7286	ENSG00000143367	0.73	6.10	8.25E-04	2.70E-03
49	Oppositely	SLC7A11	23657	ENSG00000151012	0.49	6.93	3.83E-03	1.06E-02
50	Oppositely	SCML2	10389	ENSG00000102098	0.29	4.37	4.69E-03	1.27E-02
51	Oppositely	STX1A	6804	ENSG00000106089	-0.40	2.26	8.03E-03	2.03E-02
52	Oppositely	SLC7A5	8140	ENSG00000103257	0.54	10.27	9.49E-03	2.35E-02
53	Oppositely	MMP7	4316	ENSG00000137673	-1.36	5.44	1.32E-02	3.11E-02
54	Independently	ZEB2	9839	ENSG00000169554	-3.49	3.03	1.57E-66	4.27E-64
55	Independently	LSAMP	4045	ENSG00000185565	-7.88	-0.14	2.14E-30	9.91E-29

	Category	Symbol	EntrezGene	Ensembl	logFC	logCPM	Pvalue	FDR
56	Independently	NKAIN1	79570	ENSG00000084628	-2.25	1.30	1.48E-28	5.98E-27
57	Independently	MGLL	11343	ENSG00000074416	1.61	7.78	6.12E-25	1.92E-23
58	Independently	CDH13	1012	ENSG00000140945	1.52	4.77	7.97E-25	2.48E-23
59	Independently	STC2	8614	ENSG00000113739	1.62	3.89	2.75E-22	7.08E-21
60	Independently	HTR1D	3352	ENSG00000179546	1.22	2.89	3.10E-19	6.32E-18
61	Independently	TGFB2	7042	ENSG00000092969	2.63	3.48	2.54E-13	3.22E-12
62	Independently	GFPT2	9945	ENSG00000131459	-0.94	3.82	3.65E-08	2.64E-07
63	Independently	SLC22A4	6583	ENSG00000197208	1.16	2.24	1.33E-07	8.85E-07
64	Independently	HAS2	3037	ENSG00000170961	1.69	0.89	2.70E-05	1.20E-04
65	Independently	ATF3	467	ENSG00000162772	0.78	2.81	1.57E-04	6.00E-04
66	Independently	COL7A1	1294	ENSG00000114270	0.64	7.03	1.83E-04	6.89E-04
67	Independently	LCP1	3936	ENSG00000136167	3.11	0.59	6.88E-04	2.29E-03
68	Independently	ABCA1	19	ENSG00000165029	0.38	5.54	1.02E-03	3.29E-03
69	Independently	MICALL1	85377	ENSG00000100139	0.47	6.72	1.88E-03	5.64E-03
70	Independently	IL1A	3552	ENSG00000115008	1.81	1.78	2.56E-03	7.41E-03
71	Independently	BST1	683	ENSG00000109743	0.67	2.16	3.84E-03	1.06E-02
72	Independently	GAL	51083	ENSG00000069482	-1.04	0.23	5.17E-03	1.38E-02
73	Independently	ADM2	79924	ENSG00000128165	-0.50	3.08	5.87E-03	1.54E-02
74	Independently	INHBA	3624	ENSG00000122641	-1.06	4.59	6.18E-03	1.61E-02
75	Independently	ARNTL2	56938	ENSG00000029153	0.31	7.08	9.74E-03	2.40E-02
76	Independently	FJX1	24147	ENSG00000179431	-0.85	1.47	1.29E-02	3.05E-02

Table S6 Gene list of BMI1_DN_MEL18_DN.V1_UP in OVCAR3 ZIC2-OE model

	Category	Symbol	EntrezGene	Ensembl	logFC	logCPM	Pvalue	FDR
1	Commonly	CHST3	9469	ENSG00000122863	-2.51	5.19	6.22E-227	1.19E-224
2	Commonly	LAMB3	3914	ENSG00000196878	-2.53	6.91	7.99E-144	6.37E-142
3	Commonly	ADGRE5	976	ENSG00000123146	-1.26	5.87	2.07E-109	1.08E-107
4	Commonly	PIEZO1	9780	ENSG00000103335	-1.41	7.23	1.43E-98	6.36E-97
5	Commonly	FADS3	3995	ENSG00000221968	-1.49	6.02	2.47E-95	1.05E-93
6	Commonly	ABLIM3	22885	ENSG00000173210	-2.85	2.80	4.51E-74	1.30E-72
7	Commonly	ADAM19	8728	ENSG00000135074	1.18	5.66	1.70E-70	4.47E-69
8	Commonly	ADAM12	8038	ENSG00000148848	-5.32	2.54	2.04E-62	4.42E-61
9	Commonly	PMEPA1	56937	ENSG00000124225	-3.33	5.99	8.21E-59	1.63E-57
10	Commonly	EHD1	10938	ENSG00000110047	-1.08	7.33	1.82E-53	3.25E-52
11	Commonly	KCNN4	3783	ENSG00000104783	-3.19	3.07	3.77E-48	5.84E-47
12	Commonly	MICA	100507436	ENSG00000204520	1.17	3.95	3.05E-43	3.99E-42
13	Commonly	CPA4	51200	ENSG00000128510	-2.49	3.22	1.32E-34	1.27E-33
14	Commonly	TNFSF9	8744	ENSG00000125657	-1.14	4.68	8.80E-29	6.84E-28
15	Commonly	ITGB6	3694	ENSG00000115221	-1.20	5.43	5.89E-25	3.90E-24
16	Commonly	ITGB8	3696	ENSG00000105855	-0.55	9.70	4.42E-22	2.57E-21
17	Commonly	PSAT1	29968	ENSG00000135069	0.67	7.91	1.65E-17	7.71E-17
18	Commonly	MT1F	4494	ENSG00000198417	1.05	3.95	1.48E-13	5.54E-13
19	Commonly	RREB1	6239	ENSG00000124782	0.42	6.42	5.30E-11	1.68E-10
20	Commonly	DUSP10	11221	ENSG00000143507	-0.87	3.79	1.26E-10	3.89E-10
21	Commonly	VLDLR	7436	ENSG00000147852	-0.38	6.50	1.14E-08	3.06E-08
22	Commonly	CXCL1	2919	ENSG00000163739	-2.64	6.81	1.80E-07	4.37E-07
23	Commonly	NRP2	8828	ENSG00000118257	-0.88	4.56	1.02E-06	2.34E-06
24	Commonly	ZC3H12A	80149	ENSG00000163874	-1.56	4.47	3.79E-06	8.23E-06
25	Commonly	GADD45A	1647	ENSG00000116717	-0.36	4.75	1.51E-04	2.79E-04
26	Commonly	MAP3K7CL	56911	ENSG00000156265	-0.86	1.74	2.52E-04	4.57E-04
27	Commonly	NAV2	89797	ENSG00000166833	-0.19	6.15	6.44E-03	9.92E-03
28	Commonly	ASPH	444	ENSG00000198363	-0.14	7.23	8.75E-03	1.32E-02
29	Commonly	F3	2152	ENSG00000117525	-0.31	3.10	1.15E-02	1.71E-02
30	Oppositely	PODXL	5420	ENSG00000128567	1.87	8.78	1.71E-145	1.43E-143
31	Oppositely	JAG1	182	ENSG00000101384	1.16	8.47	1.23E-119	7.36E-118
32	Oppositely	EDN1	1906	ENSG00000078401	6.13	4.71	1.05E-117	6.14E-116
33	Oppositely	CSPG4	1464	ENSG00000173546	-4.70	4.12	2.64E-61	5.62E-60
34	Oppositely	SCML2	10389	ENSG00000102098	0.99	3.46	1.50E-43	1.98E-42
35	Oppositely	TAGLN	6876	ENSG00000149591	1.72	1.94	5.67E-43	7.34E-42
36	Oppositely	TIMP3	7078	ENSG00000100234	-0.93	6.42	4.79E-40	5.59E-39
37	Oppositely	SLC7A5	8140	ENSG00000103257	0.96	9.73	5.36E-38	5.85E-37
38	Oppositely	VEGFC	7424	ENSG00000150630	-2.61	0.66	2.97E-28	2.25E-27
39	Oppositely	MMP7	4316	ENSG00000137673	-4.03	0.52	1.56E-26	1.10E-25
40	Oppositely	ANXA3	306	ENSG00000138772	1.02	6.62	1.16E-19	5.99E-19
41	Oppositely	RUSC2	9853	ENSG00000198853	0.48	5.03	1.29E-13	4.85E-13
42	Oppositely	PTHLH	5744	ENSG00000087494	1.27	4.70	1.72E-12	6.02E-12
43	Oppositely	GAB2	9846	ENSG00000033327	0.71	4.37	6.36E-12	2.15E-11
44	Oppositely	CLDN1	9076	ENSG00000163347	1.51	8.88	1.16E-11	3.83E-11
45	Oppositely	KIF21B	23046	ENSG00000116852	-1.08	2.26	1.16E-11	3.85E-11
46	Oppositely	ADRB2	154	ENSG00000169252	2.05	0.94	2.37E-07	5.71E-07
47	Oppositely	PLAUR	5329	ENSG00000011422	-0.49	4.21	9.98E-07	2.29E-06
48	Oppositely	STX1A	6804	ENSG00000106089	-0.53	2.37	1.15E-06	2.63E-06
49	Oppositely	TRIB3	57761	ENSG00000101255	0.41	6.18	3.95E-06	8.57E-06
50	Oppositely	SLC7A11	23657	ENSG00000151012	0.60	5.09	9.42E-05	1.78E-04
51	Oppositely	TUFT1	7286	ENSG00000143367	0.16	5.99	1.99E-03	3.26E-03
52	Oppositely	KLF7	8609	ENSG00000118263	0.30	4.11	3.05E-03	4.89E-03
53	Oppositely	TRIO	7204	ENSG00000038382	0.37	8.84	5.70E-03	8.84E-03
54	Independently	ITGA4	3676	ENSG00000115232	-3.98	1.55	5.93E-158	6.02E-156
55	Independently	COL16A1	1307	ENSG00000084636	-3.32	3.36	8.90E-128	6.06E-126

	Category	Symbol	EntrezGene	Ensembl	logFC	logCPM	Pvalue	FDR
56	Independently	ITGA5	3678	ENSG00000161638	-1.30	5.20	1.75E-101	8.17E-100
57	Independently	PAGE1	8712	ENSG00000068985	-3.57	0.37	4.57E-63	1.02E-61
58	Independently	MARCHF3	115123	ENSG00000173926	-0.94	5.55	3.11E-49	4.93E-48
59	Independently	KRT75	9119	ENSG00000170454	3.48	2.75	3.77E-41	4.59E-40
60	Independently	CRISPLD2	83716	ENSG00000103196	1.41	4.98	1.17E-35	1.17E-34
61	Independently	TCIM	56892	ENSG00000176907	-3.18	2.94	1.18E-33	1.11E-32
62	Independently	LHFPL2	10184	ENSG00000145685	0.67	5.43	4.74E-33	4.35E-32
63	Independently	WNT5B	81029	ENSG00000111186	1.45	1.25	2.55E-30	2.09E-29
64	Independently	C2CD2	25966	ENSG00000157617	-0.66	4.70	1.63E-26	1.15E-25
65	Independently	PLEKHO1	51177	ENSG00000023902	0.94	3.95	1.21E-23	7.54E-23
66	Independently	P2RX5	5026	ENSG00000083454	-1.77	1.29	4.57E-21	2.54E-20
67	Independently	ZNF639	51193	ENSG00000121864	0.49	5.65	4.80E-17	2.18E-16
68	Independently	PIM1	5292	ENSG00000137193	0.62	4.15	6.55E-15	2.64E-14
69	Independently	INHBE	83729	ENSG00000139269	1.14	1.87	4.25E-11	1.36E-10
70	Independently	APBB2	323	ENSG00000163697	-0.62	5.12	3.60E-10	1.08E-09
71	Independently	PAPPA	5069	ENSG00000182752	1.39	1.38	1.41E-07	3.46E-07
72	Independently	ARL4A	10124	ENSG00000122644	0.57	2.46	2.15E-07	5.20E-07
73	Independently	CXCL8	3576	ENSG00000169429	-2.58	5.44	7.61E-06	1.61E-05
74	Independently	SLC6A9	6536	ENSG00000196517	0.46	4.72	8.68E-06	1.82E-05
75	Independently	ADM	133	ENSG00000148926	-1.06	2.06	9.12E-06	1.91E-05
76	Independently	LIF	3976	ENSG00000128342	-0.90	5.56	1.64E-05	3.34E-05
77	Independently	WEE1	7465	ENSG00000166483	-0.19	6.37	7.09E-05	1.36E-04
78	Independently	PLAT	5327	ENSG00000104368	0.57	5.51	1.00E-04	1.90E-04
79	Independently	FOSL1	8061	ENSG00000175592	-1.00	3.59	8.45E-04	1.45E-03
80	Independently	GREM1	26585	ENSG00000166923	-0.66	1.91	1.51E-03	2.51E-03
81	Independently	VEGFA	7422	ENSG00000112715	0.22	5.14	3.79E-03	6.02E-03
82	Independently	SLC19A1	6573	ENSG00000173638	-0.18	5.53	1.92E-02	2.77E-02
83	Independently	ITGA3	3675	ENSG00000005884	0.35	10.45	2.71E-02	3.82E-02
84	Independently	OGFRL1	79627	ENSG00000119900	0.34	5.72	2.81E-02	3.96E-02

Table S7 Gene list of HALLMARK_WNT_BETA_CATENIN_SIGNALING in SKOV3 ZIC2-KO model

	Category	Symbol	EntrezGene	Ensembl	logFC	logCPM	Pvalue	FDR
1	Commonly	AXIN2	8313	ENSG00000168646	-3.25	2.16	3.14E-31	1.56E-29
2	Commonly	PPARD	5467	ENSG00000112033	-0.65	5.24	3.06E-19	6.25E-18
3	Commonly	FZD8	8325	ENSG00000177283	-1.62	2.82	1.52E-11	1.59E-10
4	Commonly	HDAC11	79885	ENSG00000163517	0.51	5.28	1.68E-06	9.25E-06
5	Commonly	PTCH1	5727	ENSG00000185920	-0.92	2.57	5.31E-06	2.68E-05
6	Commonly	NCOR2	9612	ENSG00000196498	0.30	7.82	1.10E-04	4.34E-04
7	Commonly	HDAC5	10014	ENSG00000108840	-0.80	4.64	2.08E-04	7.75E-04
8	Commonly	HEY1	23462	ENSG00000164683	-0.67	1.95	1.46E-03	4.50E-03
9	Oppositely	NKD1	85407	ENSG00000140807	-2.24	2.72	1.08E-50	1.47E-48
10	Oppositely	TCF7	6932	ENSG00000081059	-1.10	3.64	1.53E-19	3.21E-18
11	Oppositely	GNAI1	2770	ENSG00000127955	-1.01	5.29	6.26E-13	7.67E-12
12	Oppositely	JAG1	182	ENSG00000101384	1.25	5.83	1.20E-12	1.43E-11
13	Oppositely	TP53	7157	ENSG00000141510	-1.43	2.95	3.47E-09	2.86E-08
14	Oppositely	KAT2A	2648	ENSG00000108773	0.40	5.98	1.27E-07	8.51E-07
15	Oppositely	NUMB	8650	ENSG00000133961	0.35	7.87	7.62E-07	4.47E-06
16	Oppositely	MYC	4609	ENSG00000136997	0.72	6.26	5.04E-06	2.55E-05
17	Oppositely	PSEN2	5664	ENSG00000143801	-0.49	4.53	7.54E-06	3.69E-05
18	Independently	CCND2	894	ENSG00000118971	-12.33	4.09	3.22E-49	4.05E-47
19	Independently	MAML1	28514	ENSG00000198719	-4.61	0.72	3.87E-29	1.65E-27
20	Independently	DVL2	8321	ENSG00000157240	-0.55	4.69	2.90E-05	1.28E-04
21	Independently	DKK1	9794	ENSG00000161021	-0.24	6.26	1.01E-03	3.26E-03
22	Independently	FZD1	22943	ENSG00000107984	0.81	5.85	1.04E-03	3.34E-03
23	Independently	CTNNB1	1856	ENSG00000004975	0.30	5.67	2.53E-03	7.33E-03
24	Independently	DLL1	1499	ENSG00000168036	0.24	8.51	5.93E-03	1.56E-02

Table S8 Gene list of HALLMARK_WNT_BETA_CATENIN_SIGNALING in OVCAR3 ZIC2-OE model

	Category	Symbol	EntrezGene	Ensembl	logFC	logCPM	Pvalue	FDR
1	Commonly	FZD8	8325	ENSG00000177283	2.42	5.12	1.98E-221	3.55E-219
2	Commonly	HEY1	23462	ENSG00000164683	3.31	3.25	1.57E-147	1.36E-145
3	Commonly	AXIN2	8313	ENSG00000168646	1.90	2.35	1.79E-65	4.20E-64
4	Commonly	PTCH1	5727	ENSG00000185920	1.46	3.96	5.43E-54	9.74E-53
5	Commonly	NCOR2	9612	ENSG00000196498	-0.79	8.52	1.05E-35	1.05E-34
6	Commonly	PPARD	5467	ENSG00000112033	0.71	5.26	4.39E-32	3.87E-31
7	Commonly	HDAC11	79885	ENSG00000163517	-1.13	4.44	1.74E-16	7.67E-16
8	Commonly	HDAC5	10014	ENSG00000108840	0.21	6.17	2.85E-02	4.00E-02
9	Oppositely	JAG1	182	ENSG00000101384	1.16	8.47	1.23E-119	7.36E-118
10	Oppositely	NUMB	8650	ENSG00000133961	0.55	6.37	8.57E-35	8.33E-34
11	Oppositely	NKD1	85407	ENSG00000140807	-2.38	1.19	3.98E-33	3.66E-32
12	Oppositely	TCF7	6932	ENSG00000081059	-1.38	2.56	4.07E-26	2.84E-25
13	Oppositely	PSEN2	5664	ENSG00000143801	-0.85	2.99	5.26E-21	2.91E-20
14	Oppositely	MYC	4609	ENSG00000136997	0.95	5.54	8.94E-13	3.18E-12
15	Oppositely	GNAI1	2770	ENSG00000127955	-0.22	5.21	1.16E-05	2.41E-05
16	Oppositely	KAT2A	2648	ENSG00000108773	0.27	5.73	2.69E-05	5.37E-05
17	Oppositely	TP53	7157	ENSG00000141510	-0.12	7.12	2.62E-02	3.70E-02
18	Independently	WNT6	7475	ENSG00000115596	-2.28	2.77	1.04E-70	2.76E-69
19	Independently	SKP2	6502	ENSG00000145604	0.85	6.10	3.70E-64	8.44E-63
20	Independently	WNT5B	81029	ENSG00000111186	1.45	1.25	2.55E-30	2.09E-29
21	Independently	JAG2	3714	ENSG00000184916	-0.89	5.01	1.46E-24	9.51E-24
22	Independently	CSNK1E	1454	ENSG00000213923	-0.50	5.45	1.69E-20	9.05E-20
23	Independently	AXIN1	8312	ENSG00000103126	-0.40	5.27	9.57E-18	4.52E-17
24	Independently	CUL1	8454	ENSG00000055130	-0.41	6.46	2.62E-16	1.15E-15
25	Independently	FRAT1	10023	ENSG00000165879	-0.81	3.50	3.00E-14	1.17E-13
26	Independently	RBPJ	3516	ENSG00000168214	0.27	5.99	3.77E-09	1.04E-08
27	Independently	ADAM17	6868	ENSG00000151694	-0.25	6.72	4.62E-08	1.18E-07
28	Independently	LEF1	51176	ENSG00000138795	-0.98	1.45	3.94E-07	9.34E-07
29	Independently	HDAC2	3066	ENSG00000196591	0.22	7.81	2.31E-06	5.12E-06
30	Independently	NOTCH1	4851	ENSG00000148400	-0.44	6.50	6.35E-06	1.35E-05